Ana Teresa Salvador dos Santos Marques

Ionic donor/acceptor conjugated copolymers for optoelectronic applications

Coimbra, 2012

UNIVERSIDADE DE COIMBRA

Ionic donor/acceptor conjugated copolymers for optoelectronic applications

Provas de doutoramento
Inauguraldissertation

Doutor em Química Macromolecular
Doktor der Naturwissenschaften
(doctor rerum naturalium)

Departamento de Química da Faculdade de Ciências e Tecnologia
Universidade de Coimbra

Fachgebiet Makromolekulare Chemie
Bergische Universität Wuppertal

Submitted by
Ana Teresa Marques

Coimbra, 2012

"I love him to hell and back and heaven and back, and have and do and will."
Sylwia Plath

Para B.

Preface

Developing a project is quite a demand that could never be achieved without outside input and hence, I would like to acknowledge all the persons that directly or indirectly contribute for it.

I want to thank Professor Hugh Burrows for the scientific guidance, kindness and valuable discussions, along my years spent in Coimbra. To Professor Ullrich Scherf I thank the acceptance of the joint PhD project, supervision and for broaden my knowledge in polymer science.

To the Photochemistry and Molecular Spectroscopy Group from Coimbra University, in particular to Professor Sérgio Melo for all the support given along the development of this work, with emphasis in the single photon counting technique. I also want to express my gratitude to Professor Artur Valente for the help in the conductivity measurements and analysis and to Professor Alberto Canelas Pais and Dr. João Almeida for the molecular dynamics simulation data. To Dr. Licínia Justino I acknowledge the DFT calculations performed on several of the monomeric structures.

To Professor Johan Hofkens, Dr. Eduard Fron and Susana Rocha from the Katholieke Universiteit Leuven in Belgium, for introducing me to the single molecule spectroscopy technique and for the femtosecond experiments.

To Professor Andy Monkman, Dr. Edward Snedden from Durham University in UK for the pump and probe measurements, a crucial technique in the polymer photophysics processes understandment and Dr. Fernando Dias for some of the fluorescence lifetime kinetic analysis.

Professor Klaus Müllen and Dr. Zhihong Liu from the Max Planck Institute for Polymer Research, Mainz Germany are also acknowledged for the kind gift of the perylenediimide molecule and Dennis Weber from the Evonik Science to Business Center for the UV photoelectron spectroscopy measurements.

To the colleagues in the Coimbra University Ana, Artur, Carlos, Cláudio, Joana, Mário, Pina, Raquel, Rui, Sara, Sérgio, Telma and Viviana, I thank the help in the realization of the presented work.

To the Scherf Group, Anke Helfer and Sylwia Adamczyk for the GPC, TGA and AFM measurements, respectively, and to all the colleagues that one way or another helped me by making this thesis possible, in special Andrea, Daniel, Dietrich, Eduard, Jan-Moritz, Nils Fröhlich, Nils Koenen, Tina, Stefan and Seyfi.

To Torben for all the help in the LaTeX language and support.

Aos meus Pais e Avós, obrigada pelo apoio durante todos estes anos.

À Fundação para a Ciência e Tecnologia (FCT) pela atribuição da bolsa de Doutoramento (SFRH/BD/36666/2007).

Abstract

Conjugated polymers have attracted much attention, over the past decades, as promising electroactive materials with various applications, such as batteries, molecular electronic devices, light emitting diodes (LEDs), organic field-effect transistors (OFETs), large area photodetectors, organic photovoltaic cells and current injection lasers. Linear aromatic systems that consist of carbon bridged arylene units are of particular interest because of their unique luminescent properties for organic displays. Among the phenylene type molecules polyfluorenes (PFs) had emerged as attractive materials for display applications, due to efficient blue emission, relatively large hole mobility with trap-free transport, high photoluminescence (PL) quantum efficiencies and ability to change the electronic properties via modification of the polymer structure.

By incorporating molecular moieties with different HOMO/LUMO bandgaps, the emission can be tuned across the visible spectrum, providing excellent prospects for the polymer's application in various optoelectronic areas. Colour tuning in PFs can be achieved either by substitution, by controlling the effective conjugation length, or by blending the polymer with another emissive material. Through covalent attachment the migration of the chromophore dye remains inside the polymer matrix and thus, aggregation and poor device performance are prevented. Moreover, the incorporation of on-chain chromophoric units may allow for excitation energy transfer and singlet chromophore exciton confinement.

The goal of this work is to develop methods for increasing the electronic energy transfer within isolated conjugated fluorene based polyelectrolyte chains. Several water soluble poly{1,4-phenylene-[9,9-bis(4-phenoxy-butylsulfonate)]fluorene-2,7-diyl} (PBS-PFP) copolymers with distinct on-chain chromophore dyes were synthesized via Suzuki coupling and their solution optical properties characterized. In this perspective and based on the overlap between the emission spectra of PBS-PFP and the absorption spectra of the dyes, the following red emitters chromophores were employed: porphyrin (DPP), perylenediimide (PDI) and 4,7-bis(5-thien-2-yl)benzo[c][1,2,5]thiadiazole) (TBTT). On-chain energy transfer from the fluorene moieties was only observed in the PBS-PFP-DPP and PBS-PFP-TBTT systems, revealing that isolated PBS-PFP-PDI chains in solution do not undergo

an intermolecular energy transfer process. Furthermore, singlet-singlet electronic energy transfer in anionic fluorene conjugated polyelectrolytes (CPEs) with covalently or electrostatically bound porphyrins was compared and shown to be more efficient for the cofacial orientation of the chromophores (self-assembled PBS-PFP with an anionic porphyrin via calcium binding). PBS-PFP with on-chain chromophore dyes copolymers often show low solubility and aggregate/clusters formation in aqueous media. Therefore, the influence of organic co-solvents and cationic agents, e.g. ionic liquid (Aliquat 336), polyelectrolyte (poly(allylamine hydrochloride)) and tetraalkylammonium surfactants was studied, in the dissolution and "break-up" of aggregates.

The resonance energy transfer study (FRET) was extended to the self-assembled systems PBS-PFP with phenylenevinylene oligoelectrolytes, with the goal of tailoring their optical and electronic properties. FRET examination reveal that the self-assembled systems are sensitive to the solvent environment and to the size of the phenylenevinylene oligoelectrolyte chain.

With the aim of tailoring the optical and electronic properties and solid state morphology of conjugated materials with a hydroxy-functionalized side chain, a hydroxyalkylsbstituted polyfluorene was synthesized via the deprotection of a polymer precursor containing tetrahydropyran (THP) protecting group. Atomic force microscopy (AFM) reveal substantial morphologic differences in thin films spin coated from 1-methyl-2-pyrrolidone (NMP) and dimethyl sulfoxide (DMSO) solutions. The data reflect the polymer sensitivity towards the surrounding media, that directly influences it's aggregation behavior. In both solvents the polymer tends to form nanospheres, however in the film from NMP solution the nanospheres are further aggregated into wormlike particles.

Inhaltsangabe

In den letzten Jahrzehnten haben konjugierte Polymere immer mehr an Bedeutung beim Einsatz als elektroaktive Materialien wie z.B. in Batterien, molekular-elektronischen Bauteilen, lichtemittierende Dioden (LEDs), organische Feldeffekttransistoren (OFETs), Großflächen-Fotodetektoren, organischen Solarzellen oder Lasern gewonnen. Lineare, aromatische Systeme, die aus über Kohlenstoff-Verbrückten Phenylen-Einheitenvinylenen bestehen, sind aufgrund ihrer einzigartigen, lumineszenten Eigenschaften für organische Displays von großem Interesse. Unter den Phenylen-Derivaten haben sich Polyfluorene (PFs) aufgrund ihrer effizienten Emission blauen Lichtes, der relativ hohen Elektronenlochmobilität bei nahezu defektfreiem Transport, der hohen Photolumineszenz-Quantenausbeuten und der Möglichkeit, die elektronischen Eigenschaften über die Polymerstruktur zu ändern, als sehr attraktive Materialien für den Einsatz in Displays hervorgetan.

Durch Einbau von Bausteinen mit unterschiedlichen HOMO/LUMO-Abständen kann die Emission im gesamten Bereich des sichtbaren Lichtes verschoben werden, welches eine ausgezeichnete Grundlage für optoelektronische Anwendungen ist. Die Farbe von Polyfluorenen kann durch Substituenten, durch Beeinflussung der effektiven Konjugationslänge oder ber Vermischung mit anderen Emittern erreicht werden. Durch einen kovalenten Einbau des Farbstoffs kann hierbei die Entmischung zwischen den Farbstoffmolekülen und der Polymermatrix verhindert werden, um damit verbundenen Effekten wie Aggregation und meist geringeren Effizienzen vorzubeugen. Zusätzlich ermöglicht der direkte Einbau von Farbstoffen in die Polymerkette Energietransfereffekte und das Einfangen von Singulett Exzitonen.

Das Ziel dieser Arbeit ist es, Methoden zu entwickeln, die zu einer Verbesserung des elektronischen Energietransfers in konjugierten, fluorenbasierten Polyelektrolyten-Ketten führen. Hierfür wurden verschiedene Poly{1,4-phenylen-[9,9-bis(4-phenoxybutylsulfonat)] fluoren-2,7-diyl} (PBS-PFP)-Copolymere mit unterschiedlichen Farbstoffen über eine Suzuki-Kondensationsreaktion hergestellt und deren optischen Eigenschaften untersucht. Basierend auf der Überlappung des Emissionsspektrums von PBS-PFP und dem Absorptionsspektrums der Farbstoffe, wurden folgende Farbstoffe ausgewählt und eingebaut: Por-

phyrin (DPP), Perylendiimid (PDI) und 4,7-Bis(5-thien-2-yl)benzo[c][1,2,5]thiadiazol) (TB TT).

Der Energietransfer von den Fluorensegmenten auf den Farbstoff konnte nur bei den PBS-PFP-DPP- und PBS-PFP-TBTT-Systemen beobachtet werden, wobei für isolierte PBS-PFP-PDI Polymerketten in Lösung derartige Energietransferprozesse nicht gefunden wurden. Weiterhin wurde der Singulett-Singulett-Energietransfer in anionischen, fluorenbasierten Polyelektrolyten (*conjugated polyelectrolytes* CPEs) mit Kovalent oder elektrostatisch gebendenen Porphyrinringen verglichen, wobei sich eine cofaziale Anordnung als wesentlich effizienter herausstellt hat. PBS-PFP mit eingebauten Farbstoffen-Einheiten zeigt eine geringe Löslichkeit in Wasser und die Tendenz, in wässrigen Lösungen Aggregate bzw. Cluster zu bilden, sichtbar. Hierbei wurde der Einfluss von organischen Detergenzien und kationischen Tensiden, wie z. B. ionische Flüssigkeiten, Aliquat 336, Poly(allylaminhydrochlorid) und Tetraalkylammoniumsalzen auf das Aufbrechen und Lösen der Aggregate untersucht. Die Resonanzenergietranfer-Untersuchungen (FRET) wurden schließlich auf as selbstorganisierende System PBS-PFP/Phenylenvinylen-Oligoelektrolyt erweitert, mit dem Ziel, die optischen und elektronischen Eigenschaften gezielt zu verändern. Zwei verschiedene wässrige Lösungen von PBS-PFP wurden untersucht, die eine mit einem organischen Kosolvent, die andere mit einem nichtionischen Surfactant, bei zunehmender Phenylenvinylen-Konzentration. Die Energietransfer-Untersuchungen zeigten, dass die selbstorganisierende Systeme sehr empfindlich auf die Lösemittelumgebung und auf die Kettenlänge der Phenylenvinylen-Oligoelektrolyte sind.

Um die optischen und elektronischen Eigenschaften, sowie die Festphasenmorphologie von konjugierten Materialien über Hydroxylgruppen in der Seitenkette zu modifizieren, wurde ein entsprechendes Polyfluoren synthetisiert, welches Tetrahydropyran-Schutzgruppen als Hydroxylvorläufer enthält. Untersuchungen per Rasterkraftmikroskopie (AFM) zeigten deutlich unterschiedliche Anordnungen in Filmen, die mittels Spin Coating aus 1-Methyl-2-pyrrolidon-Lösungen (NMP) und Dimethylsulfoxid-Lösungen (DMSO) erhalten wurden. Die Resultate zeigen eine hohe Empfindlichkeit der Polymeranordnung gegenüber dem Lösemittel, die einen direkten Einfluss auf das Aggregationsverhalten ausüben. In beiden Lösemitteln bildet das Polymer kugelförmige sphärische Nanopartikel aus, wobei sich die Kugeln in dem aus der NMP-Lösung generierten Film zu wurmartigen Partikeln zusammenlagern.

Resumo

Os polímeros conjugados têm atraído, ao longo das décadas, considerável atenção como promissores materiais electroactivos para várias aplicações, tais como: diodos emissores de luz, transistores de campo eléctrico, fotodetectores de elevada área, células fotovoltaicas e lasers. De entre os polímeros conjugados os sistemas aromáticos lineares que consistem em ligações de carbono fenileno são de grande interesse em dispositivos orgânicos, devido às suas propriedades luminescentes. Na classe dos compostos de fenileno os polifluorenos emergiram como excelentes materiais, cuja aplicação em dispositivos se encontra intrinsecamente relaccionada com a sua emissão na zona do azul no espectro de ultravioleta, com o elevado rendimento quântico de fluorescência e com a facilidade de alteração das propriedades electrónicas através de simples modificação estrutural.

Nos polímeros conjugados é possível obter emissão de luz que cubra todo o intervalo do espectro do vísivel, por incorporação de mónomeros com diferentes energias entre as bandas HOMO e LUMO. Este processo é conseguido ou por substituíção das unidades monoméricas, por controlo da conjugação da cadeia polimérica, ou por dopagem do polímero com outro material, também ele emissivo. Através de ligação covalente entre as unidades de monómero e cromóforo é possível confinar a migração de transferência de energia para o cromóforo dentro da matriz polimérica; desta forma, são evitados fenómenos como a agregação e a fraca performance dos dispositivos.

O presente trabalho tem como objectivo o desenvolvimento de métodos que aumentem a transferência de energia electrónica dentro de cadeias isoladas de polielectrólitos baseados em unidades de fluoreno. Deste modo diversos copolímeros *poly{1,4-phenylene-[9,9-bis(4-phenoxy-butyl-sulfonate)]fluorene-2,7-diyl}* (PBS-PFP) com diferentes crómoforos incorporados na cadeia polimérica principal, foram sintetizados por acoplamento de Suzuki e estudadas as suas características fotofísicas. De acordo com a perspectiva mencionada e tendo por base a sobreposição espectral entre o espectro de absorção dos cromóforos e o de emissão do PBS-PFP foram seleccionados os seguintes fluoróforos emissores de luz vermelha: porfirina (DPP), perilenodiimida (PDI) e *4,7-bis(5-thien-2-yl)benzo[c][1,2,5]thiadiazole)* (TBTT). A transferência de energia das unidades de fluoreno para as de fluoróforo apenas foi obser-

vada nos copolímeros PBS-PFP-DPP e PBS-PFP-TBTT; este facto é indicativo da presença em solução de outros processos intermoleculares de desactivação dos estados excitados do copolímero PBS-PFP-PDI. O mecanismo de transferência de energia singuleto-singuleto foi provado dependente da orientação dos cromóforos, de acordo com o estudo efectuado em dois copolímeros aniónicos com diferentes orientações do fluoróforo de porfirina; sendo mais eficiente quando a porfirina se encontra numa posição cofacial relativamente à cadeia polimérica. A incorporação dos fluoróforos estimula a natureza hidrofóbica do polielectrólito aniónico PBS-PFP em solução, que resulta na formação de agregados e em fraca solubilidade. Por forma a contornar os efeitos mencionados os copolímeros foram dissolvidos em misturas de água e co-solventes orgânicos e a sua interação com surfactantes, polielectrólitos e líquidos iónicos catiónicos testada.

O mecanismo de transferência de energia de Förster foi observado em sistemas de PBS-PFP auto-agregados com oligómeros catiónicos de fenileno vinileno. De um modo geral, a emissão do sistema apresenta tanto características do copolímero como dos oligómeros; no entanto é sensível ao solvente utilizado e ao tamanho da cadeia do oligómero, sendo ideal em misturas de água/dioxano (1:1, em termos de volume) e em oligómeros de quatro unidades monoméricas.

É ainda apresentada a síntese de um copolímero não iónico, com grupos hidróxilo nas cadeias alquílicas, sintetizado através da reacção de desprotecção dos grupos tetrahidropirano do polímero percursor. O polímero apresenta diferenças nas propriedades ópticas em solução, conforme a polaridade do solvente utilizado, que se reflete na morfologia em filme e se encontra directamente relaccionado com a formação de agregados. Microscopia de força atómica realizada em filmes do polímero revelou a existência de estruturas de nano-esferas, que dependendo do grau de agregação podem apresentar uma morfologia de *wormlike*.

Contents

Nomenclature

A	acceptor
Al	aluminium
APLI	atmospheric pressure laser ionization
AFM	atomic force microscopy
BTD	benzo[1,2,5]thiadiazole
$CDCl_3$	deuterated chloroform
$C_2D_2Cl_4$	deuterated tetrachloroethane
$C_{12}E_5$	n-dodecylpentaoxyethylene glycol ether
cmc	critical micelle concentration
C_{16}TAB	hexadecyltrimethylammonium bromide
C_{18}TAB	hexadecyltrimethylammonium chloride
C_{16}TAC	octadecyltrimethylammonium bromide
COD	1,5-cyclooctadiene
CT	charge transfer
CTS	charge transfer state
CP	conjugated polymer
CPE	conjugated polyelectrolyte
DMSO	dimethyl sulfoxide
DNA	deoxyribonucleic acid
DFT	density functional theory
DPP	5,15-dibromo-10,20-diphenylporphyrin
D_2O	deuterium oxide
D	donor
E	energy transfer efficiency
EDTA	ethylenediaminetetraacetic acid
ET	electron transfer
EET	electronic energy transfer
ETL	electron transport layer

FIr6	bis(4,6-difluorophenylpyridinato)-tetrakis(1-pyrazolyl)borate
FRET	Förster resonance electronic energy transfer
GC-MS	gas chromatography-mass spectrometry
GPC	gel permeation chromatography
HOMO	highest occupy molecular orbital
HTL	hole transport layer
HTMA	poly(9,9-bis(6'-N,N,N-trimethylammonium)hexyl)fluorene phenylene)bromide
ICT	intramolecular charge transfer
IR	infrared
$Ir(ppy)_3$	tris(2-phenylpyridine)iridium
ITO	Indium tin oxide
KOAc	potassium acetate
λ	wavelength
LCD	liquid crystalline display
LC-MS	liquid chromatography-mass spectrometry
LED	light emitting diode
LEFET	light emitting field-effect transistors
LiBr	lithium bromide
LUMO	lowest unoccupied molecular orbital
MEH-PPV	poly[[(2-ethylhexyl)oxy]methoxy-1,4-phenylene]-1,2-ethenediyl]
MeOH	methanol
$MgSO_4$	magnesium sulfate
MCH	methylcyclohexane
$Ni(COD)_2$	bis(cyclooctadiene)nickel(0)
NMP	1-methyl-2-pyrrolidone
NMR	nuclear magnetic resonance
NIR	near infrared
ns	nanosecond
OFET	organic field-effect transistor
OLED	organic light emitting diode
OSC	organic solar cell
PA	polyacetylene
PAH	poly(allylamine hydrochloride)
PAni	polyaniline
PBS-PFP	poly{1,4-phenylene-*alt*[9,9-bis(4-phenoxybutylsulfonate)]fluorene-2,7-diyl}
PD	polydispersity

$PdCl_2$(dppf)	[1,1'-bis(diphenylphosphino)ferrocene]dichloropalladium(II)
$Pd(PPh_3)_4$	tetrakis(triphenylphosphine)palladium(0)
PDI	perylenediimide
Pdots	polymer dots
PEG	polyethylene glycol
PF	polyfluorene
PF2/6	poly(9,9-bis(2-ethylhexyl)fluorene-2,7-diyl)
PF8	poly[2,7-(9,9-dioctylfluorene)]
PFP	poly(fluorene-*alt*-phenylene)
ϕ_F	fluorescence quantum yield
PL	photoluminescence
PLED	polymer light emitting diode
PLQY	photoluminescence quantum yield
PMMA	poly(methyl 2-methylpropenoate)
PPG	poly(propylene glycol)
PPP	poly(*p*-phenylenevinylene)
PPV	poly(*p*-phenylene)
PPy	polypyrrole
ps	picosecond
PVA	polyvinyl alcohol
PT	polythiophene
RGB	red, green and blue
TCSPC	time correlated single photon counting
TGA	thermogravimetric analysis
THP	tetrahydropyran
TPP	tetraphenylporphyrin
TPPS	meso-tetrakisphenylporphyrinsulfonate
SANS	small angle neutron scattering
S_0	ground singlet state
S_1	lowest energy excited singlet state
SAM	self-assembled monolayer
SAXS	small angle X-ray scattering
SDS	sodium dodecylsulfate
SEET	singlet excitation energy transfer
τ	fluorescence lifetime
TBTT	4,7-bis(5-thien-2-yl)benzo[c][1,2,5]thiadiazole)

THF	tetrahydrofuran
TTP	thieno[3,2-b]thiophene
UV	ultraviolet light
UV-vis	ultraviolet-visible spectroscopy
WSCP	water soluble conjugated polymers

List of Figures

List of Tables

Chapter 1

Introduction

The advances achieved over the past decades in organic materials science, due to the urgent need for clean and renewable energy sources, has prompted the development of organic semiconductors, such as: light emitting diodes (LEDs), solar cells, electrochemical cells, organic memories and field-effect transistors (FETs) [1–3]. Continuing research on polymer electronics has shown an improvement in both devices and efficiency, and in the understanding of the underlying physical processes. Moreover, as the fundamental requirements of these materials are further revealed, it is possible to have a glance towards future use as cost effective alternatives to conventional silicon-based and other inorganic electronic systems [1, 2, 4].

Conjugated polymers (CPs) with their π-conjugated main chains and delocalized electronic structure, can be solution processed over large area substrates and, hence, are key components in the development of mechanically deformable logics circuit and printable light harvesting technologies [2], [5]. The material properties, such as conjugation length, light absorption, carrier mobilities, exciton dynamics and processability, can be varied through changes in the molecular structure. Furthermore, the possibility to combine different functionalities in a single device is of great importance in future organic electronics, especially in integrated components and circuitry [2], [3].

Synthetic polymers containing arrays of suitable chromophoric dyes, i. e. bearing donor and acceptor units, have the potential to efficiently replicate the natural light harvesting process [6]. In a simple description, after the absorption of light, the excitation energy is expected to be transfered among the polymer chromophores until it rests at the lowest energy sites [6–8]. This energy transfer mechanism has been shown to occur in dye-capped, diblock, short and branched polymers [6, 9–13]. The transfer process is dependent on the polymer conformation and conformational order [6]. This subject has been a topic of interest

in organic electronic devices that are based in conjugated molecules and it is important to determine the role that each moiety play in the device performance.

1.0.1 Principles of common optoelectronic devices

Reviews of different aspects of the field of LEDs and organic photovoltaics (OPVs) have been published, that include both the electroluminescent (EL) materials and the device physics and engineering. Organic LEDs function as OPVs in reverse, thus converting electrical current into light. There is a useful overlap in materials and cell design between the two fields [14]. While, OPV systems require efficient exciton dissociation into free charge carriers, OLEDs demand efficient recombination of free carriers to form excitons [1]. Successful OPV must be less expensive and produced for covering larger areas than OLEDs. Flexibility is of primary importance in OPV, since it enables the use of high speed manufacturing processes and minimizes the systems costs by employing light weight substrates that are easily installed on many surfaces [14].

The simplest organic LEDs comprise one active layer with the electroluminescent material and two injecting contacts: a positive (hole injection) and a negative electrode (electron injection), one of which is transparent [16], [17]. Normally the cathode metal work function is low, in order to facilitate electron injection into the active material, while the work function of the semitransparent anode is generally high. Figures 1.0.1 and 1.0.2 depict some of the most common polymer based-LED architectures and their general structures.

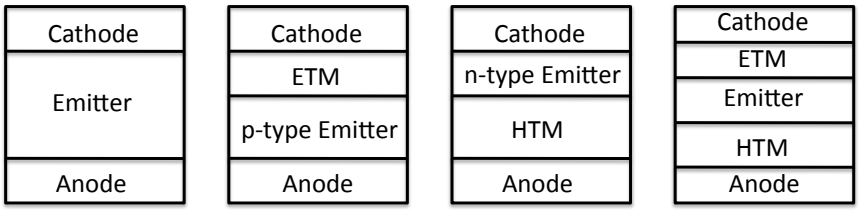

Figure 1.0.1: OLED architectures with a hole transport material (HTM) and an electron transport material (ETM). Adapted from [16].

Given that the majority of organic materials used in thin films (LEDs) normally do not transport both carrier types with similar mobilities, the recombination occurs close to one of the electrodes [17]. To achieve an efficient LED with the single layer configuration, the organic EL material needs to have a high luminescence quantum yield and to be able

[1] The electrons and holes capture one another within the polymer film, forming neutral bound excited states that are denominated excitons [15].

to facilitate the injection and transport of electrons and holes. However, a single material with such multifunctional capabilities is extremely difficult to find, and consequently, most emissive materials used in LED tend to have either p-type (hole transport) or n-type (electron transport) charge transport characteristics [18]. Therefore, the dominant factor for achieving high efficiency in a given polymer is the proper balance and confinement of the electrons and holes. Through blending high-bandgap and low-bandgap polymers in proper ratios, charge traps can be introduced in the light emitting polymer layer (LEP) [19]. Likewise, the introduction of an electron injection/hole blocking layer can confine holes to the emissive layer and enhance the electron injection [18]. However, the use of blends in technological applications is met with skepticism, given that the interface between the different functional polymers is crucial for the device performance; as a result, the synthesis of copolymers is preferred [20]. The fundamental difference between copolymers and blends is that the active functional units in a polymer are located on one single polymer chain. In contrast, in a blend the functional units are on different chains and hence, their properties depend on the blend morphology [20].

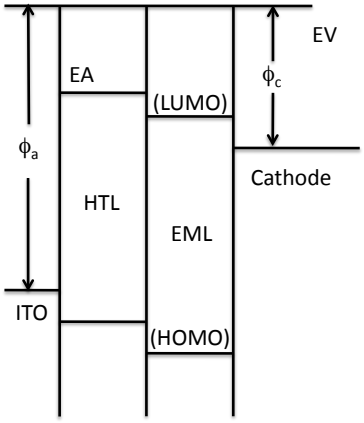

Figure 1.0.2: Simplistic electronic energy band diagram for a two-layer PLED device. The ITO anode, HTL, EML, and cathode structures are shown using the equivalence of the conduction band with the electron affinity (EA) and LUMO. The energy band diagram illustrates the equivalence of the valence band with the ionization potential (IP) and HOMO. The work function, ϕ, is also shown with reference to the vacuum potential, E_v. Adapted from [21].

A major new development involves white light-emitting diodes (OWLEDs). Currently, the common strategy in their fabrication is to use a multicomponent blend as white emissive layer, that include either two (blue and yellow) or three color (blue, green and red) polymer blend system [22]. However, the system often suffers from a rapid decrease in

efficiency and from an unstable emission spectra [23]. Furthermore, as the layers are typically deposited by spin-coating, it is difficult to choose a solvent that dissolves the material being deposited without affecting the previously deposited layers [24]. The high efficiency requirements of PWLEDs, high brightness and stable emission spectra makes devices based on a white single polymer (WSP) a preferable alternative. These polymers are commonly composed of a wide bandgap host polymer, such as polyfluorene (PF), with small amounts of different coloured chromophores covalently attached. The morphology of the emissive layer and the charge injection also determine the device performance [23]. A variety of inorganic interfacial materials combined with the Al cathode are exploited to achieve stable and efficient electron injection e. g., LiF, CsF, BaF_2, NaOH and Cs_2CO_3. As for the electron injection material, ethanol/water soluble conjugated polymers have recently been employed and show good properties [23], [25]. Figure 1.0.3 depicts a schematic diagram of a PWLED device configuration.

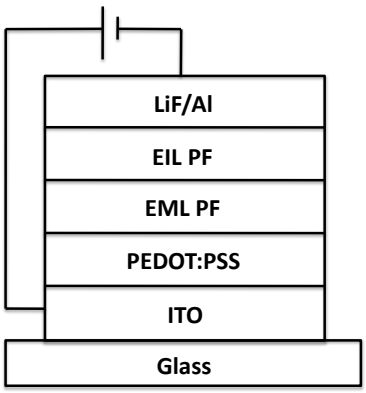

Figure 1.0.3: Schematic diagram of a device configuration of a PWLED. The white emissive layer (EML) is based on a three color PF and the and the electron injection layer (EIL) on an ethanol soluble PF. Adapted from [23].

Despite exhibiting lower power conversion efficiency in comparison to conventional inorganic technologies, polymer photovoltaic cells have attracted particular attention, due to potential applications as cost effective thin film alternatives to conventional silicon based and other inorganic systems [1], [2]. The most important figure of merit describing the performance of a solar cell is its power conversion efficiency. In addition, the accurate, reproducible and standard conform measurement of the current voltage characteristics of an organic solar cell is also essential [26]. At present, the main interest resides in bulk heterojunction solar cells (BHJ) whose structure is based on blends of conjugated polymers as electron donors and soluble fullerene derivatives as electron acceptors [1]. Most organic pho-

tovoltaic cells (OPV) have at least three interfaces: the electrode/D, D/A, and A/electrode interfaces, where D and A are the donor and acceptor semiconductors, respectively [14], see Figure 1.0.4. In order to generate a photocurrent in an OPV, optically generated excitons must be dissociated at the interface between electron donating and accepting materials.

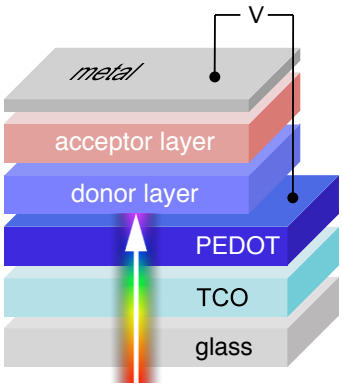

Figure 1.0.4: Typical device configuration of a bilayer organic solar cell device with planar heterojunction. On the top of the glass substrate a transparent conductive oxide (TCO) acts as anode. The PEDOT interlayer helps to avoid local shunts and the active layer consists of either a bilayer or a blend of organic semiconductors. On top, a metallic electrode acts as cathode. Reproduced with the authors permission from Ref. [26].

The energy level diagram for the main processes involved in the charge photogeneration process, within the polymer/fullerene active layer after photooxidation are shown in Figure 1.0.5. From analysis of this scheme, the key points that determine the efficiency of charge photogeneration in organic solar cells are the competition between the thermal relaxation of the CT state, and the dissociation of the CT state into a fully charge separated (CS) one [1]. In an ideal BHJ, co-continuous donor and acceptor domains with sizes related to the diffusion length of excitons should be targeted, whereas nanoscale ordering in the domains is also an important issue [2]. However, the most serious problem responsible for device instability is related with the oxidation of the Al electrode. An approach to overcome this problem is to fabricate inverted devices [27]. By reversing the polarity of the charge collection via an inverted configuration, the air stable high-work-function metal Ag can substitute Al as the anodic electrode for hole collection. This new arrangement gives a dramatic improvement in the operational lifetime, however the device suffer from a trade-off between stability and performance due to poor electrical coherence at the organic/inorganic interfaces. By incorporation of a cross-linked fullerene interlayer, the mutual diffusion between the upper

active layer and the bottom metal oxide layer can be avoided, allowing the achievement of highly efficient and stable multilayer inverted solar cells [27].

Recently, field-effect transistors (FETs) based on solution processed molecular and conjugated polymer semiconductors have been the subject of tremendous progress. This has led to a abundance of functional conjugated organic materials, among which conjugated polymers play a prominent role [28]. The mobility of an organic FET is strongly dependent on the local intramolecular structure and intermolecular packing between molecules [29]; as a result of its intrinsically connection with the relaxation energy and the transfer integral [2] [29].

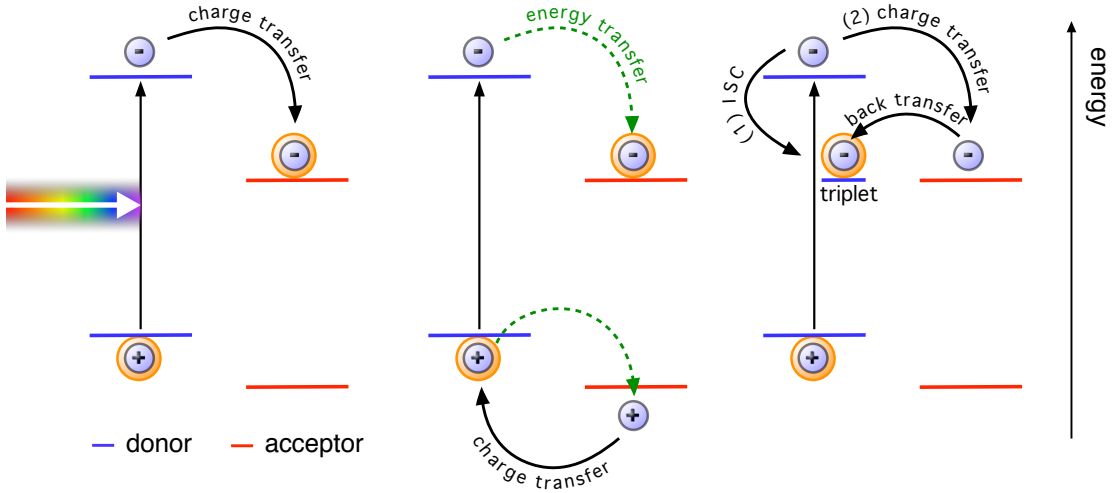

Figure 1.0.5: Typical charge transfer reactions in organic solar cells. Left: The singlet exciton on the donor material is dissociated by an electron transfer to the acceptor material. The final state is indicated by the orange frame of the charge carriers. Middle: energy transfer of the exciton from donor to acceptor, followed by a hole transfer from acceptor to donor. The final state is similar to the first described case. Right: triplet excitons can act as loss mechanisms either by intersystem crossing (ISC) or by an electron back transfer to a triplet exciton level in the donor. Reproduced with the authors permission from Ref. [26].

In fact, organic field-effect transistor OFET interfaces (Figure 1.0.6) play a crucial role in the overall performance. The source/drain metal electrode/organic semiconductor interface influences the charge carrier injection, while the gate insulator/organic semiconductor interface influence the formation, or interruption, of a conducting channel [31]. By flattering the dielectric surface with a thin polymer layer or molecular monolayer, the charge carrier traps are decreased and the surface energy of dielectric improved [31]. Most of the

[2]For further insight about the transfer integral see the work of Troisi *et al.* [30].

polymers used for OFETs operate as p-type transistors, but low-bandgap donor-acceptor copolymers also provide a route to high-mobility n-type and ambipolar FETs [29]. Several polythiophene-based OFETs have been reported with mobilities and an on/off ratio values close to silicon compounds, although the stability still must be improved for practical application. One approach is to introduce electron deficient aromatic rings (such as isoindigo) into the backbone of polythiophene to lower the HOMO level, as illustrated on the work of Lei *et al.* [32]. Recently, organic light-emitting transistors (OLETs) have been reported; these type of OFET combine in a single device the electrical switching functionality of a field-effect transistor with the ability of light generation (Figure 1.0.6). This novel class of organic devices merge the different functionalities of OFET and OLED devices and offer an ideal structure for improving the lifetime and efficiency of organic light emitting materials [3].

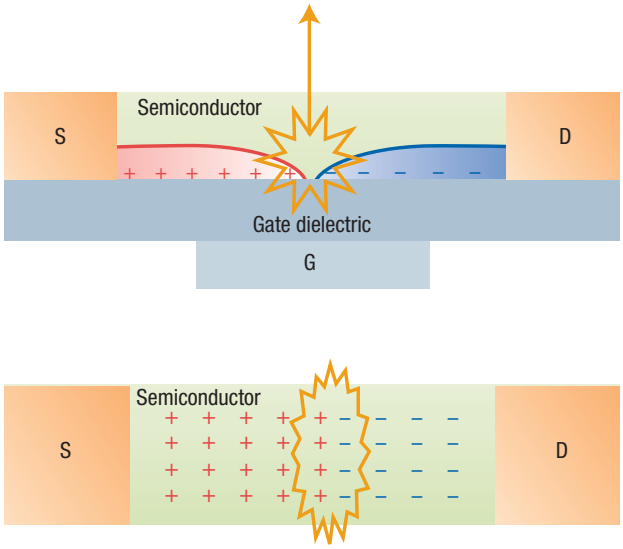

Figure 1.0.6: Scheme of a light-emitting field-effect transistor. Top: side view. Bottom: top view. The electrons and holes are injected from the drain (D) and source (S) contacts and recombine within the channel in a position controlled by the gate (G). Reproduced with permission from Ref. [3]. © (2006) Nature.

1.0.2 Conjugated polymers

Plastic semiconductors composed of conjugated organic molecules have the potential to revolutionize the electronics industry [33] When functionalized with flexible side groups, these materials become soluble in organic solvents and can be solution processed at room temperature into large-area, optical-quality thin films; these are readily fabricated into desired shapes, and can be useful in novel device applications [7]. Different types of conjugated

polymers such as polyacetylene (PA), poly(*p*-phenylene) (PPP), poly(p-phenylenevinylene) (PPV), polyaniline (PAni), polypyrrole (PPy) and polythiophene (PT) have been developed and widely investigated. Their chemistry and physics have been intensively studied and reviewed in a large number of publications [34].

The conjugated systems considered in this thesis are based on fluorene building blocks, substituted with anionic alkyl chains to provide solubility in water and organic polar solvents, and having attached on-chain fluorophores, for emission colour tuning. Consequently, the discussion of the synthetic routes and physics will only be discussed for this class of materials.

Synthetic Approaches to conjugated poly(*p*-phenylenes)

As a consequence of the development of optoelectronic applications based on conjugated polymers, significant attention has been directed to attaining stable blue electroluminescence (EL) from poly(*p*-phenylene vinylene)-type (PPV-type) or poly(*p*-phenylene) (PPP-type) polymers (Figure 1.0.7). The generation of blue light is of crucial importance for red-green-blue (RGB) full colour light-emitting devices and it can be transformed into red and green light by internal or external colour conversion [35].

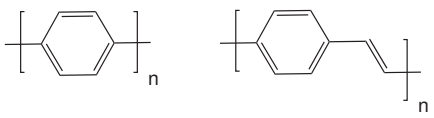

Figure 1.0.7: Structures of poly(*p*-phenylene) PPP and poly(*p*-phenylene vinylene) PPV.

Among polyphenylene-based materials, highly emissive polyfluorenes (PFs) have received particular attention during the last decade as a promising class of conjugated polymers. The excellent optical and electronic properties of 9,9-disubstituted PFs, polyindenofluorenes (PIF) (Figure 1.0.8) and fluorene-based copolymers have brought this class of materials into the focus of scientific and industrial interest [35].

The decoupling provided by bonding groups to fluorene's 9-position is noteworthy, as this allows the solubility and aggregation behavior of these compounds to be modulated independently of their electronic properties [36]. The available synthetic methods include the Suzuki cross coupling of arylboronic acids or esters with chloro-, bromo-, iodo-, or tosylaryls, the Yamamoto homocoupling of chloro-, bromo-, or iodoaryls, and the Stille cross coupling of trialkylstannylaryls with haloaryls [35].

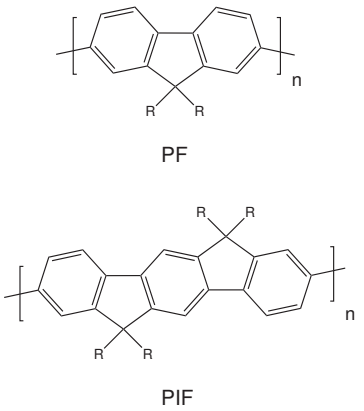

Figure 1.0.8: Structures of polyfluorene (PF) and polyindenofluorene (PIF).

The Suzuki reaction involves the coupling of an aryl or vinyl boronic acid with an aryl halide or triflate using a palladium catalyst. Its reaction mechanism is proposed to involve oxidative addition, transmetalation and reductive elimination steps, Figure 1.0.9 [37].

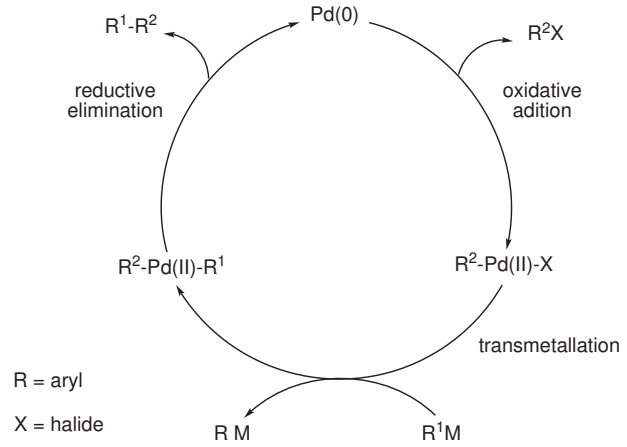

Figure 1.0.9: General catalytic cycle for the Suzuki cross-coupling. Adapted from [37].

Oxidative addition is often the rate determining step in the catalytic cycle, with the relative reactivity decreasing by the following order I > OTf > Br $\gg$ Cl. A wide range of palladium(0) catalysts or precursors can be used in the cross-coupling reaction, with $Pd(PPh_3)_4$ being the most commonly employed. However, $PdCl_2(PPh_3)_2$ and $Pd(OAc)_2$ plus PPh_3 also show good synthetic efficiency, since they are air stable and readily reduced to the active Pd(0) complexes by the organometallics used in the cross-coupling reaction [37]. Though the mechanism of oxidative addition and reductive elimination are well understood and are common processes for all cross-coupling reactions, transmetallation is highly dependent on the organometallics and reaction conditions. The addition of base exerts a remarkable ef-

fect on the transmetallation rate of organoboron reagents with metallic halides and platinic halides. Hence, the transmetallation with transition metal complexes appears to proceed well. However the choice of suitable bases and ligands is essential [37].

A way to influence the emission colour from a conjugated polymer is to control the conjugation length of chromophores contained within the macromolecule by the introduction of units that disrupt the conjugation, and hence induce a shift in the polymer emission colour [38]. The incorporation of other co-monomers into the conjugated polymer backbone can require a number of additional chemical reactions and Suzuki coupling is still the preferable synthetic method in this regard [35].

Ni(0) complex-promoted dehalogenation polycondensation of dihaloaromatic compounds X-Ar-X affords π-conjugated polymers, -(-Ar-)-$_n$. The diorganonickel(II) complexes undergo reductive coupling (or reductive elimination) reactions to give R-R (Figure 1.0.10) [39].

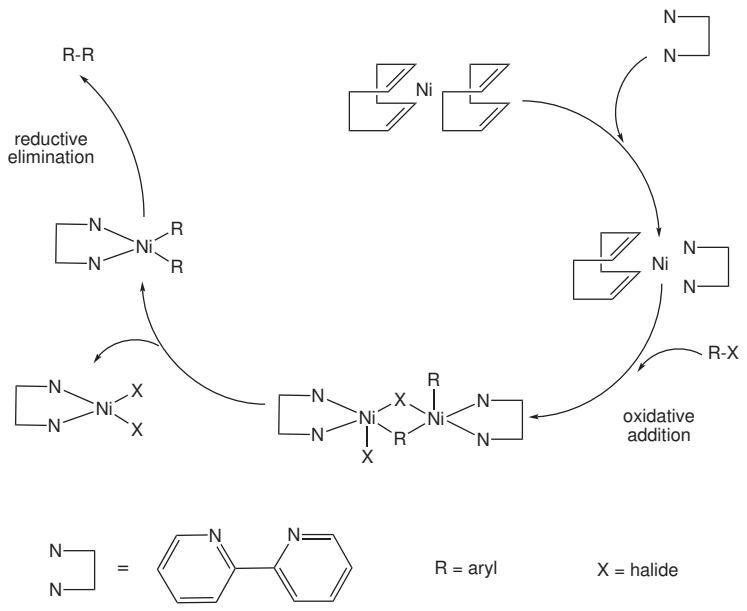

Figure 1.0.10: General catalytic cycle for the aryl-aryl Yamamoto cross-coupling reaction. Adapted from [39], [40].

Since the carbon-carbon coupling reaction is promoted by coordination of an electron-accepting olefin and an aromatic compound, the Ni-catalysed organic synthesis proceeds well with olefinic and aromatic halides. The reductive elimination via coordination of the electron-accepting olefinic halide aryl halide is essential for the catalytic reaction. Addition of electron-accepting olefins and dienes to Ni-promoted synthetic reaction systems enables the reaction, presumably by coordination of the additive to nickel. 1,5-Cyclooctadiene (cod) also serve as an activating reagent for Ni(cod)$_2$-catalyzed dehalogenative polycondensation

of dihaloaromatic compounds [39]. Both Suzuki and Yamamoto methods, can lead to high quality PFs with average molecular weights of up to 300 000, corresponding to a coupling of several hundred repeat units [35].

1.0.3 Photophysics of conjugated polymers

There is currently an intense effort to exploit the properties of conjugated polymers for the development of optoelectronic devices, which requires detailed knowledge of their photophysics. The first approach proposed that the properties of conjugated polymers could be described by a one-dimensional semi-conductor, implying that electron-electron interaction was negligible relative to electron-lattice interaction. However, nowadays there is compelling evidence that conjugated polymers do not behave fundamentally different from other organic materials [38]. As a result of the strong interaction between the electrons and the lattice in organic systems, all dynamical processes in conjugated polymers involve both electronic and atomic motions. Studies of these interactions that include: charge transport and charge transfer, exciton formation, exciton dissociation, and energy transfer, are necessary to provide the most basic understanding of electronic, as well as, optoelectronic device applications based on organic materials [35]. The physical laws that govern these dynamical processes are based on quantum mechanics for the electrons, electrodynamics for the photons, and quantum or Newton mechanics to describe the molecular part [35].

1.0.3.1 Absorption and emission properties

Following photo-excitation of a molecule in the UV-vis spectral range an electron is promoted from the highest occupied molecular orbital (HOMO) to either the lowest unoccupied molecular orbital (LUMO), or to a higher lying empty orbital [38]. The photophysical processes [3] that take place after photo-excitation are depicted on Figure 1.0.11, that illustrate the Jablownski diagram for radiative and raditionless transitions. The commonly encounter photophysical radiative processes are: 1) "allowed" singlet-singlet absorption, 2) "forbidden" singlet-triplet absorption, 3) "allowed" singlet-singlet emission (fluorescence) and 4) "Forbidden" triplet-singlet emission (phosphorescence). While, the radiationless photophysical processes comprise: 1) "allowed" transitions between states of the same spin (internal convertion), 2) "forbidden" transitions among excited states of different spin (intersystem crossing) and 3) "forbidden" transition between triplet states and the ground state (intersystem crossing) [41].

[3] The transitions that interconvert excited states with each other or with the ground state [41].

Conjugated polymer chains in solutions and films tend to twist and coil. Hence the description of a conjugated polymer chain is that of a series of linked chromophores, each of which has a different extent of π-electron delocalization. Moreover, each conjugated segment is roughly planar with its extent of conjugation limited by the twists of the polymer backbone [7]. Hence, in CPs the excess of vibrational energy of the fluorophores is transferred to their environment on a subpicosecond time scale. Via this vibrational cooling process the emission originates from the transition $S_n{}^1 \rightarrow S_n{}^0$, in accordance with Kasha's rule [4], causing an energy separation between the absorption and emission bands (the Stokes shift) [43].

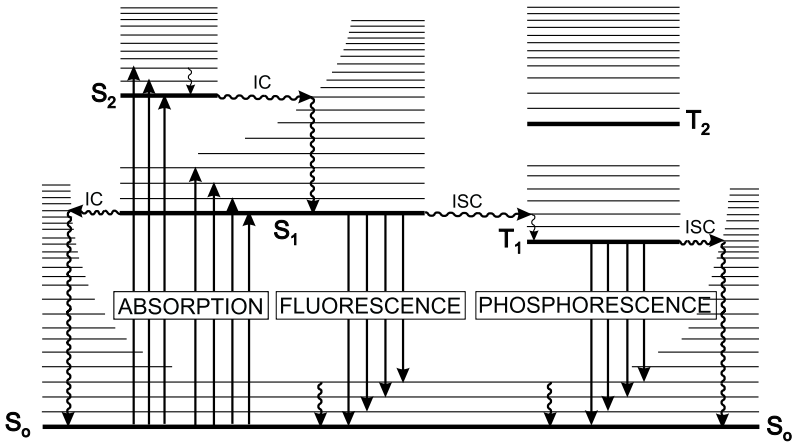

Figure 1.0.11: Perrin-Jablonski diagram showing the radiative and non-radiative transitions. S and T stands for the singlet and triplet state, respectively, IC stands for internal convertion and ISC for intersystem crossing. Reproduced with permission from Ref. [44]. © (2002) Wiley-VCH Verlag GmbH & Co. KGaA.

The material undergoes further structural relaxation and exciton migration through the energetic disorder of the bulk polymer, that causes an additional Stokes shift. These latter processes break the mirror symmetry among the $S_n{}^0 \rightarrow S_n{}^1$ and $S_n{}^1 \rightarrow S_n{}^0$ absorption and emission spectra, respectively - since absorption can be considered to be an instantaneous process allowing all possible states to absorb, whereas only the lowest energy states can emit [43]. The reasons are attributed to the relaxation of the excited polymer chain skeleton, that can give rise to a change of the electronic excitation, to the intra and interchain energy transfer towards intrinsic and extrinsic chromophores and to interchain coupling [38]. This causes the absorption spectra of CPs commonly to be structureless and broad, whereas the emission spectra is well resolved (Figure 1.0.12) [43]. The emission of PFs show a

[4]The same fluorescence emission spectrum is generally observed irrespective of the excitation wavelength [42].

structured fluorescence spectrum between 380 and 530 nm (Figure 1.0.12) attributed to at least three vibronic components; each of these vibronic bands comprises at least three different vibrational modes [45].

The optoelectronic properties of CPs are influenced upon temperature variation, as a consequence of the dynamic disorder of the material (Figure 1.0.12). The loss of vibronic structure of the absorption spectra is explained in terms of twisting vibrations along the polymer chain, that reduce the effective conjugation length and gives rise to a hypsochromic shift [5] of the absorption spectra. At lower temperatures the torsional motion along the chain is frozen, causing an increase in the effective conjugation length [38] and given the excited state a similar geometry to that of the ground state, Figure 1.0.12 [43]. The observation of a structured emission spectra at both room and low temperatures suggests that the PF emission arises from a single conjugation length. The bathocromic shift at room temperature is associated with an increase in the conjugation segment of the excited state, either by an activated relaxation process, or by energy migration to a more relaxed state [45].

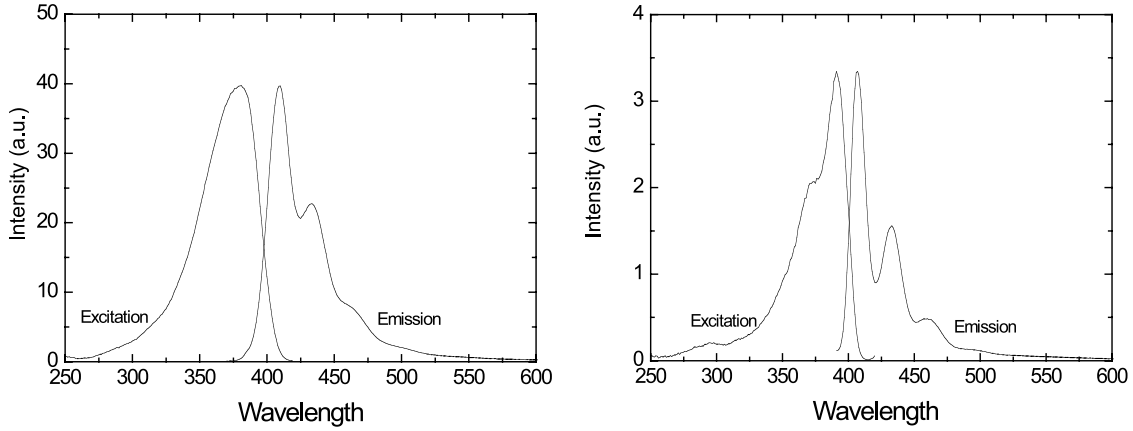

Figure 1.0.12: Excitation and emission spectra of PF2/6 in dilute methylcyclohexane solution at 295 K (a) and 77 K (b). Reproduced with permission from Ref. [43]. © (2008) Springer.

It is generally accepted that the photo-excitation of an isolated conjugated polymer chromophore produces an intrachain exciton. However, when the π-electrons in adjacent chromophores are in close proximity the formation of interchain species is possible. When two adjacent polymer chromophores share their π-electrons equally in the excited state but not in the ground state, the interchain excited state is denominated as excimer [7]; when

[5] Change of the spectral band position to a shorter wavelength, blue-shift.

the π-electrons are neutrally delocalized over multiple segments in both the ground and excited states it is considered an aggregate [6]; and it is called a polaron pair, when the charge transfer phenomena occurs via excitation of strongly interacting chromophores, leaving a radical cation, or hole polaron, on one segment and a radical anion, or electron polaron, on the other [7]. When the interchain excited states interaction imply an unequal sharing of π-electron density between segments or a partial degree of charge transfer character, the specie is labelled as exciplex [7].

The aggregation phenomena [7] plays an important role on the spectroscopic properties of oligomers and polymers. The absorption is shifted to higher energies, whereas the emission is red-shifted [8], resulting for the different separation distances and delocalization over more than one chain. In this situation, the absorption spectra is considered as a superposition of the isolated chain and aggregated complex spectra. It was found that the CPs tendency to form aggregates is dependent on the chain length, molecular constitution and solution concentration [38]. Examination of the photoluminescence spectra and fluorescence lifetime of CPs in poor solvents leads to the conclusion that interchain coupling can dramatically alter the electronic and optical properties of conjugated polymers. A decrease in the photoluminescence quantum yield [9] is normally associated to the formation of new interchain species [46].

1.0.3.2 Fluorescence lifetimes

The dynamics of intra and interchain excitation energy in CPs is crucial to understand the complex photophysical behavior of the materials. Since CPs are considered as an array of weakly coupled chromophores with slightly different excitation energies, there is a distribution of segments with different π - π^* transition energies [47]. The shorter segments have higher π - π^* transition energies than the longer ones and act as energy donors towards the low energy states.

For most luminescent polymers fluorescence lifetimes lie in the range of 100 ps to 2 ns, normally with multiple decay component, due to various processes that contribute to the radiative and nonradiative exciton recombination [43], [35]. Polyfluorenes are no exception, and their fluorescence decays are complex both in thin film and solution, with minor amplitude fast rise and decay components together with a predominant decay time (Figure 1.0.13) [43]. As shown in Figure 1.0.13 the fluorescence kinetics reflect the super-

[6] Photophysical definition: polymer segments are considered an aggregated only when the extent of π-delocalization is altered from that of a single chromophore, [7].

[7] Agglomerated conjugated polymer chains whose chromophores do not interact electronically.

[8] Bathochromic shift.

[9] A measure of the efficiency of the emission process [41].

position of two emitting species. In the work published by Dias *et al.* the slow component was found to be temperature independent, while the fast component showed a temperature dependence [45]. Dias suggested that the observed behavior was a direct consequence of the formation of an initial nonrelaxed conformer, that later decays to the ground state, giving rise to the long decay lifetime [45], [47]. However, there is still controversial and a unambiguous attribution of the fast component is lacking.

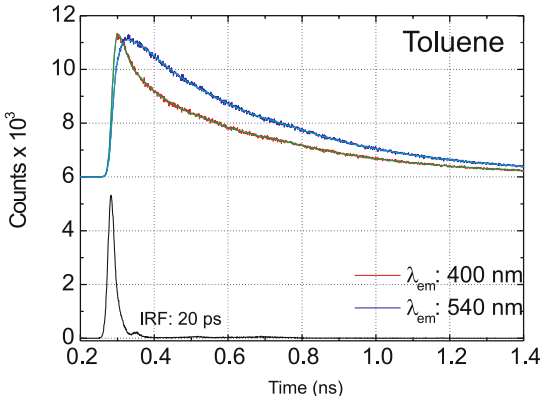

(a)

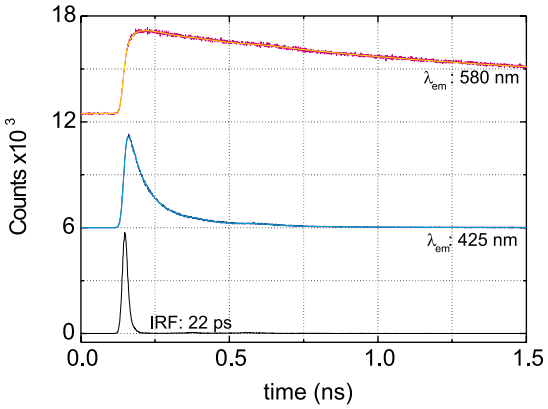

(b)

Figure 1.0.13: Time-resolved fluorescence emission decays of PFO obtained at 295 K in a) toluene solution with emission collected at 400 nm and 540 nm and b) PFO lms with emission collected at 425 nm and 580 nm. The instrument response function (IRF) is also shown. Reproduced with permission from Ref. [43]. © (2008) Springer.

Further insight into the nature of the fast component has been given by direct comparison with data obtained for the rigid ladder polymer, MeLPPP and small fluorene oligomers. In the MeLPPP case the fast decay component is not observed; in contrast, in oligomer solutions, the fast decay and rise components can be detected [43]. Furthermore, the fast

component amplitude assumes a negative value (rise time) depending on the solvent viscosity, that is a distinctive pattern of fast conformational relaxations within the polymer backbone [43], [45]. A similar pattern is observed in thin PF films observed at short wavelengths, see Figure 1.0.13.

1.0.3.3 Energy transfer

Energy transfer is a key process in the working mechanism of a wide number of optoelectronic devices based on CP systems. The most prominent example is the color tuning of the emitted light, accomplished when several materials with different optical gaps are included in the active layer, or in the polymeric chain. A distribution of segments with distinct conjugation lengths within the CP leads to the unidirectional energy migration to the lower energy sites and ultimately to its emission [48]. Figure 1.0.14 describe a simplistic scheme of the transfer of excitation energy among freely diffusing molecules, and of D and A subunits in the same molecule segments.

Electronic excitation energy is transferred between the molecules either by a trivial radiative process (emission of a photon followed by subsequent reabsorption) or by a nonradiative process [49]. Necessary conditions for the transfer phenomena to take place are that the transitions of the donor, $D^* \rightarrow D$, and acceptor, $A \rightarrow A^*$, are in ressonance and that the states are coupled by suitable D–A interactions [49]. The last requirement is fulfilled if the spectral overlap between the D emission and the A absorption, is sufficiently large [49].

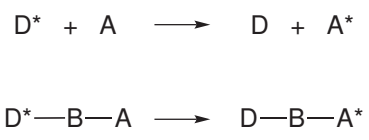

Figure 1.0.14: Transfer of excitation energy between donor (D) and acceptor (A) subunits. B denotes a bridging subunit. Adapted from [49].

The electronic coupling for excitation energy transfer can be divided into a coulomb and an intermolecular interaction part. The coulombic interactions are based on long range dipole-dipole interactions (Förster mechanism) and short range multipolar interactions. Whether the interactions due to intermolecular orbital overlap, which include electron exchange (Dexter's mechanism) and charge resonance interactions, are only short range, Figure 1.0.15 [44]. The energy transfer coulombic interaction is shown by the operational expression derived by Förster (Equation 1.1); where f_D and f_A are the oscillator strengths of

the D and A, respectively, R_{DA} is the D–A distance and J the spectral overlap integral [49].

$$k_{EET} \propto \frac{f_D f_A}{R_{DA}^6 \bar{\nu}^2} J \tag{1.1}$$

In addition to the coulomb term, Dexter derived a mathematical approach that includes an expression for the transfer rate due to the exchange mechanism. The exchange contribution depends on the overlap between the wave functions of the D and A, since the molecular orbital overlap at sufficiently large separation and decreases exponentially with increasing separation, Equation 1.2. Where J is the spectral overlap integral and L the effective orbital radius [49].

$$k_{EET} \propto Jexp\left(\frac{-2R_{DA}}{L}\right) \tag{1.2}$$

Because of the exponential attenuation of overlap of the D and A molecular orbitals with the distance between the molecules, contributions from the short range interactions are normally negligible for intermolecular separations greater than 5 Å [50].

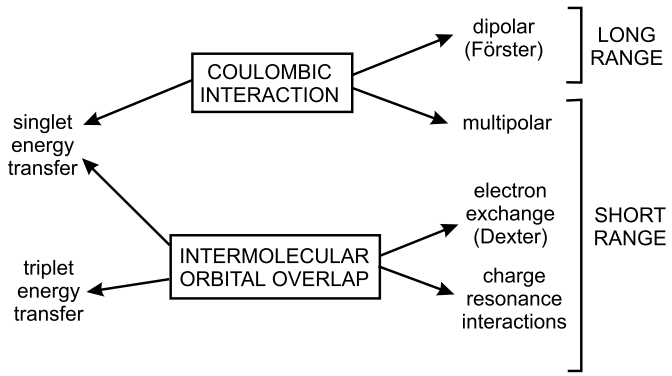

Figure 1.0.15: Types of interactions involved in nonradiative transfer mechanisms. Reproduced with permission from Ref. [44]. © (2002) Wiley-VCH Verlag GmbH & Co. KGaA.

In the CP case, the interchain migration rate is dependent on the relative internal geometries between the D and A chromophores. Förster's point-dipole model correctly reproduces the qualitative evolution of the electronic couplings with large donor-acceptor separation. However, for linear chromophores the electronic couplings and transfer rates are considerably underestimated, in comparison to the description provided by the Förster

theory. Moreover, it does not adequately account for the spatial distribution of the excitations over the nearby D and A oligomers [50]. Studies of Beljonne *et al.* highlighted the fact that in the case of solutions of conjugated macromolecules which can coil, the fast energy transfer rate has to be related to hops between stacked conjugated segments belonging to the same chain, instead of hops along the chain [48]. In summary: the actual excitation transfer rate shows a much weaker short range distance dependence than the suggested by Förster; the distance at which the Förster rate is recovered is observed to be rather large [10]; Förster theory excludes the optically dark states; and at close distances, the orientation dependence of the resonance coulomb rates alters the rates value by a factor of two [51]. Consequently, various procedures for accurately calculating the electronic coupling in CPs have been suggested to describe the nature of energy transfer, such as: the line-dipole model, the multicentric monopole expansion model and the transition density cube model [50].

The dynamical evolution of excitations in conjugated polymers is considerably more complicated than previously thought and at present, the only general qualitative conclusion made is on the excitons migration rate. In CPs, after photoexcitation the excitons migrate rapidly at early times and more slowly at later times, between localized states [50]. This kinetic behaviour gives rise to a short exciton diffusion length. This is a limiting factor in the efficiency of photovoltaic devices based in CPs and to try to overcome it, intensive research has been made on the morphology of CP films [50].

[10]Förster expression also seems to be inappropriate for systems where donors and acceptors are closely packed, as is the case of thin films [51]

Chapter 2

Experimental Part

2.1 Materials

The comercial cationic surfactants *cetyltrimethylammonium bromide* (CTAB) $CH_3(CH_2)_{15}N(CH_3)_3Br$, *cetyltrimethylammonium chloride* (CTAC) $CH_3(CH_2)_{15}N(CH_3)_3Cl$, *octadecyltrimethylammonium bromide* (OTAB) $CH_3(CH_2)_{17}N(CH_3)_3Br$ and the non-ionic *pentaethylene glycol monododecyl ether*, $C_{12}E_5$ were purchased from Sigma-Aldrich and used without further purification procedures, as well as the commercial *poly(allylamine hydrochloride)* (PAH) average Mw approx. 15 000 (GPC vs. PEG std.). *N-methyl-N,N-dioctyloctan-1-ammonium chloride*, Aliquat 336, was a kind gift from Professor Carlos Afonso from the Instituto Superior Técnico, Portugal.

2.2 NMR - spectroscopy

The ^1H and ^{13}C NMR spectra [1] were recorded on Bruker Avance III 600 (600 MHz) or Avance 400 (400 MHz) spectrometer. The chemical shifts (δ) are reported in parts per million (ppm) using the residual solvent signals as internal standards. All samples contain 10/20 mg substance in 0.5 ml of deuterated solvent. The coupling constants are reported in Hertz (Hz). The NMR measurement is presented according to the following example: *Experiment-NMR (measured frequency, solvent): δ [ppm] = δ-value (number of protons, spin multiplicity, assignment, coupling constant)* The spin multiplicity is designated as: *s* (singlet), *bs* (broad singlet), *d* (doublet), *t* (triplet), *m* (multiplet), *dd* (doublet of doublet), *dt* (doublet of triplet). The symbol Ψ stands for "Pseudo" (e.g., Ψq = pseudoquartet).

[1] Measurements performed at the Bergische Universität Wuppertal, Germany, by A. Siebert and I. Polanz.

2.3 Mass-spectroscopy

The FD-Mass-spectra were measured [2] with a Fisons Instruments Sectorfield Mass Spectrometer ZAB 2-SE-FPD and APLI experiments [3] were done in a Micromass Q-TOF Ultima API.

2.4 GC-MS and LC-MS measurements

The GC-data were obtained [4] with a GC 17A QP 5050 from Shimadzu and the LC-MS [5] on a Agilent 1100 Series connected to an ESI mass spectrometer based on MICROTOF Bruker.

2.5 Gel permeation chromatography

The non-ionic polymers molecular weights (Mn, Mw) and the polydispersity indices (PD) were measured [6] with a PSS/Agilent SECcurity GPC System with PSS SDV analytical linear M GPC columns: one precolumn (50 mm, particle size: 5 μm) and two columns (2 x 300 mm, particle size: 5 μm) were used. Detection was done with an Agilent G1315D DAD and an Agilent G 1362 RI detector to ascertain the polymer sizes and a polystyrene standard was used as calibration. The flow rate was 1 mL/min, injection volume was 100 μL with a concentration of 1 g/L.
For the anionic fluorene based polyelectrolytes a Thermo Separation Products apparatus was used [7]. The samples were dissolved in a mixture of 1-methyl-2-pyrrolidone (NMP) with 0.05 Mol/L LiBr + methyl benzoate, as interner standard and filtrated with a microfilter of 0.45 μ porosity before measurement. A GRAM (polyester without reactive reactive groups)-100/1000-7 μL (particles size) column from PSS- Polymer Standards Service was employed. Detection was done with a UV-1000 (270 nm wavelength) and a Shodex RI-71 detectors to ascertain the polymer sizes and a polystyrene standard was used as calibration. The flow rate was 0.8 mL/min, the elution time 40 min and the temperature kept at 70 °C.

[2] Measurements performed at the Max Planck Institute in Mainz, Germany.
[3] Measurements done at the Bergische Universität Wuppertal, Germany, by A. Helfer.
[4] Measurements performed at the Bergische Universität Wuppertal, Germany, by J. Dönecker.
[5] Measurements done at the Bergische Universität Wuppertal, Germany, by M. Dausend.
[6] Measurements done at the Bergische Universität Wuppertal, Germany, by A. Helfer.
[7] Measurements performed at the Max Planck Institute in Golm, Germany.

2.6 FT-IR spectroscopy

FT-IR measurements were accomplished using a Jasco FT/IR-4200 spectrophotometer with ATR unit.

2.7 Thermogravimetry

The thermogravimetry analysis [8] was performed in a Mettler TG 50.

2.8 Elemental analysis

For the samples elementar analysis a Perkin Elmer 240 B was used.

2.9 Microwave synthesis

The microwave assisted synthesis was done in a Biotage Initiator. The settings used are listed in the following order: maximum power, temperature and time.

2.10 Steady state photophysical measurements

Absorption spectra were recorded using a Shimadzu UV-2100 spectrophotometer with a minimum resolution of 0.2 nm. For the steady-state measurements, fluorescence spectra were recorded with a Horiba-Jobin-Ivon SPEX Fluorog 3-22 spectrometer and were corrected for the instrumental response of the system.
The measurements were recorded in solution and thin film. All the solvents were of spectroscopic grade and Milli-Q water was used. To ensure almost complete dissolution of the copolymers, solutions were stirred overnight.
Fluorescence quantum yields were measured using quinine sulfate in 0.5 M sulfuric acid (Φ_F = 0.546) and tetraphenylporphyrin (TPP) in toluene (Φ_F = 0.11) as references [44] [52]. Measurements of solid-state photoluminescence quantum yields were determined according to the method outlined by Monkman [53]. The quantum yields of the PBS-PFP with on-chain chromophores copolymers presented on this thesis were always determined based on the monomer ($\Phi_M{}^{Ap}$) and excimer/exciplex ($\Phi_E{}^{Ap}$) relationship, equation 2.1.

[8] Measurements performed at the Bergische Universität Wuppertal, Germany, by A. Helfer and S. Adamczyk.

$$\Phi_F^E = \frac{\Phi_E^{Ap}}{1 - (\Phi_M^{Ap}/\Phi_F^M)} \tag{2.1}$$

Where $\Phi_F{}^M$ corresponds to the model compound fluorescence quantum yield [54], [55]. Hence, $\Phi_M{}^{Ap}$ and $\Phi_E{}^{Ap}$ were calculated as the area of the deconvoluted bands of the monomer and excimer/exciplex, that in this specific case correspond to the polyfluorene and chromophore bands, respectively.

2.11 Time-resolved single photon counting

Fluorescence decays on the nanosecond time scale were measured using a home-built time-correlated single photon counting (TCSPC) apparatus as described elsewhere [56] [57], except that a Horiba-JI-IBH NanoLED, $\lambda_{exc} = 460$ nm, was used as the excitation source. Picosecond time-resolved uorescence measurements were performed using a home-built picosecond TCSPC apparatus, in which the excitation source consists of a picosecond Spectra Physics mode-lock Tsunami laser (Ti : sapphire) model 3950 (repetition rate of about 82 MHz, tuning range 700-1000 nm), pumped by a Millennia Pro-10s, frequency-doubled continuous wave (CW), diode-pumped, solid-state laser ($\lambda_{em} = 532$ nm). A harmonic generator model GWU-23PS (Spectra-Physics) is used to produce the second and third harmonic from the Ti : sapphire laser exciting beam. The samples were measured with excitation at 392 and 372 nm and the horizontally polarized output beam from the GWU (second harmonic) was first passed through a ThorLabs depolarizer (WDPOL-A) followed by a Glan-Thompson polarizer (Newport 10GT04) with vertical polarization. Emission at 90° geometry collected at magic angle polarization was detected through a double subtractive Oriel Cornerstone 260 monochromator by a Hamamatsu microchannel plate photomultiplier (R3809U-50). Signal acquisition and data processing was performed employing a Becker & Hickl SPC-630 TCSPC module. Fluorescence decays and the instrumental response function (IRF) were collected using 4096 or 1024 channels in a 0.814, 3.3 and 9.8 ps/channel scale, until 5×10^3, 3×10^3 or 1.5×10^3 counts at maximum were reached. The use of different channels acquisition, time scale and counts were related with the studied system. The full width at half-maximum (fwhw) of the IRF was about 22 ps and was highly reproducible with identical system parameters. A more detailed description of this equipment can be found in [58].

2.12 Femtosecond time resolved experiments

Fluorescence up-convertion

Fluorescence up-conversion experiments [9] were performed in an amplified femtosecond double TOPAS laser system. The power of the excitation beam was set to 150 μW. The fluorescence light emitted from the sample was efficiently collected using a lens objective. The fluorescence was then filtered using a long pass filter for suppressing the scattered light, directed and overlapped with a gate pulse (800 nm, ca. 10 μJ) derived from the regenerative amplifier onto an LBO crystal. By tuning the incident angle of these two beams relative to the crystal plane the sum frequency from the fluorescence light and the gate pulse was generated. The time resolved traces are then recorded by detecting this sum frequency light while changing the relative delay of the gate pulse versus the sample excitation time. Fluorescence gating was made under magic angle conditions in a time window of 50 ps. As detector, a photomultiplier tube (R1527p, Hamamatsu), placed at the exit of a 30 cm monochromator was used (heterodyne mode). An additional bandpass filter was placed in front of the monochromator to allow only the sum frequency light to enter. The electrical signal from the photomultiplier tube was gated by a boxcar averager (SR 250, Stanford Research Systems) and detected by a lock-in amplifier (SR830, Stanford Research Systems). The prompt response of this arrangement (including laser sources) was determined by detection of scattered light under otherwise identical conditions and found to be approximately 130 fs (FWHM). This value was used in the analysis of all measurements for deconvolution of the data sets. The sample was prepared at a concentration that yielded an absorbance of ca. 0.4 per mm at the excitation wavelength used and was contained in a quartz cuvette with an optical path length of 1 mm. To improve the signal to noise ratio, every measurement was averaged 15 times at 256 delay positions where a delay position is referred to as the time interval between the arrival of the pump and the gate pulses at the sample position. After each experiment the integrity of the samples was checked by recording the steady state absorption and emission spectra and comparing them with those obtained before the experiments. No spectral changes suggesting photodegradation were observed.

[9] Measurements performed at the Katholieke Universiteit Leuven, Belgium, by Dr. E. Fron.

2.13 Pump-probe measurements

Ultrafast spectroscopic measurements [10] were made using a conventional femtosecond non co-linear pump-probe setup. 180 fs, 4 μJ, pulses of 100 kHz repetition rate at 1.60 eV were generated using a Coherent Mira900-f Ti:Sapphire femtosecond oscillator in conjunction with a Coherent RegA 9000 laser amplifier. The output of this system was fed into a Coherent 9400-OPA, which was used to generate a single-wavelength output (390 nm) to pump, with a white-light supercontinuum (470-1000 nm) used to probe. The variable delay between pulses was controlled by means of a motorised stage, with the polarisation of both pulses orientated at 54.7^0 (magic angle) to each other using a variable quarter-waveplate. Spectral components in the probe were isolated using a monochromator (Bentham M300) incorporating visible and IR gratings, with the relative transmission change $\Delta T/T$ of the probe beam measured using a Si photodetector and lock-in amplifier referenced to the mechanically chopped pump beam.

2.14 Conductivity measurements

Solution electrical resistances were measured with a WayneKerr model 4265 automatic LCR meter at 1kHz. A dip-type conductance cell with a cell constant of 0.1178 cm, and an uncertainty of 0.02%, was used [59]. Cell constants were determined from measurements with KCl (reagent grade, recrystallized, and dried) using the procedure and data of Barthel et al. [60]. Measurements were taken at 298.15 K (± 0.02 K) Thermo Scientic Phoenix II B5 thermostat bath. Solutions were always used within 24h of preparation.

2.15 Electronic structure calculations

The molecular structure of the copolymer *poly{1,4-phenylene-[9,9-bis(4-phenoxy-butylsulfonate)] fluorene-2,7-diyl}* (PBS-PFP) based copolymer containing on-chain *N,N′-bis(4-bromo-phenyl)-1,6,7,12-tetra(phenoxy)-perylene-3,4,9,10-tetracarboxdiimide* (PDI) chromophoric units, PBS-PFP-PDI was optimized at the DFT [11] level without symmetry constraints using the GAMESS code [61]. The B3LYP (Becke three-parameter Lee-Yang-Parr) [62] [63] exchange correlation functional was employed and, due to the relative large size of the system, the 3-21G(d) basis sets were used for the expansion of the KohnSham orbitals of all the atoms. The gradient threshold for geometry optimization was taken as

[10] Experiment measured at Durham University, UK, by Dr. E. W. Snedden.

[11] Calculations done at the Universidade de Coimbra, Portugal, by Dr. L. L. G. Justino.

10^{-5} Hartree $Bohr^{-1}$. The reported DFT HOMO-1, HOMO, LUMO and LUMO+1 energies correspond to the Kohn-Sham eigenvalues.
The molecular structure of the PBS-PFP copolymer with red-emitting chomophore *4,7-di(thiophen-2yl)benzo[c][1,2,5]thiadiazole* (TBTT) units randomly distributed along the polymer chain PBS-PFP-TBTT, was also optimized by the procedure described above [61–63]. In order to reduce the computational time, the terminal $(CH_2)_4SO_3^{2-}$ in the alkyl chains, were replaced by CH_2CH_3 moieties. The gradient threshold for geometry optimization was taken as 10^{-4} hartree $bohr^{-1}$. The reported DFT $HOMO_{KS}$ and $LUMO_{KS}$ energies correspond to the Kohn-Sham eigenvalues. A second approach was used to obtain the energies of the frontier orbitals, which consisted on calculating the vertical ionisation energy and the vertical electron affinity from the ground state energies of the neutral and charged species. The HOMO energy can be approximated from the vertical ionisation energy and the LUMO energy from the vertical electron affinity.

2.16 Single molecule wide-field imaging and analysis

Wide field fluorescence microscopy experiments [12] of the copolymer PBS-PFP-PDI were performed on an inverted microscope (Olympus IX-71) equipped with a TIRF oil objective (60x, NA1.6, Olympus) and a cooled Electron Multiplying-CCD (ImagEM, Hamamatsu). The fluorene-phenylene moiety was excited with 0.1 - 0.5 kW/cm^2 from a 375 nm laser (SpectraPhysics) while the PDI subunits were excited with 1 - 5 kW/cm^2 from a 561 nm (Jive, Cobolt) diode pumped solid state laser. The laser lines were combined using a 505 dichroic (505DCLP Chroma Technology, Inc.) and further guided onto the sample through the same dichroic mirror (z561rdc Chroma Technology, Inc.). Emission from the PDI was collected through a 570 long pass and a 600/60 band (HQ570LP and HQ600/60, Chroma Technology, Inc.) while emission from fluorene-phenylene units was collected via a 430 long pass (HQ430LP, Chroma Technology, Inc.). The images were acquired with a final maximum field of view of ca. 41 × 41 μm^2 (80 × 80 nm^2 per pixel) with a frame rate depending of the excited fluorophore, more specifically, 5z when exciting PDI and 0.5 - 0.33 Hz when exciting fluorene-phenylene.

2.17 Simulation details

A trimer of PBS-PFP with on-chain red-emitting TBTT (PBS-PFP-TBTT) free in solution and in the presence of 4 and 12 C_{16}TAB molecules was studied in a box of water-dioxane

[12] Measurements performed at the Katholieke Universiteit Leuven, Belgium, by Dr. E. Fron and S. Rocha.

(70:30 %) by molecular dynamics [13] (MD) (composition of the systems is summarized in Table 6.8, Chapter 6). Polymer topology was generated by PRODRG server [64] while SPC water, dioxane and C_{16}TAB molecules were described using the original definitions of the GROMOS 96 43A1 force field [65]. A set of complementary systems in the absence of dioxane was also used as control. To keep the electroneutrality of the systems, Na^+ and Cl^- ions were added by randomly replacing solvent molecules. For simplicity, chloride ions were used instead of bromide because the latter are not implemented in the original force field, and qualitative aspects related with the structure and dynamics of such systems are not significantly influenced by, as suggested in previous works [66].
All MD simulations were carried out in the NpT ensemble and under periodic boundary conditions, resorting to the GROMACS package, version 4.0.7 [66] and the GROMOS 96 43a1 force field [65]. A standard time step of 2 fs was used for both the equilibration and production runs. Non-bonded interactions were computed on the basis of a neighbor list, updated every 10 steps. Long-range electrostatics were computed using the particle mesh Ewald (PME) method, as recommended for charged polymer simulations. For Lennard-Jones energies, a cut-off of 1.4 nm was applied. Temperature and pressure were coupled to the Berendsen external baths maintained at 25 °C and 1 bar, with coupling constants of 0.1 and 0.5 ps, respectively. To obtain a starting configuration, each system was firstly subjected to an energy minimization step. The system were then left to evolve up to 40 ns, using the LINCS algorithm [67] to keep bonds containing H atoms under positional restraint conditions. The first 10 ns were considered sufficient to attain equilibrated systems, while the last 30 ns of production runs were subsequently subjected to standard analysis, such as atom - atom (group - group) distance distributions and radial distribution functions (rdf). MD trajectories were visualized, and configuration images extracted using the VMD 1.8.6 software [68].

2.18 Surface morphological measurements

AFM measurements [14] were performed using a diInnova microscope from Bruker in the tapping mode at room temperature under ambient conditions. The silicon cantilevers used were between 215-235 μm in length and had a resonance frequency of approximate 84 kHz; the tip height was between 15-20 μm. The polymer films were prepared by spin coating of the copolymers solutions onto quartz. The solutions were previously filtered with 0.25 μm PTFE-filters.

[13] Simulations done at the Universidade de Coimbra, Portugal, by Dr. J. Almeida.
[14] Experiment measured at Bergische Universität Wuppertal, Germany, by S. Adamczyk.

2.19 Optical bandgap energies

The optical bandgaps of the copolymers were calculated by using the onset position of their absorption bands in the solid state via a tangent fitting to its UV-vis curve with subsequent convertion of the intersection with the wavelength axis from nm to eV Figure 2.19.1 following from the work of Benjamin Souharce [40].
In the case of copolymers bearing on-chain chromophore units the optical band-gaps were determined as the intersection of the absorption and emission spectra (film spectra) [69]. The HOMO levels were measured with an AC-2 from Riken Keiki Co. at the Evonik Science to Business Center in Marl Germany, based on UV photoelectron spectroscopy (UPS) [70]. The Riken setup allows the measurements to be made under ambient conditions with easy sample preparation and manipulation. All the measured copolymer films were drop casted from glass. Materials that are oxygen and moisture sensitive are not suited for the setup and their work function parameter can be red-shifted as a consequence of sample oxidation [40].

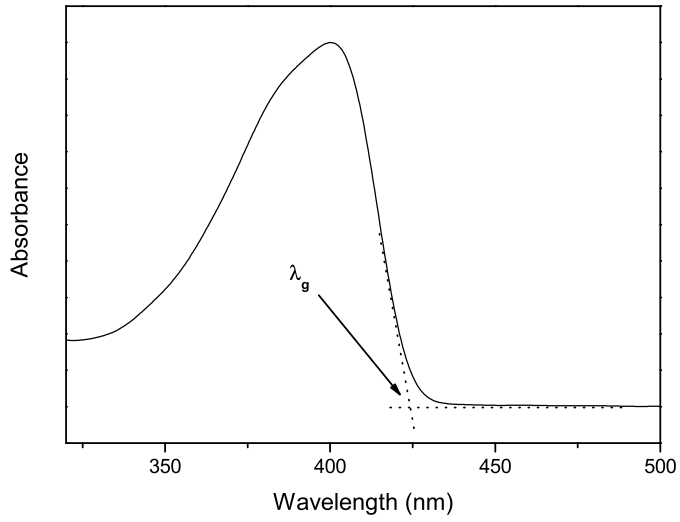

Figure 2.19.1: Band-gap determination via UV-vis spectra. Adapted from [40].

Chapter 3

Poly[9,9-bis(6-hydroxyhexyl)fluorene] a polyfluorene with non-ionic side chains

Conjugated polymers (CPs) with polar or charged side-chains show good solubility in polar solvents that, coupled with their excellent electron injecting ability, make them ideal materials for electron transport layers (ETL) in solution processed multilayer polymer light emitting diodes (PLEDs) [25], [71]. Recently, it has been proposed that this unique electron injection property arises from charged or polar groups of the polymer side chains, which can generate a positive interfacial dipole between the cathode and the organic layer [71]. Such polar, soluble conjugated polymers combine properties of conjugated polyelectrolytes and non-ionic surfactants and can be processed from enviromentally friendly solvents. Also, their neutral character eliminates the presence of mobile ions which may interfere with the devices operation. Moreover, the polar groups of the polymer side chains facilitate electron injection from high work junction metal cathodes, enhance the device lifetime and hence, make these materials useful for ETL in fluorescence PLEDs [71]. In addition, some of the spacial deposition and patterning problems in organic electronics, can be overcome [69, 72, 73].

A series of polymers comprising a nonpolar main chain and surfactant-like side chains have been developed as ETL for high efficiency PLEDs, with the aim of combining the advantages of neutral surfactants or soluble polymers (such as PEG) and conjugated polymers as ETL in PLEDs. It is common knowledge that PEG-based neutral surfactants show promising properties as cathode interfacial modication layers in OLEDs, such as avoiding the effects of counterions and prolonging the PLEDs lifetime. However, the thickness of the PEG layer in the optoeletronic devices as well as the type of metal used in the cathode have to be considered carefully, since PEG type ETL can only support aluminium (Al)

and cannot be used with other high work function metals, due to chemical instability. In this context, diethanolamino-functionalized, water soluble conjugated polymers (WSCPs) that consist of a polyfluorene main chain bearing a surfactant side chain, were designed [5]. This type of material keeps the properties of the neutral surfactants, while the main chain provide the electronic conductivity. Furthermore, the amino groups on the side chain significantly improve the electron injection of the high work function metal [5].

In the field of organic solar cells (OSCs) based on conjugated polymers, fabrication techniques for large-area devices have also become an important issue [14]. The introduction of an interfacial layer comprising a water soluble polymer between the active layer and the metal electrode show a dramatic enhancement in the open circuit voltage. Moreover, water soluble polymers can also prevent the organic soluble layer from damage, by use of orthogonal solvents in addition to reducing the work function of the cathode (due to their ionic groups) through favourable interfacial dipoles [74].

Polymers that comprise a conjugated main chain and a surfactant-like side chain also offer the opportunity to control the polymer conformation and orientation. This allows the development of appropriate architectures for nanostructured devices based on organic-inorganic hybrids [75]. These materials have an enhanced stability and are of particular interest in photovoltaic device applications as well as in solid state sensing. In both cases, the presence of polar or ionic lateral chains in CPs improve their solubility in polar media suitable for sol-gel processing. Furthermore, water-soluble polymers show a tendency to form solvent-driven molecular aggregates and ordered nanostructures, which can have a pronounced effect on the photophysical properties [76]. Additionally, zwitterionic polymer derivatives can have cellular imaging properties, which are of central importance in deciphering physiological processes and cellular structures. These polymers may therefore be used in scientific areas spanning from genomics to proteomics and pathophysiology [77].

With the goal of tailoring the optical and electronic properties and the solid state morphology of conjugated materials with a surfactant-like side chain, a hydroxyalkyl-substituted polyfluorene was synthesized via the deprotection of a polymeric precursor containing tetrahydropyran (THP) as protecting group. As discussed by Bolognesi *et al.* [73], there is an increasing interest in copolymers and homopolymers containing THP groups. This is due to the fact that these materials are relatively easy to deprotect in the corresponding alcohol, which allows a series of promising applications. One of these could be the preparation of insoluble patterns of a polyconjugated material by photolithography [73].

3.1 Synthesis

The homopolymer P-THP (**2**) was synthesized from its corresponding dibrominated monomer using Yamamoto type coupling [39]. The deprotection of the THP groups lead to the formation of P-OH (3). The overall reaction pathway is illustrated in Figure 3.3.1.

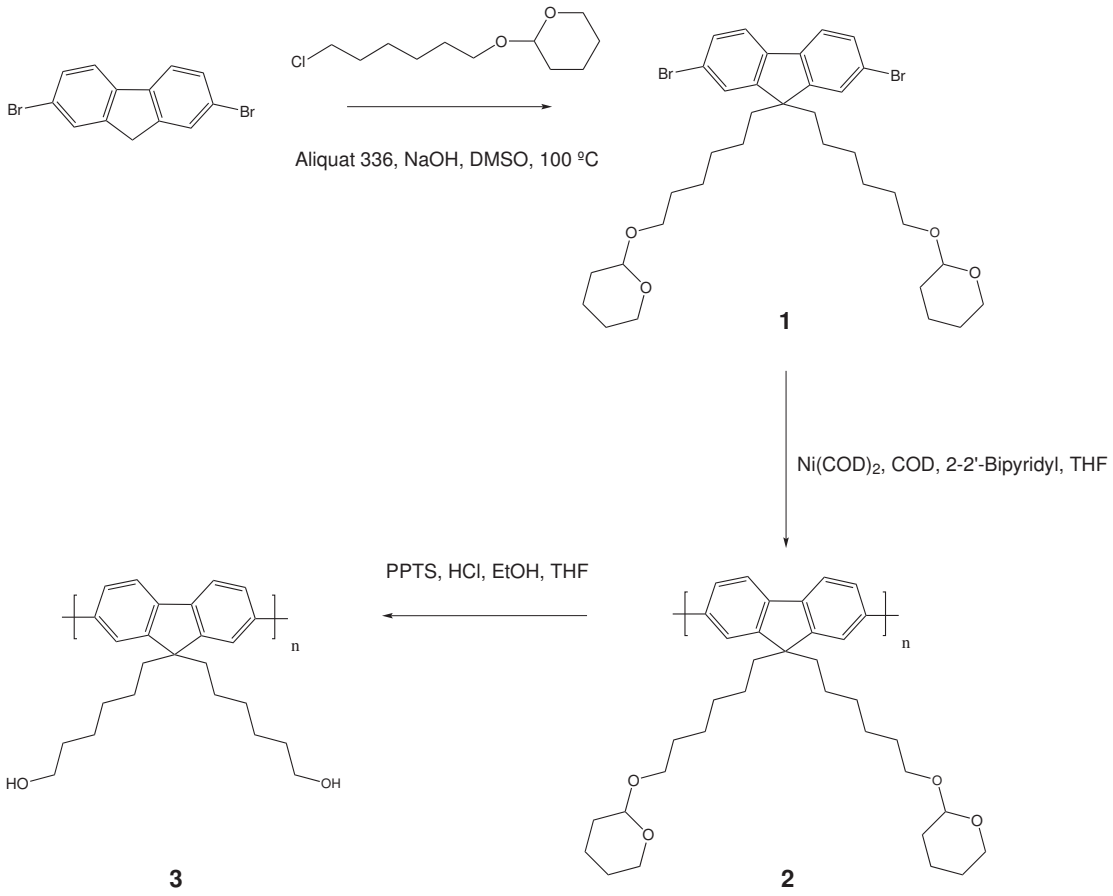

Figure 3.1.1: Overall reaction pathway to the hydroxyl functionalized polymer P-OH, **3**.

2,7-Dibromo-9,9-bis[6-(2-tetrahydropyranyloxy)-hexyl]fluorene **1**
1.02 g (3.14 mmol) of 2,7-dibromofluorene and 500 mg of the phase transfer catalyst Aliquat 336 were dissolved in 100 mL of DMSO under vigorous stirring. To remove dissolved oxygen, argon was bubbled through the solution for 30 minutes. 20 mL of a NaOH 0.5 % (w/w) solution were added and the solution changed colour to dark red. 2.07 mL of 2-(6-chlorohexyloxy)tetrahydro-2*H*-pyran were added dropwise and the mixture was heated to 100 °C under reflux overnight. The solution was poured into ice water and extracted several times with diethyl ether. The organic phase was washed with water, dried over Na_2SO_4 and the solvent was evaporated. The product was purified by column chromatography filled with deactivated aluminium oxide and hexane/ethyl acetate (5:1) as eluent, yielding 1.68

g (2.43 mmol, 77%) of **1**.
^{1}H NMR (400 MHz, $CDCl_3$): δ (ppm) = 7.51 (d, 2H, ^{3}J = 8.05 Hz, fluorene), 7.46 - 4.42 (m, 4H, fluorene), 4.51 (m, 2H, CH), 4.50 (m, 2H, CH_2), 3.81 (2H, ddd, ^{2}J = 11.09 Hz, ^{3}J = 7.70 Hz, super4J = 3.06 Hz, CH_2), 3.62 (2H, td, ^{3}J = 9.61, ^{3}J = 6.84 Hz, CH_2), 3.46 (2H, m, CH_2), 3.27 (2H, td, ^{3}J = 9.56, ^{3}J = 6.64), 1,90 (2H, m, CH_2), 1.79 (2H, m, CH_2) 1.67 (2H, m, CH_2), 1.51 (8H, m, CH_2), 1.41 (4H, m, CH_2), 1.12 (8H, m, CH_2), 0.59 (4H, m, CH_2).
^{13}C NMR (100 MHz, $CDCl_3$): δ (ppm) = 152.4, 139.1, 130.2, 126.1, 121.3, 67.5, 62.3, 55.6, 40.2, 30.7 - 19.7.
LC-MS (APLI): m/z = 692 (M^+).

Poly(9,9-bis[6-(2-tetrahydropyranyloxy)-hexyl]fluorene) P-THP, **2**
The polymer was prepared following the microwave-assisted Yamamoto type polymerization (300 W, 120 °C, 15 minutes) with 480 mg (1.73 mmol) $Ni(COD)_2$, 270 mg (1.73 mmol) 2,2 bipyridyl, 171 mg (1.58 mmol) 1,5-cyclooctadiene (COD) and 500 mg (0.72 mmol) **1** in 20 mL of dry THF. The solution was washed with 2M aqueous HCl, with a saturated aqueous $NaHCO_3$ solution, followed by a saturated aqueous EDTA solution and brine (NaCl). The solvent was removed and the residue dissolved in a small amount of chloroform. The polymer was precipitated in methanol with one drop of HCl (conc.) and extracted with methanol, acetone and ethyl acetate. The ethyl acetate fraction was further used. After drying in vacuum, 300 mg (78%) of **2** were obtained of as light yellow powder.
^{1}H NMR (600 MHz, $CDCl_3$): δ (ppm) = 7.71 - 7.87 (6H, m, fluorene, H), 4.53 (2H, m, CH), 3.30 - 3.83 (8H, m, CH_2OH), 0.87 - 2.16 (32H, alkyl H).
GPC (THF, UV detection 254 nm): Mn = 15 400, Mw = 26 400 g·mol^{-1}, PD = 1.7.

Poly[9,9-bis(6-hydroxyhexyl)fluorene] P-OH, **3**
300 mg of **2** and 28 mg of pyridinium-*p*-toluenesulfonate (PPTS) were dissolved in 50 mL of THF. 150 mL of ethanol, as well as 30 drops of conc. HCl were added and the mixture was heated at 80 °C under stirring overnight. The polymer was precipitated in water with one drop of conc. HCl and washed with water. After drying in vacuum, 200 mg (97%) were obtained as a pale yellow powder. The polymer was characterized by TGA, with the decomposition temperature starting around 360 °C.
^{1}H NMR (600 MHz, $C_2D_2Cl_4$): δ (ppm) = 7.80 (m, fluorene), 7.65(m, fluorene), 4.07 (m, CH), 3.30 - 3.55 (m, CH_2OH), 1.39 (m, alkyl, CH_2), 1.24 (m, alkyl, CH_2), 0.85 (m, alkyl, CH_2).

^{13}C NMR (150 MHz, $C_2D_2Cl_4$): δ (ppm) = 125.6 (CH, aromatic), 63.0 (CH_2OH), 21.2 - 34.4 (CH_2, alkyl). From the NMR analysis the compound has residual trapped THP units.

3.2 Optical properties

The optical and spectroscopic properties of the polymer P-OH were measured in methanol (MeOH), DMSO, NMP solution and as thin films spin-coated from NMP solution at room temperature (Figure 3.2.1). The details are given in Table 3.1 and the behaviour resemble the optical and electronic properties of other PFs [78].

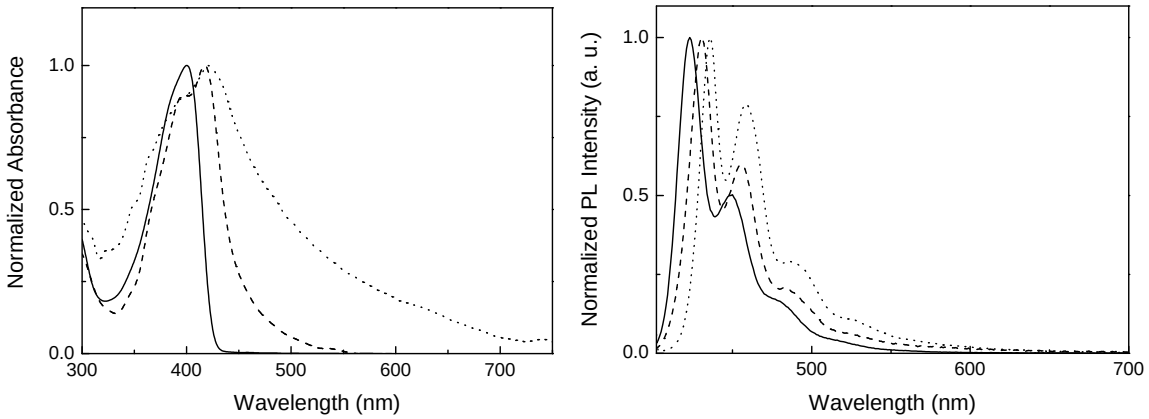

Figure 3.2.1: a) Absorption and b) emission spectra of polymer P-OH in solution. Solid line NMP, dashed line DMSO and dotted line methanol solution.

It is worth noting that in solution the polymer absorption maximum of the UV-vis spectra reveal a dependence upon the nature of the solvent, see Table 3.2. The polymer is present as isolated chains in the NMP solution, while aggregate formation is clearly visible in methanol and DMSO, via observation of a broad absorption tail and a second absorption band, at 418 nm, for P-OH in DMSO. The low energy absorption band peaking at ca. 418 nm for DMSO somewhat resembles the formation of the PFO β-phase. The very broad absorption tail for methanol indicates the formation of larger aggregates and the occurence of light scattering effects. Accordingly, the emission maxima for methanol and DMSO are red-shifted and the photoluminescence quantum efficiency (PLQY) decreases in DMSO and MeOH, compared to the NMP solution; in agreement with the proposed aggregation processes and their influence on the spectroscopic properties (Table 3.1).

Table 3.1: Optical properties of polymer P-OH in solution and thin film.

Solvent	Absorption λ_{max} (nm)	Emission λ_{em} (nm)	ϕ_F
NMP	398	422	0.83 [a]
DMSO	395, 418	430	0.42 [a]
Methanol	422	435	0.37 [a]
Film	400	432	0.11

[a] PLQY were determined using quinine sulphate in 0.5 M H_2SO_4.

A thin film of P-OH was spin-coated from an NMP polymer solution and its PLQY was determined using a calibrated integrating sphere [79] and, subsequently calculated according to the approach described by Monkman *et al.* [53] - Equations (3.1) and (3.2). Equation (3.3) was used to determine the PLQY values for the polymer solutions at room temperature.

$$\Phi_F = \frac{E_j(\lambda) - (1 - A)E_0(\lambda)}{L_e(\lambda)A} \tag{3.1}$$

$$A = \frac{L_0(\lambda) - L_j(\lambda)}{L_0(\lambda)} \tag{3.2}$$

$$\frac{\Phi_F}{\Phi_{FR}} = \frac{n^2}{n_{FR}^2} \cdot \frac{\int_0^\infty F(\lambda_F)d\lambda_F}{\int_0^\infty F_R(\lambda_F)d\lambda_F} \tag{3.3}$$

R stands for a reference compound, whose PLQY value is known and whose absorption and emission spectra has its maximum in the same range of the studied compound. The parameter n is the refractive index of the respective used solvent. $E_i(\lambda)$ and $E_0(\lambda)$ are, respectively, the integrated luminescence that result from the direct excitation of the film and the secondary excitation. A is the film absorbance, which is found by measuring the emission signal across the excitation wavelength for the two following situations: the integrated excitation when the film is directly excited, $L_i(\lambda)$ and the integrated excitation when the excitation light first hits the sphere wall, $L_0(\lambda)$. $L_e(\lambda)$ denotes the empty sphere integrated profile [53].

The results are analogous to those obtained from the concentration dependence of the cationic polyfluorene-based CPE poly{9,9-bis[6-(N,N,N-trimethylammonium)hexyl]fluorene-*co*-1,4-phenylene} dibromide (HTMA) for solutions in deuterated methanol [80]. In the

study by Wågberg study, HTMA exhibits a PL spectrum with a distinct peak at its emission maximum, followed by two well resolved vibronic side peaks at low polymer concentration. A less distinct vibronic structure, accompanied by a red-shift of the main PL peak, is observed for the HTMA emission, with a gradual tendency towards an unresolved vibronic structure, when the copolymer concentration is increased [80].

Similar behavior was found for P-OH solutions, where the photophysical properties are affected by the solvent nature (Figure 3.2.1 and Table 3.1). Although studies were not performed at different concentrations, it is clearly seen that the resulting degree of aggregation is fully controlled by the solvent quality, Table 3.2 [81]. The slight broadening of the absorption spectra in the solid state may be a result of small local variations of the π-overlap due to some conformational disorder of the polymer chains [43], [82].

Table 3.2: Physical properties of the solvents used [83].

Solvent	Dipolar moment	Dielectric constant [a]	n_D^{25}
NMP	4.09 D	32.20	1.469
DMSO	3.96 D [a]	45.00	1.479
Methanol	1.69 D	32.63	1.329

[a] [84]

The solid state emission spectrum of the PF films shows similar characteristics in shape and position to that in dilute NMP solution (Table 3.1 and Figure 3.2.2). In addition, the emission spectrum is accompanied by a bathochromic shift, see Table 3.1, with the well resolved vibronic progression being related to the stretching mode of C=C−C=C substructures of the polymer backbone (Figure 3.2.2) [82].

Fluorescence lifetimes (τ_F) of P-OH were obtained by the TCSPC technique in solution with picosecond time resolution and, as previously observed in other PFs, lie in the range of 40-500 ps with multiple decay components [43]. As depicted in Figure 3.2.3 and Table 3.3, the collected data is well fitted with double or triplet-exponential decay laws according to Equation (3.4) [43], [58].

$$I_\tau(t) = a_{i1}e^{\frac{-t}{\tau_1}} + a_{i2}e^{\frac{-t}{\tau_2}} + a_{i3}e^{\frac{-t}{\tau_3}} \tag{3.4}$$

The parameters a_{ij} with $j = 1, 2, 3$ represent pre-exponential factors and τ_i the decay time for the emission τ collected at the polymer maximum.

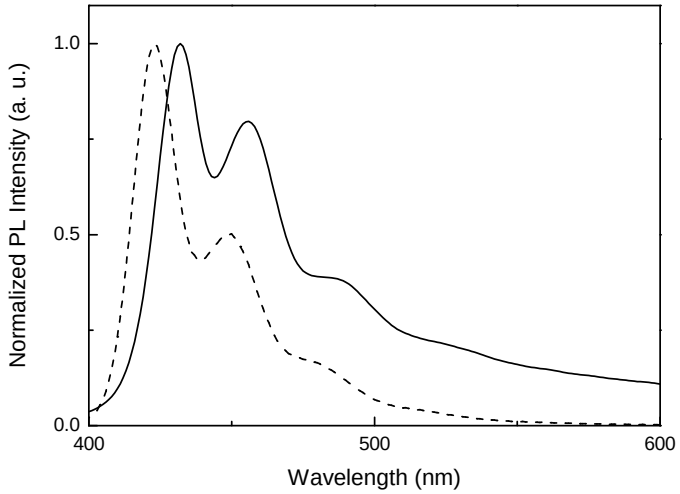

Figure 3.2.2: Normalized fluorescence spectra in thin film (solid line) and in NMP solution (dashed line).

Table 3.3: Fluorescence decay times (τ_i) and pre-exponential factors (a_{ij}) for the copolymer P-OH, obtained with excitation at 378 nm, emission at the wavelength maxima and T = 293 K.

	λ_{em} (nm)	τ_1 (ns)	τ_2 (ns)	τ_3 (ns)	a_{i1}	a_{i2}	a_{i3}	χ^2
NMP	422	0.04	—	0.40	0.119	—	0.881	0.99
DMSO	430	0.07	0.20	0.46	0.275	0.587	0.138	1.00
MeOH	435	—	0.15	0.41	—	0.934	0.066	1.01

PFs display complex fluorescence decays in thin film and in solution with minor amplitude fast rise and decay components together with a predominant decay time of hundreds of ps [43]. Decay times around 40 and 370 ps were reported by Dias *et al.* [45] for PF2/6 in methylcyclohexane (MCH) solution. Although there is still a controversy on the assignment of the fast component, it is thought that conformational relaxation and energy migration are involved [47]. In the case of fluorene based polylectrolytes (CPEs), Monkman *et al.* have suggested that in an aqueous environment, the CEPs exist as isolated polymer chains and as aggregated forms, or as clusters of variable sizes. Consequently, an additional time constant of ca. 200 ps is detected, in addition to the previously mentioned fast and longer components, [85]. Measurements of P-OH in DMSO and methanol solutions reveal the presence of an "intermediate" decay component, with 150 - 200 ps lifetime (Table 3.3) in the

same time domain as that observed by Monkman *et al.* [85]. Its contribution dominates the overall decay, particularly when the polymer is "dissolved" in methanol, the least effective solvent. Following the work of Monkman *et al.*, the observed intermediate component if the P-OH decay is attributed to polymer aggregates/clusters.

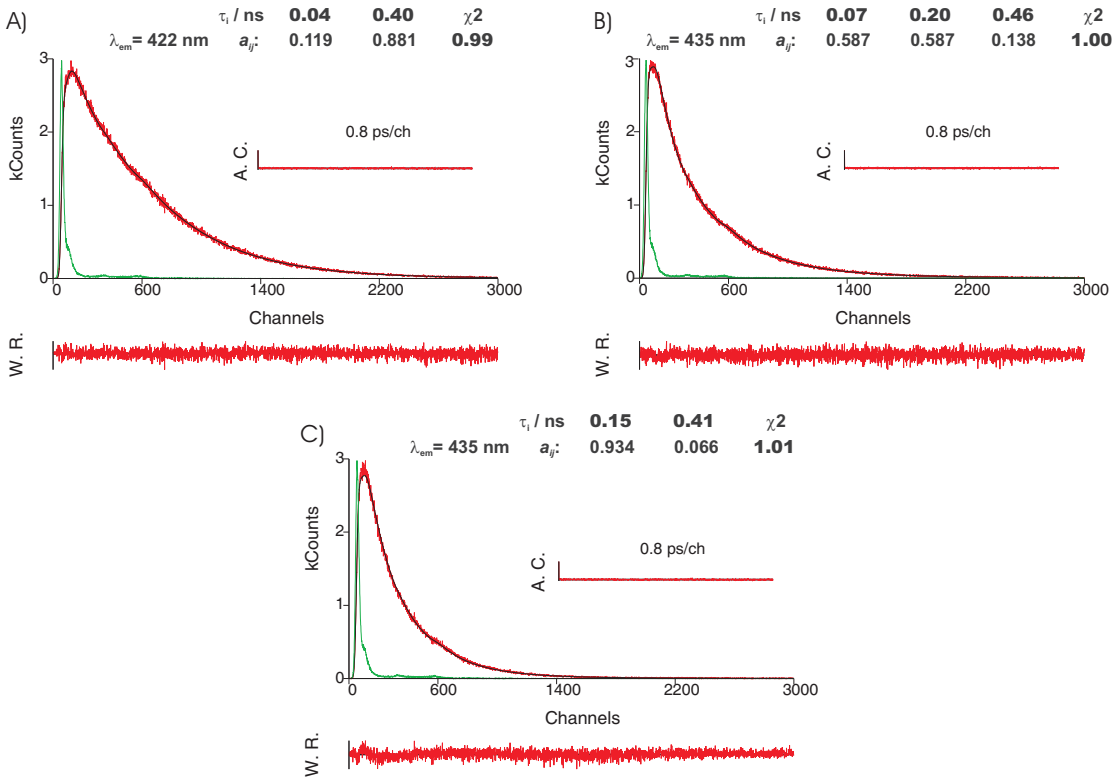

Figure 3.2.3: Fluorescence emission decay for P-OH collected at the polymer emission maximum obtained with λ_{exc} 378 nm at 298.15 K in A) NMP, B) DMSO and C) methanol. The green lines in the decays are the instrumental response function (IRF). For a better judgment of the quality of the fits weighted residuals (W.R., scale -3 $\leq \sigma \leq$ +3) autocorrelation functions (A.C.) and chi-square values (χ^2) are also presented.

This is in correspondence with the absorption/emission spectra and PLQY data and thereby, confirms that the polymer forms aggregates in DMSO and MeOH. In contrast, analysis of the polymer decay in NMP, collected at the emission maximum, show an excellent fit to the sum of two exponential functions, with 40 and 400 ps time constants (Table 3.3). The intermediate 150 - 200 ps component is no longer detected and P-OH is probably present, in the NMP solution, in the form of isolated polymer chains. Consequently, the enhancement of the PLQY, as well as the blue-shift in the absorption and emission maxima (Table 3.1), in this solvent is a direct result of the decreased aggregation. The emission originates from excited states of isolated polymer chains, with an increased PL lifetime [86].

3.3 Optical bandgap and thin film morphology

3.3.1 Energy levels and optical bandgap of polymer P-OH

The UV-vis absorption data can be combined with UPS measurements to obtain the energy level of the lowest unoccupied molecular orbital (LUMO), being the highest occupied molecular orbital (HOMO) value estimated by UPS [87]. Subsequently, the LUMO is determined by subtracting the optical band-gap as estimated from the onset of the absorption curve (λ_g) (Table 3.4) [69]. The bandgap energy (E_g) itself is calculated with Equation (3.5), where λ_g represents the onset wavelength of absorption. The correction factor ΔE = 300 meV corresponds to the exciton binding energy involved in the absorption process [40].

$$E_g(eV) = \frac{1243.125}{\lambda_g(nm)} + 0.3 \tag{3.5}$$

Table 3.4: HOMO, LUMO and bandgap levels determined by UPS for the polymer P-OH.

	HOMO	Band-gap [a]	LUMO
	eV	eV	eV
P-OH	5.58	3.17	2.41

[a] Estimated as the onset of the absorption film spectra.

As with other PF homopolymers, optical and UPS measurements on P-OH reveal HOMO and LUMO levels of ca. -5.58 and -2.41 eV, respectively. The values are comparable to those of other hydroxy-substituted polyfluorenes [69,71,88]. Furthermore, previously published work with similar polymers demonstrate that these systems work well when used as ETL [5]. It is expected that the increase of the electron injecting ability of these neutral polar-substituted conjugated surfactants, originates from their polar side chains; since they form a positive interfacial dipole between the EL polymer and the high work function metal cathode, producing a negative dipole potential for electrons [31].

The 0.09 eV HOMO level decrease of P-OH compared with the HOMO (-5.67 eV) level of PF6, should be attributed to the effect of hydroxy groups on the polymer side. Because post-polymerization treatment does not change the P-OH main chain structure, by introducing the electron withdraw units on the polyuorenes main chain, the HOMO level decreases [71]. This phenomenon was also observed in fluorene-based polyelectrolytes [89], [90]. Moreover, conjugated polymers electronic properties are strongly dependent on the morphology of

their thin films, which by its turn is affected by the polymers side-chain [91].

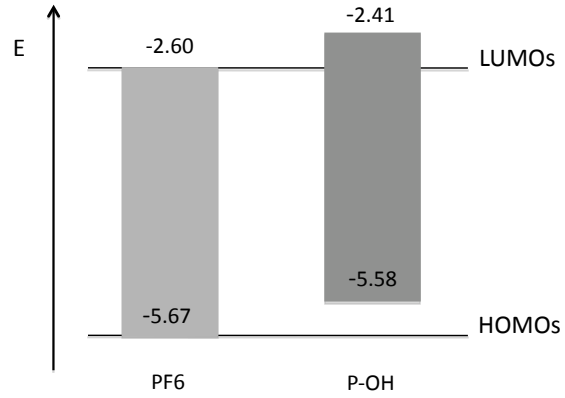

Figure 3.3.1: Energy levels (in eV) of the polymer P-OH compared to poly[-2,7-(9,9-dihexylfluorene)] (PF6) of a similar molecular weight [92].

3.3.2 Properties of polymer P-OH thin films

In the bulk state, 9,9-dialkyl-substituted PFs of sufficiently high molecular weight show a rich variety of self-organized structures, including nematic, hexagonal and lamellar phases that are highly dependent on the temperature, molecular weight, side chain structure and processing [93–95]. The self-organization is believed to be governed by a proper balance between favorable side chain - side chain interactions and by the elastic stretching of the side chains [93], [95]. In solution, PFs adopt a wormlike conformation with persistence lengths ranging from 7 to 10 nm, while in semidilute solutions, or poorer solvents, they undergo segmental aggregation [95–97]. An example is poly[-2,7-(9,9-dioctylfluorene)] (PF8) that forms a dynamic network structure in where domains of aggregates and alligned segments coexist in dilute solutions. Instead, in poor solvents PF8 forms disk or sheet-like aggregates regardless of the dilution regime [98–100].

For conjugated fluorene-based polyelectrolytes and block copolymers, the controlling of their self-assembly properties both in solution and in the solid state promises the potential for a targeted nanostructure design [101]. Polyfluorenes with surfactant-like side chains also fall into this category and therefore topography images obtained by AFM were used to investigate film morphology and aggregation behaviour of the P-OH polymer. Figure 3.3.2 depicts representative results obtained for two spin-coated films deposited in quartz from DMSO and NMP solutions. Film morphology was observed to change significantly between the two solvents and the formation of wormlike aggregates that are composed of individual nanospheres was observed for spin-coated film from NMP, whose diameter range

from ca. 16 nm to 46 nm, [102], [103]. From DMSO the formation of spherical aggregates with an average diameter of ca. 35 and 41 nm was observed. These observations point to distinct differences of the film morphology for layers made from DMSO and NMP solutions.

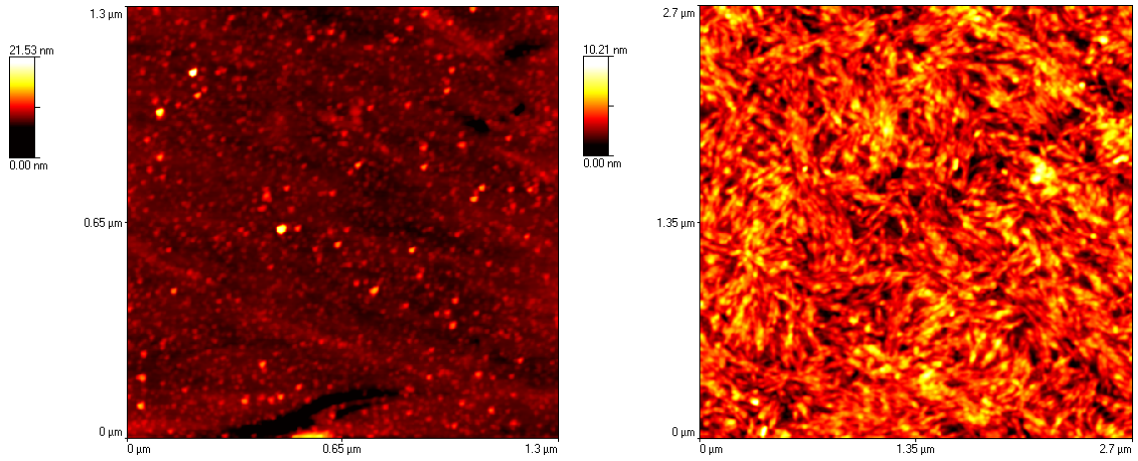

(a) (b)

Figure 3.3.2: Topographic mode AFM images in air of polymer P-OH spin coated from a) DMSO or b) NMP solutions.

Changes in the optical properties of conjugated rod-rod block copolymers in solvent mixtures of selective and nonselective solvents have been reported by Scherf *et al.* [104], where the formation of supramolecular aggregates in solvent mixtures is driven by the different polarity and solubility properties of the blocks [104]. The P-OH morphology findings can, as for the block copolymers case, be correlated to the optical absorption and emission spectra, reflecting different (pre)aggregation properties of P-OH. In both solvents P-OH tend to form nanospheres with diameters of 16 - 46 nm. However, in the film from NMP solution the nanospheres are further aggregated into wormlike particles. The data reveal the sensitivity of the polymer towards the surrounding enviroment (solvent polarity) thus, directly influencing its aggregation behavior (Table 3.2).

3.4 Conclusions

A new polyelectrolyte with non-ionic side chains was synthesized by Yamamoto coupling, via a polymer-analogous deprotection reaction of a THP side chain based-polyfluorene. After the post polymerization treatment, the majority of polymers comprised a conjugated main chain and surfactant-like side chains. The conjugated main chain provide P-OH good

conductivity, while the surfactant-like side chains should enhance its solubility in polar solvents. Solvent-induced behavior of P-OH was investigated in methanol, DMSO and NMP solutions at 25 °C. The physical differences in the solution structure are distinctive and dependent on the solvent polarity, as shown by the polymer different optical properties in solution and thin films. Indeed, aggregated species with different arrangements of the hydrophilic and hydrophobic polymeric parts, nanospheres and wormlike aggregated particles, were visualized in the AFM data.

The presence of the hydroxyl functional group grants the attractive possibility of covalent linking of phosphorescent emitters to the polymer side chains, as described by PLEDs using phosphorescent blue emitter, bis(4,6-difluorophenylpyridinato)-tetrakis(1-pyrazolyl)-borate (FIr6) and green emitter tris(2-phenylpyridine)iridium ($Ir(ppy)_3$) as dopants [71]. Moreover, high efficiency blue, green and white emitting phosphorescent OLEDs can be realized based on these neutral water/alcohol soluble conjugated polymer ETL materials [31, 105–107]. Given the morphological control of the polymer films, it is expected that P-OH with enhance the devices lifetime, by avoiding the influence of counter ions previously reported for CPEs [88], [106].

Chapter 4

Energy transfer between PBS-PFP and phenylenevinylene oligoelectrolytes

Fluorene-based conjugated polyelectrolytes (CPEs) are rigid-rod macromolecules with π-conjugated backbones and pendant ionic side groups that induce good solubility in polar solvents [77]. Hence, CPEs combine a mixture of the optoelectronic properties of conjugated polymers with the electrostatic characteristics of polyelectrolytes [108], [90]. To date, CPEs have been used as fluorescence quenching probes to detect specific analytes via electron and energy transfer mechanisms, or via analyte-induced polymer aggregation. In addition, they can act as energy donors to amplify the signal output of dye-labeled biomolecules via Förster resonance energy transfer (FRET) [109–113]. Moreover, CPEs have attracted significant attention as active materials in polymer optoelectronics such as electron injection and/or transport layers, light emitting diodes (LED), organic photovoltaics (OPV) and light emitting field-effect transistors (LEFET) [114–119]. Reports of hybrid nanodots and materials based on cationic and anionic CPEs have also been published, providing further possibilities of challenging CPE applications [76], [120].

The balance between the electrostatic properties and the interchain interactions in CPEs may lead to a rich and unique self-assembly behaviour. This behaviour is also shown by polyfluorene-thiophene diblock copolymers that form different types of aggregate structures in water, where they show poorly structured morphology, and methanol, in where large vesicular structures are present [10, 103, 121]. Furthermore, CPEs self-assemble with amphiphilic molecules, such as surfactants, forming polymer-surfactant complexes with different conformations and morphologies compared to the free polymer. Thus, their optical and chemical properties can be tuned by combining them with the appropriate surfac-

tants in a process designated by "surfactochromicity" [122–124]. Interaction with opposite charged surfactants can lead to formations of complex multilayered structures [125]. In contrast, non-ionic surfactants tend to break up interchain polymer clusters and form mixed cylindrical micelles, in which the CPE is incorporated in the core of the micelle as isolated chains [126], [127].

Förster resonance electronic energy transfer (FRET) opens the possibility of developing applications of self-assembled structures using CPEs as energy donors with appropriate energy acceptors for artificial light harvesting. As illustrated by the interaction between fluorene-phenylene based CPEs and oppositely charged energy acceptor species, such as Ru(II) complexes [128]. The emission spectrum of the fluorene based anionic poly{1,4-phenylene-*alt*[9,9-bis(4-phenoxybutylsulfonate)]fluorene-2,7-diyl} (PBS-PFP) has a good overlap with the lowest singlet-singlet transition in the absorption spectrum of tris(2,2'-bipyridyl)ruthenium(II) ($Ru(bpy)_3^{2+}$). As a result, all electronic energy from excited singlet or triplet states of the donor or acceptor can be channelled to the triplet state of the metal complex due to fast (sub-picosecond range) intersystem crossing to the emitting metal-to-ligand charge transfer (MLCT) [128]. Recently, Reynolds *et al.* [129] achieved efficient FRET in multilayer film architectures built via the inexpensive layer-by-layer (LbL) technique using two emissive conjugated polyelectrolytes. The efficiency of FRET was monitored by fluorescence spectroscopy. Therefore, it is plausible to conduct a similar energy transfer study from the anionic PBS-PFP to a series of cationic distyrylbenzene oligoelectrolytes (COEs) in solution.

4.1 Synthesis

The oligoelectrolyes DSBNI trimer, DSSNI tetramer and COE5NI pentamer were synthesized in the group of Professor Bazan from UCSB, USA, as previously described, see Figure 4.1.1 [130–132].

The copolymer PBS-PFP was synthesized from their corresponding dibrominated and diboronic acid monomers by Suzuki coupling [37], [133]. The overall reaction pathway is illustrated in Figure 4.1.2 [125], [134].

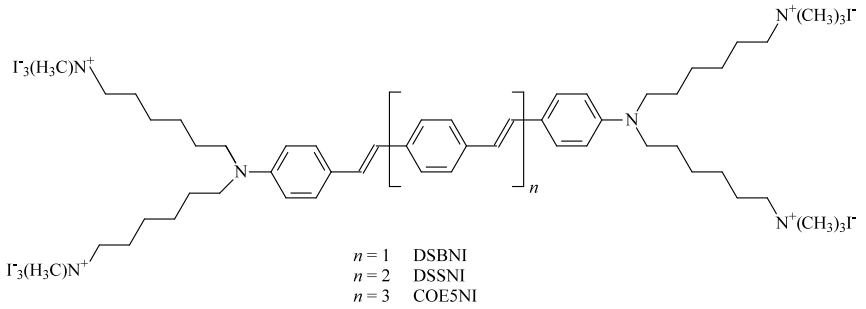

Figure 4.1.1: Molecular structures of DSBNI, DSSNI and COE5NI polyelectrolytes.

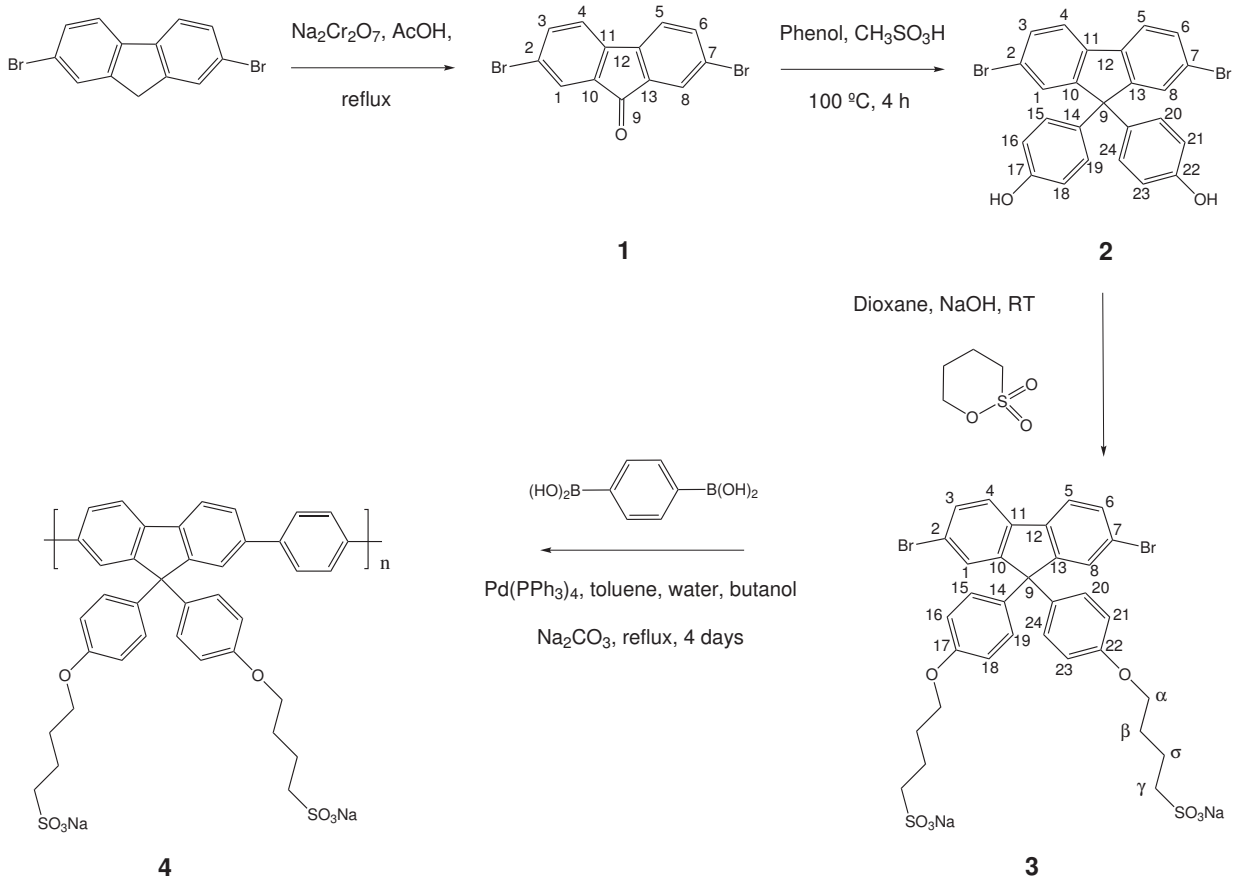

Figure 4.1.2: Overall reaction pathway to the anionic copolymer PBS-PFP (4).

2,7-Dibromofluorene-9-one **1**

10 g (30.8 mmol) of 2.7-dibromofluorene and 15.7 (60 mmol) of sodium dichromoate were refluxed in 120 mL of acetic acid under argon to 120 °C for 6 h. The reaction was cooled to room temperature, water was added and the mixture additionally stirred 10 to 15 min. The solid formed was filtered and washed repeatedly with water, until a yellow solid was obtained. The product was recrystallized from 300 mL of ethanol to yield 9.7 g (29 mmol,

94 %) of **1**.
^{1}H NMR (400 MHz, $CDCl_3$): δ (ppm) = 7.76 (d, 2H, H1, H8, ^{4}J = 1.70 Hz), 7.62 (dd, 2H, H3, H6, ^{3}J = 7.93 Hz, ^{4}J = 1.87 Hz), 7.38 (d, 2H, H4, H5, ^{3}J = 7.86 Hz).
^{13}C NMR (100 MHz, $CDCl_3$): δ (ppm) = 191, 142, 138, 135, 128, 123 and 122.
GC-MS: m/z = 309 M^+.

2,7-Dibromo-9,9-bis(hydroxyphenyl)fluorene **2**
1 (9,5 g, 28 mmol) phenol (21.2 g, 225 mmol) and methanesulfonic acid (1.9 mL, 1.9 mmol) were heated at 100 °C under argon for 4 h. The solvents were evaporated and the mixture was purified with column chromatography using a mixture of hexane/ethyl acetate (7 : 3) (v/v) as eluent. 7.8 g of a white solid were obtained (15 mmol, 55 %) of **2**.
^{1}H NMR (400 MHz, d−DMSO): δ (ppm) = 9.37 (s, 2H, H17, H22), 7.9 (d, 2H, H1, H8, ^{3}J = 8.15 Hz), 7.58 (dd, 2H, H3, H6, ^{3}J = 8.15 Hz, ^{4}J = 1.90 Hz), 7.49 (d, 2H, H4, H5, ^{4}J = 1.72 Hz), 6.90 (d, 4H, H15, H19, H20, H24, ^{3}J = 8.72 Hz) and 6.67 (d, 4H, H16, H18, H21, H23, ^{3}J = 8.72 Hz).
^{13}C NMR (100 MHz, d−DMSO): δ (ppm) = 156, 154, 138, 134, 131, 128, 123, 121, 115 and 65.
LC-MS: m/z = 307 M^+.

2,7-Dibromo-9,9-bis(4-sulfonylbutoxyphenyl)fluorene **3**
2 (5.5 g, 10.8 mmol) was dissolved under argon in a NaOH (1.7 g, 41.9 mmol) aqueous solution (154 mL). A solution of 1,4-butane sultone (2.3 g, 17 mmol) in 88 mL of dioxane was added at once to the mixture and the reaction proceed overnight at room temperature. Then the solution was heated for 30 min at 80 °C - 100 °C and cooled in a water/ice bath. The obtained suspension was filtered and the yellowish product was recrystallized first from ethanol and afterwards from dioxane to yield 3 g of white solid (3.6 mmol, 34 %) of **3**.
^{1}H NMR (400 MHz, d−DMSO): δ (ppm) = 7.91 (d, 2H, H1, H8, ^{4}J = 1.7 Hz), 7.59 (dd, 2H, H3, H6, ^{3}J = 8.14 Hz, ^{4}J = 1.79 Hz), 7.52 (d, 2H, H4, H5, ^{4}J = 1.72 Hz), 6.99 (d, 4H, H15, H19, H20, H24, ^{3}J = 8.86 Hz), 6.84 (d, 4H, H16, H18, H21, H23, ^{3}J = 8.92 Hz), 3.90 (t, 4H, CH_2, α, ^{3}J = 6.01 Hz), 2.5 (m, 4H, CH_2, γ) and 1.7 (m, 8H, CH_2, β and σ).
^{13}C NMR (100 MHz, d−DMSO): δ (ppm) = 1578, 153, 138, 136, 131, 129, 123, 121, 114, 67, 64, 51, 28 and 22.
MS: m/z = 518.7 (M^+ - $S_2O_6Na_2Br_2$).

Poly{1,4-phenylene-[9,9-bis(4-phenoxy-butylsulfonate)]fluorene-2,7-diyl} (PBS-PFP) **4**
3 (0.8 g, 1 mmol), 1,4-benzenediboronic acid (0.17 g, 1 mmol), $Pd(PPh_3)_4$ (50 mg, 0.04

mmol) and Na_2CO_3 (1 g, 9.4 mmol) were dissolved in a degassed mixture of 20 mL water and 40 mL THF and refluxed at 110 °C under argon for 4 days. Water was added and the aqueous mixture was washed several times with chloroform and concentrated to dryness. The residue was redissolved in a mixture of THF/water (1:1) (v:v) and purified by dialysis using the same solvent mixture and a membrane with a $\bar{M}n$ cutoff of 6000 - 8000 Da to yield 0.63 g (68 %) of poly{1,4-phenylene-[9,9-bis(4-phenoxy-butylsulfonate)]fluorene-2,7-diyl} as a light brown powder.
^{1}H NMR (600 MHz, d-THF 50% D_2O): δ (ppm) = 7.9 - 6.8 (Ar-H), 4.0 (CH_2, γ), 3.5 (CH_2, α), 2.8 (CH_2, β) and 1.3 (CH_2, σ).
GPC (NMP, LiBr, UV detection 360 nm): Mn = 1300, Mw = 2100 g·mol^{-1} and PD = 1.61. The molecular weights of the copolymer is likely to be considerably underestimated due to the strong interactions between the polyelectrolyte and the column material.
From TGA measurements the copolymer decomposes at 360 °C.

4.2 Optical properties of phenylenevinylene oligoelectrolytes and PBS-PFP

As described by Garner *et al.* [131] the absorption maxima for the cationic phenylenevinylene oligoelectrolytes studied (n = 1, 2, 3) occur in the range of 408 - 420nm. The red shift in absorbance maxima observed across the oligoelectrolyte series (shortest and longest oligomers posses the highest and lowest energy absorption maxima, respectively) is consistent with the effect on electronic structure as conjugation length is extended, Figure 4.2.1 and Table 4.1.

Table 4.1: Summary of the oligomers' UV-vis and PL spectra, PLQY in aqueous solutions.

Oligoelectrolyte	Absorption λ_{max} (nm)	Emission λ_{em} (nm)	ϕ_F [a]
DSBNI	408	565	0.41
DSSNI	412	595	0.06
COE5NI	420	620	0.05

[a] PLQY were determined using fluorescein at pH 12.

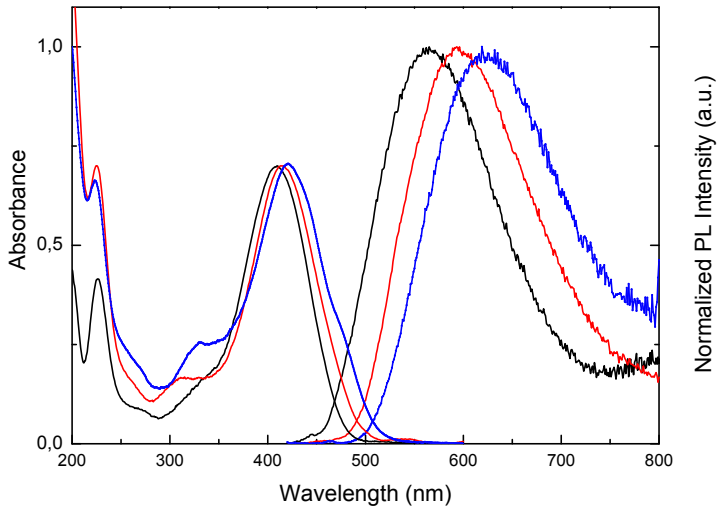

Figure 4.2.1: Absorption and fluorescence spectra of aqueous solutions of the phenylenevinylene oligoelectrolytes. Trimer DSBNI (black line), tetramer DSSNI (red line) and pentamer COE5NI (blue line).

The absorption and emission spectra of the oligomers are also dependent on the polarity of the solvent and a large hypsochromic shift in the PL maxima was observed when going from a polar to a non polar environment [131]. Consequently, in aqueous media the absorption and emission spectra are devoid of vibronic structure and the photoluminescence quantum yields (PLQY) are low, Table 4.1. Indeed this effect is more pronounced in the DSSNI and COE5NI oligomers compared to the shorter DSBNI, probably because its larger hydrophobic component may lead to aggregation and self-quenching [131].

Rigid rod poly(*p*-phenylene) based polyelectrolytes and related fluorene copolymers, such as the "hairy-rod" PBS-PFP, have a strong tendency to cluster in aqueous solutions, resulting in lower solubility and fluorescence quantum yields [80,123,135–139]. It is possible to break up the clusters/aggregates formed between the CPEs chains, either by adding a co-solvent or an appropriate surfactant [125–127,140–142]. In previous studies PBS-PFP was found to have varying solubility in water/dioxane mixtures with the greatest solubility observed within the range of 30 - 70 % 1,4-dioxane, where a balance between the hydrophobic and hydrophilic interactions is reached [123]. In a second series of experiments, PBS-PFP was dissolved in a 10^{-4} M aqueous solution of the non-ionic surfactant $C_{12}E_5$, above the surfactant critical micellar concentration (cmc, 6.5×10^{-5} M at 25 °C [143]). Aqueous solutions of the PBS-PFP copolymer show a broad absorption and fluorescence (Figure 4.2.2). Upon addition of $C_{12}E_5$, blue shifts in the absorption (ca. 7 nm) and emission maxima (ca.

10 nm) are observed, accompanied by increases in the emission intensity (not shown, in Figure 4.2.2 the spectra are normalized) and PLQY, Table 4.2.

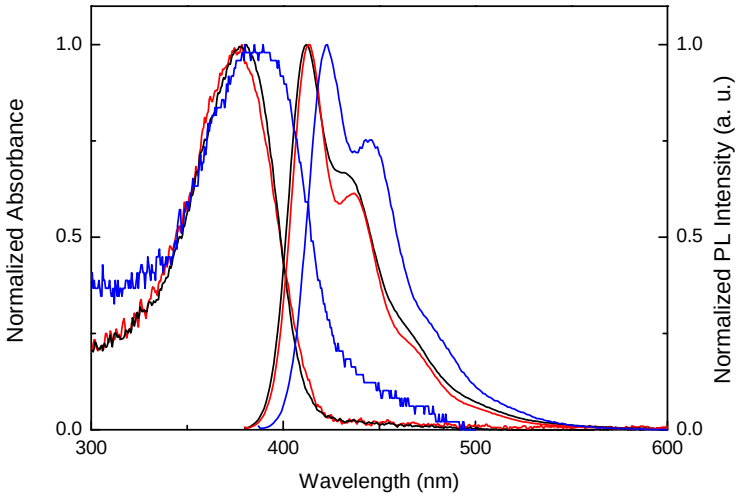

Figure 4.2.2: Absorption and fluorescence spectra of PBS-PFP. Water/dioxane (1:1, v/v) mixture (black solid line), 10^{-4} M aqueous $C_{12}E_5$ (red line) and water (blue line) solutions.

Table 4.2: Summary of the PBS-PFP UV-vis and PL spectra, PLQY in water/dioxane (1:1) and aqueous surfactant solution.

Solvent	Absorption λ_{max} (nm)	Emission λ_{em} (nm)	ϕ_F [a]
water/dioxane	376	412	0.52
aqueous 1×10^{-4} M $C_{12}E_5$	380	413	0.55
water	387	423	0.14

[a] PLQY were determined using quinine sulphate in 0.5 M H_2SO_4.

The emission spectrum of PBS-PFP in the presence of the surfactant contains increased fine vibronic structure compared to the emission in the water/dioxane solvent system. These observations are, in large part, attributed to surfactant induced breakup of polymer clusters, due to the incorporation of the copolymer into $C_{12}E_5$ aggregates [124, 126, 127]. The absorption and emission spectra, the corresponding values of absorption and emission maxima and PLQY of the PBS-PFP copolymer in the water/dioxane and non-ionic surfactant solutions are shown in Figure 4.2.2 and Table 4.2. The blue shift in the emission maxima as well as the relatively high PLQY when compared with the situation in pure water, suggest the existence of isolated copolymer chains in both solvent systems.

4.3 Singlet excitation energy transfer for light harvesting in the self-assembled PBS-PFP / phenylene-vinylene oligoelectrolytes system

With the aim of developing new self-assembled structures in which singlet-singlet excited state energy transfer is favoured, PBS-PFP was used as energy donor and the phenylene-vinylene oligoelectrolytes as acceptors (Figures 4.3.1, 4.3.2, 4.3.3 and 4.3.4). The excellent spectral overlap between the CPE fluorescence and the oligomers absorption indicates that the occurrence of energy transfer process is favoured [42].

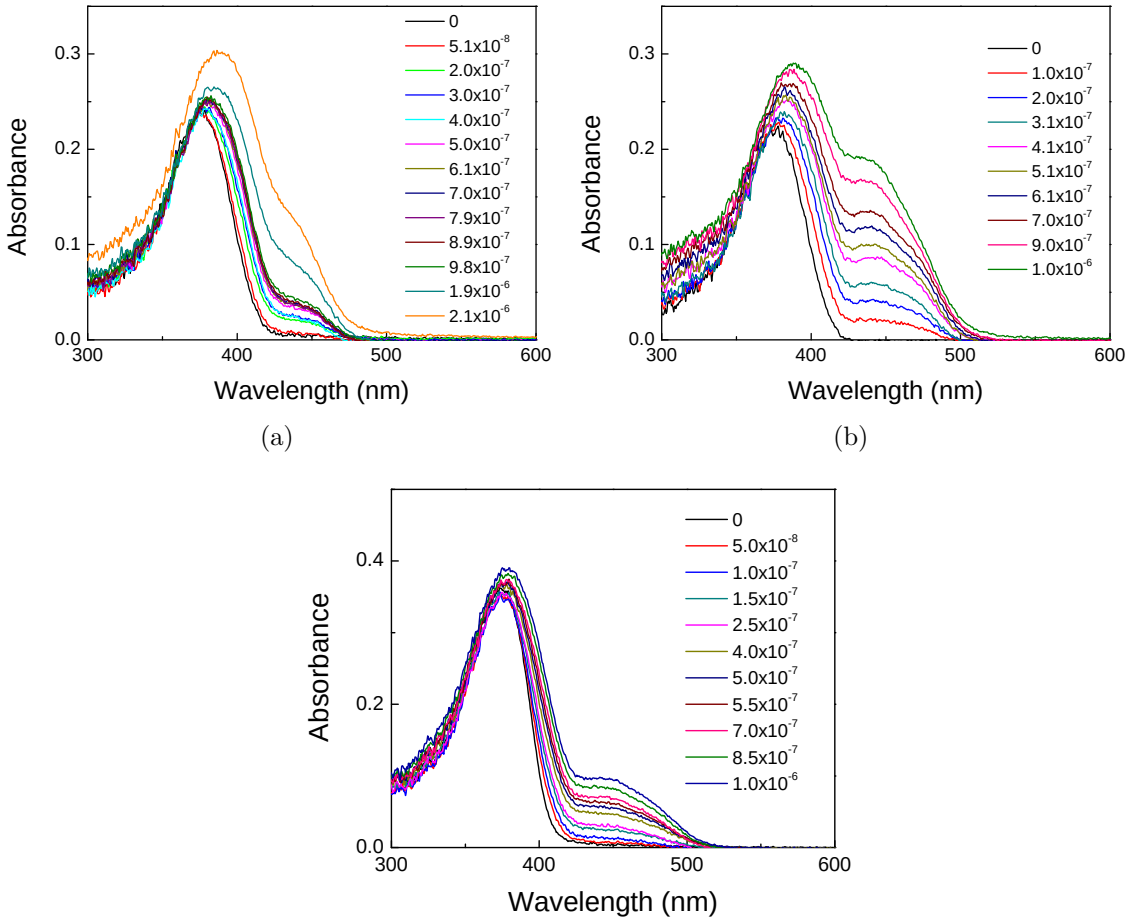

Figure 4.3.1: Absorption spectra of PBS-PFP (4.4×10^{-6} M) in water/dioxane (1:1, v/v) mixture with increasing concentrations of a) DSBNI, b) DSSNI and c) COE5NI.

The interaction between oppositely charged systems in solution was monitored using UV-vis, fluorescence spectroscopy and TC-SPC experiments. AFM was also employed to obtain further information on the aggregate morphologies. PBS-PFP concentration was kept constant (4.4×10^{-6} M, based on the copolymer monomer unit) in both solvent systems and all measurements were performed at 25 °C.

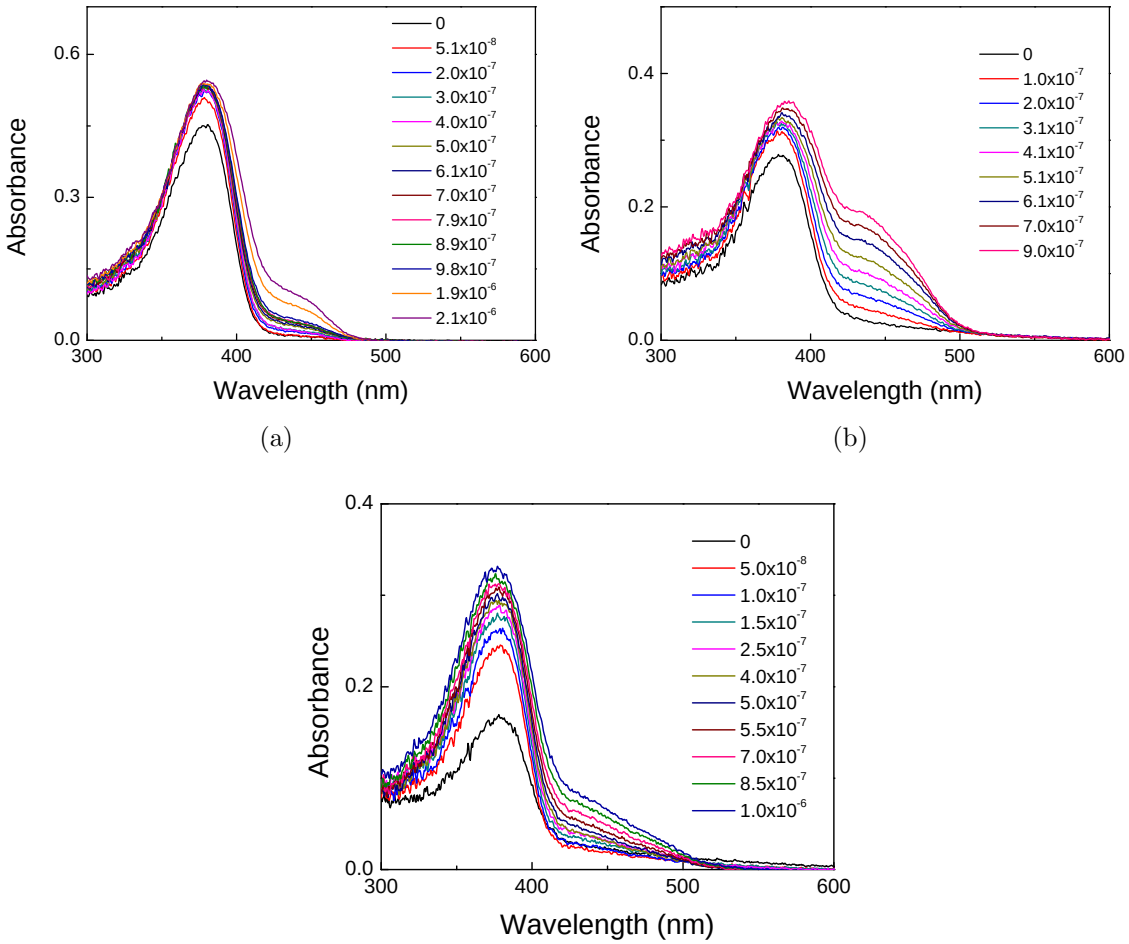

Figure 4.3.2: Absorption spectra of PBS-PFP (4.4×10^{-6} M) in 10^{-4} M aqueous $C_{12}E_5$ solution with increasing concentrations of a) DSBNI, b) DSSNI and c) COE5NI.

Figure 4.3.1 shows the absorbance spectra of PBS-PFP as the COEs are added to a polyelectrolyte water/dioxane (1:1, v/v) mixture and Figure 4.3.2 to a polyelectrolyte+surfactant solution. The absorption increases with COE concentration (the absorbance of the COEs has some overlap with that of PBS-PFP) and is accompanied by a red shift in the maxima observed in the PBS-PFP absorbance region and by the appearance of a new band in the oligoelectrolyte maximum absorption region. These are indicative of self-assembly occur-

ring between the oppositely charged materials. In water/dioxane mixture the absorption increases with higher oligolectrolyte concentrations in solution and is accompanied by a red shift of the maxima and the appearance of a new shoulder located in the oligoelectrolyte absorption maxima region. An analogous trend is observed in the surfactant containing system, although the effect is more pronounced in the water/dioxane mixture, than in the $C_{12}E_5$ solution. The increase in the absorbance region of the PBS-PFP in both solvents is explained by the increase in the oligoelectrolytes concentration and consequently intensity, since the oligoelectrolytes absorb in the same region as PBS-PFP, as previously mentioned. However, differences were observed between the two mixtures: in the surfactant solution the increase is the absorption is not as pronounced as it is in water/dioxane mixtures (Figures 4.3.1 and 4.3.2, respectively).

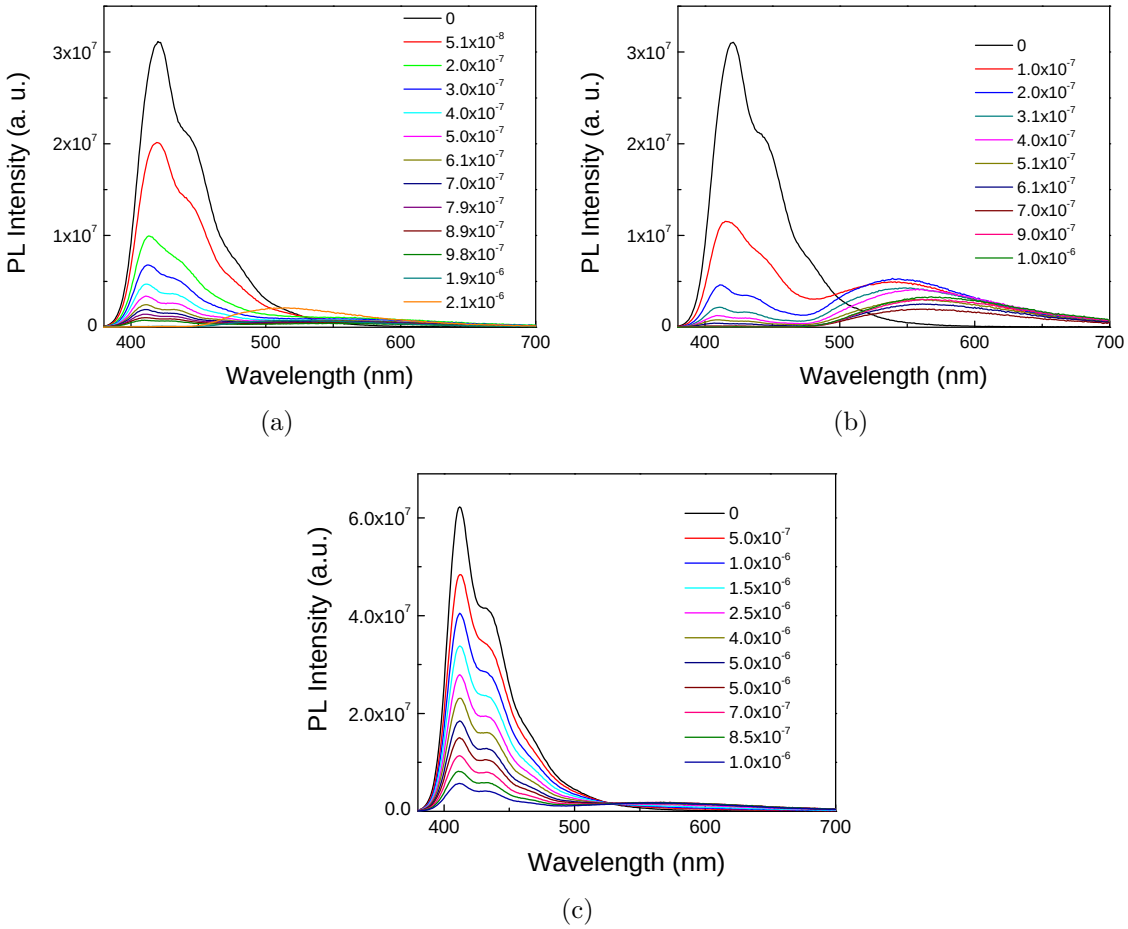

Figure 4.3.3: Emission spectra of PBS-PFP (4.4×10^{-6} M) in water/dioxane (1:1, v/v) mixture with increasing concentrations of a) DSBNI, b) DSSNI and c) COE5NI.

In addition, the changes in the absorption properties of PBS-PFP with the COEs reflect differences in the interactions between the CP and the cationic phenylenevinylene oligoelectrolytes, that are directly related with the size of the COEs chain.

In addition to monitoring the self-assembly and photophysical characteristics of the polymer/COE pairs via absorption spectroscopy the fluorescence emission properties of the donor/ac-ceptor pair interaction was also studied. Analysis of the observed PBS-PFP photoluminescence quenching phenomena (Figures 4.3.3 and 4.3.4) provide information on the surroundings of the conjugated polyelectrolytes, either quantitatively (if a kinetic model of the competitive processes can be developed) or at least qualitatively [44].

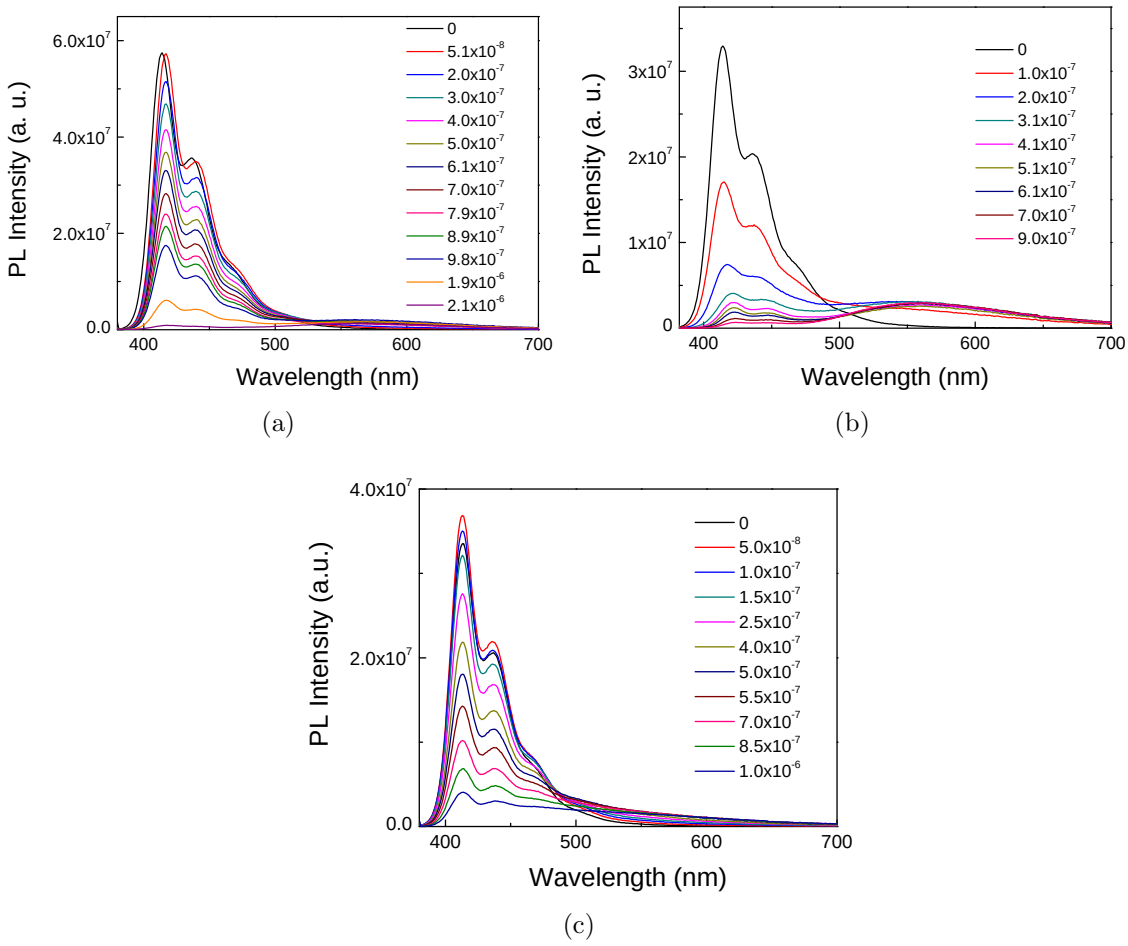

Figure 4.3.4: Emission spectra of PBS-PFP (4.4×10^{-6} M) in 10^{-4} M aqueous $C_{12}E_5$ solution with increasing concentrations of a) DSBNI, b) DSSNI and c) COE5NI.

In the presence of the oligoelectrolytes, quenching of the PBS-PFP emission is observed. In addition, a new emission band around 560-620 nm is detected and corresponds to that of the COEs (Figures 4.3.3 and 4.3.4). The FRET process in the presence of surfactant

is not as efficient as in the water/dioxane mixture. This is explained by the fact that the surfactant wraps around the copolymer chains, shielding it from the solvent environment. Overall, energy transfer occurs from the PBS-PFP copolymer to the oligoelectrolytes and the phenomenon is clearly dependent upon the solvent and oligoelectrolyte chain length as illustrated in Figure 4.3.5.

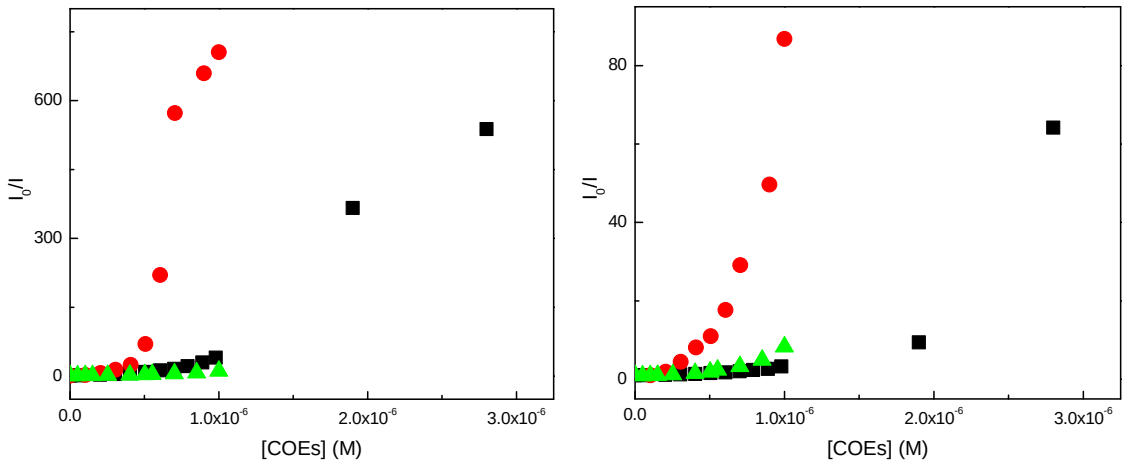

(a) (b)

Figure 4.3.5: Stern-Volmer plot for the fluorescence quenching of PBS-PFP by the phenylenevinylene oligoelectrolytes. a) water/dioxane (1:1, v/v) mixture and b) 10^{-4} M aqueous $C_{12}E_5$ solution. DSBNI (black squares), DSSNI (red circles) and COE5NI (green triangles).

This behaviour can be analyzed in terms of the Stern-Volmer plots. A first glance at Figure 4.3.5 reveals that the self-assembled systems do not follow the Stern-Volmer linear relationship expected for collisional quenching (Equation 4.1). Here I_0 and I stand for the steady-state fluorescence intensities in the absence and in the presence of quencher concentration [Q] (the oligoelectrolyte acceptors) respectively, k_q the quenching rate constant, τ_0 the donor (PBS-PFP) excited state lifetime in the absence of the quencher and K_{SV} is the Stern-Volmer constant [42] [44].

$$\frac{I_0}{I} = 1 + k_q \tau_0 [Q] = 1 + K_{SV}[Q] \tag{4.1}$$

The nonlinear region is in agreement with static interaction between PBS-PFP and the oppositely charged oligoelectrolytes. The data could be fitted into a linear behaviour for COEs concentrations below 10^{-7} M that rapidly turned nonlinear was fitted into the Stern-Volmer representation (Figure 4.3.6). The quenching parameters/data for the linear are

presented for the water/dioxane (1:1, v/v) mixture only (Table 4.3), given the complexity of the PBS-PFP/COE/surfactant system. The k_q values are also presented in Table 4.3, this parameter was determined using the average lifetime (τ_0), of 560 ps for PBS-PFP in a water/dioxane (1:1, v/v) mixture. As has previously been observed in a system involving a cationic poly poly{9,9-bis[6-(N,N,N-trimethylammonium)hexyl]fluorene-2,7-diyl-*co*-1,4-phenylene} dibromide (HTMA) self-assembled with anionic porphyrins [144–146], the calculated k_q values are orders of magnitude greater. This difference within the quenching rates supports the idea of self-assembly.

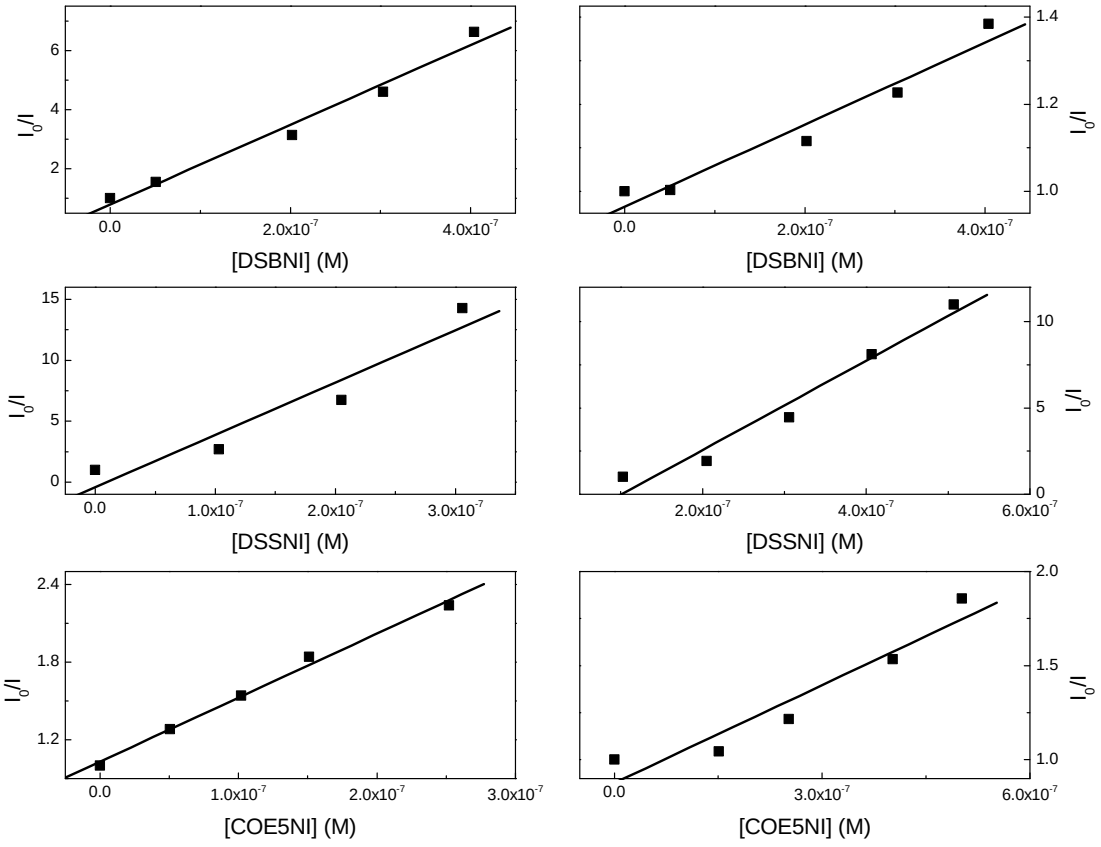

Figure 4.3.6: Stern-Volmer plots for the PBS-PFP quenching phenomena at low phenylene-vinylene oligoelectrolytes concentration. Water 50% dioxane (v/v) mixture (left) and 10^{-4} M aqueous $C_{12}E_5$ solution (right).

Given the negative charge of PBS-PFP, it is expected that the quenching procedure will be sensitive to the charge of the oligoelectrolytes, the ionic strength of the solution, the surfactant environment and the rate of quencher diffusion near the copolymer [42]. To obtain further insight into the COE quencher effects on PBS-PFP, the following Stern-Volmer linearity deviations were considered: the quenching sphere of action and the formation of

a non-fluorescent complex [42] [44].

Table 4.3: Experimental quenching constants using the linear Stern-Volmer relationship of PBS-PFP in water/dioxane (1:1, v/v) mixture.

	K_D (M^{-1})	R^2	$k_q = K_D/\tau_0$ [a] ($M^{-1}\cdot s^{-1}$)
DSBNI	1.34×10^7	0.980	2.39×10^{16}
DSSNI	4.29×10^7	0.915	7.66×10^{16}
COE5NI	4.85×10^6	0.993	8.66×10^{15}

[a] $\tau_0 = 560$ ps

4.3.1 Deviations from the Stern-Volmer Equation: combined dynamic and static quenching

Treatment using the Stern-Volmer Equation and corrections for formation of a non-fluorescent complex the ratio I_0/I is multiplied by the fraction of uncomplexed fluorescent molecules that leads to Equation 4.2.

$$\frac{I_0}{I} = 1 + (K_D + K_S)[Q] + K_D K_S [Q]^2 \tag{4.2}$$

This modified form that takes into account both the dynamic (K_D) and the static (K_S) mechanisms is second order in terms of the quencher concentration [Q], which balances the upward curvature that is observed when both quenching mechanisms occur for the same fluorophore [42], [44]. The dynamic contribution can be determined from fluorescence lifetime measurements (Equation 4.3).

$$\frac{\tau_0}{\tau} = 1 + K_D[Q] \tag{4.3}$$

However, there are cases of weak association between fluorophores and quenchers that do not actually form a stable ground state complex. Instead, it seems that the static component is a result of the quencher being located near the fluorophore at the moment of excitation. These closely spaced (centered) fluorophore-quencher pairs are immediately quenched and appear to be dark complexes [42]. These observations are interpreted in terms of another

type of static quenching called the sphere of action. If a quencher is located outside the sphere of action, it has no effect on the fluorophore. Hence, the solution fluorescence intensity decreases upon increasing the Q concentration, while the fluorescence decay excitation is unaffected [42] [44]. The modified Stern-Volmer relation that translates this set of circumstances is described by Equation 4.4, where V is the volume of the sphere and N the Avogadro number.

$$\frac{I_0}{I} = (1 + K_D[Q])e^{[Q]VN/1000} \tag{4.4}$$

The upward-curving Stern-Volmer plots for the PBS-PFP quenching for the different phenylenevinylene oligoelectrolytes was analysed by the two combined static and dynamic quenching methods described, Equations 4.3 and 4.4. As illustrated in Figures 4.3.7 and 4.3.8, the data fit in the sphere of action model, up to a certain oligoelectrolyte concentration, especially when the copolymer is dissolved in the water/dioxane (1:1, v/v) mixture.

Indeed, the extent of quenching is affected by the environment that surrounds the fluorophore. This fact is well illustrated when PBS-PFP is dissolved in aqueous $C_{12}E_5$, and may be due to the complex morphology of the self-assembled system copolymer+surfactant+oligomer. Protection against quenching has been observed for probes bound to macromolecules and cyclodextrins, as indicated in ref. [42]. The macromolecules provide protection from the solvent, but not from diffusing quenchers. Furthermore, the charge of the quenchers has a dramatic effect on the extent of quenching. In general, these effects can be expected to be present with charged quenchers and absent for neutral ones [42].

Based on the fitting results obtained for the quenching of PBS-PFP by the oligoelectrolytes, the experimental quenching data will be only presented for the sphere of action quenching model in PBS-PFP water/dioxane (1:1, v/v) mixture.

The quenching constants determined, see Table 4.4, are several orders of magnitude greater than purely diffusion controlled systems in water, $k_q \approx 10^{10}$ - 10^{13} M^{-1} s^{-1} [42, 144, 147]. Pinto *et al.* observed similar values for apparent quenching constants in their self-assembled systems of a cationic PF with several anionic porphyrins ($K_D = 10^7$ - 10^9 M^{-1} and $k_q = 10^{16}$ - 10^{18} M^{-1} s^{-1}) [144]. According to their interpretation, the quenching does not occur simply via a dynamic process but by electrostatic interactions (ion pairing) between the oppositely charged donor (PF) and acceptor (porphyrin) and subsequent energy transfer within self-assembled species [144].

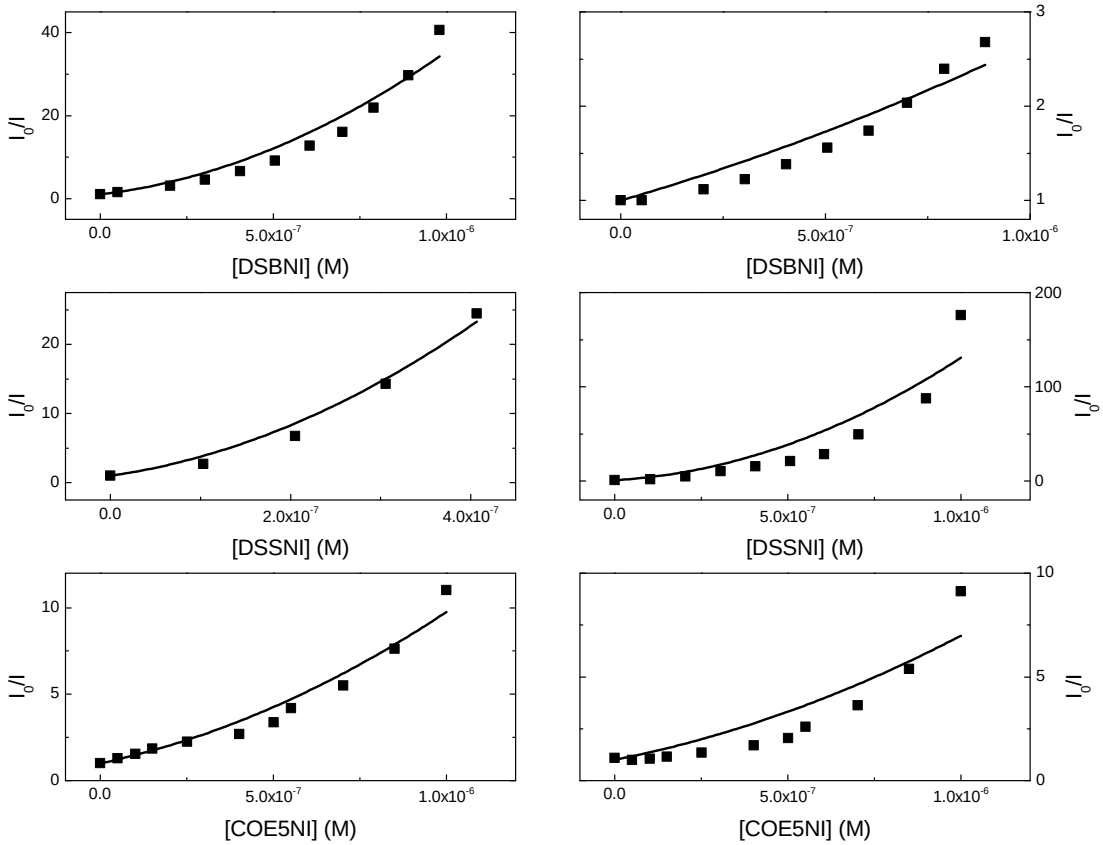

Figure 4.3.7: Deviations of the Stern-Volmer plots according to the formation of a non-fluorescent complex. Water/dioxane (1:1, v/v) mixture (left) and 10^{-4} M aqueous $C_{12}E_5$ solution (right).

The oligomers are expected to bind strongly to the anionic PBS-PFP, due to the four available cationic trimethylammonium groups, $N(CH_3)_3^+$. The data show a correlation of the quenching efficiency with the positive oligomer charge and size, Table 4.4 and Figure 4.3.8. With COE5NI in solution, the quenching efficiency is low, compared to the other two oligomers. These observations suggest that the fluorescence quenching of CPEs by charged macromolecules do not just involve mechanisms of electron or energy transfer. The dependence of the quenching efficiency on the oligomer size resembles the fluorescence quenching mechanism of poly[2,5-bis(3-sulfonatopropoxy)-1,4-phenylene-*alt*-1,4-phenylene) (PPP-$OPSO_3$) with cationic dendrimer materials [148]. The larger macrolomecules allow more interactions with the polymer backbone, causing the polymer to distort and possibly wrap around the macromolecule surface. This leads to conformational changes in the polymer and enhances the coupling among the electronically excited state and the ground state leading to a "self-trapping" effect [148].

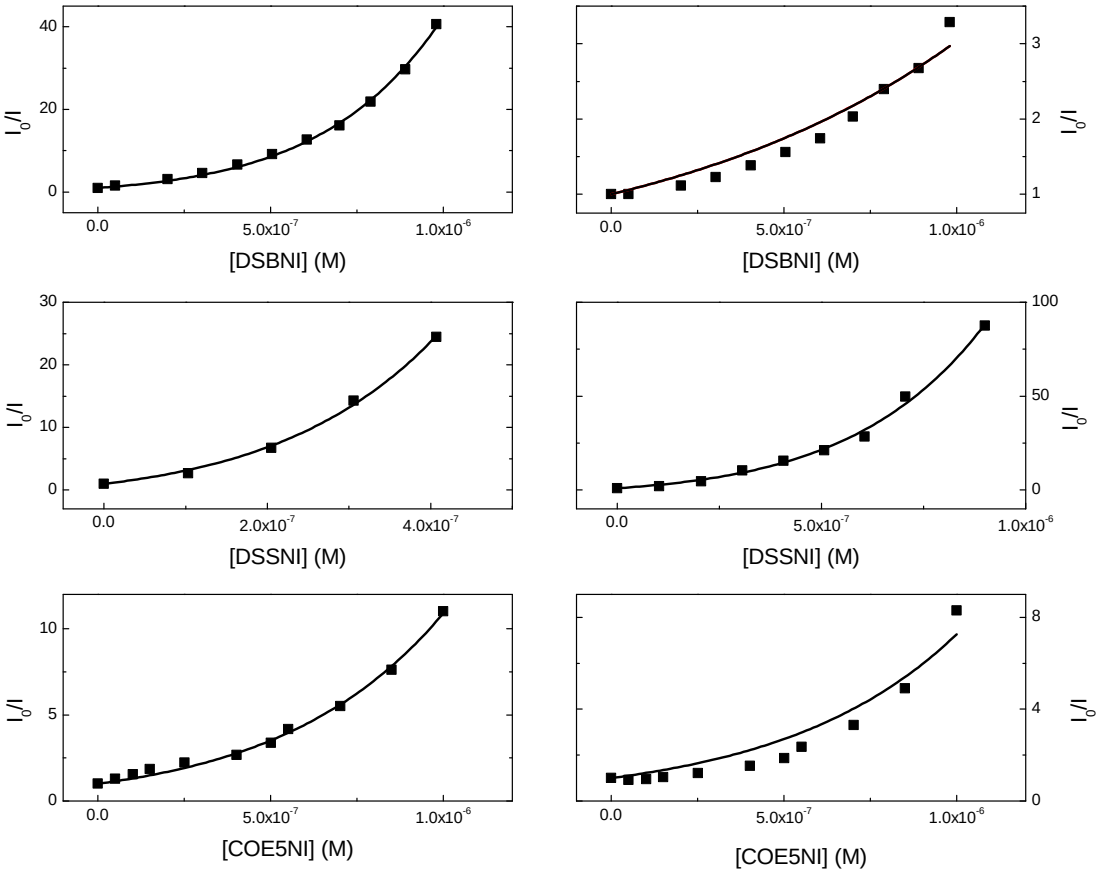

Figure 4.3.8: Deviations of the Stern-Volmer plots according to the quenching sphere of action. Water/dioxane (1:1, v/v) mixture (left) and 10^{-4} M aqueous $C_{12}E_5$ solution (right).

For chemical and biosensor applications, it is desirable to have a fluorophore-quencher pair with a high K_{SV} [149] [150], as is the case of the fluorescence quenching efficiency of the conjugated polymer poly[lithium 5-methoxy-2-(4-sulfobutoxy)-1,4-phenylenevinylene] (MBL-PPV) with the well known electron transfer (ET) protein cytochrome c (cyt c), whose K_{SV} exceeds 10^8 M^{-1}. The high efficiency ($K_{SV} = 10^8$ M^{-1}) is attributed to a combination of ultrafast photoinduced ET between the polymer and the acceptor and to the formation of bound complexes (static quenching) that is due to the oppositely charged polyelectrolytes [150].

Regarding the higher K_D (K_{SV}) values of the PBS-PFP quenching with phenylenevinylene oligoelectrolytes, the systems could be used, in a broad context, for sensing purposes. Understanding the quenching dynamics of functionalized fluorescent conjugated polymers is critical to the design of chemical and biological sensory materials. The Stern-Volmer analysis reveals that a combination of static and dynamic processes contributes to the quenching mechanism of PBS-PFP system in the presence of the cationic oligoelectrolytes. The nonlinear behaviour is attributed to a combination of static quenching and to an

energy transfer between the anionic PF and the acceptors, as well to the "self-trapping" effect that is dependent on the oligoelectrolyte size [151].

Table 4.4: Experimental quenching constants using the sphere of action model for PBS-PFP in water/dioxane (1:1, v/v) mixture.

	K_D (M^{-1})	x [d] ($r^3 \cdot mol^{-1}$)	R^2	$k_q = K_D/\tau_0$ [e] ($M^{-1} \cdot s^{-1}$)	$V = x \cdot 1000/N$ (r^3)	$R = 3 \cdot V/(4\pi)^{1/3}$ (r)
I[a]	3.68×10^{6}	2.20×10^{6}	0.998	6.75×10^{15}	3.66×10^{-15}	4.72×10^{-15}
II[b]	1.18×10^{7}	3.55×10^{6}	0.997	2.11×10^{16}	5.89×10^{-15}	7.60×10^{-15}
III[c]	1.03×10^{6}	1.68×10^{6}	0.995	1.84×10^{15}	2.79×10^{-15}	3.60×10^{-15}

[a] DSBNI
[b] DSSNI
[c] COE5NI
[d] V·N/1000
[e] τ_0 = 560 ps

4.4 Time-resolved fluorescence of the self-assembled PBS-PFP / phenylenevinylene oligoelectrolytes system

Figures 4.4.1 and 4.4.2 show the time-resolved fluorescence decays of the anionic PBS-PFP polyelectrolyte with increasing cationic oligoelectrolytes concentration. Excellent fits of the emission decays collected at the PBS-PFP maxima could be achieved by using sums of three discrete exponentials, Figure 4.4.3 (see Chapter 3 for the global analysis equation). This is in agreement with the observations made for fluorescence decays of fluorene-based polymers that frequently need more than one exponential for a good fit and fluorene-based polyelectrolytes are no exception [124], [145]. As discussed by Dias *et al.*, the component with a few hundred picoseconds lifetime is attributed to the decay of a singlet exciton located in the backbone [47]. The assignment of the shortest component is still doubtful and not free of uncertainties. However, it is generally assumed that it is associated with the conformational relaxation and energy migration along the polymer chain [45]. Furthermore, its contribution on the overall decay depends on the degree of polymer aggregation, as suggested for the cationic HTMA case [145], [146].

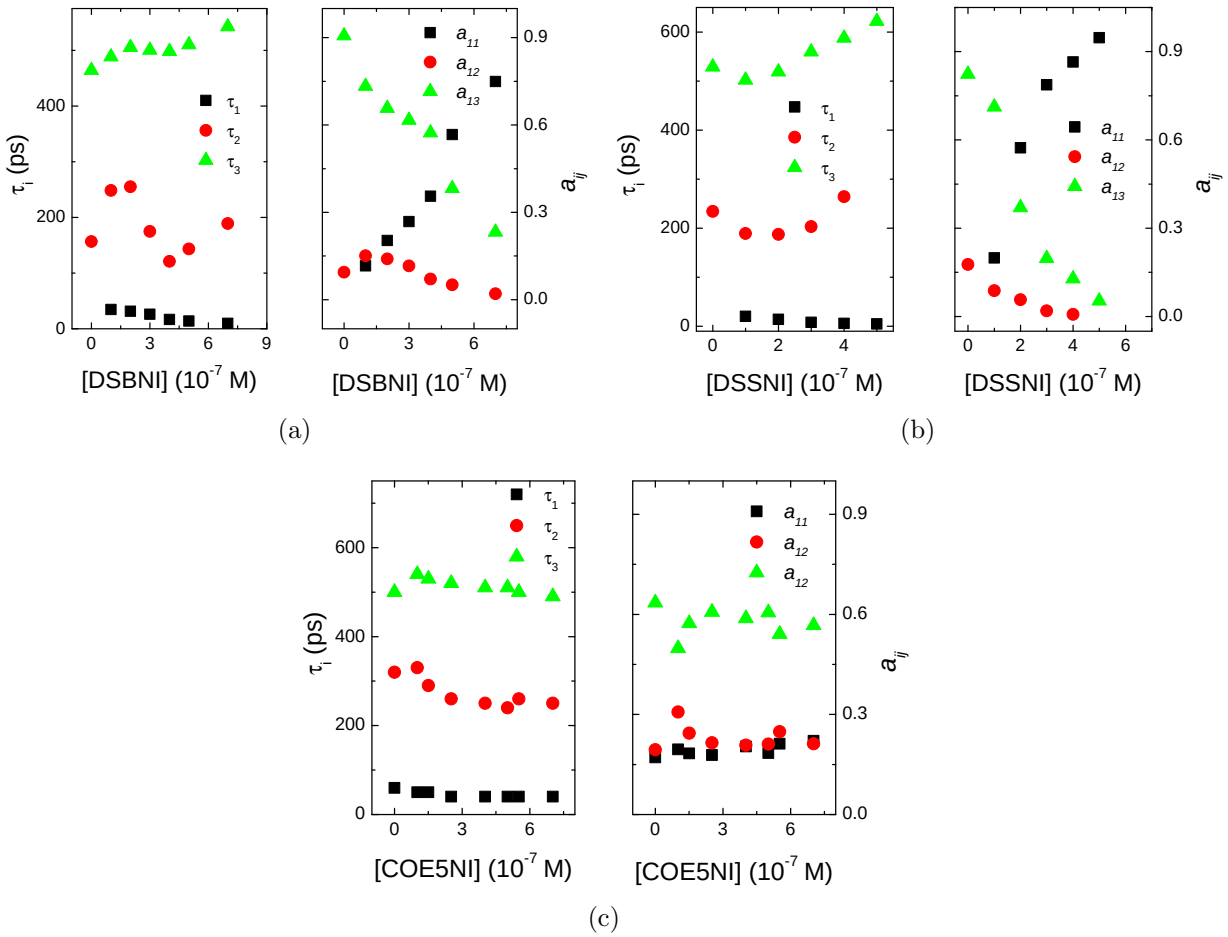

Figure 4.4.1: Fluorescence decay times (τ_i) and amplitudes (a_{ij}) of PBS-PFP in water/dioxane (1:1, v/v) mixture with increasing phenylenevinylene oligoelectrolyte concentration. a) DSBNI, b) DSSNI and c) COE5NI.

In a study presented by Monkman *et al.* about the surfactant effect on the energy and charge-transfer processes in deoxyribonucleic acid (DNA) detection using a conjugated fluorene-based polyelectrolyte, time-resolved analysis was used to demonstrate the effect of surfactant on DNA sequence detection quantitatively [85]. The CPE/DNA system data was fitted with three discrete exponential terms ($j = 3$). The three CPE phases were associated with time constants of around 600, 200 and 15 ps and the intermediate time constant of 200 ps was then assumed to be related to the presence of polymer clusters [85].

For the decay kinetics depicted in Figure 4.4.3 without a) and with b) surfactant, the collected results reveal differences in the decay profile in the two cases, with respect to the fast and the slowest components. This observation indicates that the surfactant eliminates strong intra-chain quenching components in the copolymer, which is supported by the enhancement of PBS-PFP PLQY in $C_{12}E_5$, see Table 4.2. Despite the fact that there are no

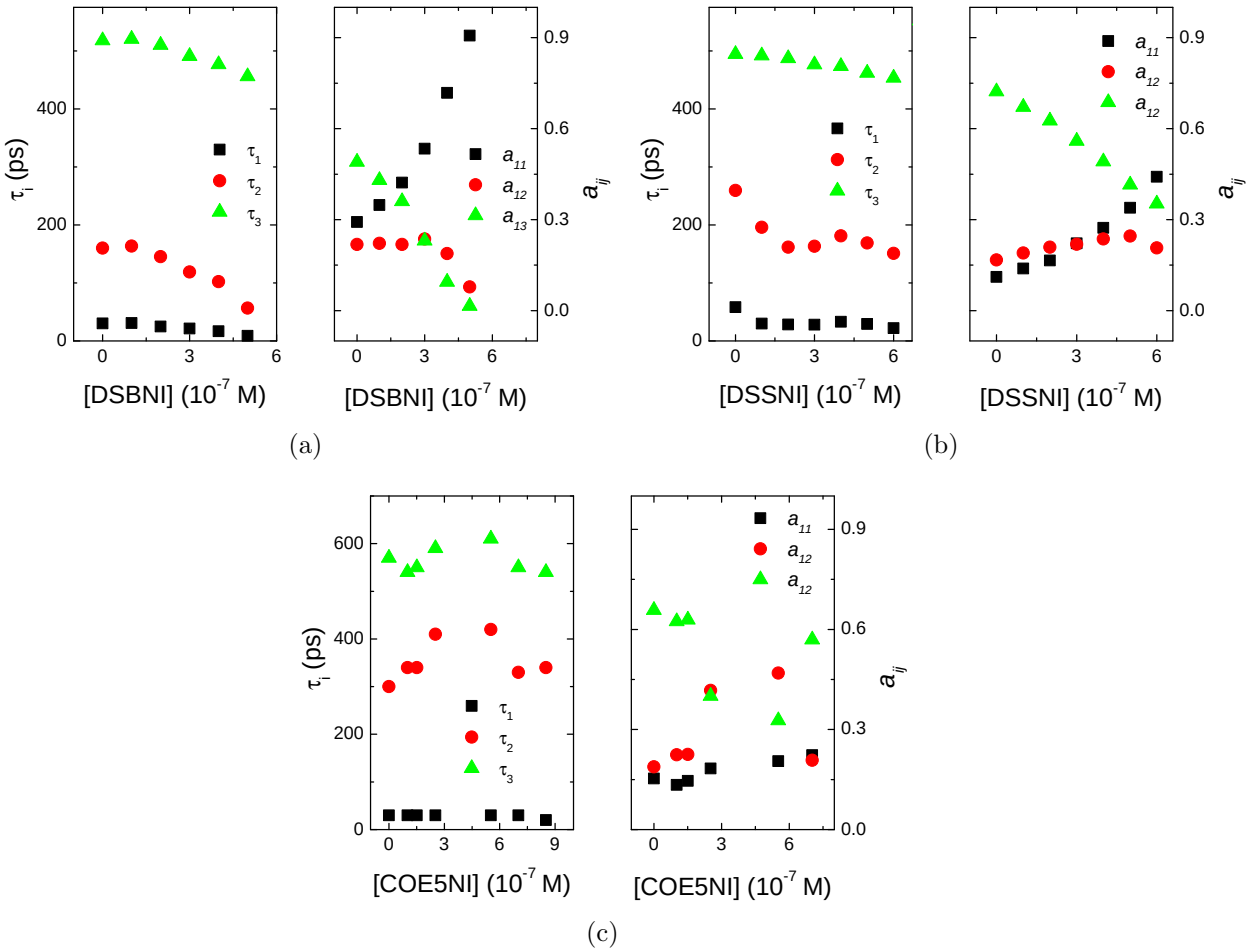

Figure 4.4.2: Fluorescence decay times (τ_i) and amplitudes (a_{ij}) of PBS-PFP in aqueous $C_{12}E_5$ (10^{-4} M) solution with increasing distyrylbenzene oligoelectrolyte concentration. a) DSBNI, b) DSSNI and c) COE5NI.

major changes in the intermediate decay component, the surfactant increases its contribution by reducing the average size of the clusters and by making them closer to the isolated polymer chains, as proposed by Monkman [85]. However, a reduction in the average lifetime was observed from 560 in water/dioxane to 490 ps, which may be a consequence of environmental polarity changes [86]. In the PBS-PFP non-ionic surfactant solution, the longest lifetime increases initially slightly with the oligomer DSBNI and COE5NI concentration, as do the two faster components τ_1 and τ_2. Nevertheless, this increase does not continue and all the three components are quenched above a certain cationic oligoelectrolyte concentration. In contrast, when DSSNI (the tetramer) is added to the CPE solution, all the decay components experience a decrease in the lifetime. The longer decay, τ_3, that represents the isolated polymer chain lifetime, is the component most affected in the energy-transfer

process. In the presence of oligomers τ_3 does not suffer major changes, but its amplitude is reduced. The decrease of the pre-exponential amplitude with the phenylenevinylene oligoelectrolyte concentration confirms that the long-decay component (τ_3) is not connected with the presence of the oligoelectrolytes [128].

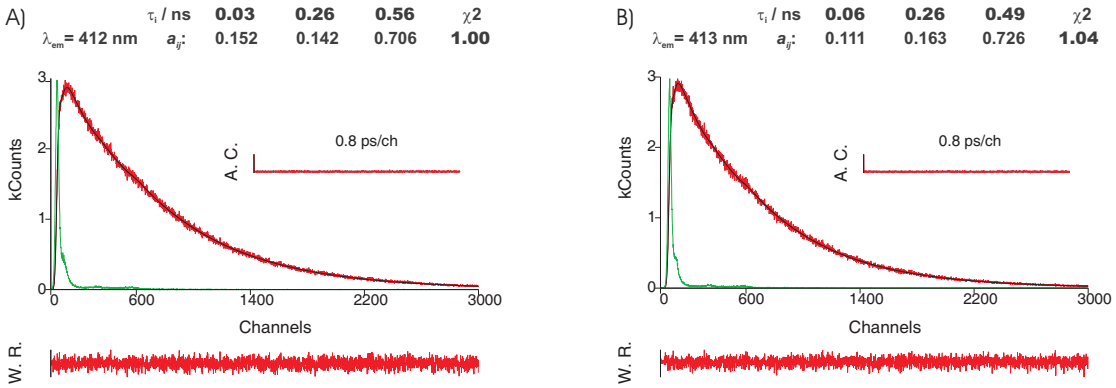

Figure 4.4.3: Fluorescence emission decay for PBS-PFP collected at 412 nm obtained with λ_{exc} 372 nm at 298.15 K. A) in water/dioxane (1:1, v/v) mixture and B) in 10^{-4} M $C_{12}E_5$ solution. The green lines in the decays are the instrumental response function (IRF). For a better judgment of the quality of the ts weighted residuals (W.R., scale $-3 \leq \sigma \leq +3$), autocorrelation functions (A.C.) and χ^2 are also presented.

Equally important is the fact that the pre-exponential amplitude associated with the fastest decay component increases and, thus, its origin may lie in the singlet-singlet energy migration from the fluorene-based polyelectrolyte to the cationic oligomers, which predominantly involves Förster energy transfer (FRET). This has previously been reported for the PBS-PFP/tris(bipyridyl)ruthenium(II) self-assembled system in solution [128]. The nature of τ_2 is still unclear but it is often observed with this type of polyelectrolytes and it is questionably assigned to exciton migration, either on-chain or within copolymer aggregates [85, 144–146].

The general scheme proposed for energy transfer from PBS-PFP to the cationic oligomers is shown in Figure 4.4.4. For a simple reading the energetic processes was illustrated only for the oligomer DSBNI. The phenylenevinylene oligoelectrolytes excited state energy values are presented for all the compounds.

The lifetime variation in the presence of the three cationic oligomers suggests that some of the changes observed may be due to the formation of polymer aggregates. This has been seen in the PBS-PFP fluorescence quenching by calcium(II) in dioxane-water [152] mixtures, and in the interaction of carboxylate poly(phenylene ethynylene) CPEs with metal ions [153]. The possibility that the divalent cation induces aggregation of the CPE is sup-

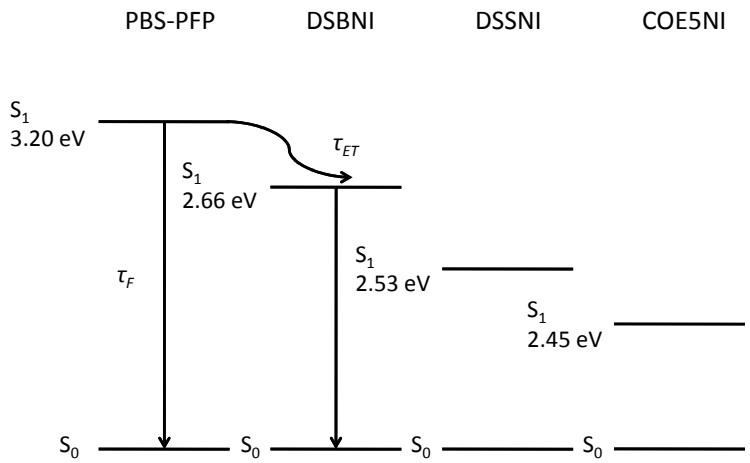

Figure 4.4.4: Schematic energy diagram for PBS-PFP and oligoelectrolytes. Energies were taken from the intersection of the absorption and emission spectra for the cationic oligomers and from ref. 33 for the CPE.

ported by molecular dynamics simulations [152]. The intermediate decay component τ_2 tends to increase at higher oligoelectrolyte concentrations, probably due to polymer aggregation with the positively charged acceptors. This process is well illustrated for the DSSNI case, and shows how the oligomer size plays an important role in the FRET process. From the collected data it is expected that the surfactant $C_{12}E_5$ encapsulates the CPE in elongated cylindrical micelles which protect the CPE (donor) from the acceptor. Consequently, the Förster transfer rate will be reduced. For PBS-PFP in the absence of surfactant, the phenylenevinylene oligoelectrolyte induces an increase in the lifetime, while in $C_{12}E_5$ solutions and in the presence of COEs, a decrease in the longest lifetime was observed. This is attributed to CPE-CPE quenching and/or to a dynamic quenching of the high isolated polymer chain population generated through a surfactant effect [85].

4.5 Self-assembly of PBS-PFP properties in films

Ortony and Bazan characterized the DSBNI aggregates by liquid-AFM [154]. Wormlike micelles were observed that showed degrees of surface order over a length scale of approx. 100 nm. Furthermore, cross-sectional analyses revealed structures with an average diameter of 4.4 nm and a height of 0.84 nm. Several roughly elliptical micelles structures were visualized with lengths less than 400 nm and within the corresponding length of one DSBNI molecule ($\approx$ 3.6 nm) to the elliptic major axis [154].

On the spin coated DSBNI solution (2.2 mM) the same roughly elliptical structures were found with average sizes of ca. 49 - 120 nm (Figure 4.5.1). These measurements,

performed above the DSBNI aggregation concentration (0.51 mM), are associated with formed oligoelectrolyte cylindrical micelles. However, in the studied case no major changes were noticeable on the AFM phase image of PBS-PFP spin coated with DSBNI, Figure 4.5.1.

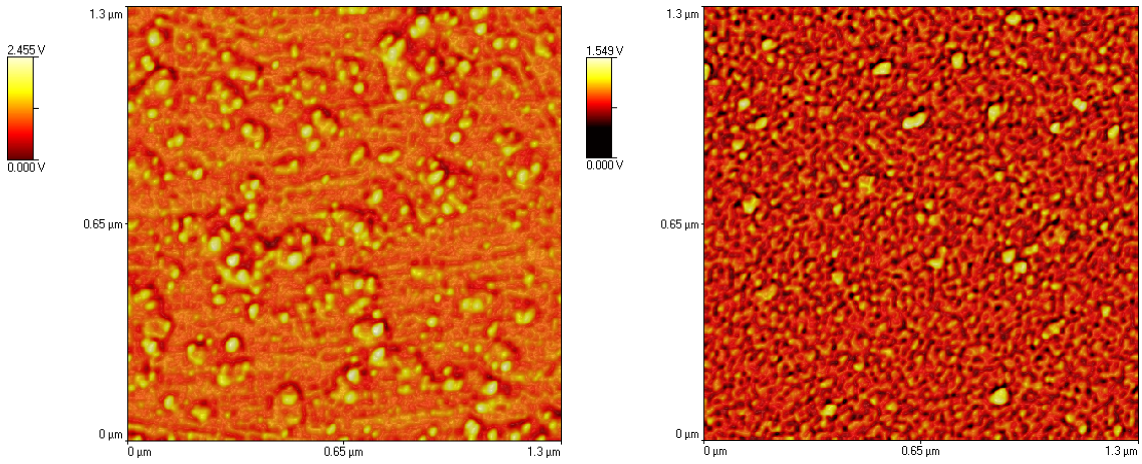

(a) (b)

Figure 4.5.1: AFM phase images spin coated on quartz a) DSBNI 2.2 mM aqueous solution and b) PBS-PFP (3 mg/mL) in water/dioxane (1:1, v/v) mixture with ca. 6.5 μM DSBNI.

4.6 Conclusions

The chapter discussed the self-assembly mechanism between PBS-PFP polyelectrolyte and cationic phenylenevinylene oligoelectrolytes based on steady state and time resolved fluorescence measurements. The collected data imply that intrinsic energy transfer to the phenylenevinylene oligoelectrolytes quenches the fluorescence intensity of PBS-PFP, and that the efficiency can de "tuned" by controlling the oligoelectrolyte size.

The influence of the non-ionic surfactant $C_{12}E_5$ on the energy transfer of the PBS-PFP/phe-nylenevinylene oligoelectrolyte systems was investigated and compared with water/dioxane (1:1, v/v) mixtures of the same systems. The PL decrease of PBS-PFP was found to be ca. 10% inferior in aqueous 1×10^{-4} M $C_{12}E_5$ solutions, in comparison to the water/dioxane (1:1, v/v) mixture. The observation is in accordance with previously mentioned studies by Burrows and coworkers [126–128]. In the presence of $C_{12}E_5$, PBS-PFP exists as isolated copolymer chains that are surrounded by the non-ionic surfactant, with the sulfate groups of the PBS-PFP side chain, extended into the aqueous domain. Moreover, molecular dynamics conducted in PBS-PFP oligomers solvated in a 30% dioxane solvent

box, suggest that dioxane has a "coating" effect and displaces water from the copolymer immediate environment. This limits the accessibility of the aqueous media to the oligomers, while the sulfonate groups and sodium counter-ions are solvated by water [123]. Despite this, it is possible for the phenylenevinylene oligoelectrolyte molecules to interact with the anionic copolymer, resulting in an efficient FRET mechanism.

Non-linear Stern-Volmer plots were found for the PBS-PFP/cationic oligoelectrolytes quenching dynamics. This nonlinear behavior was attributed to a combination of static quenching and an energy transfer enhancement of the quenching as a result of energy migration along the polymer backbone. The systems were fitted into two models that include combinations of dynamic and static mechanisms counterparts. In spite of the system complexity, the "quenching sphere of action" model appears to best translate the assembly PBS-PFP/phenylenevinylene oligoelectrolytes.

Time-correlated fluorescence decays of PBS-PFP were obtained and collected at the PBS-PFP absorption (372 nm) and emission maxima (412 nm), respectively. The decays were fitted with sums of three discrete exponential functions. The long-decay component, τ_3, attributed to PBS-PFP isolated chains, remains roughly constant, in both solvent systems, with increasing DSSNI concentration. However,τ_3 increases slightly when DSBNI and COESNI are added to PBS-PFP solutions of water/dioxane (1:1, v/v) and decreases in the surfactant copolymer solution. The quenching of the pre-exponential amplitude a_{13}, with the phenylenevinylene oligoelectrolytes concentration, confirms that the long decay component is not connected with the presence of the oligoelectrolytes [128]. The two fast constants, τ_1 and τ_2, follow the same discussed τ_3 tendency. Moreover, the pre-exponential amplitude associated with the short decay component, a_{11}, increases with the oligomers concentration as the PBS-PFP lifetime is quenched; thus, τ_1 is attributed to the singlet-singlet energy migration from the PBS-PFP to the oligoelectrolytes that takes place in the self-assembled complex [128]. Attribution of τ_2 is controversial, still it makes sense to think about aggregated species as being responsible for the τ_2 time constant [85], [86].

Atomic force microscopy shows roughly elliptical micelles with average sizes of ca. 49 - 120 nm for spin coated DSBNI aqueous solution (2.2 mM). However, AFM data from films of the self-assembled system PBS-PFP/DSBNI didn't shown the existence of defined aggregates, probably due to the low oligomer concentration: 6.5 μM DSBNI to 3.9 mM (3 mg/mL) of PBS-PFP.

Chapter 5

PBS-PFP with on-chain chromophores

Fluorene copolymers that can emit colours over the entire visible range (red, green and blue) are becoming essential in full colour display PLEDs fabrication. As a consequence, they have been extensively studied and synthetised particularly via Suzuki and Yamamoto routes [21], [155]. Improvements in the polymeric emitters with good color purity are becoming, necessary to further explore and develop efficient PLED materials [156]. Controling energy transfer between different chromophores within a single polymer carrying different groups, is crucial for the final emission color, in particular for achieving white light emission; since the close proximity of the constituents usually results in the dominant emission from the lower bandgap material [19], [157]. Although the chromophore is incorporated within the conjugated polymer chain, both intra and interchain processes are likely to be important.

Colour tuning in organic conjugated polymers (CP) through FRET involves dipole-dipole interaction between two different on-chain or side-chain moieties. Energy transfer may also involve an exchange mechanism (Dexter), following exciton hopping. In donor-acceptor polymers the transfer mechanism normally includes diffusion within the D, followed by transfer from the D to the A moieties. Thus, involving nonradiative transfer from the D to the A [158]. However and according to Hofkens *et al.* [159], FRET is not restricted to nonradiative transfer from a D in an excited state to a ground-state A, but can also occur between donor and acceptor molecules with different spin multiplicities. The transfer processes allowed within the Förster formulation are those for which no changes, in the electron spin in the acceptor transition, occur. Hence, the transfer of excitation energy from a chromophore residing in the first excited singlet state to another chromophore either in excited singlet or triplet state, is also possible and a competing deactivation pathway [159], [160].

In order to meet application driven functionalities key properties of PBS-PFP polyelectrolyte, such as the bandgap energy, carrier transport, absorption spectrum, HOMO and LUMO energy levels, can be tuned through synthetic modications of the copolymer core by the incorporation of on-chain chromophores, as depicted in Figure 5.0.1.

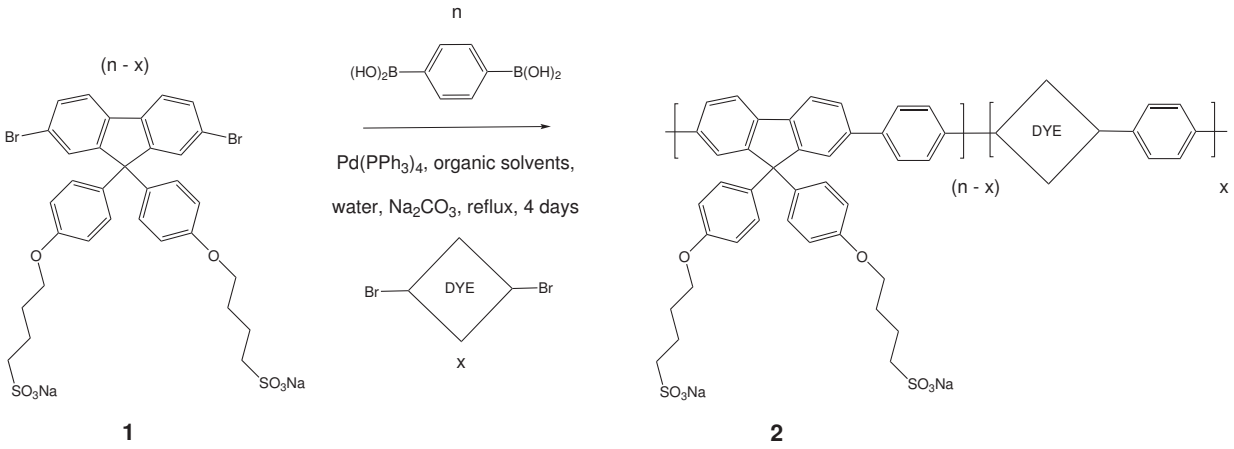

Figure 5.0.1: Copolymerization of PBS-PFP with dibrominated dyes via Suzuki route.

5.1 Synthesis

The preparation of the PBS-PFP was described previously, see chapter 4. Several PBS-PFP derivatives with different chromophoric units of the main chain were synthesized via statistical copolymerization of 2,7-dibromo-9,9-bis(4-sulfonylbutoxyphenyl)fluorene **1** and suitable bisbrominated dyes with benzene(1,4)-diboronic acid, in a Suzuki-type aryl-aryl cross coupling **2** (Figure 5.0.1) [37, 133, 134]. The comonomers were chosen based on their absorption maxima and spectral overlap with the polyelectrolyte emission. The copolymers have been characterized by GPC, although their Mw is likely to be considerably underestimated due to the interactions between the polyelectrolytes and the column material. This will be further discussed in subchapter 5.4.

5.2 PBS-PFP with main chain dye chromophores

5.2.1 PBS-PFP with on-chain perylenediimide units

Perylenediimides (PDIs) and their derivatives, having compact and electron deficient cores, as well as high chemical, thermal and photo-stability, are archetypal components in a variety of photofunctional materials. They have demonstrated great potential as n-type

semiconductors in organic field effect transistors (OFETs), organic solar cells, organic light emitting devices (OLEDs), xerographic materials, laser dyes and biosensors [161–164]. PDIs have strong absorption in the visible region with high extinction coefficient (ϵ of ca. 50 000 M^{-1} cm^{-1}) and their characteristic absorption and emission features are not affected by the presence of solubilizing substituints at the imide nitrogen. The introduction of bulky groups at the N-aryl moieties allow the PDI molecule to achieve the desirable solubility in appropriate solvents [162], [165]. Further solubility increase can be accomplished with introduction of alkoxy substituints at the perimeter of the perylene nucleus [165].

At the single molecule level, PDI based systems have been employed to study photoinduced electron transfer processes, because of to their accessible oxidation and reduction potentials. Furthermore, energy transfer and hopping processes that lead to efficient single photon emission, have also been demonstrated to occur in these systems [166], [167].

The backbones of CP can be covalently linked to appropriate functional groups to provide specific physical and chemical properties. Electron-donor polymers substituted with electron acceptor groups are promising candidates with potential new properties and applications. In this perspective, PDI has been chosen for incorporation in the main chain of CPs, either covalently attached as pendant groups, or as chain termini [9], [168]. According to work developed by Müllen and coworkers [9], PF end-capped with PDIs have been shown to be suitable materials for probing the fundamental processes of energy transfer via single molecule spectroscopy, since they possess only one or two chromophores in a well-defined spatial relationship. In addition, statistical copolymers bearing PDI units have been successfully used to make LEDs with emission colours covering the whole visible spectra. PFs copolymers with pendant PDI groups can incorporate a high dye concentration, without affecting the PF backbone electronic properties and show complete energy transfer, both in solution and solid state. Given that PDI groups are excellent electron acceptors for use in photovoltaic devices, PF-PDI copolymers with pendant groups are potentially good candidates for organic solar cell application [9, 169, 170].

Because of the vast applications potential of PF-PDI copolymers, it is important to study and understand their conformational aspects and energy transfer pathways. The particular interest is in the case of a water soluble fluorene based polyelectrolyte, where it may be possible to tune their properties, by controlling the material morphology. The photophysical properties and dynamics of a PBS-PFP based copolymer with statistical PDI units have been explored upon excitation of the PBS-PFP and PDI parts by single molecule spectroscopy, steady state, time resolved fluorescence measurements and ultrafast transient absorption measurements.

5.2.1.1 Synthesis

The statistical PBS-PFP-PDI copolymer was synthesized from the corresponding di-brominated monomers and di-boronic acid via a Suzuki route [37], [133]. The chemical sctrutures of PDI dye and PBS-PFP-PDI copolymer are depicted in Figure 5.2.1. The reaction ratio of *n-x* to *x* is 95 to 5.

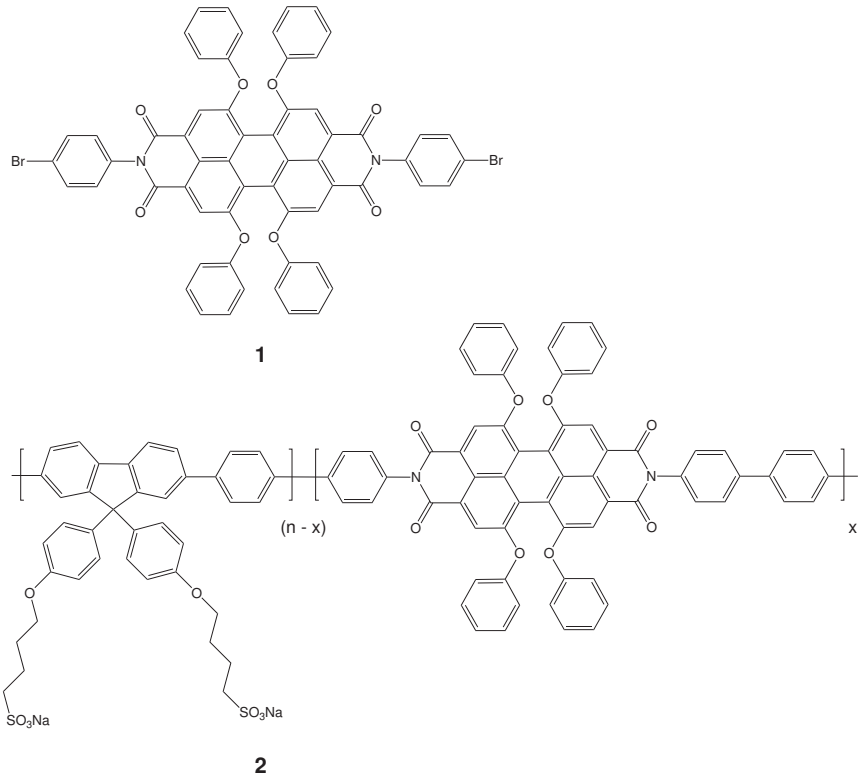

Figure 5.2.1: Chemical structures of the PDI monomer (1) and the copolymer PBS-PFP-PDI (2).

N,N'-bis(4-bromophenyl)-1,6,7,12-tetra(phenoxy)-perylene-3,4,9,10-tetracarboxdiimide PDI **1** was synthesized in the working group of Professor Klaus Müllen in the Max Planck Institute for Polymer Research, Mainz, Germany as described previously [9].

Poly{1,4-phenylene}-co-{[9,9-bis(4-phenoxy-butylsulfonate)]fluorene-2,7-diyl}-alt-{N,N'-bis (4-bromophenyl)-1,6,7,12-tetra(phenoxy)-perylene-3,4,9,10-tetracarboxdiimide}
(PBS-PFP-PDI) **2**.
A mixture of 2,7-dibromo-9,9-bis(4-sulfonylbutoxyphenyl)fluorene (0.783 g, 0.95 mmol), N,N'-bis(4-bromophenyl)-1,6,7,12-tetra(phenoxy)-perylene-3,4,9,10-tetracarboxdiimide PDI (0.053 g, 0.05 mmol), 1,4-benzenediboronic acid (0.166 g, 1 mmol), $Pd(PPh_3)_4$ (50 mg),

Na_2CO_3 (1.0 g, 9.4 mmol) in 50 mL of toluene, 5 mL of water and 5 mol of butanol, were reacted for 4 days under reflux. The aqueous layer was washed with chloroform and concentrated to dryness [134] [124]. The residue was redissolved in a mixture of water and THF 50% (v/v), and then purified by dialysis using a membrane with a cut-off of 3500 g·mol^{-1}. Based on the monomer/PDI ratio in the starting reaction mixture, the copolymer is expected to contain on average 5% PDI units. Total yield of the copolymer PBS-PFP-PDI was 374 mg of a light red powder (47%). From TGA measurements, the copolymer has a decomposition temperature at 370 °C.
^{1}H NMR (400 MHz, d-THF 50% D_2O): δ (ppm) = 8.2 (ar-H PDI), 7.8 - 7.0 (ar-H PDI and ar-H fluorene), 4.2 (CH_2, α), 3.1 (CH_2, γ), 2.1 (CH_2, β) 1.5 (CH_2, σ).
FTIR 1652, 1662 and 1698 (sh) cm^{-1} for the imide groups and 1507.5, 1578 and 1600 cm^{-1} for the perylene skeleton [171] [172].
GPC (NMP, LiBr, UV-detection 360 nm) Mn = 1400, Mw = 2100 g·mol^{-1}, and PD = 1.50.

5.2.1.2 Steady state spectroscopic measurements

The absorption and photoluminescence emission spectra of the PBS-PFP-PDI copolymer were recorded both in water and water/dioxane (1:1, v/v) mixture. The steady-state spectra in water/dioxane are shown in Figure 5.2.2. The spectroscopic data observed for the PBS-PFP-PDI in the two solvents are summarized in Table 5.1.

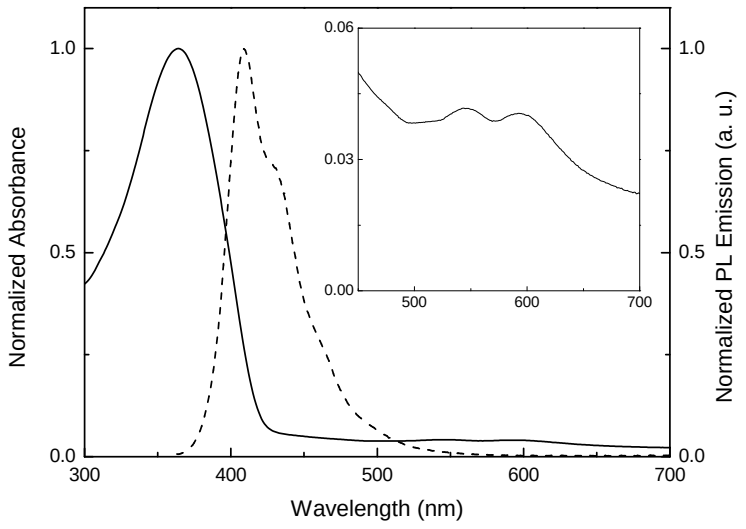

Figure 5.2.2: Absorption and emission spectra of the PBS-PFP-PDI copolymer in a water/dioxane (1:1, v/v) mixture. The inset depicts the 400 - 700 nm region of the PBS-PFP-PDI absorption shown in the main plot.

Table 5.1: Absorption and emission maxima and photoluminescence quantum yield (ϕ_F) of PBS-PFP-PDI copolymer.

Solvent	Absorption λ_{max} (nm)	Emission λ_{em} (nm)	ϕ_F [a]
water	369	424	0.08
water/dioxane	360	409	0.55

[a] PLQY were determined using quinine sulphate in 0.5 M H_2SO_4.

The absorption spectra of PBS-PFP-PDI shows an intense absorption band at 360 nm characteristic of the poly(fluorene-*alt*-phenylene) backbone and a very weak absorbance in the 400 - 615 nm region associated with the incorporated on-chain PDI units [9], [160]. Considering the high molar extinction coefficient of PDI, the small absorbance value (ca. 4% when compared with the PF absorption band) mirrors a low degree of PDI incorporation (Figure 5.2.2). As has been reported for related systems [123], the use of the organic co-solvent is expected to avoid aggregation in solution. In particular, the blue-shift in the emission maximum upon the addition of dioxane and the increase in the fluorescence quantum yield (Table 5.1) suggests the existence of isolated copolymer chains in the water/dioxane mixture [121], [123].

The emission spectra of the copolymer in both solvents (excitation at 360 nm) shows only fluorescence arising from PF units, although, as depicted in Figure 5.2.3, there is a good spectral overlap between the homopolymer PBS-PFP emission and PDI absorption. Upon direct excitation into the PDI unit at 540 nm, no emission from the PDI chromophore could be detected, suggesting a very efficient nonradiative deactivation of the PDI excited state in these solvents, as has been reported for related systems [160]. The photoluminescence quantum yield (PLQY) of the PDI molecule in dioxane is close to unity [173], the value drops to 0.06 in water/dioxane (1:1, v/v) (reference used Rhodamine 6G in ethanol). This indicates the presence of new deactivation pathways of the PDI local excited state, due to the water content in the solution and/or aggregation. For the copolymer in water/dioxane the fluorescence quantum yield was found to be 0.55 in dioxane. This value drops to 0.08 in water and is likely associated with aggregation, which is further supported by the 15 nm red-shift of the emission maxima when compared to the water/dioxane mixture [123].

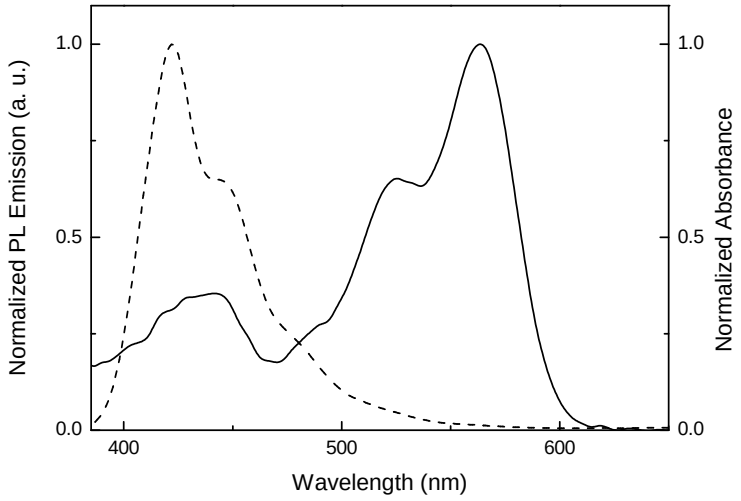

Figure 5.2.3: Spectral overlap between homopolymer PBS-PFP emission and PDI absorption.

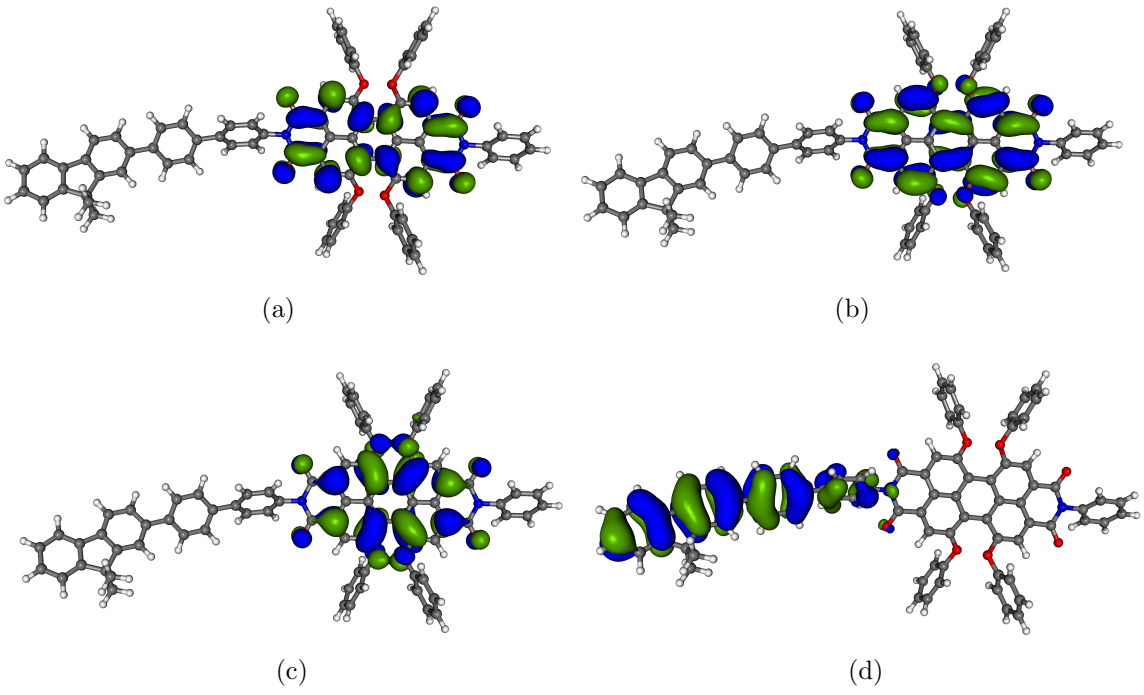

Figure 5.2.4: Contour plots of the HOMO-1, HOMO, LUMO and LUMO+1 orbitals of a PDI-phenylene-fluorene model oligomer as calculated at the B3LYP/3-21G* level. a) LUMO+1 = -1.58 eV, b) LUMO = -2.84 eV, c) HOMO = -5.20 eV and d) HOMO-1 = -5.46 eV.

DFT calculations illustrate that the PDI unit is not electronically coupled to the PFP backbone (see above Figure 5.2.4) such that electronic energy transfer between the two

parts occur only via dipole-dipole interaction (Förster transfer). This is in agreement with studies by Beljonne *et al.* on polyindenofluorenes end-capped with a perylene derivative, which showed rather slow on-chain energy transfer to the perylene dye end-caps, but fast interchain energy transfer [48].

In order to understand the energy transfer process the Förster radius (R_0) for PBS-PFP and PDI was calculated from Equation 5.1 [41], [42]. Where $J(\tau)$ is the overlap integral that expresses the degree of spectral overlap between the donor emission and the acceptor absorption. Hence, the spectral overlap between the PBS-PFP polymer and the PDI chromophore, together with the PDI molar absorption coefficient and the donor fluorescence yield, were used to calculate the Förster radius (R_0), which is the distance at which energy transfer occurs with 50% efficiency [41], [42]. This leads to a Förster radius of 47 Å. Distances ranging from 20 to 40 Å, have previously been calculated for related fluorene containing macromolecules [128, 144, 160, 174, 175].

$$J_\tau = \int_0^\infty F_D(\lambda)\epsilon_A(\lambda)\lambda^4 d\lambda = \frac{\int_0^\infty F_D(\lambda)\epsilon_A(\lambda)\lambda^4 d\lambda}{\int_0^\infty F_D(\lambda)d\lambda} \tag{5.1}$$

Based on the dependence of k_{ET} (Equation 5.2) with the distance between the donor and acceptor (r) [42] with τ_D = 512 ps [128] and R_0 = 47 Å, the following values were obtained for $k_{ET} = 2.06\times10^9$ s^{-1} (r = 47 Å) and 4.72×10^{11} s^{-1} (considering the van der Waals radius, r = 19 Å). From the fluorescence decay measurements, the decay time associated with the energy transfer process (which can also be attributed to conformational relaxation processes) [128] leads to a rate constant of 1.67×10^{10} s^{-1}, see Figure 5.2.5.

$$k_{ET} = \frac{1}{\tau_D}\left(\frac{R_0}{r}\right)^6 \tag{5.2}$$

More details on the distance of the rate transfer are given by the efficiency of the energy transfer (E), also depicted in Figure 5.2.5. That is defined as the fraction of photons absorbed by the donor that are transferred to the acceptor [42]. Equation 5.3 shows that the transfer efficiency is strongly dependent on the distance, particularly at shorter D-A distances.

$$E = \frac{k_T(r)}{\tau_T^{-1} + k_T(r)} \tag{5.3}$$

The fact that no energy transfer is observed through PDI emission, although the calculations indicate its possibility, suggests that an alternative photophysical pathway (such as charge transfer from the fluorene to the PDI [160]) exist with isolated CPE chains in water/dioxane mixture.

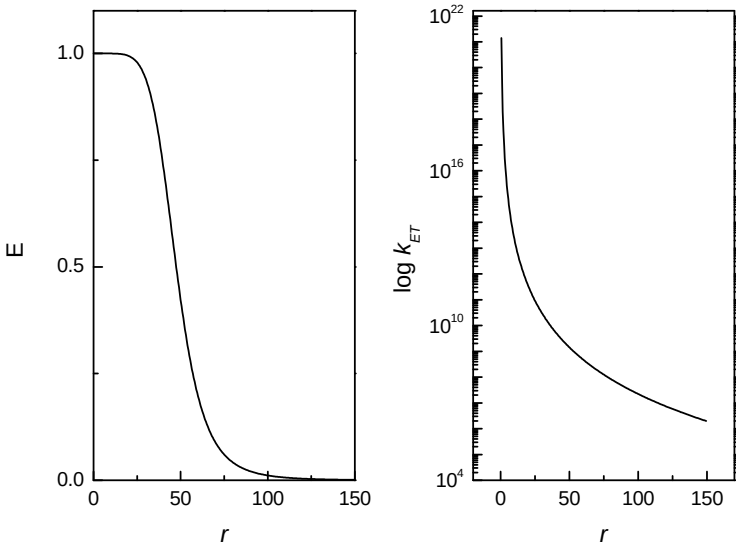

Figure 5.2.5: Dependence of the energy transfer efficiency (E) on the donor acceptor distance (left) and variation of the rate of energy transfer as a function of the donor acceptor distance for the PBS-PFP-PDI system (right).

5.2.1.3 Single-molecule wide field imaging

The detection of single molecules is made possible by the sensitivity and selectivity of fluorescence microscopy [176], [177]. Despite the complexity of the system under study, single-molecule experimental set-ups typically focus on extracting as much information as possible, in addition to measuring the fluorescence emission. Properties studied by the technique involve the determination of the emission wavelength and polarization, the emission dynamics (with nanosecond accuracy), as well as, the excited-state lifetime of the emitting fluorophore. Furthermore, by detecting over several emission bands, different types of fluorophores can be followed simultaneously, making single-molecule particularly useful in the study of CPs with D-A moieties [177].

In solution, all the chromophores of the CP are roughly equivalent and the probability for emission from each chromophore is more or less the same. This behaviour is different when the polymer chains are immobilized in a matrix, since each polymer backbone has a unique conformation and environment and the individual chromophoric properties are

altered [178]. As a result, the fluorescence emission becomes qualitatively identical to that of a single emitter (as in an "energy trapping" process) characterized by intermittent non-fluorescent periods and single-molecule emission patterns, corresponding to the emission of the "trapped" chromophore [177], [178].

Hofkens and co-workers have previously analysed fluorene based copolymers with attached PDI dye chromophores [160], [179]. To avoid any motion or rearrangement of the polymer chains the molecules were immobilized into PMMA thin film by spin coating and the copolymer concentration kept low, to ensure that only a single copolymer chain is present within a diffraction-limited spot. The intensity trajectories could be constructed by plotting the integrated intensity of the single-polymer emission as a function of fluorescence time [180]. Figure 5.2.6 shows the case of two emission levels that indicate the presence of two chromophores. The emission pattern of the first step corresponds to the linear combination (sum) of the emission of both dye (I) and the second reflects only the emission of the last surviving dye (II) (Figure 5.2.6). If more than four chromophores are present then the probability of observing energy transfer for the PDI-based system becomes signicant [179].

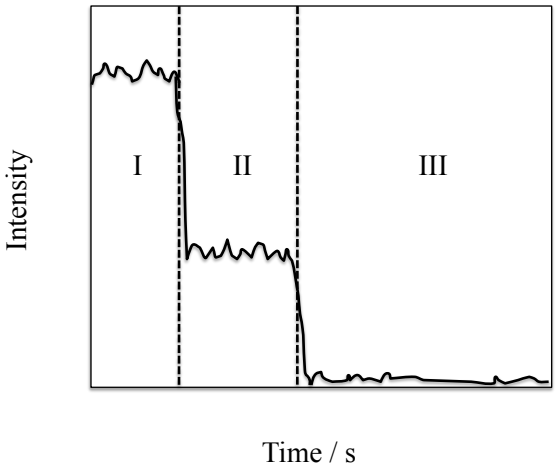

Figure 5.2.6: Fluorescence intensity traces of an emission spot containing the contributions of two PDI chromophores. Based on the intensities, the trace was divided into steps, corresponding to the emission of two (step I) and a single (step II) PDI chromophore. Adapted from [179].

In order to determine the PDI fraction that is actually incorporated in the PBS-PFP-PDI single chain wide field imaging experiments were employed [179]. For this, wide-field images and fluorescence intensity trajectories were recorded of individual polymer chains dispersed in a PVA film, as in the work described by Fron *et al.* and Delport *et al.* [160], [181]. Two excitation lasers were used, 375 and 561 nm, to selectively excite the PBS-PFP and

PDI units. Control experiments indicate that the PVA used as the matrix show no emissive spots when excited at 375 nm. Upon excitation of the PBS-PFP moieties emission from PDI units was observed, indicating that excitation energy transfer does take place form PBS-PFP to the PDI as energy donor and acceptor, respectively. This also suggests that the process occurs more efficiently in a solvent free environment, possible associated with changes in both polarity and polymer chain conformation (folding) (Figure 5.2.7).

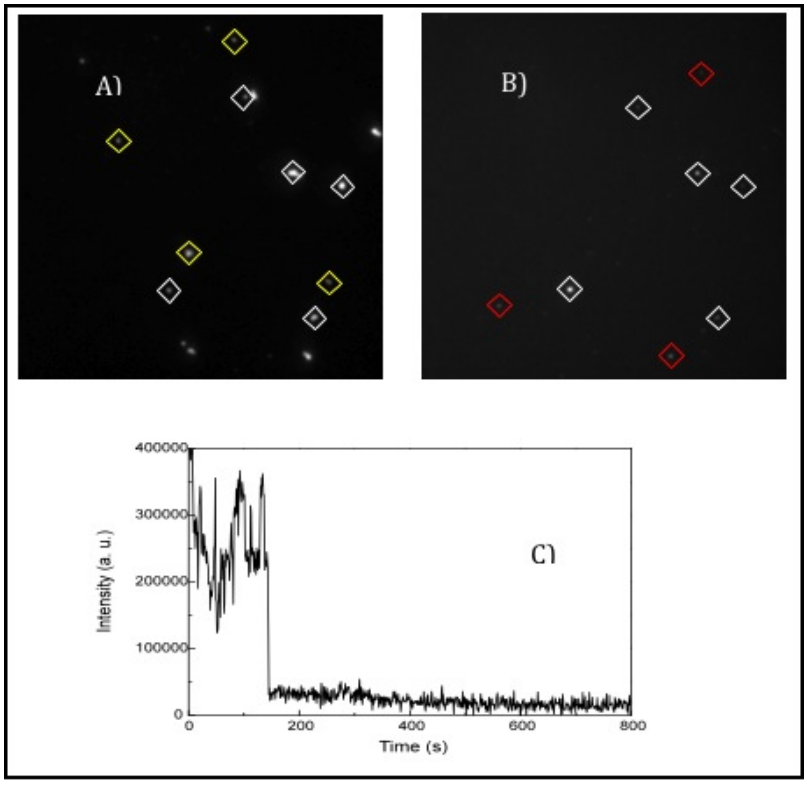

Figure 5.2.7: Wide-field images and fluorescence intensity trajectory of individual PBS-PFP-PDI copolymers dispersed in a PVA film. (A) Wide-field image recorded with 375 nm excitation light. The PBS-PFP units are absorbing moieties and fluorescence is emitted by either PF (yellow spots) or PDI incorporated in the copolymer chain (white spots). (B) Wide-field image recorded with 561 nm excitation light of the same area as Figure 5.2.7A. The PDI units are the absorbing and emitting species in this image; the red spots show "isolated" PDI spots without a corresponding PBS-PFP spot in Figure 5.2.7A. The white spots are PDI chromophores unambiguously attached to PBS-PFP. Figure 5.2.7C represents an intensity-time scan of a PBS-PFP-PDI copolymer containing one PDI chromophore.

The single molecule wide field technique was also used to estimate the number of PDI units incorporated within a single polymer chain. The emission occurring from the polymer

chains was first visualized upon 375 nm excitation and the observed area selected. A movie was then recorded of this area with 561 nm excitation, until all the molecules were photobleached. Via this method, it was possible to identify the PBS-PFP-PDI copolymers and build the copolymer fluorescence intensity time trajectories. Afterwards, a control movie was made with 375 nm excitation to check if all the copolymers were still present and whether the PBS-PFP units were still emitting (Figure 5.2.7). Based on these, the exact number of PDI units present in each copolymer could be determined. The resulted histogram is depicted in Figure 5.2.8 and the majority of the observed copolymers show the presence of one PDI subunit in the PBS-PFP-PDI molecule. The number of intensities levels observed can be assumed to correspond to the number of PDI units. On the basis of the wide-field experiments 272 copolymer molecules were visualized with 375 nm excitation, of which 63% also reveal emission when excited with 561 nm wavelength (copolymer fraction that contains on-chain PDI chromophores) and 36% not (PBS-PFP fraction).

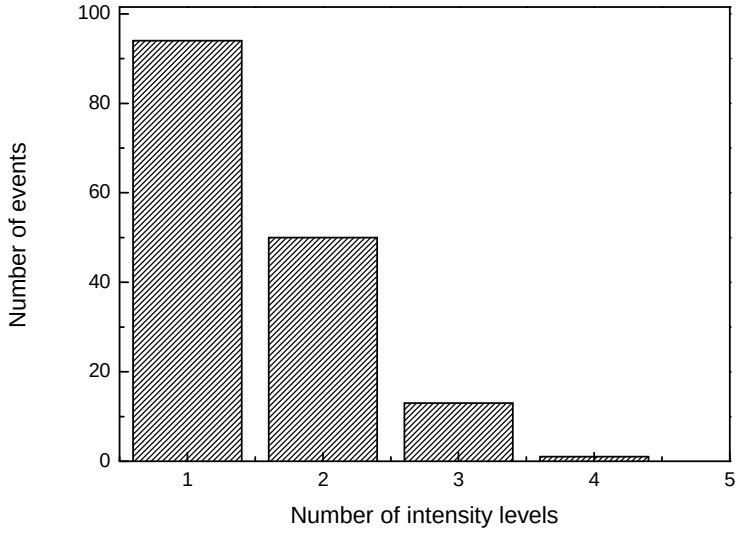

Figure 5.2.8: Number of fluorescence intensity levels corresponding to the number of PDI units in single PBS-PFP copolymer chain.

5.2.1.4 Time-resolved fluorescence measurements

For a better understanding of the excited state behaviour of the PBS-PFP-PDI copolymer, time-resolved fluorescence experiments were performed in the two solvent systems studied and collected at the copolymer emission maxima (Table 5.2 and Figure 5.2.9). The fluorescence decays observed at the polyfluorene emission maximum were best fitted with double and triple-exponential decay laws, according to the Equations 5.4 and 5.5.

$$I_\tau(t) = a_{i1}e^{\frac{-t}{\tau_1}} + a_{i2}e^{\frac{-t}{\tau_2}} \tag{5.4}$$

$$I_\tau(t) = a_{i1}e^{\frac{-t}{\tau_1}} + a_{i2}e^{\frac{-t}{\tau_2}} + a_{i3}e^{\frac{-t}{\tau_3}} \tag{5.5}$$

For the model PDI compound in dioxane a mono-exponential decay was obtained with a lifetime of 5.65 ns, which is close to the value previously reported for PDI compounds, 5 - 6 ns [166].

Table 5.2: Fluorescence decay times (τ_i) and pre-exponential factors (a_{ij}) for the copolymer PBS-PFP-PDI, obtained with excitation at 372 nm, emission at the PF wavelength maxima and T = 293 K.

	λ_{max} (nm)	τ_1 (ns)	τ_2 (ns)	τ_3 (ns)	a_{i1}	a_{i2}	a_{i3}	χ^2
water	420	0.01	0.10	0.70	0.915	0.063	0.022	1.10
water/dioxane	410	0.06	—	0.52	0.079	—	0.921	1.01

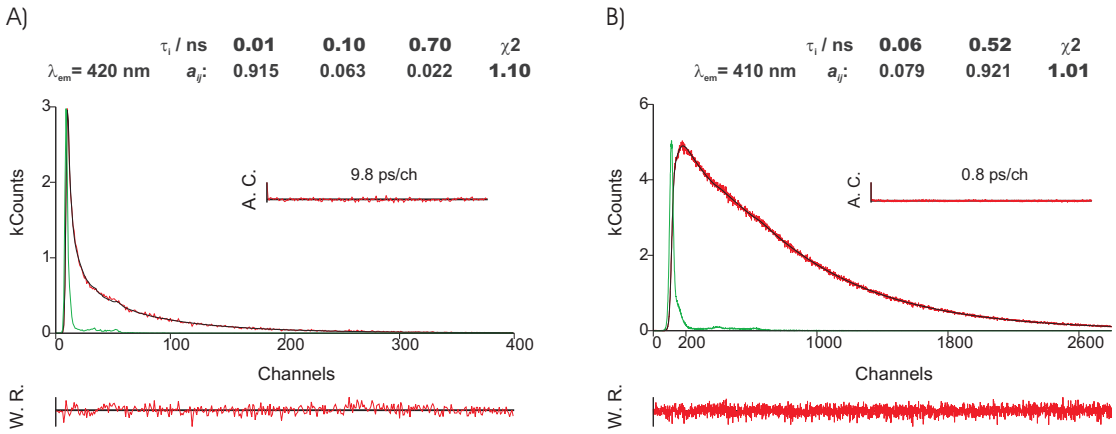

Figure 5.2.9: Fluorescence emission decay for PBS-PFP-PDI collected at the polymer emission maximum obtained with λ_{exc} 372 nm at 293 K in A) water and B) water/dioxane (1:1, v/v) solutions. The green lines in the decays are the instrumental response function (IRF). For a better judgment of the quality of the fits weighted residuals (W.R., scale -3 $\leq \sigma \leq$ +3) autocorrelation functions (A.C.) and chi-square values (χ^2) are also presented.

As discussed elsewhere for related systems [45, 47, 160] the fast component observed is believed to include contributions from both energy migration (either on-chain or inter-chain in water) in the excited singlet state between the fluorene and the PDI and conformational relaxation within the PFP backbone (also observed with the homopolymer, poly(fluorene-*alt*-phenylene). The fast process in water/dioxane (1:1, v/v) has a time constant of 60 ps, attributed to a combination of conformational relaxation and/or singlet exciton hopping processes along the chain [47] [144]. The longest time component, which dominates the decay, is clearly identified with the decay of the relaxed PFP relaxed structure. In agreement with previous studies on related conjugated polyelectrolytes [85], the component with 100 ps lifetime found in water is attributed to copolymer aggregates (clusters) and, hence, is not observed for the copolymer in water/dioxane, a better solvent for this polymer. The dominance (in terms of amplitudes) of the two shortest components in water and of the longest components in the water/dioxane (1:1, v/v) mixture is fully consistent with the suggestions from the PLQY data (Table 5.1), that excited state quenching is a consequence of aggregation.

5.2.1.5 Femtosecond fluorescence up-conversion and pump-and-probe experiments

The excited states of polyfluorenes have characteristic optical absorptions that can be divided into 1) singlet excited state absorption, 2) excited state absorption of the first triplet state and 3) absorption of charged species. Excited state absorption spectroscopy techniques are particularly useful for investigating the generation of non-emissive species such as triplet and charged states and its interaction with the singlet state [43]. Ultrafast transient absorption spectra can be measured with pump probe system, which can resolve spectra and decays with sub-picosecond resolution [43, 182]. As stated by Monkman *et al.* the accuracy of the singlet excited state induced absorption is made by comparison between the decay and excitation dependence of the absorption, with the stimulated singlet emission signal and the fluorescence lifetime [43,183–186]. Under high excitation powers, the formation and observation of other long-lived excited states is possible. These are charged species that after photoexcitation cause the separation of the electron and hole, leading to the formation of a pair of polaron-type (or charged transfer) charged states on adjacent chains [43, 187, 188]. In solution it is also possible to generate charged species, that can be formed by an electron transfer reaction with a strongly electron acceptor donor or solvent and, since these are "dark" states (their decay does not result in the emission of light) can be investigated by absorption techniques [43].

With the aim of further investigating the nature of any fast processes in aqueous and dioxane/water solutions of the PBS-PFP-PDI copolymer, such as the formation of a charge transfer (CT) or other short-lived states, ultrafast transient absorption experiments were performed. In the work by Fron *et al.* [160] femtosecond transient absorption in a PF-PDI copolymer reveals another deactivaction pathway for the copolymer that is dependent on the solvent polarity. When Frons' PF-PDI copolymer was dissolved in a THF solution, a rising signal at 730 nm on a nanometer time scale was observed. By contrast, in toluene solutions no rise signal was observed and the absorbing species detected in THF was attributed to the radical anion formation of the PDI chromophore (probably thought formation of a charge transfer state), since its absorbing wavelength region range has a correspondence to previous reported studies on the PDI radical anion [160, 164, 189]. In high polarity solvents the energetic position of the CT state is lower than the PDI local excited state (LES), due to an energetic stabilization induced by the polarity of the solvent, that leads to a change in the free energy of the charge separation and consequently ends with a CT state formation [160]. Based on the finding described by Fron *et al.* and according to the polarity of the solvents (dielectric constant ε: toluene 2.38 $\leq$ THF 7.58 $\leq$ water 80.16 [52]) it is expected that water will easily induce formation of a CT state in the polyelectrolyte PBS-PFP-PDI system.

Femtosecond fluorescence up-conversion experiments were performed in a water/dioxane (1:1, v/v) mixture of the PBS-PFP-PDI copolymer to attempt to obtain further insight into any fast processes, such as the formation of any charge transfer (CT) or other short-lived state, Figure 5.2.10.

However, we could not detect any fluorescence emission signal from the PDI moiety (600 nm) probably due its low quantum yield. Detection at 450 nm reveal a triexponential fluorescence decay with an 8 ps rise signal, a 60 and a 550 ps decay components (Figure 5.2.10). The decay components have identical lifetimes to those seen in the ps time-resolved measurements and whose attribution has already been discussed. The assignment of the fast risetime component is at present unclear, but may be related to a vibrational relaxation process within the first electronic excited state of the copolymer backbone.

Pump probe experiments have previously been conducted on PFs to characterize ultrafast processes such as the origin of the "green emission", attributed to the formation of a delocalized charge transfer state (CTS defect) which decays radiatively [43, 190, 191]. Similar CT states can be formed when PF chains are copolymerized with charge acceptors and PBS-PFP-PDI is a good example.

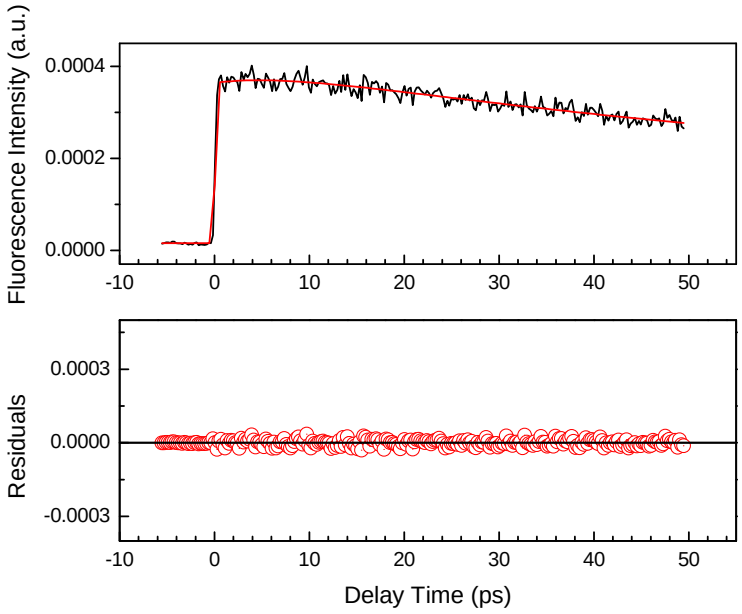

Figure 5.2.10: Femtosecond time resolved experiment of PBS-PFP-PDI in a water/dioxane (1:1, v/v) mixture. Excitation wavelength 370 nm and detection at 450 nm.

The PDI random repeat units have a strong acceptor character and may lead to the formation of stable, but non-emissive, CT or radical pair states. These states will alter the PBS-PFP-PDI copolymer photophysics, though are not necessarily observable in TCSPC or femtosecond fluorescence up-conversion experiments. Initial experiments using ns time resolution were unsuccessful, suggesting any transients formed have much shorter lifetimes. Instead, pump probe measurements with fs time resolution were performed, following exciting PBS-PFP-PDI solutions in the PFP band at 390 nm in water and water/dioxane mixture. The transient absorption spectra obtained are shown in Figures 5.2.11 and 5.2.12.

The transient absorption spectra in the two solvents (water and water/dioxane solutions) are very similar and show two photoinduced absorption bands at 550 and ca. 760 nm (Figure 5.2.12). In addition, there is stimulated emission at 470 nm. The longer wavelength and more intense absorption is fully formed within the timescale of the first measurement ($<$ 400 fs) and is attributed to the singlet exciton population of the PFP backbone (the literature value for polyfluorene excited singlet absorption is approximately 770 nm, 1.6 eV) [43]. The second broad band overlaps with the former and is centred around 500 - 550 nm. The kinetic results measured at 760 nm on long timescales ($>$ 10 ps) are consistent with the time constants obtained via TCSPC, Table 5.3 and Figure 5.2.13. However, additional short components (0.99 in water and 5.7 ps in water/dioxane) are detected, and feed the 500 - 550 nm photoinduced absorption band (Figure 5.2.12).

A tentative assignment of this short wavelength component can be made following pulse radiolysis studies on the polymers PF2/6 [192] and poly[2,7-(9,9-bis(2'-ethylhexyl)fluorene)-*alt*-1,4-phenylene] in chloroform solutions [193]. For these systems transient absorption spectra were observed with maxima around 540 - 560 nm, which were assigned unambiguously to the positively charged species (positive polarons, radical cations) of the polymers formed by one-electron oxidation reaction with the chloroform radical cation [192].

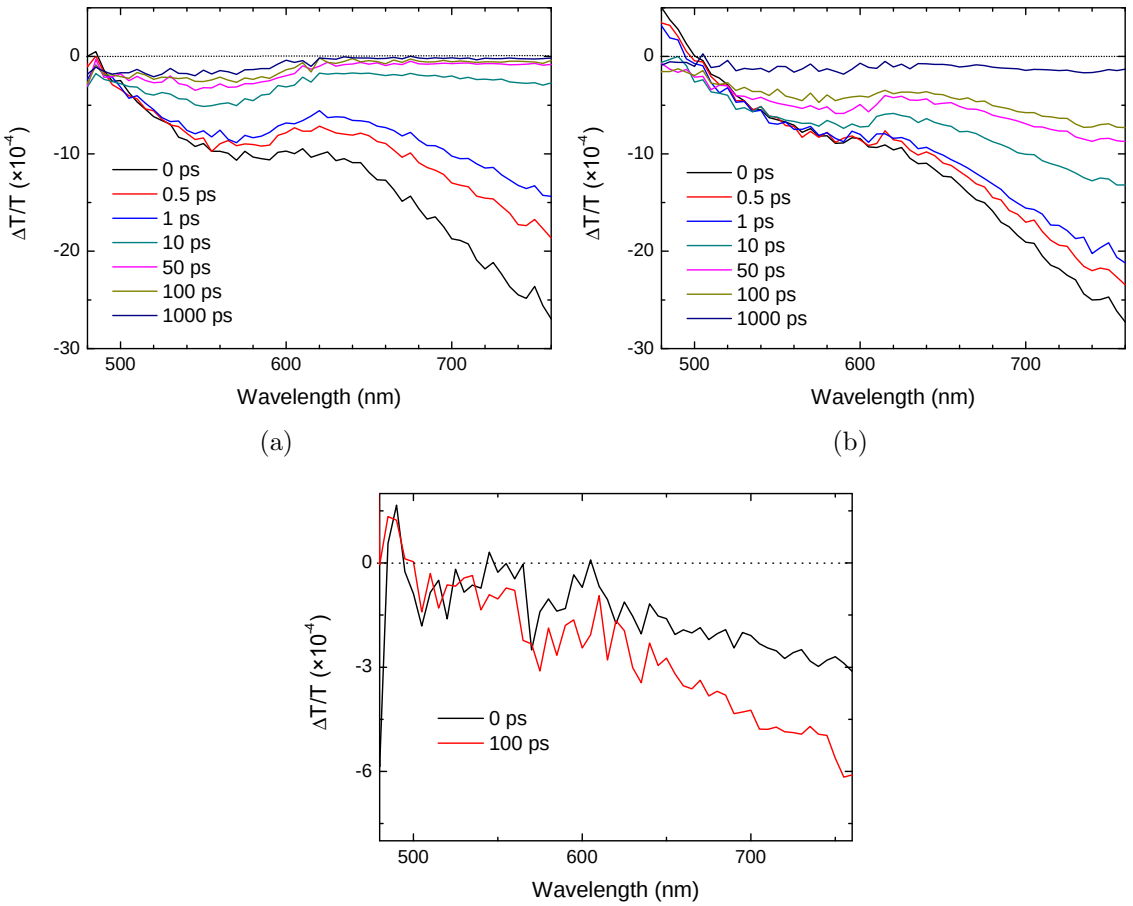

Figure 5.2.11: Evolution of the transient absorption spectra following excitation (390 nm) of PBS-PFP-PDI a) in water (5 μJ cm^{-2}), b) water/dioxane (1:1, v/v) (5.5 μJ cm^{-2}) and c) dilute water/dioxane (1:1, v/v) (19 μJ cm^{-2}) mixtures.

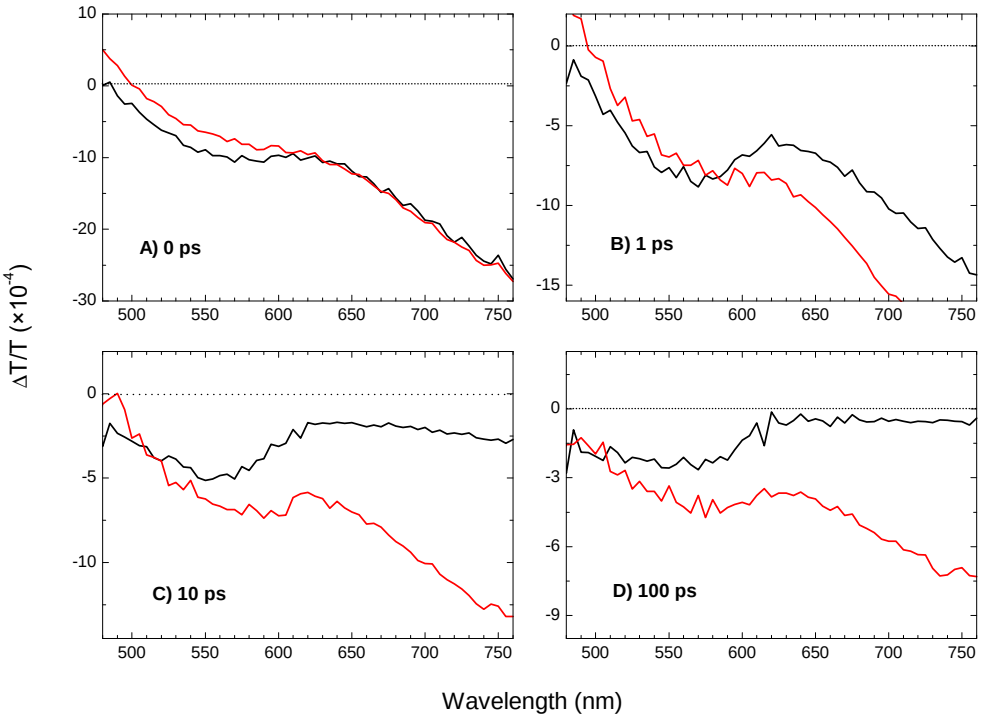

Figure 5.2.12: Evolution of the transient absorption spectra following excitation (390 nm) of PBS-PFP-PDI in water solution (black line) and water/dioxane (1:1, v/v) mixture (red line).

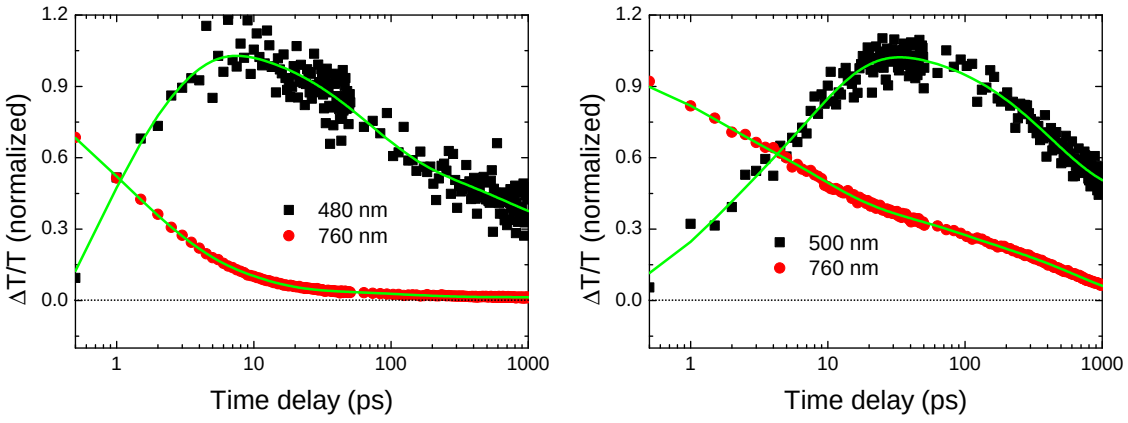

(a) (b)

Figure 5.2.13: Single-wavelength transient absorption kinetics of PBS-PFP-PDI, as recorded at selected probe wavelengths (as marked) in a) water and b) water/dioxane (1:1, v/v). The results of multi-exponential fitting have been included. A summary of the relevant fitting parameters is included in Table 5.3.

This suggests that upon excitation of PBS-PFP-PDI in water and dioxane-water, electron (or charge) transfer occurs from the polymer backbone to the PDI unit. In contrast, if singlet excitation energy transfer is the dominant pathway, it would be expected the PFP singlet excited state to decay with formation of the excited singlet state absorption (ESA) of PDI. The main peak at 685 nm is rather narrow while the second peak is broad. No significant transient absorption is seen in this region following decay of the PFP singlet exciton.

Table 5.3: Summary of fitting parameters from the collected transient absorption data, as obtained using the model of Equation 5.6. For the water and water/dioxane (1:1, v/v) solutions, the τ_1 component was linked as part of global fitting. An excellent fit to the data was obtained in all cases.

	λ_{max} (nm)	τ_1 (ns)	τ_2 (ns)	τ_3 (ns)	a_{i1}	a_{i2}	a_{i3}
I [a]	480	0.99±0.05	121±0.07	long	-1.63±0.05	0.62±0.01	0.42±0.01
	760	0.99±0.05	7±1	600±300	0.63±0.09	0.30±0.06	0.213
II [b]	500	5.7±0.2	470±40	long	-0.99±0.01	0.64±0.02	0.42±0.02
	760	5.7±0.2	60±30	600±300	0.47±0.02	0.14±0.05	0.28±0.03
III [c]	760	2.7±0.2	40±2	518±3	0.173±0.005	0.194±0.003	0.620±0.003

[a] water.

[b] water/dioxane (1:1, v/v).

[c] dilute water/dioxane (1:1, v/v).

$$\frac{\Delta T}{T} = a_{i1}e^{\frac{-t}{\tau_1}} + a_{i2}e^{\frac{-t}{\tau_2}} + a_{i3}e^{\frac{-t}{\tau_3}} \tag{5.6}$$

Furthermore, according to Janssen *et al.* [194] photoinduced electron transfer is more favorable in polar solvents due the stabilization of the charge-separated state. Therefore, in water or water co-solvent mixtures, fluorescence quenching of PFP by PDI involves predominantly electron or charge transfer, either on-chain or inter-chain. Aggregation is certainly ocurring in water and there are indications from the relative amplitudes of the fast polyfluorene decay components that it may also be present in dioxane-water at the relatively high concentrations used in these experiments.

It has been shown that although organic co-solvents do help break up aggregates of CPEs, it still occurs at high polymer concentrations, even in good solvents [195]. Therefore, pump-probe experiments were carried out in more dilute copolymer solutions in the

water/dioxane mixture, following excitation at 390 nm. Results are presented in Figure 5.2.11 c). It is clear, from both spectra and kinetic traces that there is no evidence for a long lived state in the 500 to 550 nm region, Figures 5.2.11 and 5.2.13; only fluorene singlet exciton photoinduced absorption was detected. With the PFP singlet photoinduced absorption at 760 nm (too short to be detected in the TCSPC measurements) may correspond to that seen in fluorescence upconversion. The remaining components are consistent with the TCSPC data. Overall, the results indicate that electron (or charge) transfer involves an interchain process.

5.2.2 PBS-PFP with on-chain porphyrin units

For red emission in fluorene based conjugated polymers, either polar moieties, such as electron donor substituted pyran derivatives, or non polar ones involving extensive π conjugation, such as perylene derivatives or porphyrin-type macrocyclic compounds have been studied [196], [197].

Porphyrin systems exhibit intense spectral response bands in the near-IR region and possess good chemical, photo-, and thermal stability and are excellent candidates for photovoltaic applications. Owing to appropriate HOMO and LUMO energy levels and very strong absorption of the Soret band (400 - 450 nm region), as well as, the Q-bands (500 - 700 nm region), porphyrin derivatives are sensitive to all colours of the spectrum; and, hence, are suited as photosensitizers for dye-sensitized solar cells (DSCs) [198], [199]. Their valuable photophysical properties [200] allow their use in a large number of practical applications apart from DSCs, such as molecular photonic devices and artificial photosynthesis systems [201–205]. Recently, two and three-dimensional (symmetrical) porphyrin arrays have been investigated [206]. The simplest of these involves linking a number of porphyrins together using covalent chemistry [207], [208] and the more complex assemblies have been prepared using noncovalent chemistry [209]. Furthermore, porphyrin dendrimers are able to mimic highly ordered ringlike structure of natural light-harvesting complexes [210]. Also, porphyrins bearing hydrophilic pendant groups interact with relevant biomolecules, such as nucleic acids, polypeptides and proteins [211]. In addition, porphyrins are excellent systems for testing models of electronic energy transfer in conjugated polymers [50, 51, 124, 212].

The ability to design molecules and integrate them into organic-organic and inorganic-organic composites provides a unique pathway in the formulation of materials for desired novel applications [213]. Systems involving PFs and red emitting porphyrins are particularly good candidates for FRET, because of the excellent spectral overlap between the donor emission and the acceptor absorption, as has previously been demonstrated [144, 184, 197, 214–216]. In particular, the Förster model for electronic energy transfer using point dipoles

appears to break down at small PF-porphyrin distances and the efficiency of energy transfer is suggested to show considerable differences if the two, D and A, moieties are colinear or cofacial [51].

An anionic poly(fluorene-*alt*-phenylene) with porphyrin units incorporated randomly on the backbone was synthesized, PBS-PFP-DPP and its singlet-singlet electronic energy transfer studied in solution.

5.2.2.1 Synthesis

The chemical sctrutures of DPP porphyrin and PBS-PFP-DPP copolymer are depicted in Figure 5.2.14. The reaction ratio of *n-x* to *x* is 90 to 10.

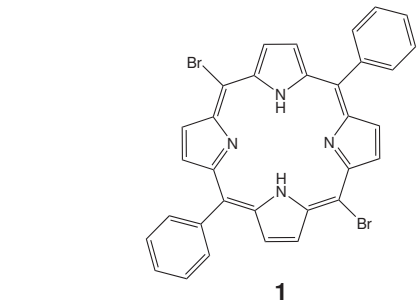

1

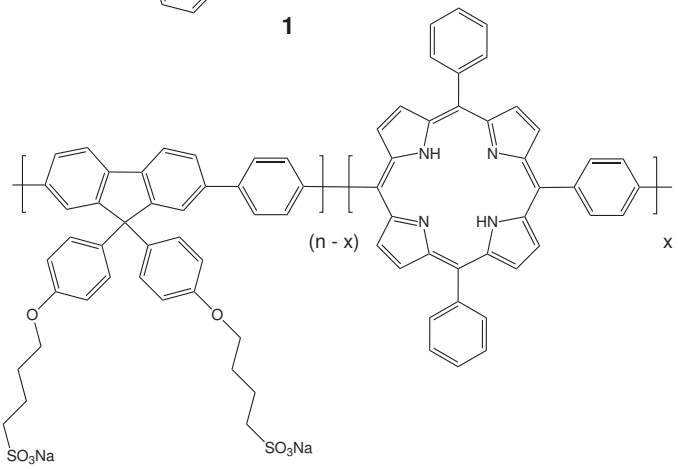

2

Figure 5.2.14: Chemical structures of the DPP monomer (1) and the copolymer PBS-PFP-DPP (2).

5,15-Dibromo-10,20-diphenylporphyrin **1**, DPP, was synthesized in the working group of Professor M. M. Pereira in the University of Coimbra, Portugal. The synthesis of dipyrromethane and 5,15-diphenylporphyrin was carried out with slight modifications of previously described methods [217] [218].

Dipyrromethane, ^{1}H NMR (600 MHz, $CDCl_3$): δ (ppm) = 7.7 (br s, 2H), 6.6 (m, 2H), 6.2 (ψq, 2H, J = 2.9 Hz), 6.1 (m, 2H), 4.0 (s, 2H).
^{13}C NMR (150 MHz, $CDCl_3$): δ (ppm) = 129.1, 117.3, 108.3, 106.4, 26.3.

5,15-Diphenylporphyrin, ^{1}H NMR (600 MHz, $CDCl_3$) : δ (ppm) = 10.3 (s, 2H, H*meso*), 9.4 (d, 4H, ^{3}J = 4.5, H_β), 9.1 (d, 4H, ^{3}J = 4.5, H_β), 8.3 - 8.3 (m, 4H, Ph-H_o), 7.8 - 7.8 (m, 6 H, Ph-$H_{m,p}$), -3.1 (br s, 2H, NH).
^{13}C NMR (150 MHz, $CDCl_3$): δ (ppm) = 147.2, 145.3, 141.4, 134.9, 131.6, 131.1, 127.7, 127.0.
MS(APCI-TOF), m/z: 462.176 M^+.

5,15-Dibromo-10,20-diphenylporphyrin, DPP **1**.
300 mg of 5,15-diphenylporphyrin (0.58 mmol) were dissolved in 300 mL $CHCl_3$ and 2.4 mL of pyridine. The mixture was cooled to 0 °C and 240 mg of N-bromosuccinimide (1.22 mmol, 2.1 eq) were added and the solution was stirred for 60 min. The reaction was quenched with acetone (50 mL) and the solvent was evaporated yielding a product that was washed with methanol [218]. Recrystallization from toluene/MeOH gave 347 mg of the title compound as purple crystals (0.56 mmol, 96%).
^{1}H NMR (400 MHz, $CDCl_3$): δ (ppm) = 9.62 (d, ^{3}J = 4.7 Hz, 4H, H_β), 8.8 (d, ^{3}J = 4.7 Hz, 4H, H_β): δ (ppm) = 8.2 - 8.1 (m, 4H, Ph-H_o), 7.8 - 7.7 (m, 6H, Ph-$H_{m,p}$), -2.7 (br s, 2H, NH).
The HOMO values of the DPP were measured using atmospheric pressure photoelectron spectrometry (Riken Keiki AC-2) and the LUMO calculated from the HOMO and optical band-gap (determinated via the intersection of the absorption and emission thin film spectra) [219–221].
HOMO = -5.04 eV and LUMO = -3.17 eV.

{*Poly1,4-phenylene*}-*co*-{*[9,9-bis(4-phenoxy butylsulfonate)]fluorene-2,7-diyl-alt*-{*1,4-phenylene(5,15-diphenylporphyrin)*}, PBS-PFP-DPP **2**.
For the preparation of the copolymer PBS-PFP-DPP, a mixture of 2,7-dibromo-9,9-bis(4-sulfonylbutoxyphenyl)fluorene (0.742 g, 0.90 mmol), 5,15-dibromo-10,20-diphenylporphyrin, DPP (0.062 g, 0.10 mmol), 1,4-benzenediboronic acid (0.166 g, 1 mmol), $Pd(PPh_3)_4$ (50 mg) and Na_2CO_3 (1.0 g, 9.4 mmol) in 40 mL of THF and 20 mL water, were reacted for 4 days at 110 °C. The aqueous layer was washed with chloroform and concentrated to dryness. The residue was extracted with dichloromethane via Soxhlet, redissolved in a mixture of water and THF 50% (v/v) and purified by dialysis using a membrane with a cut-off of

3500 g·mol^{-1}. Based on the monomer/DPP ratio in the starting reaction mixture, the copolymer is expected to contain on average 10% (mole percent) DPP units. Total yield of the copolymer PBS-PFP-DPP was 655 mg (91%). The copolymer decomposition temperature was estimated as 390 °C by TGA.
^{1}NMR (600 MHz, d-dioxane 50% D_2O): δ (ppm) = 8.9 - 8.9 (ar-H DPP), 8.2 - 6.6 (ar-H DPP and ar-H fluorene), 4.1 - 3.9 (CH_2, α), 3.0 - 2.9 (CH_2, γ), 2.0 - 1.9 (CH_2, β and σ).
GPC (NMP, LiBr, UV-detection 360 nm) Mn = 1000 g·mol^{-1}, Mw = 1400 g·mol^{-1}, PD = 1.4.

5.2.2.2 Steady state measurements

The anionic copolymer poly(fluorene-*alt*-phenylene)-porphyrin (PBS-PFP-DPP) (Figure 5.2.14) was studied by UV-vis absorption, photoluminescence (PL) spectroscopy and time-resolved fluorescence (TCSPC) measurements. Anionic fluorene based conjugated polyelectrolytes tend to aggregate in aqueous solution to form ill defined clusters [123]. To minimize the aggregation, measurements have been made in a water/dioxane (1:1, v/v) solution mixture and in aqueous solutions of 1×10^{-4} M non-ionic surfactant n-dodecylpentaoxyethylene glycol ether, $C_{12}E_5$.

In both solvent systems two characteristic absorption regions are observed in the UV-vis absorption spectrum, which are attributed to the poly(fluorene-*alt*-phenylene) backbone (broad absorption at 365 nm) and to the on-chain porphyrin (DPP) units (various bands between 420 and 650 nm) Table 5.4, Figures 5.2.15 and 5.2.16.

Table 5.4: Parameters of PBS-PFP-DPP in water/dioxane (1:1, v/v) mixture and 1×10^{-4} M aqueous $C_{12}E_5$ solution.

Solvent	Absorption λ_{max} (nm)	Emission λ_{em} (nm)	ϕ_F PF [ab]	ϕ_F DPP [ab]
water/dioxane	365, 420 (PF, DPP)	410, 650 (PF, DPP)	0.41	0.013
aqueous $C_{12}E_5$	367, 425 (PF, DPP)	411, 655 (PF, DPP)	0.34	0.017

[a] PLQY were determined using quinine sulphate in 0.5 M H_2SO_4.
[b] Measured with excitation at the PF absorption maximum.

The strong, narrow absorption peak at 420 nm and the four smaller absorption peaks between 520 and 650 nm correspond to the so-called "Soret" and "Q" bands, respectively,

typical of porphyrins [222]. The presence of four absorptions in the Q band region, corresponding to the (0,0) and (0,1) vibronics of the Q_x and Q_y bands, confirms that the porphyrin is present as its free base. Excitation of PBS-PFP-DPP at 365 nm leads to emission from both PF and DPP, while excitation at 420 nm shows only emission from the DPP units (Figures 5.2.15 and 5.2.16).

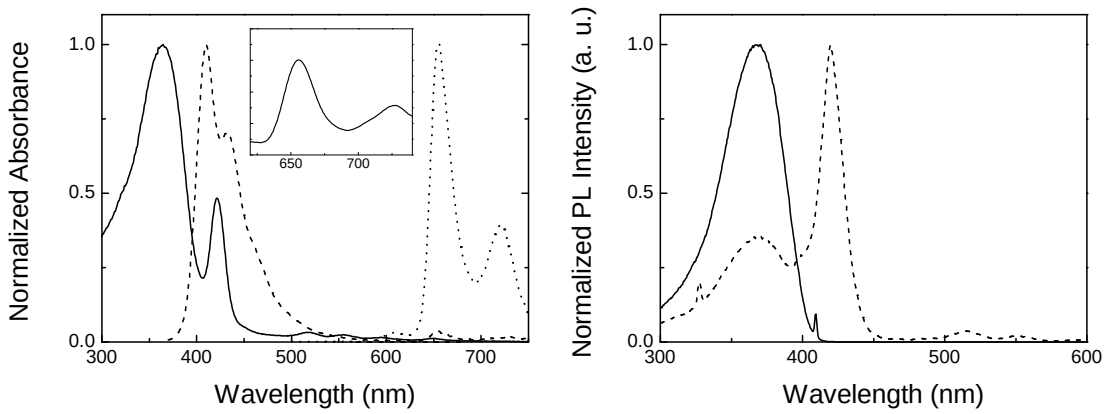

Figure 5.2.15: Left, absorption and emission spectra of PBS-PFP-DPP in water/dioxane (1:1, v/v) mixture, with excitation at 365 nm (dashed line) and 420 nm (dotted line). The inset depicts the 600 - 750 nm region of the PBS-PFP-DPP emission shown in the main plot. Right, fluorescence excitation spectra with emission at 410 nm (solid line) and emission at 655 nm (dashed line) of PBS-PFP in water/dioxane.

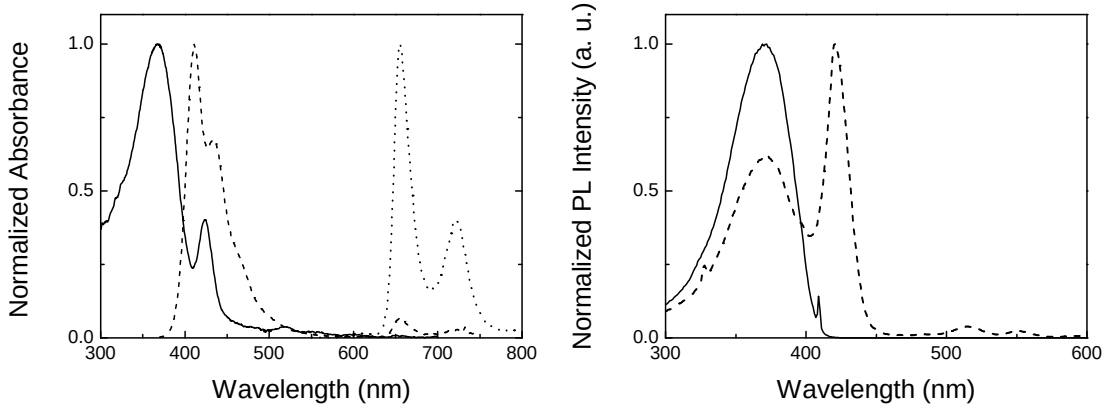

Figure 5.2.16: Left, absorption and emission spectra of PBS-PFP-DPP in 1×10^{-4} M aqueous $C_{12}E_5$ solution, with excitation at 365 nm (dashed line) and 420 nm (dotted line). Right, fluorescence excitation spectra with emission at 410 nm (solid line) and emission at 655 nm (dashed line) of PBS-PFP in 1×10^{-4} M aqueous $C_{12}E_5$.

Fluorescence excitation spectra for emission in the porphyrin region reveals two maxima in the PF and DPP region, demonstrating efficient electronic energy transfer from the fluorene to the porphyrin units. However, differences in the relative intensities are observed between water/dioxane and in 1×10^{-4} M aqueous $C_{12}E_5$ solutions. In particular, the ratio of PF to DPP intensities is higher in $C_{12}E_5$ solution than in water/dioxane. Small angle X-ray scattering (SAXS), cryotransmission electron microscopy, molecular dynamics simulations [127], together with small angle neutron (SANS) scattering on PBS-PFP solutions with $C_{12}E_5$ [126], strongly suggest that in the presence of surfactant, the conjugated polymer is present as a mixed cylindrical aggregate in which the polymer backbone is surrounded by a layer of surfactant molecules. The surfactant is expected to cause the following effects on the PBS-PFP-DPP copolymer: increasing its backbone rigidity and decreasing the solvent access to the PFP chain. Given the increased rigidity of the PBS-PFP-DPP system, on-chain exciton migration will be facilitated and consequently, the efficiency of energy transfer to the porphyrin unit enhanced.

Photoluminescence quantum yield (PLQY) measurements made for the PBS-PFP-DPP copolymer dissolved in the two solvent systems, water/dioxane (1:1, v/v) and aqueous $C_{12}E_5$ solution, are presented in Table 5.4. The energy transfer quantum yields for PFP to DP units is greater in $C_{12}E_5$ solution than in water/dioxane co-solvent. As discussed above this may be associated with the decrease in the copolymer conformational disorder when encapsulated by the surfactant. There is a slight decrease in the PLQY values for the copolymer PBS-PFP-DPP compared with that of the polymer without the porphyrin chromophore, PBS-PFP, for the same solvents, 0.52 in water/dioxane and 0.55 in $C_{12}E_5$ (see chapter 4). In part, this may result from photogenerated excitons being transferred to the DPP units. However, the sum of PLQY for the PF and DPP units emission is, in both cases, inferior to that of PBS-PFP in the two solvents [124], [123], indicating that some other mechanism is also involved.

As shown in Figure 5.2.17, there is a strong overlap between the 0-0 emission band of the homopolymer PBS-PFP and the Soret absorption of the DPP. As the emission from the Soret band is weak, it acts as a "dark" state and the emission arises preferentially from the lowest energy Q_x band [184].

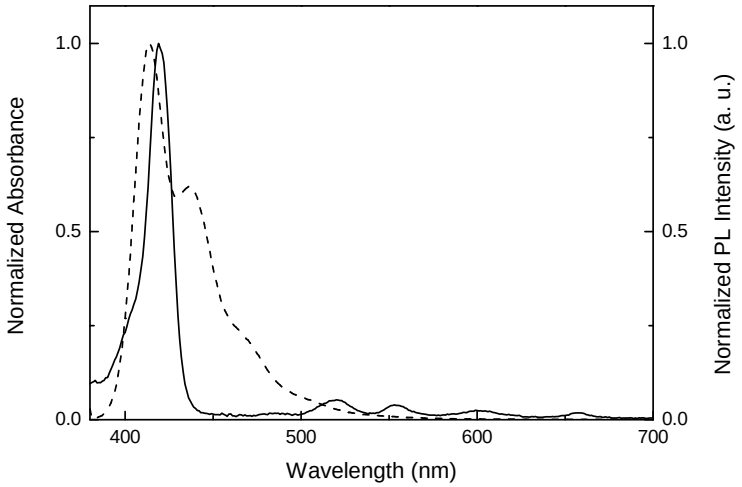

Figure 5.2.17: Spectral overlap between the donor PBS-PFP emission (dashed line) and the acceptor DPP absorption (full line).

5.2.2.3 Time-resolved fluorescence measurements

Fluorescence decays were obtained in the water/dioxane (1:1, v/v) mixture and aqueous 1×10^{-4} M $C_{12}E_5$ solution, on excitation in the PFP unit (372 nm) and collected at the PF and DPP emission maximum (Figures 5.2.18, 5.2.19 and Table 5.5). A value of 550 - 590 ps (τ_3) that dominates the decay, together with a shorter lifetime value of ca. 50 - 60 ps (τ_1) is found when the data is collected at 410 nm (Figures 5.2.18 and 5.2.19) in agreement with previous observations [45]. The longer decay lifetime (τ_3) has a value very close to the previously described for PBS-PFP dispersed in the $C_{12}E_5$ micellar system [124], [128] and is attributed to the natural decay of the PF backbone [124]. The fast component (τ_1) is suggested to be related either to the formation of an initially formed non-relaxed conformer, that decays giving rise to a more stable one [45], or to on-chain energy transfer process [45]. Nevertheless, sums of two and three discrete exponentials functions (dependent on the solvent system used) were needed to fit the excited state data collected at 650 nm (Figures 5.2.18 and 5.2.19).

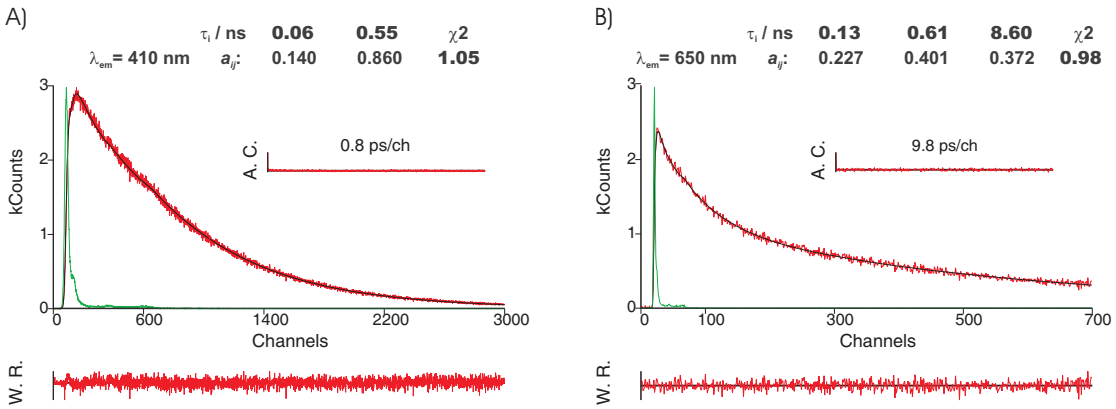

Figure 5.2.18: Fluorescence emission decay for PBS-PFP-DPP in water/dioxane (1:1, v/v) mixture obtained with λ_{exc} 372 nm at 298 K and collected at A) 410 nm and B) 650 nm. The green lines in the decays are the instrumental response function (IRF). For a better judgment of the quality of the fits weighted residuals (W.R., scale $-3 \leq \sigma \leq +3$) autocorrelation functions (A.C.) and chi-square values (χ^2) are also presented.

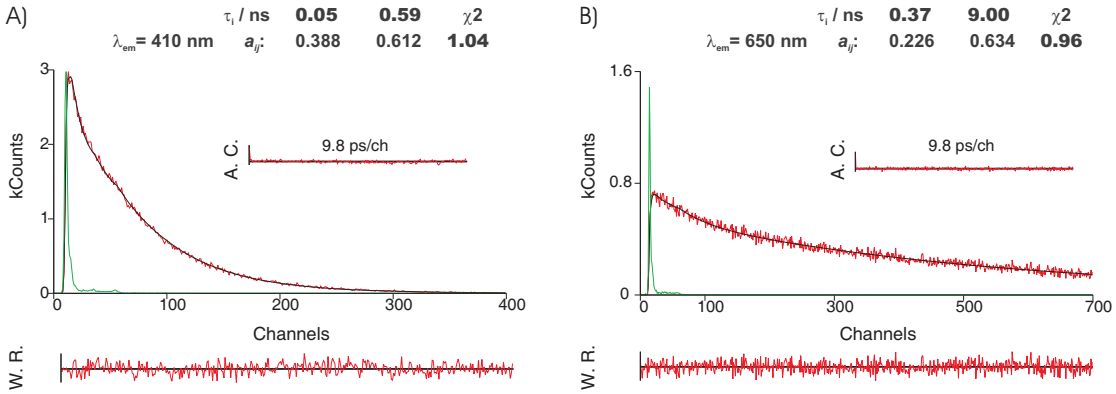

Figure 5.2.19: Fluorescence emission decay for PBS-PFP-DPP in 1×10^{-4} M aqueous $C_{12}E_5$ obtained with λ_{exc} 372 nm at 298 K and collected at A) 410 nm and B) 650 nm. The green lines in the decays are the instrumental response function (IRF). For a better judgment of the quality of the fits weighted residuals (W.R., scale $-3 \leq \sigma \leq +3$) autocorrelation functions (A.C.) and chi-square values (χ^2) are also presented.

Table 5.5: Fluorescence decay times (τ_i) and pre-exponential factors (a_{ij}) for the copolymer PBS-PFP-DPP, obtained with excitation at 372 nm, emission at the wavelength maxima and T = 298 K.

	λ_{max} (nm)	τ_1 (ns)	τ_2 (ns)	τ_3 (ns)	τ_4 (ns)	a_{i1}	a_{i2}	a_{i3}	a_{i4}	χ^2
water/dioxane	410	0.06	—	0.55	—	0.140	—	0.860	—	1.05
	650	—	0.13	0.61	8.60	—	0.227	0.401	0.372	0.98
aqueous $C_{12}E_5$	410	0.05	—	0.59	—	0.388	—	0.612	—	1.04
	650	—	0.37	—	9.00	—	0.366	—	0.634	0.96

In water/dioxane, an intermediate decay component of 130 ps is observed. A similar decay time of approximately 130 ps has been reported previously for the cluster morphology adopted by polyelectrolytes in solution [85]. However, this seems unlikely in the present case and in agreement with suggestions of a closely related self-assembled porphyrin/conjugated polyelectrolyte system, the nature of the time constant is more likely to be related with exciton migration along the polymer chain [144]. This component becomes longer lived (370 ps) and more important in $C_{12}E_5$ solutions, the system showing more efficient energy migration from PFP to DPP units. The 8.60 - 9.00 ns decay lifetime collected at 650 nm is assigned to emission from the DPP units, in agreement with the values published for PPV and PF doped with porphyrins [216], [223].

5.2.2.4 Meso-tetrakisphenylporphyrinsulfonate self-assembled with PBS-PFP via calcium (II) binding

With PBS-PFP-DPP, the porphyrin is expected to be collinear with the PF units. A second PF-porphyrin energy transfer system in which the anionic porphyrin meso-tetrakisphenylporphyrinsulfo-nate (TPPS) is self-assembled by calcium(II) ions to the homopolymer PBS-PFP (Figure 5.2.20), will be discussed in this subchapter. In this new system the PF and porphyrin units are expected to be cofacial [51].

Pinto *et al.* have previously described the photophysics of a cationic PF system self-assembled by electrostatic interactions to TPPS [144]. These self-assembled systems have the advantage that by tuning the solvent and stoichiometry, it is possible to control the amount of porphyrin and, possibly, structural morphology and disorder of the materials. The characterization of the hydrophilic porphyrin has been described elsewhere [224]. The absorption and emission spectra of PBS-PFP were recorded in the same solvents used with

PBS-PFP-DPP, water/dioxane (1:1, v/v) and 1×10^{-4} M aqueous $C_{12}E_5$ (above the surfactant critical micelle concentration, cmc = 6.5×10^{-5} M in water at 25 °C [225]). Calcium^{2+} modulates the self-assembly between the two negatively charged components. Energy transfer from the PBS-PFP to the anionic porphyrin is evident from the PL spectra (Figure 5.2.21).

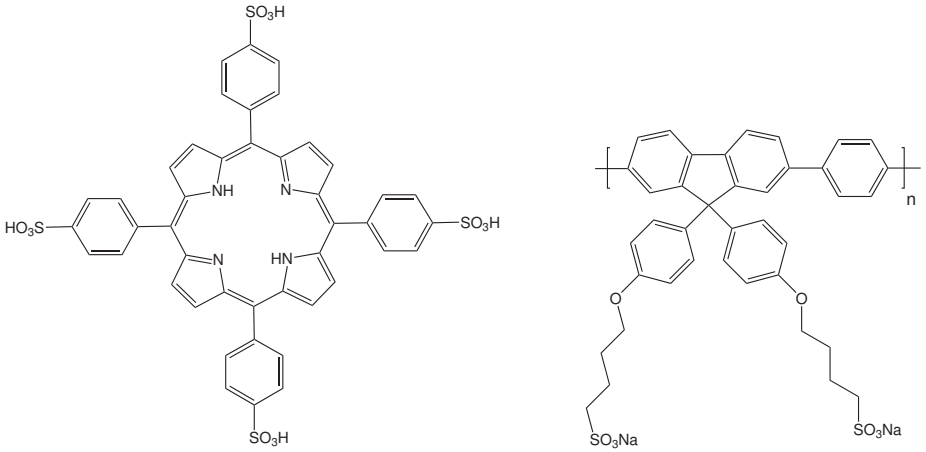

Figure 5.2.20: Chemical structures of the electronic energy acceptor TPPS (1) and the anionic donor copolymer PBS-PFP (2).

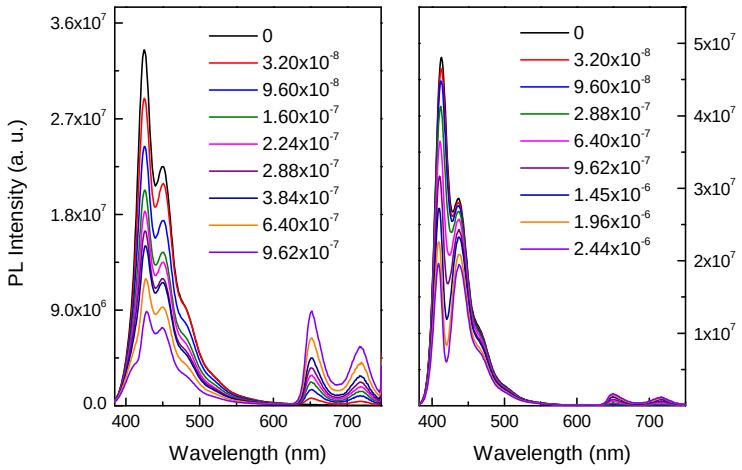

Figure 5.2.21: Photoluminescence spectra of PBS-PFP/Ca^{2+} with increasing TPPS concentrations in water/dioxane (1:1, v/v) (left) and in 1×10^{-4} M aqueous $C_{12}E_5$ solutions (right). Ca^{2+} concentration 2×10^{-3} M.

By adding different concentrations of porphyrin to the polyelectrolyte at fixed Ca^{2+} concentration (2×10^{-3} M) there is a decrease in the fluorescence band in the PF region and a corresponding increase in the emission band of the TPPS (λ_{max} = 650 nm). The quenching effect is most pronounced when the polyelectrolyte is dissolved in the water/dioxane co-solvent solution mixture, Figure 5.2.22.

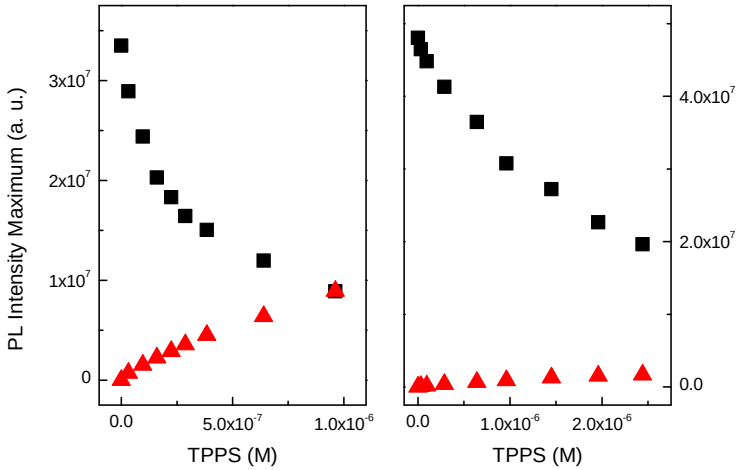

Figure 5.2.22: Photoluminescence maximum intensity as a function of TPPS concentration in water/dioxane (1:1, v/v) (left) and in 1×10^{-4} M aqueous $C_{12}E_5$ solution (right). PBS-PFP emission (squares) and TPPS emission (triangles).

Significant differences are seen in energy transfer from PF to porphyrin units in the on-chain and self-assembled systems, in agreement with the predictions of Wong *et al.* [51]. In addition to the of orientation effect of the donor-acceptor units, other non-radiative deactivaction processes may be possible in the PBS-PFP-DPP copolymer, including charge transfer, triplet formation, exciton - exciton annihilation and molecular excimer formation [184, 226, 227]. However, given the low light intensity and dilute solutions used, the latter two processes are unlikely.

For the self-assembled system, control experiments of the effect of 2×10^{-3} M Ca^{2+} on the PL of the PBS-PFP copolymer solutions were also performed and no significant differences were observed in the spectral shape or maximum, as depicted in Figure 5.2.23. Nevertheless, the PLQY decreases in the presence of Ca^{2+} as a consequence of the metal interaction with the polar copolymer side chains inducing its aggregation [152]. The photoluminescence deactivation by Ca^{2+} of the copolymer in the water/dioxane mixture is 30% more effective than in the surfactant solution (see Figure 5.2.23). The spectral changes observed in the PL spectra (Figure 5.2.24) are mainly due to the strong attenuation by the overlap of the absorption of the porphyrin Soret band and the PBS-PFP copolymer

fluorescence (Figure 5.2.17) [144]. PBS-PFP emission quenching is more pronounced in the water/dioxane mixture (Figure 5.2.21 and Table 5.6) since calcium ion induces strong copolymer-aggregation [152] and the large aggregates are likely to favour energy transfer from multiple PBS-PFP units towards TPPS.

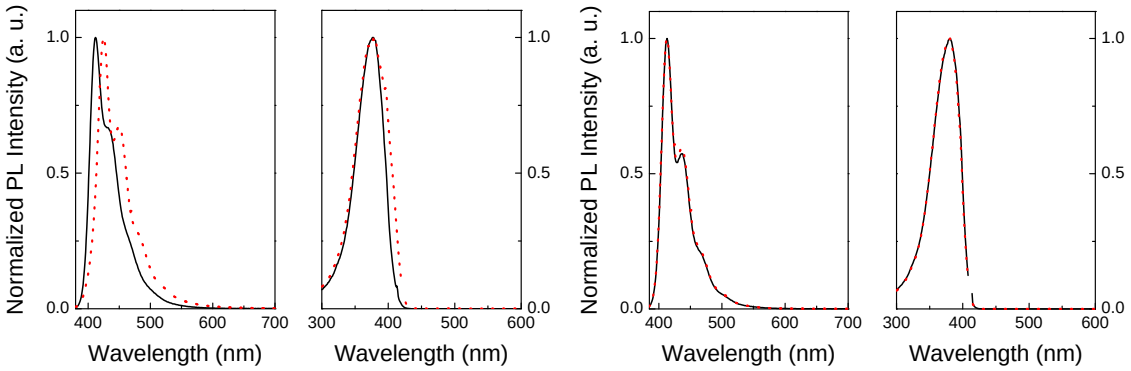

Figure 5.2.23: Emission and excitation spectra of PBS-PFP (10^{-6} M) a) in water/dioxane (1:1, v/v) with excitation at 375 nm and emission at 414 nm and b) 1×10^{-4} M aqueous $C_{12}E_5$, with excitation at 378 nm and emission at 412 nm. Solid line in the absence of Ca^{2+} and dotted line with 2×10^{-3} M Ca^{2+} in solution.

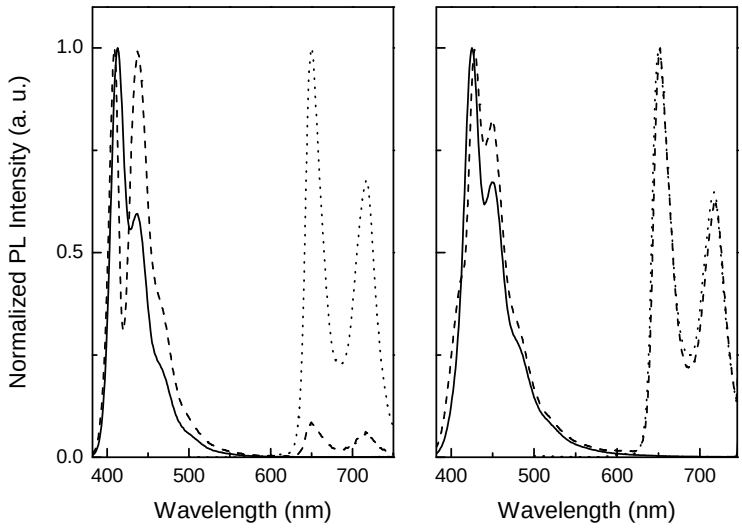

Figure 5.2.24: Photoluminescence spectra of PBS-PFP without TPPS (solid line) and with maxima TPPS concentration (dashed line), obtained with excitation in the PF absorption maximum and TPPS emission (dotted line) obtained with excitation at 420 nm, in water/dioxane (1:1, v/v) (right) and in 1×10^{-4} M aqueous $C_{12}E_5$ (left).

In contrast, for the self-assembled system in the presence of the non-ionic surfactant, a lower PLQY was found for the TPPS upon excitation of PBS-PFP (Table 5.6). It is known that $C_{12}E_5$ wraps around the copolymer forming supramolecular structures that shield the CPE from the aqueous solvent [141], [222]. This means that calcium ions are likely to only bind to the exposed sulfonate groups on a single PBS-PFP chain, such that energy transfer is from one CPE molecule to the bound porphyrin.

Table 5.6: Photoluminescence quantum yields of PBS-PFP/Ca^{2+} self assembled with TPPS in water/dioxane (1:1, v/v) and 1×10^{-4} M aqueous $C_{12}E_5$ (Ca^{2+} concentration 2×10^{-3} M).

Solvent	TPPS (M)	ϕ_F PF [a] λ_{exc} 382 (nm)	ϕ_F TPPS [b] λ_{exc} 382 (nm)
water/dioxane (1:1, v/v)	2.44×10^{-6} M	0.06	0.07
1×10^{-4} M $C_{12}E_5$	2.44×10^{-6} M	0.05	0.03

[a] PLQY were determined using quinine sulphate in 0.5 M H_2SO_4.
[b] PLQY were determined using tetraphenylporphyrin in toluene.

Fluorescence decays of the system PBS-PFP+Ca^{2+}+TPPS, with increasing anionic porphyrin concentration were collected at the PBS-PFP emission maxima. The decays were fitted with sums of three discrete exponential functions and the corresponding decay times and amplitudes, as a function of the porphyrin concentration, were plotted, Figure 5.2.25.

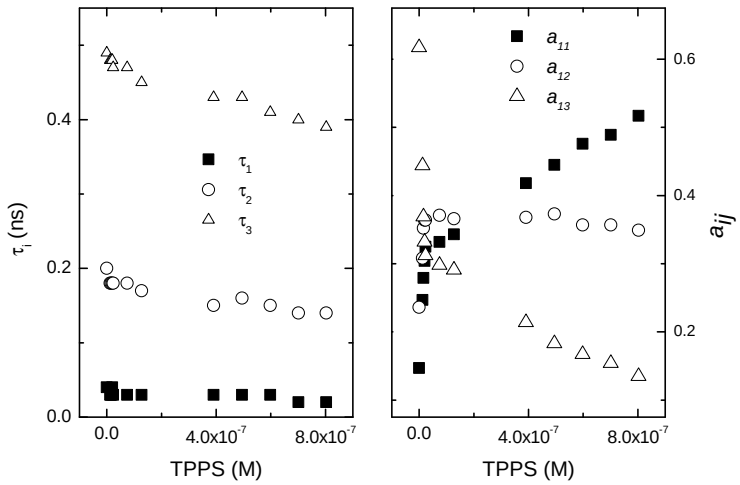

Figure 5.2.25: Fluorescence decay times (τ_i) and amplitudes (a_{ij}) of PBS-PFP (10^{-6} M) with Ca^{2+} (1×10^{-3} M) in 1×10^{-4} M aqueous $C_{12}E_5$ as a function of TPPS concentration.

The dependence of the decay times and amplitudes, presented in Figure 5.2.25 is similar to the behaviour observed for the system involving the cationic fluorene based polyelectrolyte HTMA-PFP and different anionic hydrophilic porphyrins [144]. The long component (τ_3) has a value very close to that previously reported for PBS-PFP with $C_{12}E_5$ in water [124] and the presence of calcium does not seem to affect the lifetime of the polyelectrolyte (Figure 5.2.26). The PBS-PFP lifetime is, as previously observed in the PL data, quenched with increasing porphyrin concentration (Figure 5.2.25). Attribution of the fastest component (τ_1 ca. 20 ps for a TPPS concentration of 8.03×10^{-7} M) is still troublesome and it has been attributed to both energy transfer and conformational relaxation of the copolymer chain [144] [45]. However, with the present system and based on the decay profile and data of Figure 5.2.27, a rise time (ca. 7 ps at 8.03×10^{-7} M TPPS) is attributed to the fast component, providing evidence that energy transfer is taking place and dominating the deactivation pathways occurring in the excited states of the self-assembled donor/acceptor system. The origin of the intermediate lifetime component, τ_2, has been discussed previously and attributed to exciton migration, either on-chain or intra-chain (within aggregates) [85], [144].

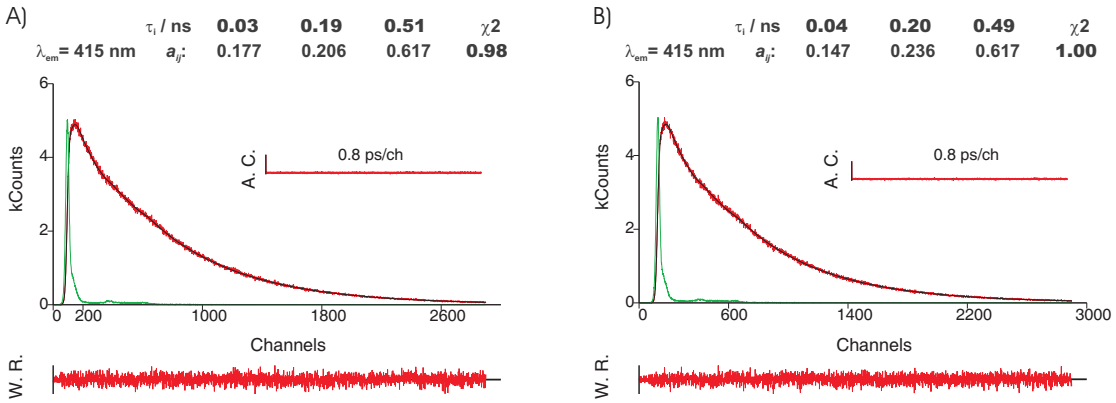

Figure 5.2.26: Fluorescence emission decay for PBS-PFP (10^{-6} M) in aqueous 1×10^{-4} M $C_{12}E_5$ at 415 nm, obtained with λ_{exc} 392 nm at 298 K and collected at A) in the absence of Ca^{2+} and B) with 1×10^{-3} M Ca^{2+} in solution. The green lines in the decays are the instrumental response function (IRF). For a better judgment of the quality of the fits weighted residuals (W.R., scale $-3 \leq \sigma \leq +3$) autocorrelation functions (A.C.) and chi-square values (χ^2) are also presented.

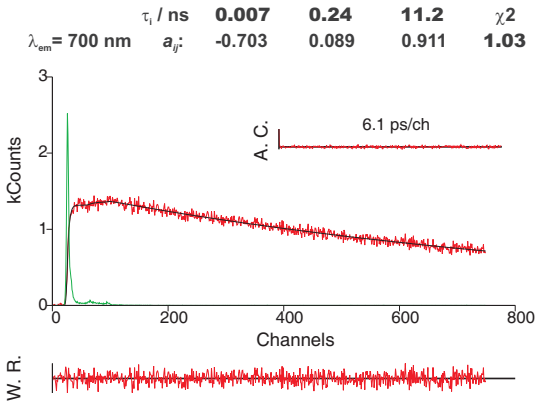

Figure 5.2.27: Fluorescence emission decay for PBS-PFP (10^{-6} M) in aqueous 1×10^{-4} M $C_{12}E_5$ at 700 nm and at the maximum TPPS concentration, obtained with λ_{exc} 392 nm at 298 K. The green lines in the decays are the instrumental response function (IRF). For a better judgment of the quality of the fits weighted residuals (W.R., scale $-3 \leq \sigma \leq +3$) autocorrelation functions (A.C.) and chi-square values (χ^2) are also presented.

The FRET of the self-assembled system is always more efficient when compared to the PBS-PFP-DPP copolymer. This resembles the behaviour described for MEH-PPV porphyrin blends [228]. As demonstrated by Morgado and co-workers the distribution of the porphyrin chromophore within the polymer does not match the one for the self-assembled system and the copolymer. Hence, the differences in the efficiency of the energy transfer and the concentration quenching effects might contribute for the observations. The results are also in complete agreement with the ideas of Wong *et al.* on cofacial energy transfer in PF-porphyrin systems being more efficient than in the collinear case [51].

Although the porphyring ring and polymer backbone may not be perfectly parallel, a small deviation from cofacial geometry is not likely to significantly affect the FRET efficiency. Despite the questioned validity of the use of point dipoles in Förster theory [41], [42], to treat electronic energy transfer between these donor and acceptor units, it is instructive to compute the Förster radius R_0. Table 5.7 comprises the R_0 values for the PBS-PFP-DPP copolymer and the self-assembled system PBS-PFP/TPPS. As expected, the R_0 value vary for the two systems according to PBS-PFP/TPPS $\leq$ PBS-PFP-DPP (R_0 for PBS-PFP-DPP is $\approx$ to 60 Å). However, the efficiency of the porphyrin PL runs counter the expectation on the basis of the Förster theory, as the copolymer PBS-PFP-DPP is the least efficient, despite the larger R_0 values [229]. As mentioned before, other factors than the Förster efficiency govern the PBS-PFP-DPP copolymer PL efficiency [229].

Overall, the computed values calculated for the Förster distance are comparable to what had been determined for the singlet-singlet Förster transfer, of fluorene-based poly-

electrolytes and oppositely charged complexes and porphyrins [128, 144, 229, 230].

Table 5.7: Computed Förster radius, R_0, for the PBS-PFP-DPP copolymer and self-assembled system PBS-PFP/TPPS.

Solvent	System	R_0 (Å)
water/dioxane	PBS-PFP-DPP	62
	PBS-PFP/TPPS	47
aqueous $C_{12}E_5$	PBS-PFP-DPP	61
	PBS-PFP/TPPS	50

5.2.3 PBS-PFP with on-chain thiophene/benzothiadiazole derivative units

Polymeric devices based on polyfluorenes (PFs) have disadvantages related to their inefficient injection of charges into the polymer layer, as well as, the tendency to form long wavelength green defects (attributed to excimers or ketonic defects) in the solid state [78, 231, 232]. The incorporation of conjugated heterocyclic acceptor units greatly influences the properties of this CP, helping to overcome the PF drawbacks and facilitate the control of the optoelectronic properties [231–233]. Typical, aromatic heterocyclic acceptors involve electron deficient nitrogen containing compounds, such as benzo[1,2,5]thiadiazole (BTD) and quinoxaline [234–237]. BTD based polymers possess particularly interesting electro-optical properties and have found applications in photovoltaics, electroluminescence devices and field-effect transistors [27, 238–240].

Copolymers featuring PFs with BTD units and thieno[3,2-b]thiophene have already been synthesised and their performances tested for PLED applications and photovoltaic cells [11, 231, 241–248]. The properties of the BTD group can be modulated by linkage to other units such as thiophenes (e.g. the 4,7-di(thiophen-2-yl)benzo[c][1,2,5]thiadiazole - TBTT) [249–251] and, thus, the strength of the intramolecular charge transfer (ICT) interaction between the electron donor (D) and electron acceptor (A) units can extend the absorption bands into the near-infrared [243, 252–255].

Recenty, sensors based on semiconducting polymer dots (Pdots) and luminescent vesicles based on conjugated organic chromophores, such as BTD and TBTT have been reported [256–259]. The vesicles, are obtained either by dispersion of an organic solution of the

material in water, or by cooling in a hydrocarbon solvent. Their colour can be tuned from blue to red, by adjusting the energy of the singlet excited state and the compounds can be mixed in varying proportions without affecting aggregate morphology. The palette of colours each individual is capable to generate, covers more than 75% of the scope of current liquid crystalline displays (LCDs) [259].

A variety of fluorescent sensors based on electron or energy transfer have been developed to take advantage of aggregation between water-soluble conjugated polyelectrolytes (CPEs) and added analytes [229, 260, 261]. To overcome the drawback of CP properties in aqueous solution, such as low fluorescence quantum yield, poor solubility and unpredictable sensor response, induced by their strong propensity to self-assemble into aggregates [262–265], conjugated polyelectrolytes that feature sterically congested, branched polyionic side groups were synthesised. In order to modulate their photophysical properties, BTB and TBTT were introduced into the CPE backbone [139]. Such water soluble CPs with on-chain BTD and TBTT units offer good opportunities to avoid interfacial mixing, upon fabrication of multilayer polymer optoelectronic devices by solution processing and, can dramatically improve charge injection from high work function metal cathodes that greatly enhance the device performance [88].

Two anionic water soluble poly(fluorene-*alt*-phenylene) copolymers, with different percentages of the red-emitting chomophore 4,7-di(thiophen-2yl)benzo[c][1,2,-5]thiadiazole - TBTT - randomly distributed along the polymer chain, were synthesised via Suzuki coupling. For energy transfer studies the phenyl spacer was replaced by a non-conjugated monomer and the results obtained of the new PBS-PFP-TBTT copolymer compared to the previous fully conjugated TBTT copolymers. In addition, an anionic PFP copolymer containing blue-, green and red light emitting moieties was synthesized via the same route. All the copolymers with on-chain thiophene derivatives units were fully characterized.

5.2.3.1 Synthesis of PBS-PFP-TBTT copolymers

The strutures of the TBTT monomer and the PBS-PFP-$TBTT_x$ copolymers are depicted in Figure 5.2.28 and the polymerization results in Table 5.8. The reaction ratio of n-x to x is 90 to 10 for PBS-PFP-$TBTT_{10}$ and 80 to 20 for the PBS-PFP-$TBTT_{20}$.

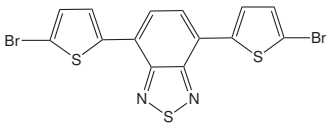

1

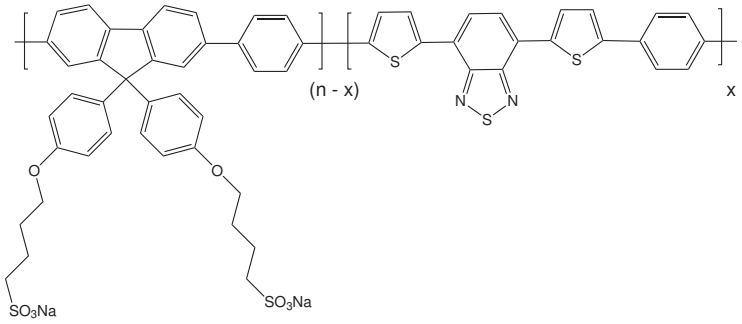

2

Figure 5.2.28: Structures of the TBTT monomer (1) and the copolymers PBS-PFP-TBTT$_x$ (2).

4,7-bis(5-bromothiophen-2-yl)benzo[c][1,2,5]thiadiazole (TBTT) **1**, was synthesised according to the procedures reported in the literature [255, 266–268] [1].
^{1}H NMR (400 MHz, CD_2Cl_4, 353 K): δ (ppm) = 7.1 -7.1 (d, 2H, ^{3}J = 4.1 Hz), 7.7 (s, 2H, H-Ar), 7.7 - 7.8 (d, 2H, ^{3}J = 4.1 Hz).
^{13}C NMR (100 MHz, CD_2Cl_4, 353 K): δ (ppm) = 115.1, 125.4, 125.7, 127.7, 131.1, 140.9, 152.5.
MS(FD): m/z = 457,4 M^+.

Poly{1,4-phenylene}-co-{[9,9-bis(4-phenoxy butylsulfonate)]fluorene-2,7-diyl}-stat-{4,7-bis(5-thi
en-2-yl)benzo[c][1,2,5]thiadiazole)} copolymers (PBS-PFP-TBTT$_x$) **2**.
For the copolymer preparation, a mixture of 2,7-dibromo-9,9-bis(4-sulfonylbutoxyphenyl)-fluorene (1-x mmol), 4,7-bis(5-bromothiophen-2-yl)benzo[c][1,2,5]thiadiazole (x mmol)1,4-benzenediboronic acid (0.166 g, 1 mmol) $Pd(PPh_3)_4$ (50 mg), Na_2CO_3 (1.0 g, 9.4 mmol) in 20 mL of THF and 40 mL degassed water, was reacted for 4 days at reflux. The aqueous layer was washed with chloroform and concentrated to dryness [134] [124]. The residue was redissolved in a mixture of water and THF 50% (v/v) and purified by dialysis using a membrane with a cut off of 3500 Da.

[1]Synthesis and caracterization of the compound done by Dr. Dietrich Breusov from Professor Scherf's Group, Bergische Universität Wuppertal, Germany

The TBTT percentage incorporated in the copolymer was estimated from the elemental analysis data, using the nitrogen atom contribution, see Table 5.8. The copolymers were characterized by TGA, with the decomposition starting around 380 °C for PBS-PFP-$TBTT_{10}$ and 385 °C for PBS-PFP-$TBTT_{16}$.
^{1}H NMR (600 MHz, D_2O 50% d-Dioxane; ppm): δ (ppm) = 8.3 - 7.2 (ar-fluorene and ar-TBTT), 4.3 (CH_2, α), 3.2 (CH_2, γ), 1.7 - 1.2 (CH_2, β and σ).
GPC (NMP, LiBr, UV-detection 360 nm) Mn = 2100 g·mol^{-1}, Mw = 3100 g·mol^{-1}, PD = 1.5 for PBS-PFP-$TBTT_{10}$ and Mn = 2700 g·mol^{-1}, Mw = 5800 g·mol^{-1}, PD = 2.1 for PBS-PFP-$TBTT_{16}$.

Table 5.8: Polymerization results.

Copolymer	1-x (mmol fluorene)	x (mmol TBTT)	TBTT incorporation (%)	Reaction Yield (%)
PBS-PFP-$TBTT_{10}$	0.90	0.10	10	45
PBS-PFP-$TBTT_{16}$	0.80	0.20	16	[a]

[a] The copolymer has water trapped within its structure.

5.2.3.2 Steady-state spectral characterization

The UV-vis absorption spectra, Figure 5.2.29, of the copolymers in water/dioxane (1:1, v/v) mixture show two maxima at 370 - 380 nm and at 450 nm corresponding to the PFP and on-chain TBTT units, respectively [269] [252]. From the broad absorption in the PFP region, the copolymer PBS-PFP-$TBTT_{16}$ shows evidence of aggregation in solution, even in the presence of the organic co-solvent. The fluorescence spectra of the two copolymers PBS-PFP-$TBTT_{10}$ and PBS-PFP-$TBTT_{16}$ when excited in the PFP absorption band also display two maxima at 410 - 415 nm and 650 - 660 nm, Figure 5.2.29. The latter (650 - 660 nm band) arises from energy transfer of PFP to the TBTT units and from TBTT emission, since the chromophore also absorbs in the PF region. As expected, the emission is more intense in the copolymer with the higher percentage of chromophore (Figure 5.2.29) [243] [270]. However, given the TBTT on-chain incorporation, estimated by elemental analysis, such a difference in the absorption and emission intensities between the copolymers is not expected.

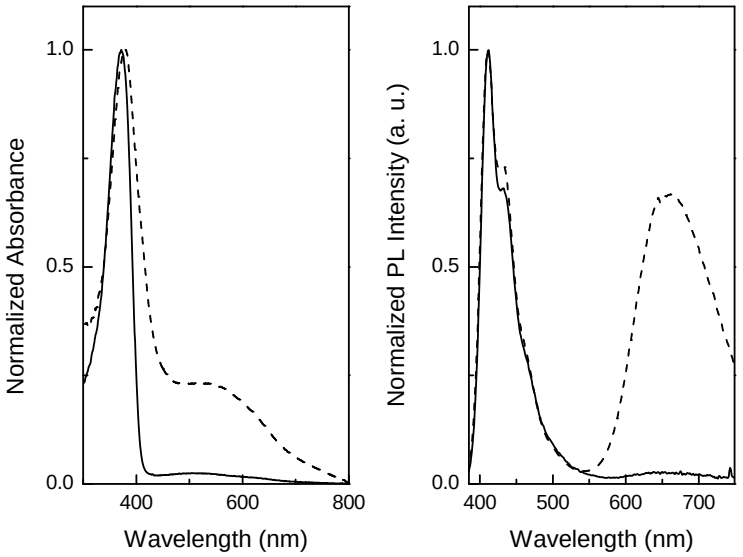

Figure 5.2.29: Absorption and emission spectra of the PBS-PFP-$TBTT_{10}$ (solid line) and PBS-PFP-$TBTT_{16}$ (dashed line) in water/dioxane (1:1, v/v) mixture.

As in the PBS-PFP-PDI case, single molecule wide-field imaging was used to estimate the TBTT average number of chromophores contained per copolymer chain. PBS-PFP-$TBTT_{10}$ was analyzed via the technique and the collected histogram displayed a majority of one TBTT chromophore in the PBS-PFP-$TBTT_{10}$ molecule (graph not shown). The wide-field imaging experiments revealed the presence of free individual TBTT molecules. This denotes that the data collected from the elemental analyzes also takes into account unattached dye and, hence, the TBTT on-chain incorporation percentage is lower that 10%. The simple fact that these are ionic polymeric materials, with hydrophobic and hydrophilic parts that easily form clusters in solution, may contribute for the trap of unreacted dye and solvent within some of the polymeric chains.

For both systems the spectral overlap between the homopolymer PBS-PFP and the acceptor TBTT, Figure 5.2.30, was used to calculate the Förster distance (R_0) at which resonance energy transfer is 50% efficient [41], [42]. In this case the R_0 value is 41 Å, which is comparable to the literature [128], [144] and previously obtained values (chapter 4 and subchapter 5.2.2).

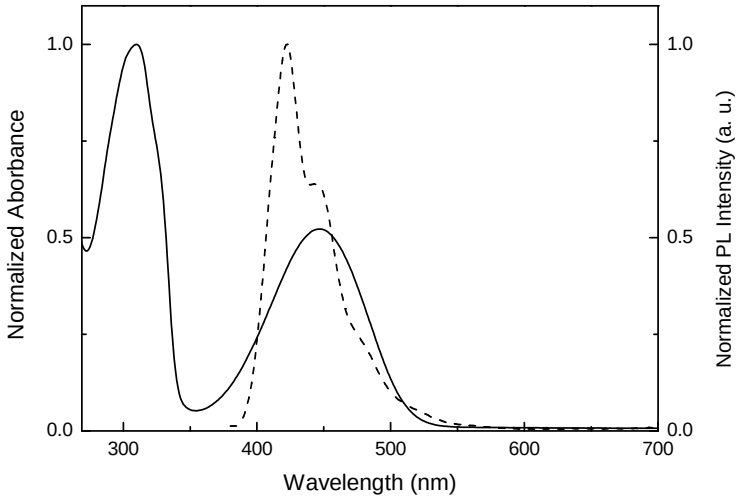

Figure 5.2.30: Spectral overlap between the donor PBS-PFP emission (dashed line) and the acceptor TBTT absorption (full line).

5.2.3.3 Aggregation in solvent mixtures

The behaviour of the anionic PF-TBTT copolymers in a water/methanol (1:1, v/v) mixture was studied and compared with the results obtained in water/dioxane solution with the same percentage of organic co-solvent. Both copolymer solutions were transparent, however, under UV light of 365 nm the solutions presented different colours according to the solvent mixture used (Figure 5.2.31).

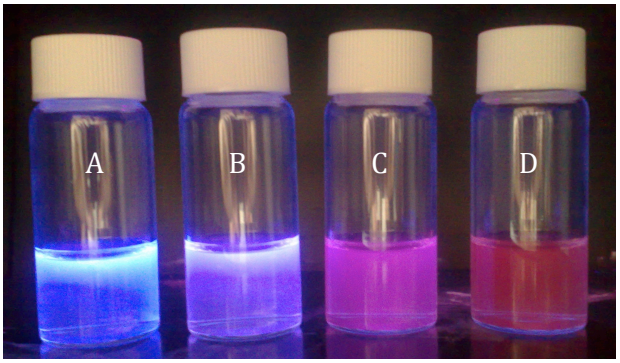

Figure 5.2.31: Photograph with copolymers dissolved in the co-solvent mixtures. A) PBS-PFP-TBTT$_{10}$, C) PBS-PFP-TBTT$_{16}$ in water/dioxane (1:1, v/v), B) PBS-PFP-TBTT$_{10}$ and D) PBS-PFP-TBTT$_{16}$ in water/methanol (1:1, v/v).

The photoluminescence (PL) spectrum of the two copolymers in the water/dioxane (1:1, v/v) mixture exhibit a distinct vibronic structure for the PFP emission, with the main

band located at 410 nm and two relatively well-resolved vibronic peaks at 425 and 460 nm (Figures 5.2.32 and 5.2.33). A less distinct vibronic structure and a quenched PF emission accompanied by a red-shift on the PFP and TBTT emission maximum is observed in the water/methanol (1:1, v/v) mixture. This effect is more evident in the copolymer PBS-PFP-$TBTT_{16}$ (Figure 5.2.33) and coupled with the broadened absorption in the PFP region strongly suggests the copolymer associates into clusters in the water/methanol mixture [123, 126, 141], enhancing the TBTT emission.

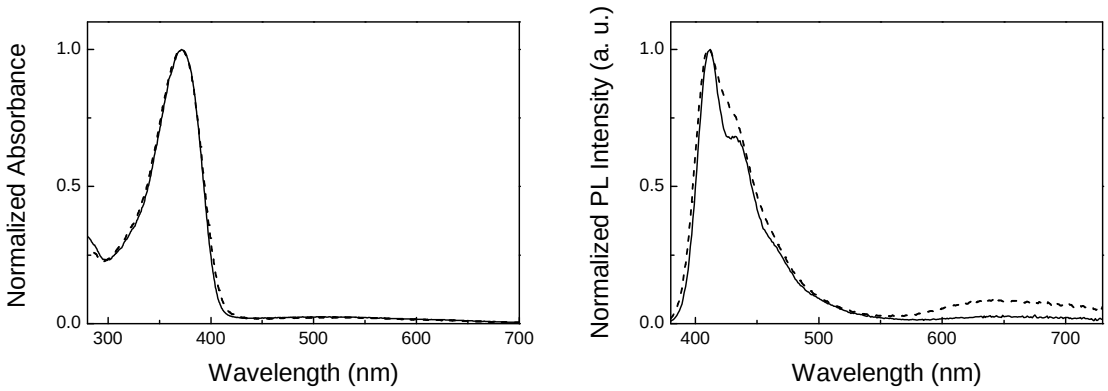

Figure 5.2.32: Absorption (left) and photoluminescence spectra (right) of PBS-PFP-$TBTT_{10}$ in water co-solvent mixtures. water/dioxane (solid line) and water/methanol (1:1, v/v) (dashed line).

Pu and Li have noted that the fluorescence of fluorene-based CPE with attached BTD units is sensitive to the solvent polarity, and when aggregated structures are formed the BTD emission is enhanced [271]. Since the LUMO is located on the TBTT units (Figure 5.2.34) there is a charge redistribution upon copolymer excitation due to the strong electron-accepting character of the chromophore unit. As with the system system by Liu *et al.*, it is likely that aggregated structures are formed, where the TBTT group is in a hydrophobic environment and protected from the water molecules, that favour the chromophore emission [271]. Fluorescence quantum yields (Table 5.9) measured are inferior to those determined for the homopolymer PBS-PFP when dissolved in water co-solvents [127]. The PLQY also decrease with increasing fraction of TBTT; in part this may be due to aggregation, but it is possible that the heavy sulfur atom of the chromophore may enhance intersystem crossing [270].

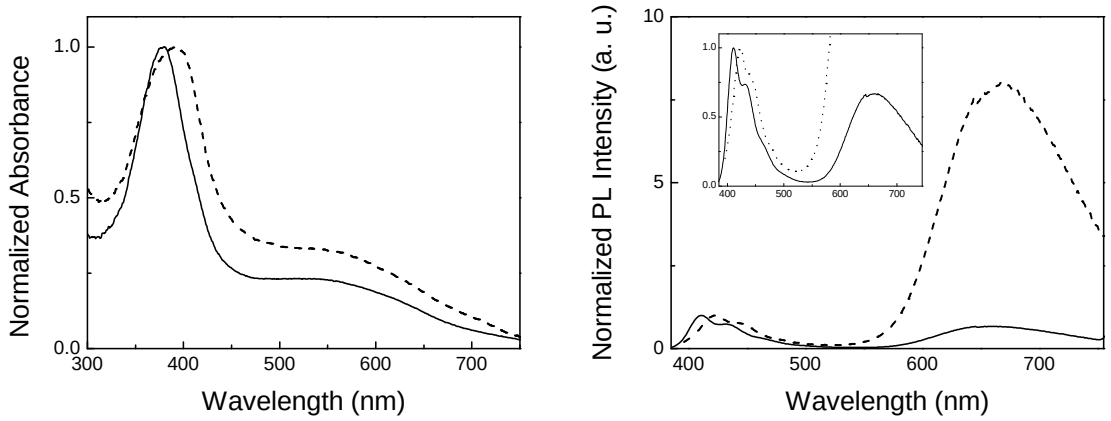

Figure 5.2.33: Absorption and photoluminescence spectra of PBS-PFP-TBTT$_{16}$ in water co-solvent mixtures. Water/dioxane (solid line) and water/dioxane (dashed line).The inset depicts the PF emission region for the two solvent mixtures.

Table 5.9: Photophysical parameters of PBS-PFP-TBTT$_x$ in water/dioxane and water/methanol (1:1, v/v) mixtures.

Copolymer	Solvent	Absorption λ_{max} (nm)	Emission λ_{em} (nm)	ϕ_F PF [a] [b]	ϕ_F TBTT [a] [b]
PBS-PFP-TBTT$_{10}$	water/dioxane	370, 510 (PF, TBTT)	411, 650 (PF, TBTT)	0.43	0.02
	water/methanol	372, 520 (PF, TBTT)	411, 650 (PF, TBTT)	0.39	0.03
PBS-PFP-TBTT$_{16}$	water/dioxane	380, 520 (PF, TBTT)	411, 660 (PF, TBTT)	0.21	0.11
	water/methanol	390, 550 (PF, TBTT)	423, 670 (PF, TBTT)	0.003	0.09

[a] PLQY were determined using quinine sulphate in 0.5 M H_2SO_4.

[b] Measured with excitation at the PF absorption maximum.

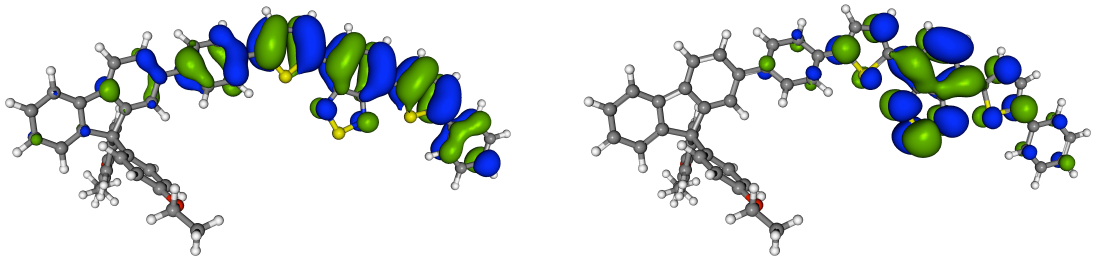

(a) (b)

Figure 5.2.34: Contour plots of the a) HOMO and b) LUMO orbitals of the PBS-PFP-$TBTT_x$ calculated at the B3LYP/3-21G* level. HOMO = -4.95 eV and LUMO = -2.64 eV.

5.2.3.4 Time-resolved fluorescence decays of the PBS-PFP-$TBTT_x$ copolymers.

Figures 5.2.35, 5.2.36 and Tables 5.10 and 5.11 show the fluorescence decays kinetic profiles and lifetime constants for the PBS-PFP-$TBTT_{10}$ and PBS-PFP-$TBTT_{16}$ copolymers, respectively, in both solvent mixtures; collected at room temperature with excitation at 392 nm and at the PFP and TBTT chromophore emission maxima. Excellent fits of emission decays collected at the PFP emission maximum could be achieved with sums of two or three exponential functions, depending on the copolymer nature and solvent mixtures used (Figures 5.2.35 and 5.2.36).

Table 5.10: Fluorescence decay times (τ_i) and pre-exponential factors (a_{ij}) for the copolymer PBS-PFP-$TBTT_{10}$, obtained with excitation at 392 nm, emission at the wavelength maxima and T = 293 K.

	λ_{em} (nm)	τ_1 (ns)	τ_2 (ns)	τ_3 (ns)	τ_4 (ns)	a_{i1}	a_{i2}	a_{i3}	a_{i4}	χ^2
water/dioxane	410	—	0.25	0.51	—	—	0.267	0.733	—	1.05
	660	—	—	0.45	2.52	—	—	0.470	0.530	1.06
water/methanol	410	0.04	—	0.51	—	0.264	—	0.736	—	1.08
	650	0.09	—	0.53	2.68	0.256	—	0.354	0.390	1.07

Table 5.11: Fluorescence decay times (τ_i) and pre-exponential factors (a_{ij}) for the copolymer PBS-PFP-TBTT$_{16}$, obtained with excitation at 392 nm, emission at the wavelength maxima and T = 293 K.

	λ_{em} (nm)	τ_1 (ns)	τ_2 (ns)	τ_3 (ns)	τ_4 (ns)	a_{i1}	a_{i2}	a_{i3}	a_{i4}	χ^2
water/dioxane	410	0.02	0.18	0.47	—	0.422	0.245	0.333	—	0.96
	660	—	0.16	0.58	2.46	—	0.191	0.253	0.556	1.16
water/methanol	410	0.01	0.05	0.57	—	0.977	0.013	0.010	—	1.19
	660	—	0.14	0.68	2.32	—	0.291	0.335	0.375	1.16

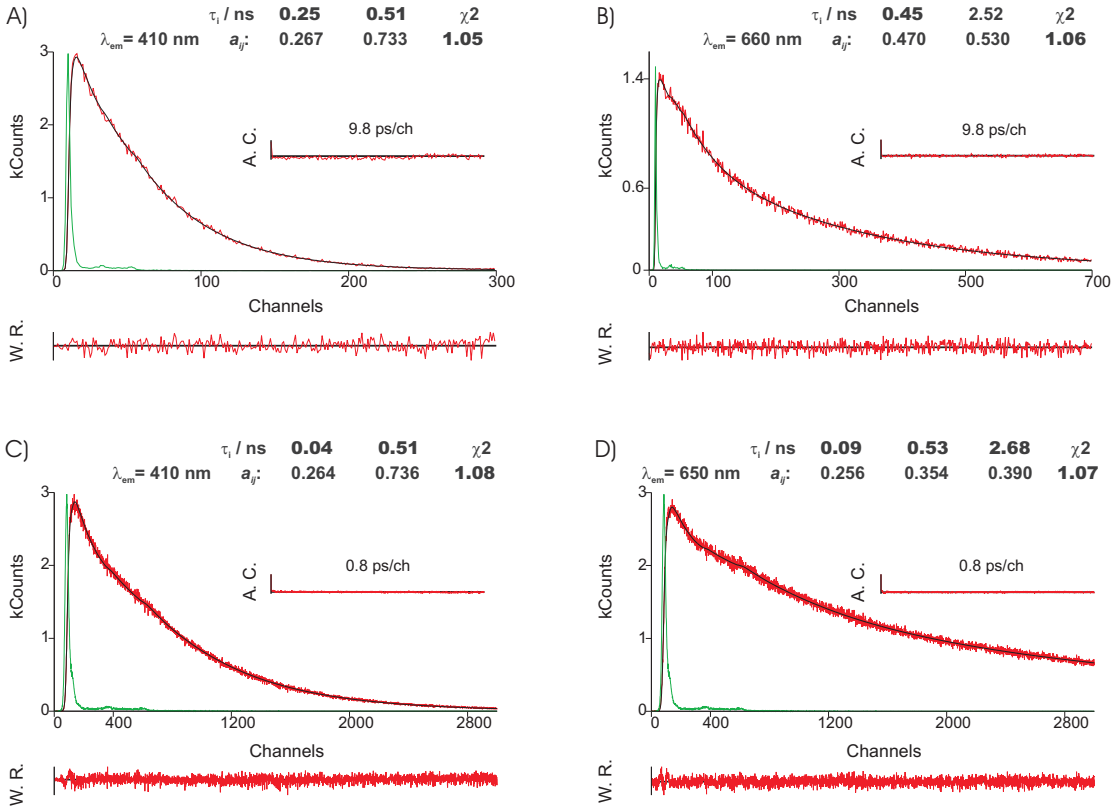

Figure 5.2.35: Fluorescence emission decay for PBS-PFP-TBTT$_{10}$ obtained with λ_{exc} 392 nm at 293 K and collected at PFP and TBTT emission maximum. A) and B) in water/dioxane (1:1, v/v) mixture. C) and D) in water/methanol (1:1, v/v) mixture. The green lines in the decays are the instrumental response function (IRF). For a better judgment of the quality of the fits weighted residuals (W.R., scale -3 $\leq \sigma \leq$ +3) autocorrelation functions (A.C.) and chi-square values (χ^2) are also presented.

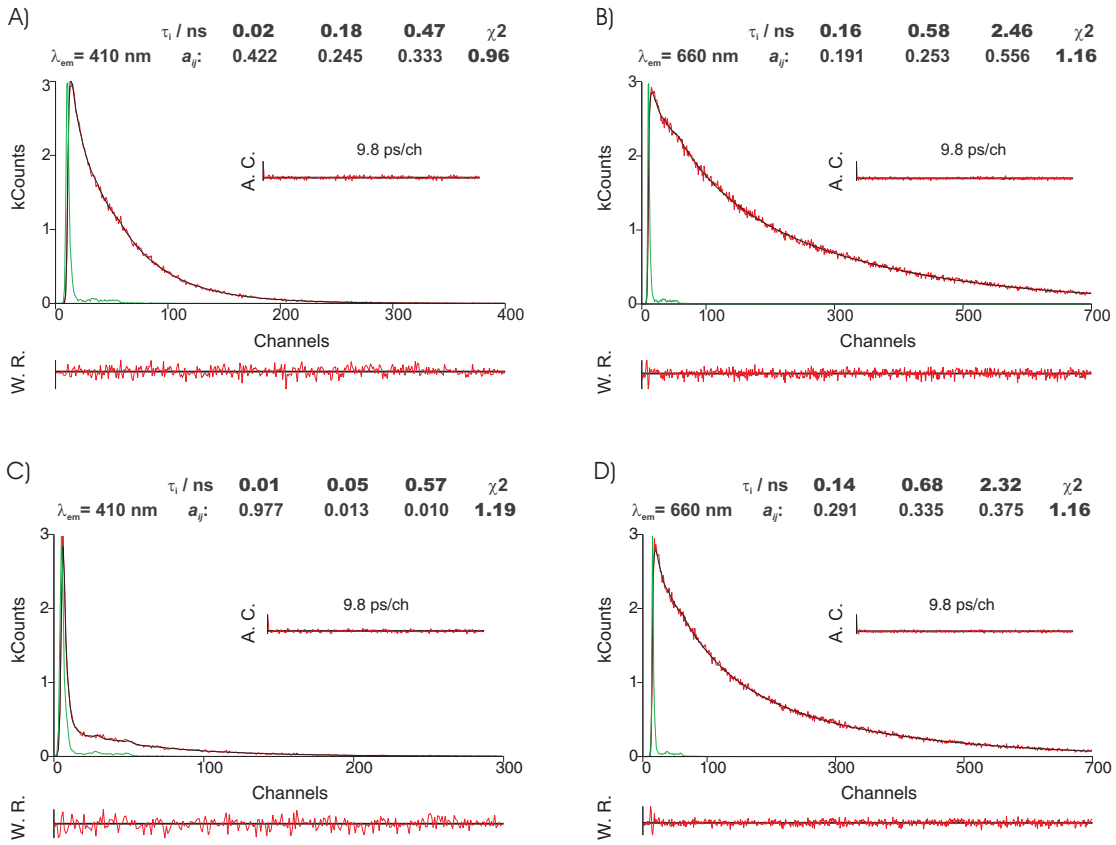

Figure 5.2.36: Fluorescence emission decay for PBS-PFP-TBTT$_{16}$ obtained with λ_{exc} 392 nm at 293 K and collected at PFP and TBTT emission maximum. A) and B) in water/dioxane (1:1, v/v) mixture. C) and D) in water/methanol (1:1, v/v) mixture. The green lines in the decays are the instrumental response function (IRF). For a better judgment of the quality of the fits weighted residuals (W.R., scale -3 $\leq \sigma \leq$ +3) autocorrelation functions (A.C.) and chi-square values (χ^2) are also presented.

In both water co-solvent mixture the fast decay component is attributed either to the formation of an initial nonrelaxed conformer, that gives rise to a more stable one; or to energy transfer to TBTT on-chain moieties. This is not observed in the copolymer PBS-PFP-TBTT$_{10}$, when dissolved in water/dioxane where FRET is not efficient, due to the low molar chromophore concentration [45], [47]. The lifetimes of 160 - 250 ps have already been observed for PF based polyelectrolytes and are believed to be due to cluster morphologies in solution [86]. However, as with the on-chain porphyrin copolymer discussed earlier in this chapter, the amplitude associated with the 160 - 250 ps lifetimes in water/dioxane is greater than in water/methanol (Tables 5.10 and 5.11); hence, exciton migration along the polymer chain, should be the dominant contribution [144]. The intermediate component varying from 450 to 530 ps appears as a decay time at both wavelengths and is more important at 410 nm than at 640 nm. This component is identified with the PFP lifetime,

which is quenched for higher TBTT content. When the decay is collected at 650 - 660 nm (Tables 5.10 and 5.11) a longer lifetime component is found that is independent of the TBTT content and therefore assigned to the TBTT fluorescence lifetime. As reported by Dias *et al.* [270], the population of TBTT singlet state occurs during the excited states lifetime of PFP and later decays with a 2.4 - 2.6 ns time domain.

5.2.3.5 Synthesis of PBS-PFP-TBTT copolymer with interrupted chain conjugation

Electronic energy transfer can result from different interaction mechanisms, that may be due to coulombic interaction, or to intermolecular orbital overlap. The coulombic interactions feature long range dipole-dipole interactions - as is the case of the Förster mechanism - and short range multi-polar interactions [44]. The interactions that arise from the intermolecular orbital overlap - like Dexter mechanism - as well as, charge resonance effects are of short range. Hence, for singlet-singlet energy transfer all types of mentioned interactions are involved, whereas triplet-triplet energy transfer only happens due to the orbital overlap [44].

For allowed transitions between donor and acceptor, the coulombic interaction is predominant even at short distances. In the case of the forbidden transitions among the donor and the acceptor the coulombic interaction is negligible and the exchange mechanism is only effective at short distances (< 10 Å), since it requires a overlap of the molecular orbitals [44] [272]. In summary, the major distinction between the exchange energy transfer concept and the coulombic is that in the former case, either collisions are required or aggregation maybe present, while in the latter they are not. Furthermore, in the exchange energy transfer the excitation is transferred from the donor to the acceptor analogous through a moving particle, which transfers momentum to others particles with which collides. In the induced dipole mechanism, the excitation is transferred throught space [41].

Based on the distinction between the physical principles of energy transfer presented, a copolymer of PBS-PFP-spacer-TBTT (Figure 5.2.37) has been synthesized and fully characterized. The spacer units comprise a monomer of 2,2'-(4,4'-(propane-2,2-diyl)bis(4,1-phenylene))bis(4,4,5,5-tetra-methyl-1,3,2-dioxaborolane (Figure 5.2.38) repeat units and allows the acceptor-donor separation distance to be superior to the van der Waals radius, 19 Å, of the previous 1,4-benzenediboronic acid spacer. A notable feature of this copolymer is that each subunit can be selectively excited with monochromatic light [273], as a result of the suppressed conjugation.

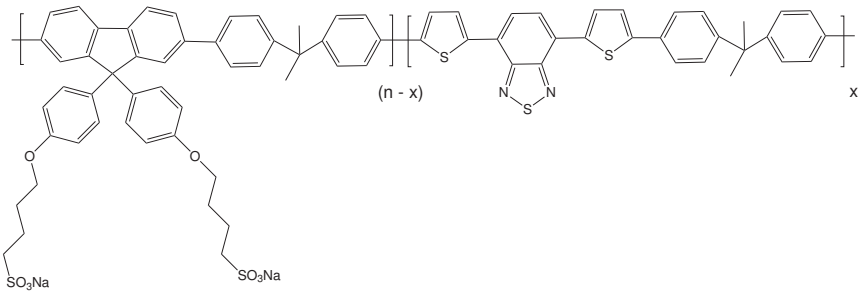

Figure 5.2.37: Structure of the PBS-PFP-TBTT copolymer with interrupted conjugation.

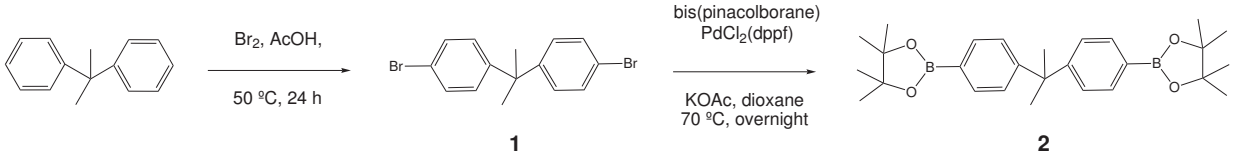

Figure 5.2.38: Overall reaction procedure for the arylboronic ester spacer synthesis.

4,4'-(propane-2,2-diyl)bis(bromobenzene) **1**.

A solution of 2.5 M Br_2 (6 eq) in acetic acid was added at room temperature to 2 g (10.2 mmol, 1 eq) of propane-2,2-diyldibenzene, in an argon environment. Afterwards the reaction was heated to 50 °C and carried overnight. The mixture was washed several times with an aqueous NaOH solution and the organic phase extracted with dichloromethane and dried over $MgSO_4$. The obtained white product (4.6 mmol, 96 %) was characterized by GC-MS and used directy without further purification methods on the next step.

CG-MS: m/z = 354 M^+.

2,2'-(4,4'-(propane-2,2-diyl)bis(4,1-phenylene))bis(4,4,5,5-tetramethyl-1,3,2-dioxaborolane) **2**.

The palladium-catalyzed cross-coupling reaction of the bis(pinacolborane) (7.50 g, 17.70 mmol, 3 eq) , with **1** (3.48 g, 9.85 mmol, 1 eq) was achieved following the procedure of Miyaura *et al.* [274]. The reaction was catalyzed by $PdCl_2$(dppf) (3 mol %) overnight at 70 °C in the presence of KOAc (4.5 equiv) in dry dioxane (130 mL) under argon. Water was added to the mixture and the product extracted with dichloromethane. The solvents were evaporated and the product dried over $MgSO_4$. The product was purified by colum chromatography, using deactivated silica and a mixture of hexane 5% ethyl acetate as eluent. 2.5 g (7.1 mmol, 72 %) of a white powder were obtained.

^{1}H NMR (600 MHz, $CDCl_3$) : δ (ppm) = 7.7 (d, 4H, ^{3}J = 8.3 Hz) 7.2 (d, 4H, ^{3}J = 8.3 Hz) 1.7 (s, 6H) 1.3 (s, 24H).

^{13}C (150 MHz, $CDCl_3$): δ (ppm) = 153.7, 136.6, 126.3, 83.6, 43.5, 30.5, 24.8.
CG-MS: m/z = 448 M^+.

Poly{propane-2,2-diyl-para-phenylene}-co-{[9,9-bis(4-phenoxy butylsulfonate)]fluorene-2,7-di-yl}-stat-{4,7-bis(5-thien-2-yl)benzo[c][1,2,5]thiadiazole)} copolymer (PBS-PFP-TBTT). A mixture of 2,7-dibromo-9,9-bis(4-sulfonylbutoxyphenyl)fluorene (0.742 g, 0.9 mmol), 4,7-bis(5-bromothiophen-2-yl)benzo[c][1,2,5]thiadiazole (46.3 mg, 0.1 mmol), **2** (0.448 g, 1 mmol) $Pd(PPh_3)_4$ (50 mg), Na_2CO_3 (1.0 g, 9.4 mmol) in 20 mL of THF and 40 mL degassed water, was reacted for 4 days at reflux. The aqueous layer was washed with chloroform and concentrated to dryness [134] [124]. The residue was redissolved in a mixture of water and THF 50% (v/v) and purified by dialysis using a membrane with a cut off of 3500 Da. The reaction ratio of *n-x* to *x* is 90 to 10. Total yield of the copolymer PBS-PFP-TBTT was 590 mg (70%) and its decomposition temperature starts around 395 °C (TGA measurement).
^{1}H NMR (600 MHz, D_2O 50% d-THF; ppm): δ (ppm) = 8.0 - 6.9 (ar-fluorene and ar-TBTT), 4.0 (CH_2, α), 2.9 (CH_2, γ), 1.9 (CH_3, spacer) 1.7 - 1.3 (CH_2, β and σ).
GPC (NMP, LiCl, UV-detection 360 nm) Mn = 2200 g·mol^{-1}, Mw = 3500 g·mol^{-1}, PD = 1.6.

5.2.3.6 Photophysical properties of the PBS-PFP-TBTT copolymer with interrupted chain conjugation

Individual studies on electronic energy transfer (EET) have addressed particular issues on the distance dependence, polarity changes, bridge mediated EET, concerted conformational motion, quantum effects and coupled soliton involvement, among others [49, 199, 273, 275–283]. Consequently, the energy transfer mechanism work was extended to a longer spaced monomer as a bridge between the PFP donor moieties and the TBTT acceptor units. Thus, the singlet-excited state of the PFP donor can participate in long-range EET to the TBTT chromophore through FRET, with the process driving-force attributed to a reasonably large energy gap; being Dexter transfer inhibited for the on-chain processes. An additional motivation for studying the dynamics of EET in multicomponent molecular systems, stems from the fact that in conjugated polymers, Förster theory might not be appropriate to explain the long range intrachain energy migration that has been observed in certain cases [7], [284]. However, σ-skeleton-based bridges are not completely insulating and may provide a small but demonstrable electronic coupling supporting singlet excitation energy transfer (SEET) [49, 285, 286].

The copolymer absorption and emission spectra recorded in a water/dioxane (1;1, v/v) mixture are depicted in Figure 5.2.39. The shape of the copolymer absorption spectra do

not change when compared to the individual component TBTT (Figure 5.2.40). The localized bands of the individual polymer chromophore units are well resolved and easily recognized through comparison with the model compounds. This is specially true in the TBTT monomer units that display a pronounced absorption, which a maximum centered at approx. 500 nm.

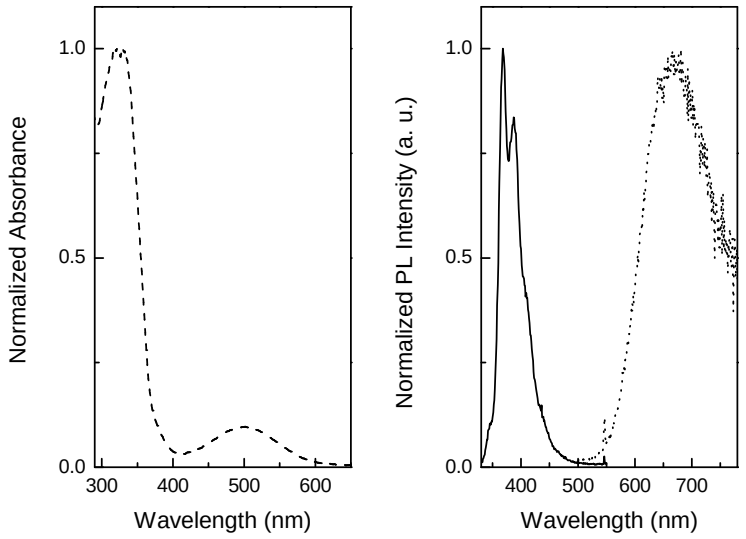

Figure 5.2.39: Absorption and emission spectra of the PBS-PFP-TBTT copolymer with interrupted conjugation in water/dioxane (1:1, v/v) mixture. Excitation at 325 nm (solid line) and 486 nm (dotted line).

A narrowing of the PFP emission band and an increase in the vibrational structure was perceptible upon excitation, together with a blue-shift on the emission maxima. This is attributed to different copolymer conformations in the ground and excited states. The excitation spectra, Figure 5.2.40, exhibit two clearly distinct absorption bands dependent on the emission wavelength (PFP and TBTT emission maxima). The specific shape of the peak collected at 670 nm is red-shifted towards the absorption spectra of the TBTT monomer. The observed red-shift upon going from the TBTT monomer to the copolymer indicates that the conjugation is extended by two more phenyl rings [287].

Absorption and emission spectral bands associated with the spacer unit differ markedly from the PBS-PFP-$TBTT_{10}$, with the maximum located at higher energy, as the molecular length increases [288–290]. The length dependence is a consequence of the energy gap between donor and spacer units becoming bigger as the molecular length increases.

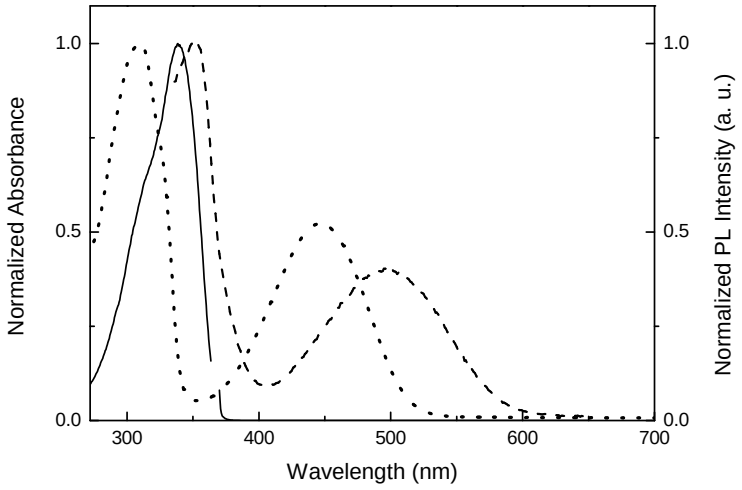

Figure 5.2.40: Excitation spectra of the PBS-PFP-TBTT copolymer with interrupted conjugation water/dioxane (1:1, v/v) mixture. Emission at 368 nm (solid line) and 670 nm (dashed line). The absorption spectrum of the monomer dye TBTT was also included (dotted line).

Analysis of the decay profile for the investigated copolymer PBS-PFP-TBTT are in agreement with the absorption and fluorescence solution findings. The decay profile collected at 400 nm (PFP emission) reveals the presence of a fast component (10 ps), an intermediate decay time of 120 ps, and a slower decay time of 470 ps (Figure 5.2.41). The decay component attribution has been made previously and will not be further discussed. A single exponential fit was found for the TBTT emission region, at λ_{em} = 600 nm, with a lifetime of 3.36 ns, Figure 5.2.41. No evidence for the typical PF decay lifetime was detected at this wavelength and hence, the lifetime is unambiguously attributed to the isolated TBTT decay.

Studies of the distance dependence for electron and energy transfer have resulted in a fairly good relationship between the electronic structure of the intervening medium and the attenuation factor (β). π-conjugated spacers span a very large range of β between fully conducting (when β is close to zero) to insulating (when β is greater than 0.5 $Å^{-1}$) [49]. By contrast, σ-spacers always present the same value of β, which is close to unity [49]. The dependence on the conformational changes of the bridge structure is responsible for the attenuated excitation energy (EET) and electron (ET) transfer.

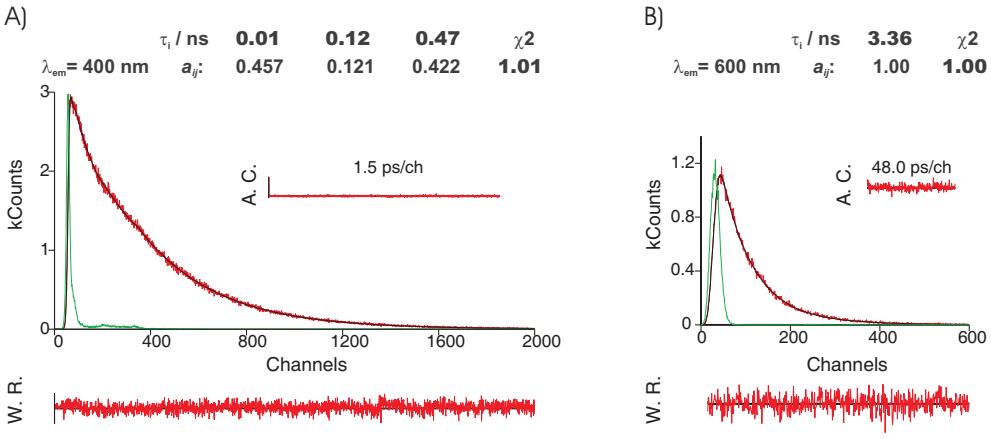

Figure 5.2.41: A) Fluorescence emission decay for PBS-PFP-TBTT in water/dioxane (1:1, v/v) mixture obtained with λ_{exc} 392 nm at 293 K and collected at the PFP emission maximum and B) obtained with λ_{exc} 460 nm at 293 K and collected at the TBTT emission. The green lines in the decays are the instrumental response function (IRF). For a better judgment of the quality of the fits weighted residuals (W.R., scale -3 $\leq \sigma \leq$ +3) autocorrelation functions (A.C.) and chi-square values (χ^2) are also presented.

5.2.3.7 Attempt preparation of PBS-PFP based white light emitting copolymer

The design of luminescent materials for use in LED devices is as critical to device performance as in the process of constructing the device itself [21], [291]. Processability, purity, thermal and oxidative stability, emission colour and luminance efficiency are among most important materials properties required for a system to be viable in commercial LED device applications [21], [18]. To improve the device performance, low-work function cathodes have been used to increase the electron injection, while multilayer devices have been fabricated with separate electron-transport and a hole-transport emissive polymer [16, 292, 293]. For electronic devices, the interface between the different functional polymers is crucial for the performance [20]. Another approach for increasing device external quantum efficiency is to synthesize emissive copolymers containing both hole and electron-transporting moieties. This design strategy is expected to produce polymeric materials with improved electron affinity and charge balance [292].

White light emission can be tuned by adjusting the composition of the RGB units and by controlling the partial energy transfer to green- or red-emissive units in the polymer chain. Reported strategies to obtain white light electroluminescence include the use of single polymer systems that contain chemically doped chromophores, to overcome problems of multilayers and blend systems [294]. Several studies have succeeded in realizing efficient

white PLEDs devices with simultaneous blue, orange, or red, emission from polyfluorene based polymers [22, 294, 295]. Single polymers containing RGB emitting units in the backbone have also been reported [24, 294, 296, 297].

Oligomers and polymers containing thiophene rings have attracted considerable attention as candidate materials for use in molecular devices. In the past decade the evolution of new synthetic routes has allowed remarkable advances in the production of high molecular weight and structurally well-defined materials. Furthermore, reproducible methods for the large-scale synthesis of thieno-acenes, namely thieno[3,2-b]thiophene have been reported by Smith *et al.* [298]. This allows high purity fluorene and thieno[3,2-b]thiophene-based copolymers to be easily obtained [244].

To fulfill the necessary requirements to achieve white EL a single polymer system was developed with different emission components based on the control of energy transfer and charge trapping between the chromophores in the designed polymer. A small amount of red- and green-emitters TBTT and thieno[3,2-b]-thiophene (TTP), respectively, were incorporated into the main chain of a blue-light-emitting anionic polyfluorene (PBS-PFP). Thieno[3,2-b]thiophene was chosen as green-chromopore based on previous studies published by Lim *et al.* [244]. Lim was able to achieve pure green emission with an LED device based on poly(9,9'-dioctylfluorene-*alt*-thieno[3,2-b]-thiophene) (PFTT), synthesized via a palladium-catalyzed Suzuki coupling reaction [244]. The feed ratio of TBTT and TTP was tuned accorded to previous publications of polyfluorene copolymers with red and green units in the backbone. According to those studies white EL is accomplished with low compositions of green and red-emitting chromophores within the polyfluorene main chain [244, 299, 300].

5.2.3.8 Synthesis of PBS-PFP-TTP-TBTT copolymer

The structure of the PBS-PFP-TTP-TBTT copolymer is shown in Figure 5.2.42. The reaction ratio of *n-x-y* to *x* and to *y* is n-x-y = 99.60 to x = 0.20 and y = 0.20. 2,5-Dibromothieno[3,2-b]thiophene (TTP, purity: > 98.0 % GC) was purchased from TCI Europe and used without further purification.

Poly{1,4-phenylene}-co-{[9,9-bis(4-phenoxy butylsulfonate)]fluorene-2,7-diyl}-stat-{2,5-thieno[3,2-b]thiophene}-stat-{4,7-bis(5-thien-2-yl)benzo[c][1,2,5]thiadiazole)} copolymer (PBS-PFP-TTP-TBTT).

A mixture of 2,7-dibromo-9,9-bis(4-sulfonylbutoxyphenyl)fluorene (0.996 mmol, 821.2 mg), 2,5-Dibromothieno[3,2-b]thiophene (2.0×10^{-3} mmol, 0.60 mg), 4,7-bis(5-bromothiophen-2-

yl)benzo[c]-[1,2,5]thiadiazole (2.0×10^{-3} mmol, 0.92 mg),1,4-benzenediboronic acid (0.166 g, 1 mmol) $Pd(PPh_3)_4$ (50 mg), Na_2CO_3 (1.0 g, 9.4 mmol) in 5 mL of butanol, 50 mL of dry toluene and 5 mL degassed water, was reacted for 4 days at reflux. The aqueous layer was washed with chloroform and concentrated to dryness [134] [124]. The residue was redissolved in a mixture of water and THF 50% (v/v) and purified by dialysis using a membrane with a cut off of 3500 Da. Total yield of the copolymer PBS-PFP-TTP-TBTT was 450 mg (76%). The copolymer was characterized by TGA, with the decomposition temperature starting around 365 °C.

^{1}H NMR (600 MHz, D_2O 50% d-Dioxane; ppm): δ (ppm) = 8.0 - 6.9 (ar-fluorene), 4.0 (CH_2, α), 3.6 (CH_2, γ), 2.9 (CH_2, β) 1.9 - 1.3 (CH_2, σ).

GPC (NMP, LiBr, UV-detection 360 nm) Mn = 1800 g·mol^{-1}, Mw = 2700 g·mol^{-1}, PD = 1.5. The very low concentration of TTP and TBTT units enable its percentage incorporation determination in the copolymer via ^{1}H NMR and elemental analysis.

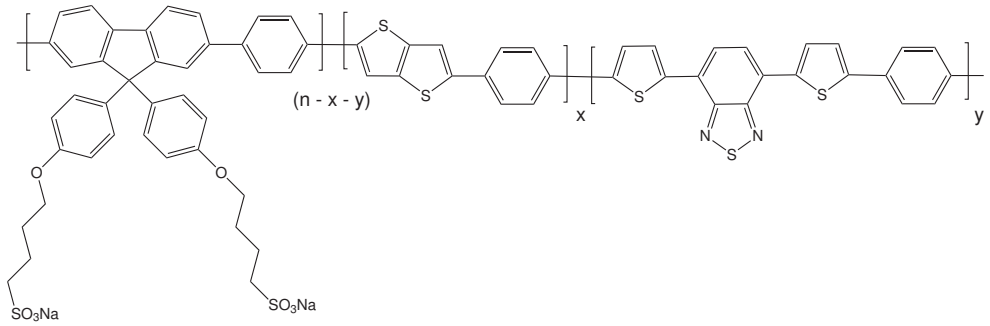

Figure 5.2.42: Structure of the PBS-PFP-TTP-TBTT copolymer with green and red emitting on-chain monomers.

5.2.3.9 Steady state and time resolved fluorescence measurements

Figure 5.2.43 show the normalized UV-vis absorption and photoluminescence spectra of the PBS-PFP-TTP-TBTT copolymer in a water/dioxane (1:1, v/v) mixture. PFP-TTP-TBTT exhibit similar UV-vis and PL spectra to that of PBS-PFP (Table 5.12), due to the low amount of the chromophores (0.2 %). The PLQY of PBS-PFP-TTP-TBTT was measured in the water/dioxane solution mixture and found to be 0.60, the value falls within the range of PL quantum efficiency determinated for the PBS-PFP homopolymer under the same conditions (52%), Table 5.12. Unfortunately, the photophysical characteristics of the RGB copolymer reveal the TTP and TBTT units make almost no contribution to the absorption and emission spectra, due to their low concentration in the copolymer chain. Future studies should address the concentration effect in addition to studying the light

emitting behaviour of PBS-PFP-TTP-TBTT thin film.

Table 5.12: Absorption and emission maxima and PLQY of PFP-TTP-TBTT copolymer and PBS-PFP homopolymer in water/dioxane (1:1, v/v) mixture.

Copolymer	Absorption λ_{max} (nm)	Emission λ_{em} (nm)	ϕ_F [a]
PBS-PFP	376	412	0.52
PBS-PFP-TTP-TBTT	366	410	0.60

[a] PLQY were determined using quinine sulphate in 0.5 M H_2SO_4.

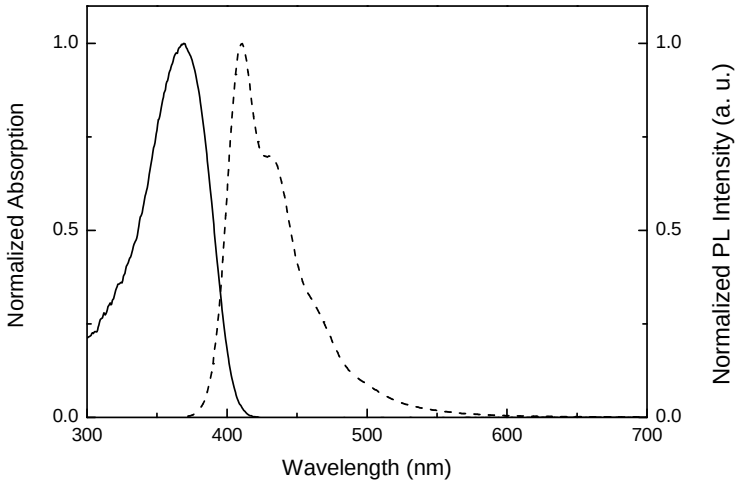

Figure 5.2.43: Absorption (solid line) and photoluminescence (dashed line) spectra of PBS-PFP-TTP-TBTT in water/dioxane (1:1, v/v) mixture.

Fluorescence lifetimes of the copolymers in solution were best fitted with biexponential and triexponential decay laws according to Equation 5.7. With a_{ij} = (i = 1, 2; j = 1, 2 and i = 1, 2, 3; j = 1, 2, 3) see Figure 5.2.44.

$$I_\lambda(t) = \sum_{ij} a_{ij} e^{\frac{-t}{\tau_j}} \tag{5.7}$$

The decay time values are in good agreement with the values obtained for fluorene based polyelectrolytes [124], [145]. The difference on the fitting equation used for PBS-PFP-TTP-TBTT and homopolymer can be attributed to the different copolymer size, since the intermediate component is not observed in the PBS-PFP-TTP-TBTT decay, and/or

to different copolymer in solution morphology [85], [123]. No longer lifetimes components were detected at the TTP and TBTT emission range in the RGB copolymer decay.

The above information confirms the low incorporation of the chromophores. Thus, the material structure reveal promising application for white PLEDs fabrication, in comparison with the results presented by several groups [294, 296, 297]. However, the PL in solution and EL in film behavior are not necessarily the same, and the PFP-TTP-TBTT copolymer should be tested in an EL device and its maximum brightness and current efficiency measured.

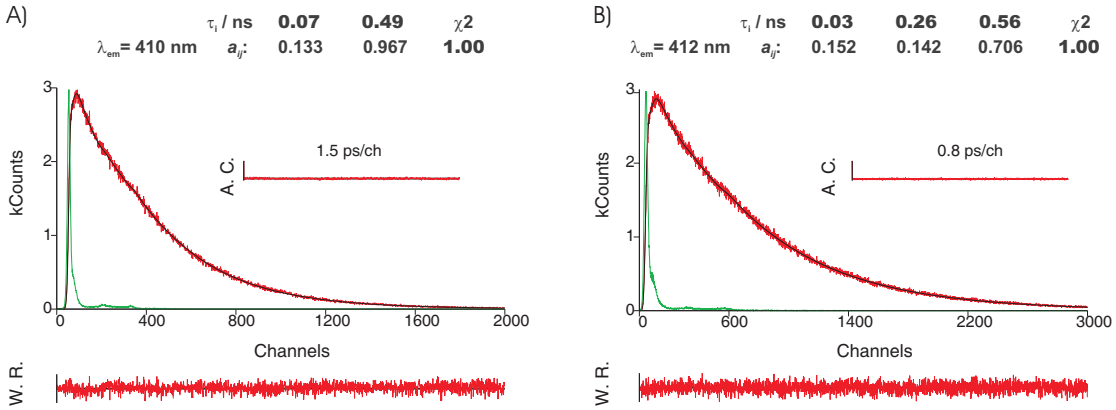

Figure 5.2.44: Fluorescence emission decay obtained with λ_{exc} 392 nm at 298.15 K in water/dioxane (1:1, v/v) mixture for A) PBS-PFP-TTP-TBTT collected at 410 nm and B) PBS-PFP collected at 412 nm. The green lines in the decays are the instrumental response function (IRF). For a better judgment of the quality of the fits weighted residuals (W.R., scale -3 $\leq \sigma \leq$ +3), autocorrelation functions (A.C.) and χ^2 are also presented.

5.3 Optical bandgaps of the PBS-PFP copolymers with on-chain chromophores

A series of structural modifications involving the conjugated backbone has been examined in efforts to optimize the integration of CPEs in optoelectronic devices [301]. Accurate estimation of the strength of an electron deficient unit can be obtained from the LUMO level value. Comparison of the electron affinities, between two acceptor units, should only be performed for similar conjugated backbone and identical side chains [1].

The bandgap properties of the several PBS-PFP copolymers were investigated by ultraviolet photoelectron spectroscopy (UPS) which allowed the determination of the HOMO. The LUMO was determined as difference of HOMO and optical bandgap energy estima-

tion, from the interception of the absorption and emission spectra, Table 5.13 and Figure 5.3.1. The HOMO energy levels of the copolymers are between -5.72 eV and -5.56 eV with only small variations, which consequently, indicates that the HOMO is mainly independent of the incorporation of the acceptor units (Table 5.13). Only for PBS-PFP-$TBTT_{16}$ is a slight 0.1 eV increase of the HOMO energy observed, probably caused by the TBTT incorporation. The LUMO levels are decreased by ca. 0.3 eV upon the incorporation of the acceptor chromophore and reveal that the LUMO is localized on the chromophore segments, as suggested previously on the DFT calculations performed for the PBS-PFP-PDI and PBS-PFP-$TBTT_x$ copolymers (see subchapters 5.2.1 and 5.2.3).

Table 5.13: HOMO, LUMO and bandgap levels determined by UPS of the several PBS-PFP anionic copolymer with on-chain chromophores.

Copolymer	HOMO eV	Bandgap eV	LUMO eV
PBS-PFP	5.60	3.27 [a]	2.33
PBS-PFP-PDI	5.72	3.07	2.65
PBS-PFP-DPP	5.67	3.07	2.60
PBS-PFP-$TBTT_{10}$	5.66	2.98	2.68
PBS-PFP-$TBTT_{16}$	5.56	2.92	2.64

[a] Estimated as the onset of the film absorption spectra.

The 2,1,3-benzothiadiazole derivative (TBTT) unit appears to be the most promising acceptor for photovoltaic applications, given the copolymer's lower bandgaps. The bandgap of the PBS-PFP-$TBTT_x$ copolymers gradually decreases from 2.98 to 2.92 eV as a function of the acceptor segment content. However, multicyclic fused aromatic rings with enforced planarity also show great promise as on-chain chromophoric functionalities, since high hole mobilities often result [1]. The resulting HOMO and LUMO level values calculated for the PBS-PFP-DPP copolymer fall among the typical values published for PF-porphyrin polymers (HOMO = -5.29 to -5.25 eV and LUMO = -3.29 to -3.24 eV) [302]. The PBS-PFP-PDI bandgap properties differ from those previous found for donor-acceptor copolymers based on a naphthalene-bisimide (LUMO = -3.91 to -3.80 eV and HOMO = -6.13 to -6.10 eV) or PDI (LUMO = -3.61 eV and HOMO = 5.93 eV) moieties as electron-acceptor and connected to polyfluorene as the electron-donor [303], [304]. The bandgap decrease in the

PBS-PFP-PDI is caused by the decrease in the LUMO energy level accompanied only, by slight increase in the HOMO energy [303].

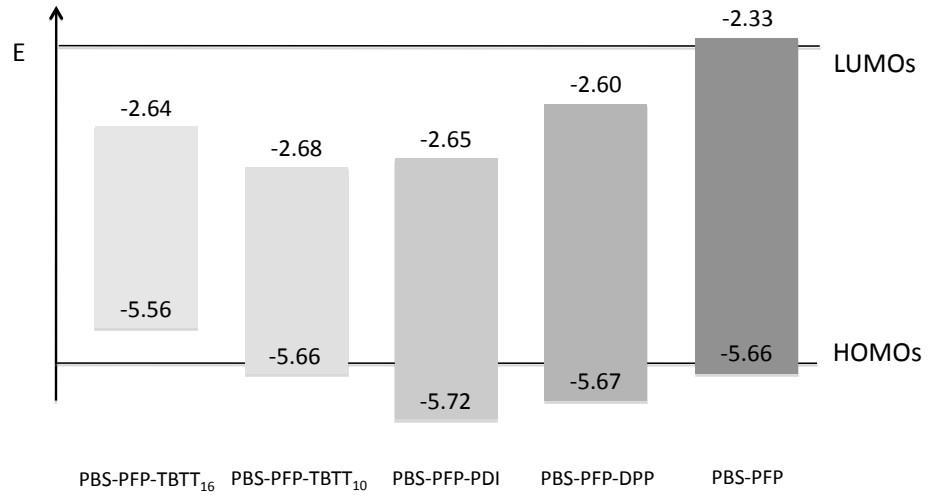

Figure 5.3.1: Energy levels (E in eV) of the several PBS-PFP anionic copolymer with on-chain chromophores.

5.4 Conclusions

Several anionic conjugated polyelectrolyte (CPE) composed of phenylene-*alt*-fluorene repeat units with randomly distributed on-chain chromophores have been synthesised and their photophysical behaviour studied in different solvent mixtures. The absorption and emission spectra, together with the excited state behavior, are strongly dependent on the chromophore used. The optical bandgaps have been determined and the HOMO level found to be intrinsically related with the PBS-PFP units, while the LUMO varies with the electronic properties of the dye.

The low molecular weights values determined experimentally are explained by the copolymer interactions with the column packing material. These probably underestimated the actual macromolecule weight values. The interactions between the polyelectrolytes and the matrix of the organic sorbent can either be positive (repulsion) or negative (attraction) and are caused by the competition of the chain units with the eluent molecules or polar co-solvents, electrostatic interactions, entropy hindrances, among others. The asymmetry of the chromatogram peaks, observed in all the GPCs measurements, is caused by the nature of the flexible chain macroions due to their ability to change their size when the ionic strength of the solution is varied, or the concentration altered. Owing to the existence of a concentration gradient and of the corresponding difference in the ionic strength inside the

chromatographic zone, the macromolecules acquire more uncoilded conformations at the edges. Hence, the polyelectrolyte chromatographic zone in pure solvents is formed by the action of strong concentration effects, such as the expansion of the polyelectrolyte association, that eliminate the influence of the molecular mass and its distribution, preventing a correct assignment of the copolymer size [305].

The optical spectra of the copolymer PBS-PFP-PDI in water and water/dioxane mixtures showed no significant energy transfer or emission from the PDI chromophore. However, single chain wide-field imaging in PVA films confirmed incorporation of the PDI dye within the PFP polymer chain, although at a low percentage. Time-resolved PL, femtosecond fluorescence and ultrafast transient absorption experiments in water and water/dioxane mixture, indicate the presence of fast PL decay components and suggest that there is an efficient nonradiative decay pathway in this system, that involves electron (or charge transfer) leading to quenching of both the PFP and PDI emission.

Time-resolved experiments and steady state measurements have been conducted in solution to unravel the role of energy transfer in two fluorene based conjugated polyelectrolyte systems containing porphyrin units. The first one with on-chain porphyrin moieties and the second one a self-assembled structure with an anionic porphyrin bound electrostatically by Ca^{2+}. Energy transfer in the on-chain PBS-PFP-DPP case should compete with other deactivaction processes, such as radiative decay of the singlet excitons photogenerated on the donor-acceptor conjugated chains and copolymer conformational changes. The existing difference between the overall energy transfer efficiency among the PBS-PFP-DPP copolymer and the self-assembled system is attributed to differences in the porphyrin chromophore content and thus, to the efficiency of the on-chain energy migration. As previously reported by Morgado and coworkers [228] for a MEH-PPV porphyrin blend and in a MEH-PPV-porphyrin copolymer the energy transfer efficiency values are similar, in terms of efficiency, only when the copolymer possesses the highest porphyrin concentration. In addition, the spacial extent, intermolecular separation and relative orientations of transition dipole densities on the donor and acceptor PF-porphyrin copolymers, determine the rate of electronic excitation transfer, as observed in the case for the cofacial and collinear orientations between the donor and the acceptor.

The aggregation behaviour of two hairy-rod copolymers with various red emitting TBTT unit percentages randomly distributed along the main chain, has also been studied in solutions of different polarity. Two binary solvent mixtures composed by water and dioxane or methanol were investigated. In the water/dioxane solvent a clear blue-shift is seen in the fluorescence spectrum, accompanied by a well defined vibronic structure on the emission spectra. Quantitative differences in the copolymer spectral shifts and quantum yields

were observed, in the water/methanol mixture. Moreover the energy transfer from the PFP to the TBTT units is enhanced in the methanol water solution, with the emission spectra of the copolymer with the higher TBTT incorporated percentage (PBS-PFP-$TBTT_{16}$) being dominated by the chromophore emission. Normally both Förster and Dexter mechanisms are involved on the energy transfer process. To study the effect of energy migration a non-conjugated linker was included between the PBS-PFP and the TBTT units, the phenylene spacer was replaced by 2,2'-diphenylpropane-4,4'-diyl. The new copolymer has now a specific emission dependent on the excitation wavelength and no, or only residual energy transfer, via the Dexter mechanism, was observed.

The possibility of designing new polymeric architectures for white light emission via the metal catalysed cross coupling was the input for the synthesis of PBS-PFP-TTP-TBTT. The percentage of on-chain green and red-emitting chromophore units was kept low based on previous literature reports. However, and as a consequence, the copolymer has only blue photoluminescence in solution from the PBS-PFP part. Nevertheless, white light emission from a single polymer main chain may be possible in fabricated EL devices, where the emission component from the lower excitation on-chain chromophore is often drastically enhanced [244]. Future work should be directed towards building an EL device to test this specific copolymer property.

Chapter 6

Systems of surfactant and polyelectrolyte with PBS-PFP based copolymers

Water soluble photoluminescent polymers can be formed by π-π conjugated hydrophobic backbones with charged side groups and consequently, are highly sensitive to external agents such as pH, ionic strength, polarity and to the presence of small molecules [306]. Because of this, conjugated polyelectrolytes (CPEs) show considerable potential as chemical and biological sensors [110, 122, 307–313]. In addition, research on these systems has led to their rapid development for use in areas such as p-n heterojunctions, bioimaging applications, PLEDs, photovoltaic devices and light-emitting field-effect transistors (LEFETs) [77, 114, 116–118, 120, 128, 229, 314–316]. However, the aqueous and polar media in which these studies are carried out frequently induce the aggregation of the polymer hydrophobic backbone, rendering a less soluble material with a lower emission efficiency. With the aim of increasing the sensitivity and other properties of water soluble conjugated polymers, efforts have been made to develop methods for increasing CPE solubility in aqueous and polar solvents. The interaction of the polymer hydrophobic backbone and hydrophilic side chains with surfactants is a promising approach to enhance the emission efficiency and other properties of the CPEs [122, 317].

It has proved possible to break up aggregates of the anionic PBS-PFP copolymer in aqueous solution by using nonionic alkyloxyethylene surfactants, as shown by NMR spectroscopy, small angle and X-ray neutron scattering (SANS and SAXS, respectively) and fluorescence spectroscopy [124, 126, 140, 318, 319]. In addition, 1,2-dilauryl-3-acetylarginyl-*rac*-glycerol (1212R) - a synthetic alternative to the biocompatible surfactant lecithin - was observed to induce PBS-PFP micelle behavior. A stable, water-soluble aggregate in

which the polymer exists as isolated chains is formed, opening the window for applications of PBS-PFP for sensing in biological systems [142]. There exist several examples of PBS-PFP+surfactant interaction and it is interesting to note that not all the surfactant-polyelectrolyte complexes function similarly. For instance, the influence of several cationic tetraalkylammonium surfactants with different structures (alkyl chain length, counterion, or double alkyl chain) and of anionic surfactant sodium dodecylsulfate (SDS) has been monitored by emission spectroscopy and conductivity measurements [125]. The cationic surfactants lead to the appearance of a new emission band, that according to the authors is due to energy hopping to defect sites (keto defects), caused by the increase of PBS-PFP interchain interaction; favored by charge neutralization and by hydrophobic interactions [125]. Copolymer aggregation is induced by the cationic surfactants at concentrations well below the surfactant critical micelle concentration (cmc), while in the presence of the anionic SDS, this is inhibited due to the electrostatic repulsion between the surfactant and the negatively charged polymer [125]. A deeper insight into the driving force for PBS-PFP+surfactant interaction can be seen from photophysical and molecular dynamics studies in the presence of gemini C_sH_{2s}-α,ω-$((CH_3)_2N^+C_mH_{2m+1}Br^-)_2$ surfactants (m-s-m), with different spacer (s) and alkyl chain (m) lengths [320] [320]. The interaction is described as mainly electrostatic between the oppositely charged tetraalkylammonium group of the surfactant and the sulfonate group of the polymer. However, for surfactant concentrations around the cmc, the polymer aggregates are disrupted and incorporated into the surfactant micelles. This leads to increases in the polymer emission and PLQY. Molecular dynamics simulations, showed that the hydrophobic part of the geminis interact preferentially with the copolymer backbone and electrostatic interactions are favored when the spacer length is close to the intercharge separation in the polymer [320].

The effect of cationic surfactants, cationic polyelectrolytes and a cationic ionic liquid on the anionic conjugated PBS-PFP with on-chain chromophores, has been investigated and is discussed in this chapter. It is expected that at low concentration the cationic agents may induce aggregation, but at high concentration will enhance the photoluminescence of the several PBS-PFP copolymers by separation of the polymer chains. This will reduce the quenching by nonemissive interchain aggregates via incorporation of the CPEs into cationic agents+polymer complexes.

6.1 PBS-PFP copolymers and tetraalkylammonium surfactants

The amphiphilic chain structure of surfactants makes them particularly favourable to reside at air-water and other interfaces. The micelle formation of a surfactant in solution is induced by the hydrophobic interactions between their hydrocarbon tails balanced by hydration and electrostatic effects. The core of the micelle can be pictured as similar to a small oil droplet with the surfactant head groups located at the surface. Figure 6.1.1 show the wide range of different surfactant self-assembly structures [143, 321, 322].

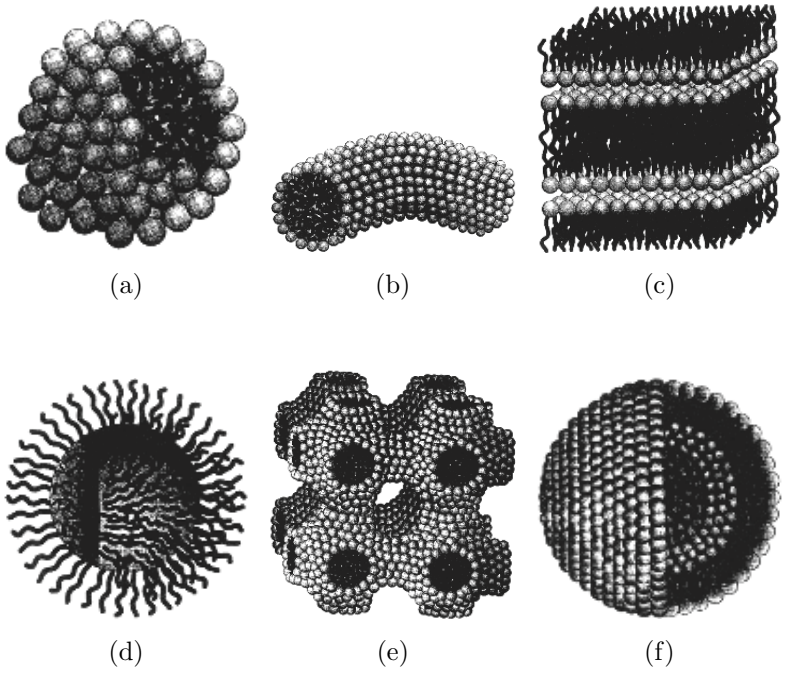

Figure 6.1.1: Examples of surfactant self-assembly structures. a) Spherical micelle. b) Cylindrical micelle. c) Lamellar phase. d) Reversed micelle. e) Bicontinuous structure. f) Vesicle. Reproduced with permission from Ref. [143]. © (2003) Wiley-VCH Verlag GmbH & Co. KGaA.

Cationic surfactants are frequently depicted as quaternary salts and their solution properties have been evaluated in terms of cmc, degree of counter ion dissociation (α), sphere-to-rod transition, aggregation number and various thermodynamic properties. That reflect the several combinations of the surfactant hydrophobic tail with the hydrophilic group and the counter ion species [322], [323]. Hexadecyltrimethylammonium bromide salts have a tendency to form rodlike (or wormlike) micelles. However, the formation of such rodlike

micelles depends upon both the concentration and nature of the counter ion attached, e. g. the chloride ion tend to give origin to spherical micelles [322]. In the alkyltrimethylammonium bromide the majority of the studies involve alkyl chain lengths of up to sixteen carbons and hence, the octadecyltrimethylammonium halides have undergone more limited investigation. Mostly due to C_{18}TAB relatively low cmc and solubility in water (Table 6.1). In addition to normal micelle formation, C_{18}TAB can also form reverse micelles and microemulsions in nonpolar medium [324], [325].

The propensity of polymers to arrange as single strands or aggregates, in a particular solvent, can be manipulated via the hydrophobicity and charge properties of the side chain [326]. In addition, the interaction between polyelectrolytes and surfactants can lead to various self-assembly motifs [327]. Depending on the polyelectrolyte and surfactant properties, the polyelectrolyte/surfactant complexes can assume wide morphologies as: 1) single-stranded substoichiometric complexes in aqueous solution, 2) stoichiometric complexes in nonaqueous solution, 3) polymer/micelle complexes, 4) vesicles and 5) liquid crystals [327–333].

The effect of chain length and counter ion of alkyltrimethylammonium halides C_nTAX in solutions of PBS-PFP with on-chain chromophore segments has been followed by electrical conductivity, UV-vis absorption and emission spectroscopy and TCSPC measurements. Here n represents the carbon aliphatic chain length, with the quartenary ammonium group as the terminal group (n = 16 and 18) and X the halide counter ion (Table 6.1).

Table 6.1: Values of cmc and degree of counter ion dissociation, α, for the alkyltrimethylammonium halide surfactants at 298.15 K.

Surfactant	cmc	α	Reference
C_{16}TAB	9.64×10^{-4} M	0.238	[323]
C_{18}TAB [a]	3.80×10^{-4} M	0.257	[322]
C_{16}TAC	1.72×10^{-3} M	0.520	[334]

[a] Determined at 303.15 K.

6.1.1 PBS-PFP-PDI and hexadecyltrimethylammonium bromide complexes

As discussed in the previous chapter the PBS-PFP-PDI fluorescence in nonpolar media involves emission from both PFP and PDI groups. The latter is suggested to involve an

interchain process thus, revealing that isolated copolymer chains in solution do not undergo efficient intramolecular energy transfer. However, quenching of the PBS-PFP excited state by PDI is observed in aqueous media and ultrafast pump-probe studies in water and water/dioxane mixture show that electron transfer can occur from the PFP units to the PDI. The extent of this increases with aggregation, in agreement with it being mostly an interchain process. Since the competition between energy and electron (charge) transfer depends upon the polarity of the medium, the interaction of the positively charged surfactant hexadecyltrimethylammonium bromide (C_{16}TAB) with the negatively charged PBS-PFP-PDI copolymer is expected to provide interesting observations [126], [127]. Therefore, the effect this surfactant on the photophysics of PBS-PFP-PDI was studied in solution.

6.1.1.1 Fluorescence spectra

Various concentrations of the cationic surfactant C_{16}TAB were added to a solution of PBS-PFP-PDI in water/dioxane (1:1, v/v) (approx. 5×10^{-6} M, in terms of the copolymer repeat unit), Figure 6.1.2.

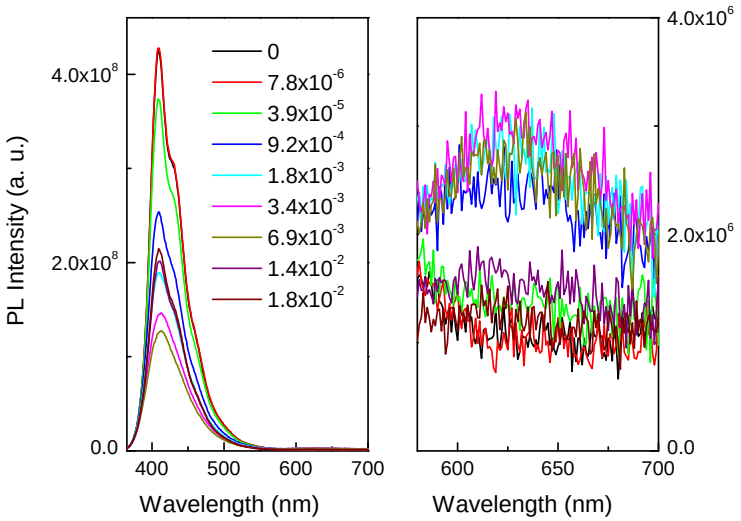

Figure 6.1.2: Left, emission spectra of PBS-PFP-PDI (5×10^{-6} M) with increasing CTAB concentrations (M) in water/dioxane (1:1, v/v) mixture. Right, long wavelength region of the emission spectra of PBS-PFP-PDI (5×10^{-6} M) with increasing CTAB concentrations (M) showing a new emission maximum located at 635 nm.

As previously reported, for the interaction between PBS-PFP and C_{16}TAB [125], the emission of the copolymer below the surfactant cmc is partially quenched. The PLQY value of 0.17 found for the PBS-PFP homopolymer/C_{16}TAB system is typical for highly ag-

gregated systems (Table 6.2). The surfactant induces changes of the PBS-PFP-PDI PL intensity, which are also attributed to aggregation. Above 3.4 mM C_{16}TAB concentration, the emission intensity increases and the (emission) vibrational fine structure is recovered. However, no significant shift is observed for the absorption and emission maxima (Figures 6.1.2 and 6.1.3). The decrease of the PLQY upon C_{16}TAB addition (from 0.55 to 0.47) may indicate the presence of additional excited state deactivation pathways for the PBS-PFP-PDI aggregates (Table 6.2). There is a very weak PDI based emission in the 600 - 650 nm region (at C_{16}TAB concentration ranging from 9.2×10^{-4} M to 6.9×10^{-3} M) upon excitation in the PFP band (Figure 6.1.2). This suggests that some energy transfer can occur from the PFP units to the PDI chromophore in the hydrophobic surfactant medium, as shown by the fluorescence excitation spectra with observation at 635 nm (Figure 6.1.3).

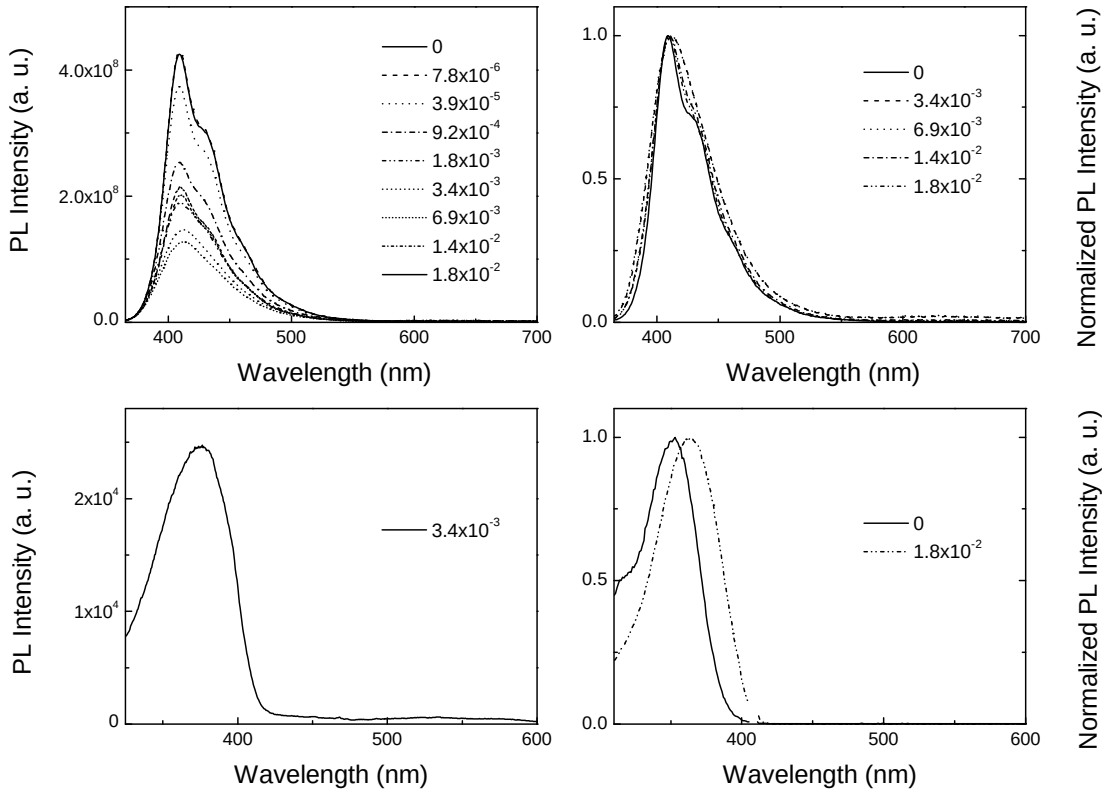

Figure 6.1.3: PL emission spectra of PBS-PFP-PDI with increasing C_{16}TAB concentrations (M) in water/dioxane (1:1, v/v) mixture (top left). Normalized PBS-PFP-PDI emission spectra at surfactant concentrations above the cmc (top right). PL excitation spectra of PBS-PFP-PDI with 3.4 mM CTAB concentration in water/dioxane (1:1, v/v) mixture for emission at 635 nm (bottom left). PL excitation spectra of PBS-PFP-PDI in the absence of the surfactant and at maximum surfactant concentration for emission at 409 nm (bottom right).

Table 6.2: Absorption and Emission Maxima and PLQY of PBS-PFP-PDI and PBS-PFP in water/dioxane (1:1, v/v) and with C_{16}TAB.

	0 M C_{16}TAB			1.8×10^{-2} M C_{16}TAB		
	Absorption (nm)	Emission (nm)	Φ_F	Absorption (nm)	Emission (nm)	Φ_F
PBS-PFP-PDI	360	408	0.55	363	409	0.47
PBS-PFP	372	410	0.52	380	416	0.17

For a better understanding of the copolymer-surfactant system, the surfactant cmc was estimated for the water/dioxane mixture by electrical conductivity measurements and found to be 4.0 (±0.3) mM (Figure 6.1.4), in excellent agreement with the concentration where the spectral changes in the PBS-PFP-PDI copolymer emission occur. The cmc is significantly higher than that of C_{16}TAB in water (9.64×10^{-4} M at 25 °C) [335].

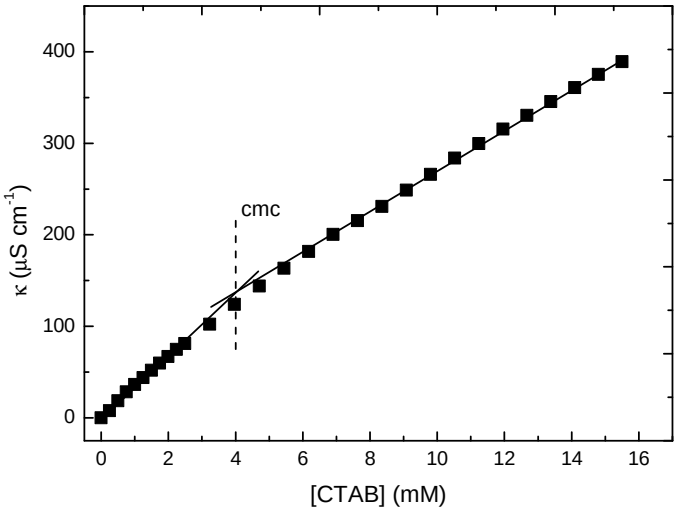

Figure 6.1.4: Specific electrical conductance, κ, of C_{16}TAB in dioxane/water (1:1, v/v) at 298.15 K. vertical dashed line show the critical micelle concentration (4.0±0.3 mM) as obtained by the intersection of the two straight lines method (e.g. [323]).

6.1.1.2 Fluorescence lifetimes

Time resolved fluorescence studies have also been carried out, for the investigated copolymer at the maximum surfactant concentration. The decays were collected at both the PF emission maximum and within the PDI emission range and fitted in three exponentials.

The results are shown in Figure 6.1.5 and Table 6.3.

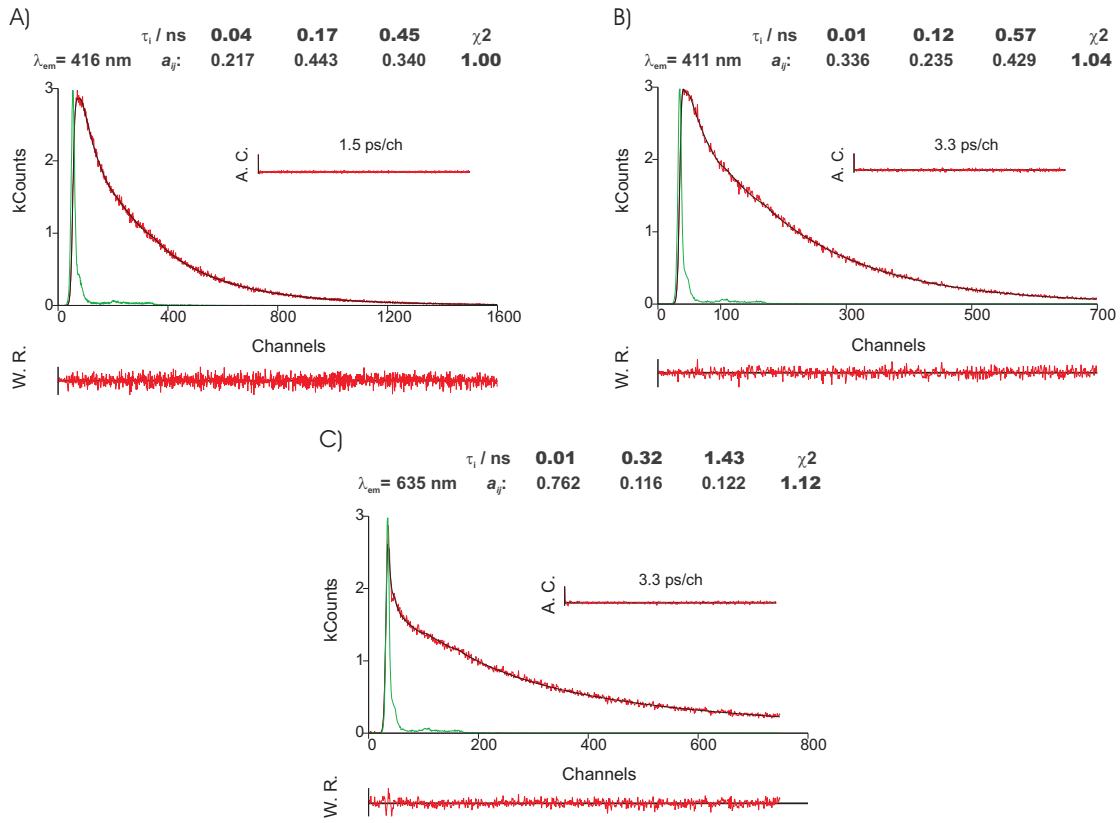

Figure 6.1.5: Fluorescence emission decay for A) homopolymer PBS-PFP in water/dioxane (1:1, v/v) mixture and 18 mM C_{16}TAB obtained with λ_{exc} 392 nm at 298 K and λ_{em} 416 nm. Fluorescence emission decays for the copolymer PBS-PFP-PDI in water/dioxane (1:1, v/v) mixture and 18 mM C_{16}TAB obtained with the same conditions and collected at B) with λ_{em} 411 nm and C) with λ_{em} 635 nm. The green lines in the decays are the instrumental response function (IRF). For a better judgment of the quality of the fits weighted residuals (W.R., scale $-3 \leq \sigma \leq +3$) autocorrelation functions (A.C.) and chi-square values (χ^2) are also presented.

The assignment of the decay time components in CPE, when in the presence of surfactants or other polyelectrolytes, is not easy or consensual. When the system is investigated in the presence of the cationic surfactant C_{16}TAB, an additional longer lifetime component (1.43 ns) is found at 635 nm in the emission range of the PDI chromophore (Table 6.3 and Figure 6.1.5). Moreover, the shortest component decay time for PBS-PFP-PDI in the presence of C_{16}TAB is found to decrease to a value of 10 ps. This may indicate, in contrast to the "good" solvent system water/dioxane, the presence of an additional deactivation process, such as interchain energy hopping, competing with conformational relaxation (CR)

and on-chain excitation energy transfer (ET).

Table 6.3: Fluorescence decay times (τ_i) and pre-exponential factors (a_{ij}) for the copolymers PBS-PFP-PDI and PBS-PFP in water/dioxane (1:1, v/v) mixture with 18 mM C_{16}TAB, obtained with excitation at 372 nm, emission at the wavelength maxima indicated and T = 298.15 K.

	λ_{max} (nm)	τ_1 (ns)	τ_2 (ns)	τ_3 (ns)	a_{i1}	a_{i2}	a_{i3}	χ^2
PBS-PFP	416	0.04	0.17	0.45	0.217	0.443	0.340	1.00
PBS-PFP-PDI	411	0.01	0.12	0.57	0.336	0.235	0.429	1.04
	635	0.01	0.32	1.45	0.762	0.116	0.122	1.12

These results are all in agreement with the surfactant inducing aggregation of the CPE. Comparable decay components (ca. 0.32 and 1.43 ns) have previously been reported by Fron *et al.* [160] for a non-ionic PF copolymer with random on-chain PDI chromophores in polar solvents. The authors suggested the occurrence of a photoinduced charge transfer (CT) process. Ultrafast pump-probe experiment in water/dioxane (chapter 5) confirms this with PBS-PFP-PDI. The decay time observed in the region of the PDI emission (1.43 ns) is considerably shorter than that of the isolated chromophore (5.65 ns), suggesting a competing deactivation process in the micellar environment, which may involve charge transfer.

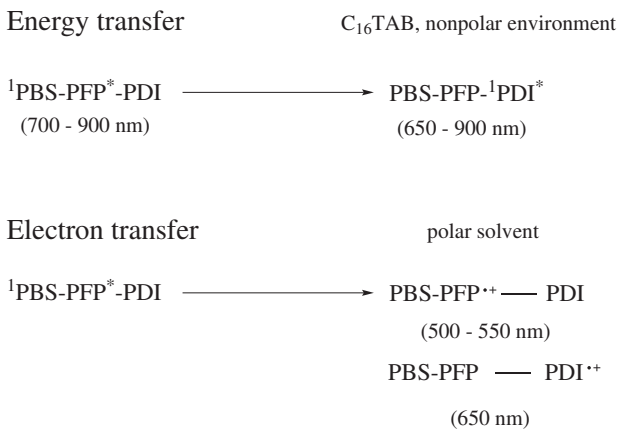

Figure 6.1.6: Schematic kinetic pathway for PBS-PFP-PDI in water, water/dioxane (1:1, v/v) mixture and in the presence of the cationic surfactant C_{16}TAB upon excitation of the PFP unit.

Based on the collected data, both energy and electron (or charge) transfer are possible with PBS-PFP-PDI upon excitation of the PFP copolymer units. The kinetic pathways, depicted above in Figure 6.1.6, show that this can be mediated by control of the polarity of the environment through use of surfactants.

6.1.2 PBS-PFP-TBTT$_x$ and alkyltrimethylammonium halide surfactant complexes

The effect of adding alkyltrimethylammonium halide surfactants to dilute solutions of the PBS-PFP-TBTT$_x$ copolymers described in the previous chapter was studied by fluorescence (steady state and time resolved), electrical conductivity and molecular dynamics. Molecular dynamics helps provide insights into copolymer+surfactant interactions in solution.

6.1.2.1 Photoluminescence spectra

At surfactant concentrations below the cmc, a decrease in the emission maxima in the PFP region was observed, accompanied by an enhancement in the TBTT emission (Figure 6.1.7 [1]). The surfactant effect on the copolymers is clearer in the fluorescence quantum yield measurements (Table 6.4).

Table 6.4: PLQY of PBS-PFP-TBTT$_x$ in water/dioxane (1:1, v/v) mixture with alkyltrimethylammonium halide surfactants.

	PBS-PFP-TBTT$_{10}$		PBS-PFP-TBTT$_{16}$	
	$\Phi_F{}^a$ (PFP)	$\Phi_F{}^a$ (TBTT)	$\Phi_F{}^a$ (PFP)	$\Phi_F{}^a$ (TBTT)
C_{16}TAB	0.43	0.02	0.21	0.11
C_{18}TAB	0.21	0.11	0.05	0.17
C_{16}TAC	0.11	0.13	0.02	0.20

[a] PLQY were determined using quinine sulphate in 0.5 M H_2SO_4.

[1] The emission data is only shown for the copolymer PBS-PFP-TBTT$_{10}$, since the spectroscopic changes happen in the same emission region and surfactants concentration for both copolymers.

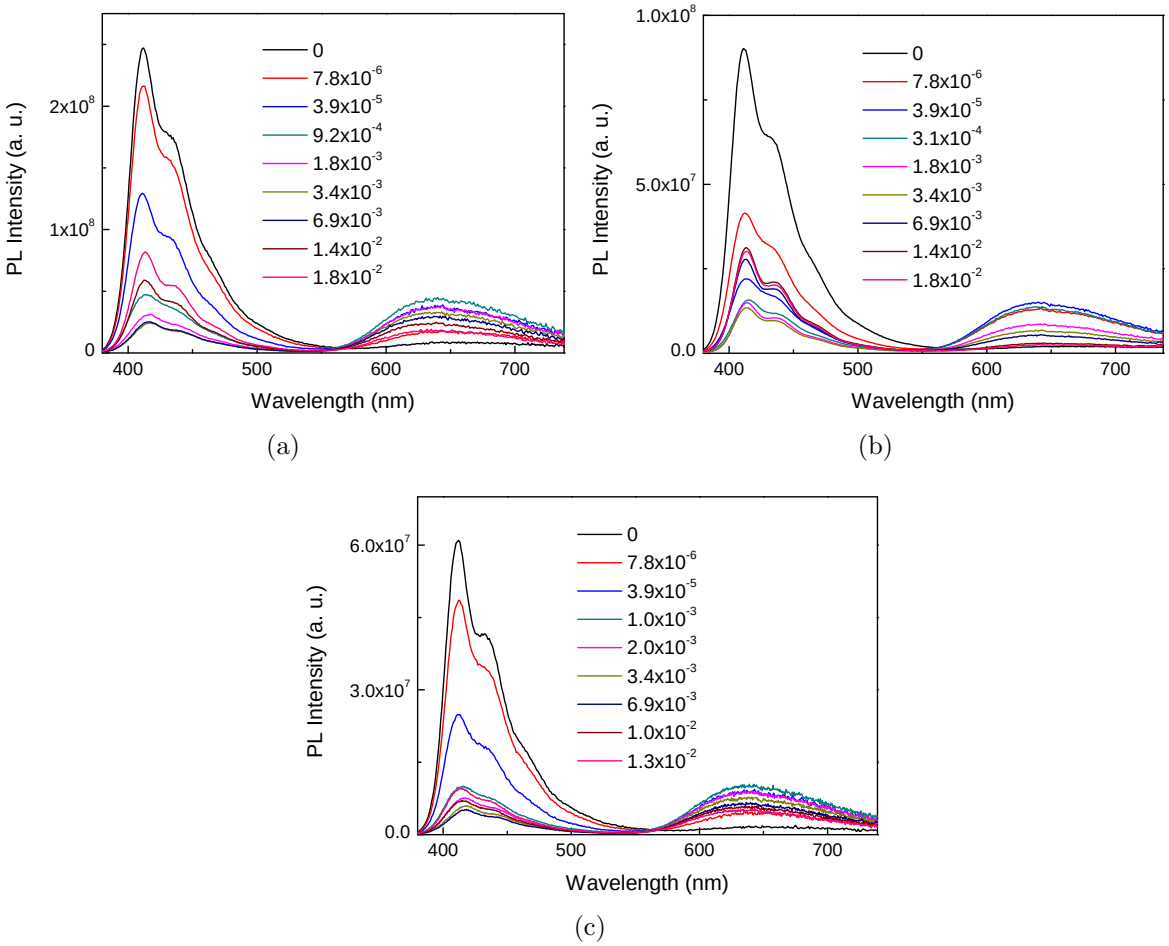

Figure 6.1.7: Photoluminescence emission of PBS-PFP-TBTT$_{10}$ in water/dioxane (1:1, v/v) mixture in the presence of the alkyltrimethylammonium halide surfactants. a) C_{16}TAB, b) C_{18}TAB and c) C_{16}TAC.

The data is consistent with the interaction between the copolymers and surfactants leading to a change in the copolymer morphology adopted. However, when increasing the cationic surfactants concentrations above its cmc an increase in the PFP maximum intensity was observed. The PL increase has been related to the "break-up" of aggregate clusters in solution, which also explains the diminish TBTT emission for the above mentioned cationic surfactant concentrations. As in the PBS-PFP-PDI case, PBS-PFP-TBTT$_x$ copolymers show a different behaviour from what was observed with the homopolymer PBS-PFP, where C_{16}TAB produces a marked quenching in the polyelectrolyte emission [125]. From the emission data collected, C_{16}TAC seems the most efficient in the copolymer solubilization and C_{18}TAB the least promissing, Figure 6.1.8. This may be related with the counter-ion effect, as well as, with the increase of aggregated structures in solution (C_{18}TAB

itself forms elongated micelles easily).

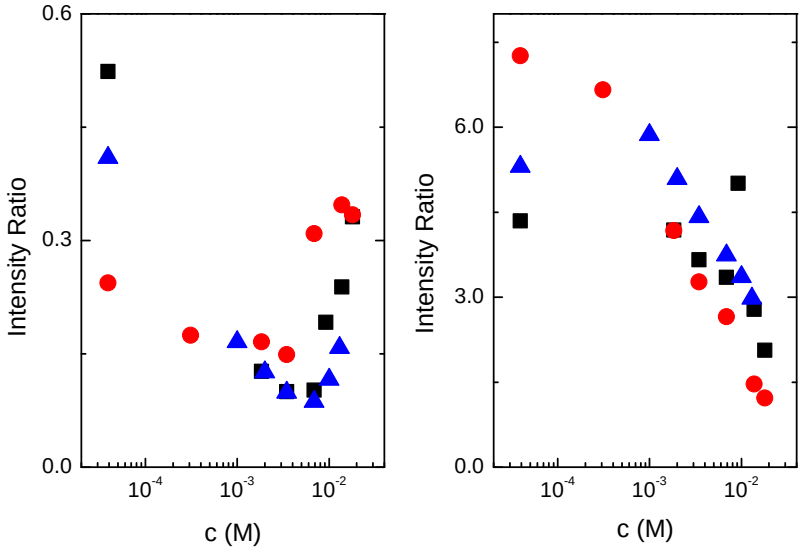

(a)

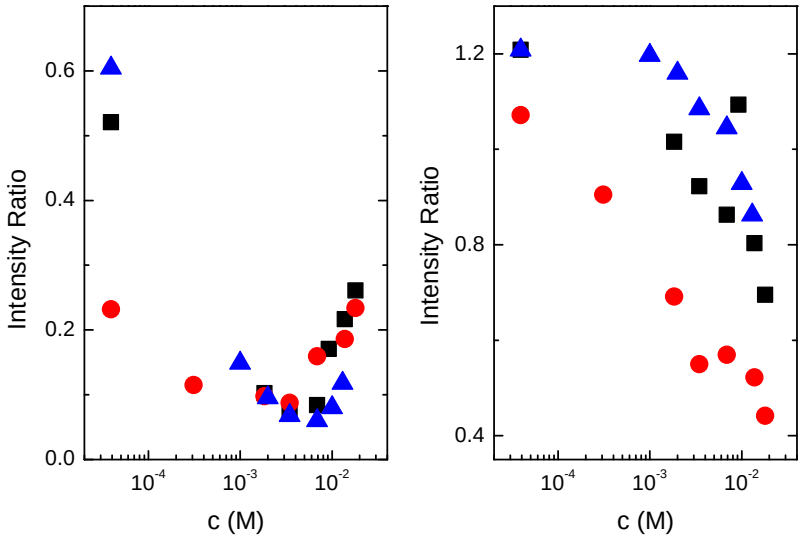

(b)

Figure 6.1.8: Photoluminescence intensity ratio collected at 411 nm (left) and 650 nm (right) as a function of the cationic surfactant concentration. a) copolymer PBS-TBTT$_{10}$ and b) copolymer PBS-TBTT$_{16}$. Black squares C_{16}TAB, red circles C_{18}TAB and blue triangles C_{16}TAC.

To attempt to probe whether the copolymers behaviour is due to the ionic or hydrophobic interaction, light-scattering experiments were performed. Spectrofluorimeters can successfully be used for light-scattering, allowing molecular weights and second virial

coefficients determination, as well as, the observation of an external agent effect on the scattering [336]. The intensity of the scattered light was determined with a Horiba-Jobin-Ivon SPEX Fluorog 3-22 spectrometer with excitation and observation at 705 nm using 1 mm slits. Sets of solutions of different concentration were prepared and the intensity given directly by the spectrofluorimeter. However, ill defined behavior was observed and the data obtained ambiguous. Hence, to test if the effect of surfactant addition was a result of charge neutralization of the anionic copolymer by the cationic surfactants, NaBr was added to a 1×10^{-5} M (in terms of monomer unit) solution of PBS-PFP-TBTT$_{16}$ in water/dioxane (1:1, v/v) (Figure 6.1.9). The increased intensity in the PFP region for NaBr concentrations above 1 mM can be attributed to charge neutralization of the anionic copolymer, that results in a higher copolymer solubility in the medium (Figure 6.1.9). The TBTT emission above 1 mM is slightly quenched, which may support the previous statement.

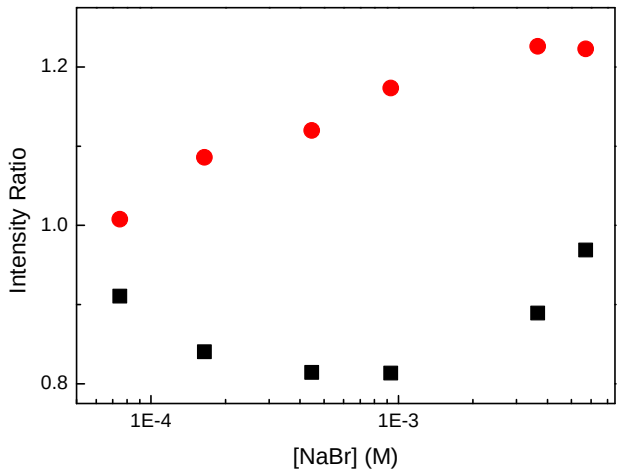

Figure 6.1.9: Intensity ratio as a function of NaBr concentration for the PBS-PFP-TBTT$_{16}$ copolymer (1×10^{-5} M in terms of monomer units). Black squares, PBS emission region and red circles, TBTT emission region.

6.1.2.2 Fluorescence lifetimes

Time resolved experiments were performed to reveal the effect of the cationic surfactants on the emission kinetics. The fluorescence decays of the copolymers PBS-PFP-TBTT$_x$ were obtained at the surfactants maximum concentration (Tables 6.5 and 6.6).

Table 6.5: Fluorescence decay times (τ_i) and pre-exponential factors (a_{ij}) for the copolymers PBS-PFP-TBTT$_{10}$ in water/dioxane (1:1, v/v) mixture with alkyltrimethylammonium halides, obtained with excitation at 392 nm, emission at the wavelength maxima.

	λ_{em} (nm)	τ_1 (ns)	τ_2 (ns)	τ_3 (ns)	τ_4 (ns)	a_{i1}	a_{i2}	a_{i3}	a_{i4}	χ^2
water/dioxane	410	—	0.25	0.51	—	—	0.267	0.733	—	1.05
C_{16}TAB[a]	410	0.05	—	0.52	—	0.586	—	0.414	—	1.03
	640	0.04	—	0.66	3.23	-0.212	—	0.226	0.774	1.04
C_{18}TAB[b]	410	—	0.14	0.46	—	—	0.448	0.552	—	0.92
	650	0.01	—	—	3.28	0.958	—	—	0.042	1.03
C_{16}TAC[a]	413	0.02	0.10	0.56	—	0.520	0.304	0.176	—	0.97
	650[c]									

[a] T = 298.15 K.

[b] T = 306.15 K.

[c] Counting efficiency not enough to built up a fluorescence kinetic decay.

Table 6.6: Fluorescence decay times (τ_i) and pre-exponential factors (a_{ij}) for the copolymers PBS-PFP-TBTT$_{16}$ in water/dioxane (1:1, v/v) mixture with alkyltrimethylammonium halides, obtained with excitation at 392 nm, emission at the wavelength maxima.

	λ_{em} (nm)	τ_1 (ns)	τ_2 (ns)	τ_3 (ns)	τ_4 (ns)	a_{i1}	a_{i2}	a_{i3}	a_{i4}	χ^2
water/dioxane	410	0.02	0.18	0.47	—	0.422	0.245	0.333	—	0.96
C_{16}TAB[a]	414	0.02	0.12	0.52	—	0.608	0.172	0.219	—	0.96
	660	0.01	—	0.45	2.58	-0.916	—	0.265	0.735	1.10
C_{18}TAB[b]	413	0.01	0.07	0.56	—	0.837	0.122	0.040	—	0.99
	660	0.01	0.29	—	2.27	-0.920	0.920	—	0.731	1.07
C_{16}TAC[a]	413	0.01	0.08	0.55	—	0.883	0.045	0.073	—	0.97
	650[c]									

[a] T = 298.15 K.

[b] T = 306.15 K.

[c] Counting efficiency not enough to built up a fluorescence kinetic decay.

In the presence of the cationic surfactants, the decays collected at the fluorene emission region (410 - 414 nm) gave mostly a biexponential decay for the copolymer PPS-PFP-$TBTT_{10}$ (with the exception of C_{16}TAC) and a triexponential for PBS-PFP-$TBTT_{16}$. In both copolymers a rise time was observed for the shortest component (10 - 50 ps) when the decay was collected at the TBTT emission region (640 - 660 nm). This is a clear evidence that upon excitation there is energy transfer, either on-chain or interchain, between the excited singlet states of the fluorene and the TBTT chromophore. The 470 - 660 ps decay component (τ_3), that represents the isolated copolymer chain lifetime, is the most affected in the energy transfer process. In the presence of cationic surfactants the τ_3 value does not undergo significant changes, but its amplitude is reduced. Furthermore, in the presence of C_{18}TAB when the decay is collected at the TBTT emission maximum, τ_3 disapears from the overall fluorescence kinetics. The slow decay component, 2.58 and 3.23 ns (τ_4), is assigned to the decay of the TBTT chromophore on-chain units (see chapter 5). The actual nature of the τ_2 component is unclear [86]; apparently in this particular case it seems to be intrinsically related with the copolymer+surfactant complexes. In fact, it is highly quenched in the presence of the surfactant and its amplitude increases when the long chain surfactant, C_{18}TAB, is added to the copolymer solution. As discussed earlier, hexadecyltrimethylammonium salts are well known for the formation of rodlike (or wormlike) micelles. Yue *et al.* [327] observed that anionic polyelectrolytes+C_{18}TAB complexes exist in a series of structures of different sizes, chemical compositions and morphologies, depending on the relative concentration of the polyelectrolyte and surfactant. A similar correlation of the interaction between the anionic PBS-PFP-$TBTT_x$ copolymers and C_{18}TAB can be suggested. As for the C_{16}TAC case, the differences in the fluorescence decays are explained by the counter ion; this also plays an important role in micelle formation and geometry. This will be discussed in detail in the next subsection.

6.1.2.3 Electrical conductivity

The electrical specific conductance of surfactants (C_{16}TAB and C_{16}TAC) in the presence of PBS-PFP-$TBTT_{10}$ and PBS-PFP-$TBTT_{16}$ was measured. This provides an excellent method for characterizing ionic micelles or other aggregate species present in solution [125]. At the simplest level, the experimental specific conductance (κ) of the mixed solutions can be considered to be the sum of the following contributions: surfactant (κS), polymer (κP) and interactions between surfactant and polymer ($\Delta\kappa$P-S). Hence, in the absence of any polymer-surfactant interactions the latter term is zero.

For correct interpretation of the results in the water/dioxane (1:1, v/v) mixture it is necessary to determine the cmc of the cationic surfactants. In a water dioxane (1:1, v/v)

mixture, C_{16}TAB and C_{16}TAC show critical micelle concentrations (cmcs) equal to 4.0 ($\pm$0.3) and 4.2 ($\pm$0.3) mM and degrees of counterion dissociation, α, of micelles of 0.62 ($\pm$0.01) and 0.58 ($\pm$0.01), respectively (see Figure 6.1.10 and Table 6.7).

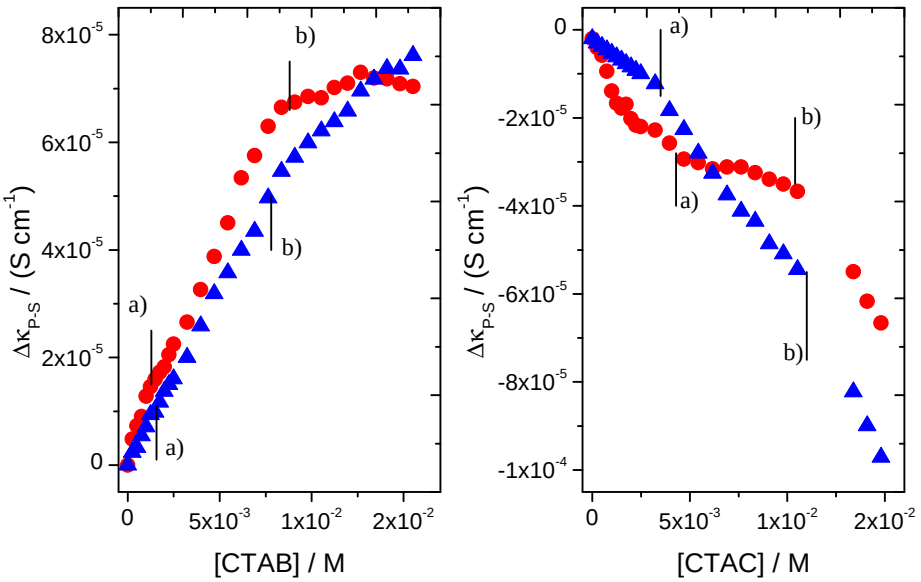

Figure 6.1.10: Effect of interactions between copolymer PBS-PFP-TBTT$_{10}$, 1×10^{-5} M (red circles) and PBS-PFP-TBTT$_{16}$, 1×10^{-5} M (blue triangles) and surfactants on the specific conductance, $\Delta\kappa_{P\text{-}S}$, as a function of surfactant concentrations, in dioxane/water mixed solutions at 25 °C. Vertical lines shows: a) cac and b) psp.

These values are higher than those found in water: C_{16}TAB 0.964 mM, C_{16}TAC 0.238, and 1.72 mM and 0.52, respectively [323], [334]. Solvation of the surfactants by an organic (hydrophobic) species may be expected to lead an increased solubility of the surfactant tail in solution, delaying the aggregation of the surfactant unimers to form micelles and hence increasing the cmc of the surfactant. Similarly increasing the percentage of dioxane in the solvent mixture decreases the dielectric constant [337] and, consequently, the electrostatic interactions between the ionic groups of the surfactant in micelles also decrease, thus increasing the degree of dissociation of counterions. It was found that the effect of the solvent on the degree of bromide dissociation of micelles is more significant then that of chloride. From studies of electrical conductivity as a function of surfactant concentration (Figures 6.1.10 and 6.1.11), very similar behavior is seen with C_{16}TAB and C_{16}TAC, suggesting both are dominate by CTA^+ polyelectrolyte interaction. However, marked differences are seen in the plot of $\Delta\kappa$, the behavior shows more pronounced changes in C_{16}TAC in water/dioxane

(1:1, v/v). This may be due to the formation of elongated structures.

Table 6.7: Effect of PBS-PFP-TBTT$_x$ conjugated polyelectrolytes on the aggregation and micellization parameters of C_{16}TAB and C_{16}TAC in water/dioxane (1:1, v/v) mixture, at 298.15 K.

	cac (mM)	α	ΔG_a^0 (kJ/mol)	psp (mM)
C_{16}TAB	4.0 (±0.3)[a]	0.62 (±0.01)	-30.9 (±0.9)[b]	—
C_{16}TAB + PBS-PFP-TBTT$_{10}$	1.3 (±0.1)	0.42 (±0.01)	-40 (±1)	8.8 (±0.5)
C_{16}TAB + PBS-PFP-TBTT$_{16}$	1.6 (±0.2)	0.57 (±0.01)	-35 (±1)	7.8 (±0.6)
C_{16}TAC	4.2 (±0.3)[a]	0.58 (±0.01)	-32 (±1)[b]	—
C_{16}TAC + PBS-PFP-TBTT$_{10}$	4.3 (±0.8)	0.53 (±0.06)	-33 (±1)	10 (±01)
C_{16}TAB + PBS-PFP-TBTT$_{16}$	3.5 (±0.3)	0.41 (±0.06)	-36 (±1)	11 (±0.6)

[a] This value corresponds to the cmc.

[b] Free energy of micellization.

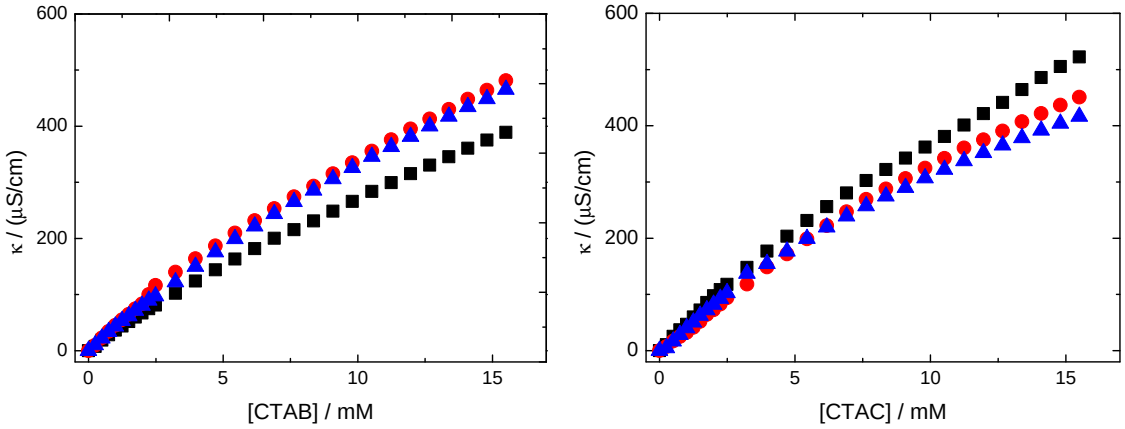

(a) (b)

Figure 6.1.11: Effect of copolymer on the total electrical conductance of cationic surfactants+PBS-PFP-TBTT$_x$. a) C_{16}TAB and b) C_{16}TAC. Black squares: surfactant, red circles: PBS-PFP-TBTT$_{10}$ and blue triangles: PBS-PFP-TBTT$_{16}$.

Taking the length of a fluorene-phenylene unit to be 3/2 higher of a fluorene monomer (0.75 nm [338]) and assuming 5 - 10 monomer units, the length of a fully extended polymer

chain will be in the range 5.6 - 11.2 nm. This is larger than the diameter of a spherical C_{16}TAB micelle (approx. 3.5 nm [339]) which means the PBS-PFP-TBTT/C_{16}TAB aggregates cannot be spherical, but more probably have a cylindrical structure. In addition, above the surfactant cmc, the concentration of micelles is about 100 times higher than that of the polymer, which suggests that at higher surfactant concentration there will be a distribution of one polymer chain per micelle. These effects can explain the observed spectroscopic behaviour. At low surfactant concentration, formation of surfactant-CPE aggregates is observed and lead to a decrease in the PFP emission and energy transfer to the TBTT units. Above the cmc, the copolymer is present as isolated chains in cylindrical micelles and the PFP emission is practically restored. This is supported by further analysis of the electrical conductivity data.

The observed behaviour can be justified by an surfactant effect over the polymer structure. In solution at low concentrations (approx. 10 mM) C_{16}TAC micelles are spheres, that have a tendency to transformed from rod micelles to wormlike ones, at concentrations above 10 mM [339]. Knowing that the polymer has a flexible and rod-like structure, it can be suggested that the presence of the surfactant elongated micelles will contribute for the decreasing of intra and intermolecular polymeric interactions. By forcing the copolymer to adopt a non-aggregate conformation more electrical charge is exposed to the media, and thus, the degree of condensation decreases. While C_{16}TAC addition is characterized by strong hydrophobic and electrostatic interactions ($\Delta\kappa_{\text{P-S}} \leq 0$) [145]. Comparing C_{16}TAC and C_{16}TAB, it is evident that the counterion can select whether rods or spherical micelles are formed in solution [340]. Furthermore, from the effect of the two surfactants on the electrical conductance behavior it can be concluded that the surfactant counterions do not play an important role on the interaction mechanism between cationic surfactants and the conjugated polyelectrolyte. However, there are differences compared with pure surfactants.

The addition of surfactant to a conjugated polyelectrolyte solution leads to a three different regimes (2 break points) of electrical conductance as a function of surfactant concentration. The first transition can be attributed to the critical association concentration (cac) and the second transition point to the polymer saturation point (psp) which, for the sake of simplicity, can be considered as equal to the onset of bulk micelle formation (Figure 6.1.10). These data have been calculated from the intersection of the data regression lines method based on the occurrence of two linear regimes at surfactant concentrations above and below cac or psp, in the plots of κ=f([S]) (see subchapter 6.1.1.1, Figure 6.1.4, as example) [341]. Both aggregation and psp are dependent on the surfactant. The cac of C_{16}TAB occurs at concentrations well below the cmc, whilst for C_{16}TAC taking into account the experimental error the cac is similar to the corresponding cmc, see Figure

6.1.10. This has a direct consequence on the psp, with psp values for C_{16}TAC being higher than those found for C_{16}TAB. However, for each surfactant, the cac and the psp values are independent of the copolymer.

In order to understand the thermodynamics involved in the surfactant+PBS-PFP-TBTT$_{16}$ interactions, the free energy of aggregation, ΔG_a^0, was calculated through equation 6.1. Here R is the gas constant, T the absolute temperature, and X is the cac, or the cmc in the absence of polymer, in mole fraction units.

$$\Delta G_a^0 = (2 - \alpha)RT \cdot lnX \tag{6.1}$$

The degree of counterion dissociation, α, is calculated from the following relation $m_{c>b}$ / $m_{0\leq c<a}$. The subscripts indicate the points (see Figure 6.1.10) that delimit the segment with each slope for plots of specific conductance as a function of surfactant concentration, c (not shown) [342]. The analysis of ΔG_a^0 values (Table 6.7) shows that the aggregation of C_{16}TAB is favoured by the presence of the copolymers, with the highest energetic gain occurring for PBS-PFP-TBTT$_{10}$, which may be due to the lower PBS-PFP-TBTT$_{16}$ solubility. This energetic gain, although minor when compared with micellization, also occurs for the C_{16}TAC surfactant. The ΔG_a^0 values lead to the conclusion that while for C_{16}TAB the free energy gain is due to a small value of cac and α, for C_{16}TAC it is essentially the dissociation degree of counterions that controls the ΔG_a^0; and subsequently, favouring the aggregation rather than micellization. In both cases it can be suggested that the polyelectrolytes can induce the formation of large and more dense surfactant aggregates, with the phenomenon being more pronounced for PBS-PFP-TBTT$_{16}$ copolymer.

A point worth noticing is related with the effect of the polymer nature over the C_{16}TAB and C_{16}TAC properties. Figure 6.1.10 reveals the differences between the PBS-PFP-TBTT$_{16}$ and PBS-PFP-TBTT$_{10}$ profiles. In the concentration range below the cac the effect of PBS-PFP-TBTT$_{10}$ on the surfactant conductivity is predominant, which can be justified by the higher copolymer solubility and consequent greater ability to interact with the surfactant. Furthermore, in PBS-PFP-TBTT$_{10}$ containing solutions and for [S]>psp, $\Delta\kappa$ does not change (C_{16}TAB) or has a smaller value (C_{16}TAC) upon increase of surfactant concentration. This suggests that the polymer has negligible or less significant contribution for the overall electrical conductivity of the solution.

6.1.2.4 Molecular dynamics simulations

Molecular dynamics provides further details on the behavior and nature of the PBS-PFP-PFP$_x$/alkyltrimethylammonium halides complexes. Based on the photophysical and

electrical conductivity data it is suggested that the copolymers form dispersions in water, that can be broken up by addition of organic co-solvents and oppositely charged surfactants [125], [126]. To gain further insight into the origin of the co-solvent effect, in breaking up the polymer clusters, molecular dynamics simulations were carried out on one oligomer (consisting of two PBS-PFP units and one TBTT unit) solvated with a solvent box containing water and dioxane (70% and 30%, respectively); as previously described by Burrows and coworkers [127], [320]. To the oligomer model of PBS-PFP-TBTT in the water/dioxane mixture, several molecules of the cationic surfactant C_{16}TAB were added. Three different and distinct simulations (A, B and C) have been carried out, as summarized in Table 6.8.

Table 6.8: Investigated systems. The number of molecules and counterions are indicated for each system.

	PBS-PFP-TBTT (oligomer)	C_{16}TAB	SPC Water	Dioxane	Na^+	Cl^-
System A	1	—	4684	435	4	—
System B	1	4	4365	453	—	—
System C	1	12	4324	448	—	8

The initial simulation - system A, absence of surfactant - show that the backbone is more rigid than the phenoxybutylsulfonate chains, although the incorporation of the TBTT chromophore confers a certain flexibility to the oligomer backbone (Figure 6.1.12 a)). From the snapshot and data presented in Figure 6.1.12 a) and Table 6.9, respectively, it can be noted that dioxane acts as a coater and displaces water from the oligomer medium. As a consequence, this limits its accessibility to the hydrophobic oligomer chain, while the sulfonate groups and sodium counter ions are preferably solvated by water, as observed by Burrows [320]. Previous studies using different types of binary solvent mixtures (water-methanol, water-dioxane and water-acetonitrile) have indicated the co-solvent effect is not simply a result of changes in polarity, but attributed to specific interactions of the co-solvent with the conjugated charged copolymer backbone [320].

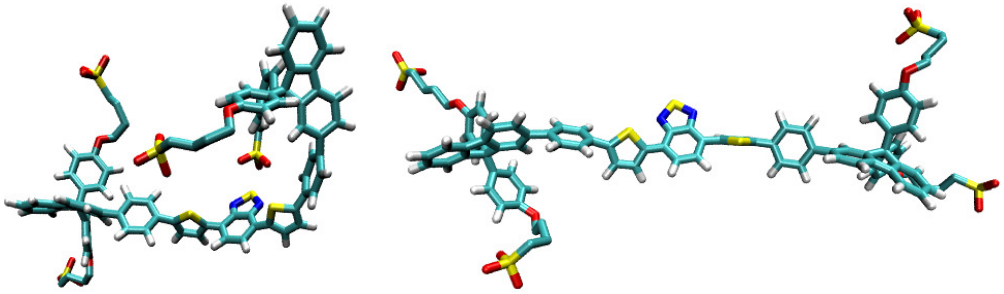

(a) (b)

Figure 6.1.12: Snapshots of PBS-PFP-TBTT oligomer extracted from the MD simulations calculated at 25 °C, illustrating (a) the typical bended conformation of the copolymer free in water/dioxane, in contrast with (b) the typical extended conformation that the copolymer adopt for the same solvent mixture in the presence of 12 molecules of C_{16}TAB.

The simulations were also conducted in the presence of surfactant (Table 6.8 systems B and C). In the snapshot depicted in Figure 6.1.13 can be seen how closely the surfactant interacts with the oligomer, forming a "core-shell" type structure with the hydrophobic copolymer backbone, surrounded by the polymer side chains mixed with the surfactant orientated towards the bulk solvent mixture exterior. The simulations strongly suggest that at least one surfactant molecule is necessary for each CPE repeat unit. It can also be seen that the tails of the surfactant intercalate between the oligomer backbone and hence, induce the separation of clusters, Figure 6.1.12 and Table 6.9. Further evidence of these changes arises from the radial distribution functions of the C_{16}TAB hydrophobic chains, relative to the central carbons of the fluorene, sulfonate and BTD groups of the copolymer, Figure 6.1.14.

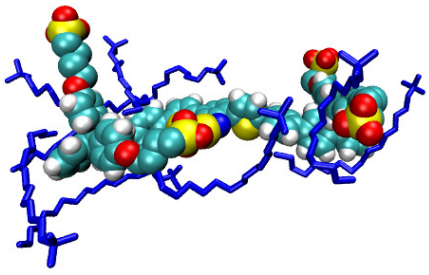

Figure 6.1.13: Snapshot extracted from the MD trajectory for the system composed of PBS-PFP-TBTT oligomer and 12 molecules of C_{16}TAB in water/dioxane, illustrating the copolymer-C_{16}TAB interaction. Hydrophobic chains of C_{16}TAB are preferentially in contact with the polymer, while respective polar heads are exposed to the bulk.

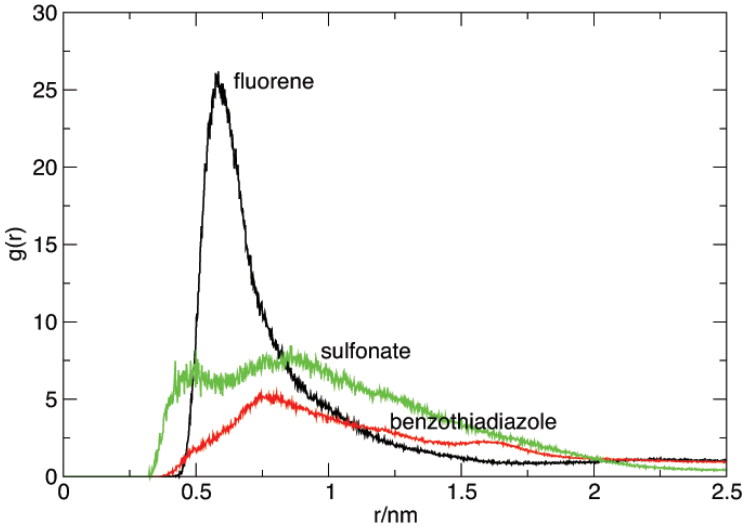

Figure 6.1.14: Radial distribution function of the hydrophobic chains of C_{16}TAB relative to the central carbons of the fluorene groups, sulfonate gropus in the lateral chains and sulfur atom in the BTD group of the copolymer, calculated from the MD simulations carried out at 25 °C for the system PBS-PFP-TBTT (oligomer) + 12 C_{16}TAB in water/dioxane.

Table 6.9: Average conformation of the trimer as extracted from the MD simulations at 25 °C. The overall conformation is described in terms of average distances (mean±SD) between fluorene groups ($d_{FL\text{-}FL}$), fluorene goups and sulfonate groups of the lateral chains ($d_{FL\text{-}SO^{3-}}$), as well as benzothiadiazole (BTD) and the sulfonate groups of the lateral chains ($d_{BTD\text{-}SO^{3-}}$).

	$d_{FL\text{-}FL}$ (nm)	$d_{FL\text{-}SO^{3-}}$ (nm)	$d_{BTD\text{-}SO^{3-}}$ (nm)
System A	2.2 (±0.2)	1.0 (±0.1)	1.1 (±0.5)
System B	2.4 (±0.2)	1.3 (±0.1)	1.4 (±0.4)
System C	2.7 (±0.1)	1.2 (±0.1)	1.7 (±0.4)

This strongly supports the suggestion that the breakup of the polymer clusters is associated with micellization and incorporation of isolated chains of the PBS-PFP-$TBTT_x$ into copolymer-surfactant aggregates [127]. The distance tends to increase with the amount of surfactant molecules. The effect of interaction between the surfactant and the conjugated polyelectrolyte is, thus, strongly suggested by MD simulations. That demonstrate the tendency to form copolymer-surfactant aggregates, in which isolated chains of PBS-PFP-TBTT are included. The changes are similar to those observed upon addition of

organic co-solvent; moreover, they occur at much lower concentrations, highlighting the importance of surfactant binding to the polyelectrolyte.

Figure 6.1.15 depicts the progressive surfactant effect upon break up of aggregation and the growth of the surfactant+CPE complexes. The force that holds the CPE in a cluster (in solution) is though to be due largely to a hydrophobic interaction. The cationic surfactants weaken this hydrophobic force, causing the CPE to adopt a more linear morphology, whose immediate consequence is manifested via increase an in the PL emission and electrical conductance.

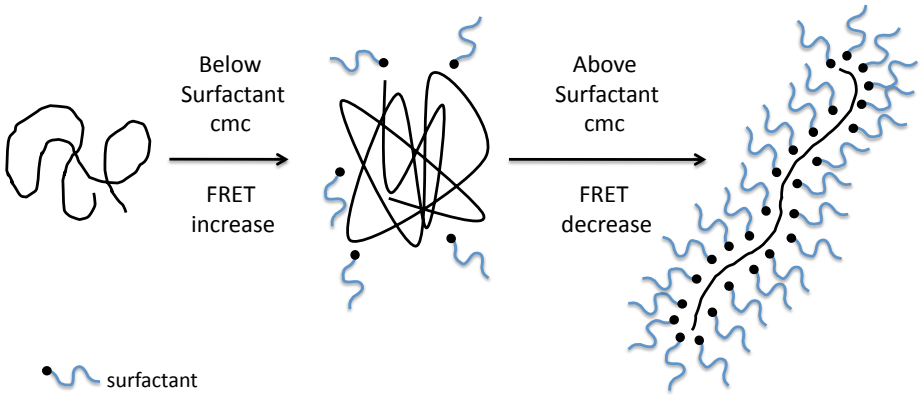

Figure 6.1.15: Schematic diagram that represents the predicted system constituents in three stages: pure copolymers emission, addition of surfactants, aggregation, and formation of copolymer+surfactant complexes.

6.2 PBS-PFP copolymers and poly(allylamine hydrochloride)

Interactions between polyelectrolytes result from the dual character of high charges and rigidity of the macromolecule chain. These are affected by charge density and possible acid-base reaction of functional groups. In the latter case, it can lead to strong or weak macromolecular interactions, depending on the pH of the media. The more usual morphologies of polyelectrolytes are flexible chains. However, rigid rod-like, e. g. poly(phenylene), or spherical, e. g. globular proteins, can also occur [343]. Considerable theoretical and experimental efforts have been conducted to understand the origin of cluster formation in semidilute solutions of highly charged polyelectrolytes. The suggested explanation involves charge fluctuation forces among several polyions, due to counterion sharing or attraction by expansion of the condensed layers between charged rods [332]. Polyelectrolytes can be

classified into natural, modified natural and synthetic. In addition, they can be grouped in terms of their charge as polyanioins, polycations and polyampholytes [2] [343].

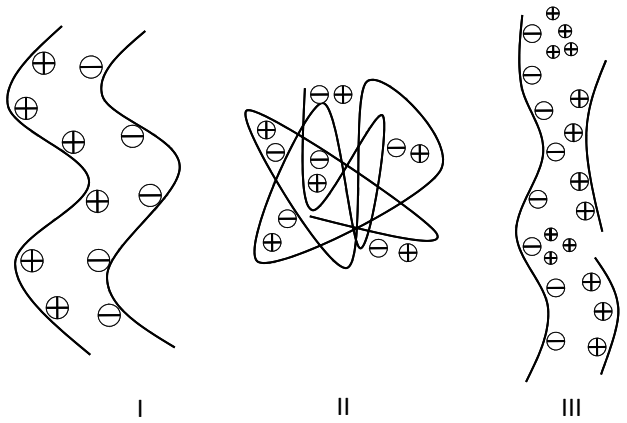

Figure 6.2.1: Polyelectrolyte complex models of ordered and less ordered schoichiometric complexes: I) ladder model, II) scrambled egg model and III) sequential model. Adapted from Koetz *et al.* [343].

Investigation of the interaction between polyelectrolytes and other uncharged and oppositely charged polymers, are important in the development of new fields of application and in the optimization of those already known [344]. The mixing of aqueous solutions of polyions carrying charges of opposite sign results in the formation of aggregated systems, that are generally referred to as polyelectrolyte complexes (PECs) or interpolyelectrolyte complexes [345]. Polyanion-polycation complex (symplexes) formation is a well known phenomenon and is associated predominantly on coulombic interactions [346]. However, other types of non coulombic interactions, such as hydrogen bonding, dipole forces, van der Waals and hydrophobic interactions, can also play a significant role in the structures and stabilization of these complexes [345]. PECs, have a variety of compositions with diverse structures and relatively large dimensions, which are easily tailored by changing the environment parameters: e. g. mixing ratio, concentration, solution pH, ionic strength or temperature, either during or after the complexes formation [347]. When polyelectrolytes with weak ionic groups and large differences in the molecular weight are mixed in a non stoichiometric ratio, the structures formed normally consist of a large host macromolecule; sequently complexed with oppositely charged shorter guest polyions (Figure 6.2.1). In the case of polyions with strong ionic groups and similar molar mass a 1:1 schoichiometric ratio is frequently observed. The final supramolecular structures of the aggregated complexes may be described

[2] Polyelectrolytes which bear both cationic and anionic repeat groups

by different models: ladder structure with fixed ionic cross links, or a more chaotic model structure with a statistical charge compensation (scrambled egg), Figure 6.2.1.

The mixing of polyanion and polycation solutions results in spontaneous aggregation, leading to the release of counterions, see Figure 6.2.2. In the case of high charge densities, the small molecular counterions of free polyelectrolytes are located near the macroions, mainly because of the counterion condensation effect. PEC formation between polyions with weak ionic groups and signicantly different molecular weights in non stoichiometric systems, results in soluble complexes that consist of hydrophilic single-stranded and hydrophobic double-stranded segments. If the long host molecules are in excess, the non-complexed segments keep the PECs in the solution state [332].

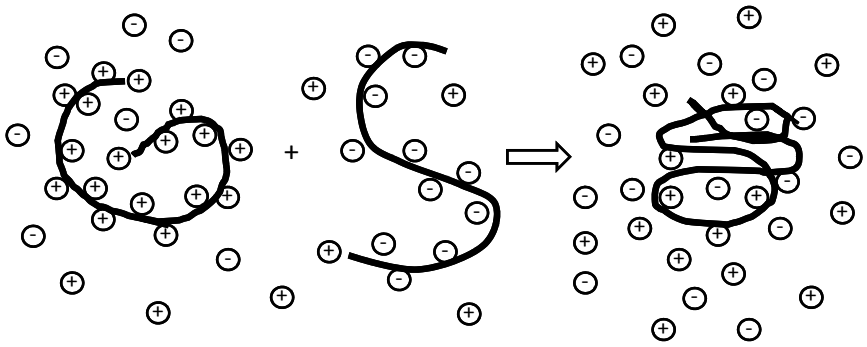

Figure 6.2.2: Polyelectrolyte complex formation scheme. Adapted from Radeva [332].

Molecular self-assembly in such systems can provide a useful synthetic route to many interesting supramolecular structures. Covalent and ionic self-assembly methods have been employed on the multilayer thin film construction, with cooperative electronic and optical properties, including electroluminescence, second harmonic generation and photoinduced electron transfer [348]. Complex formation between two oppositely charged polyelectrolytes can easily be followed by emission spectroscopy, if one of the macromolecules is either labelled or has chromophoric units [349]. Furthermore, the effects of different salts on the dissociation behavior of the two water-soluble PECs, in addition to the effect of the chain length, have also been considered [349], [350].

Poly(allylamine hydrochloride) (PAH), Figure 6.2.3, with positively charged side chains attached to the polymer chain, was tested as a spatially aligned polymer scaffold for aggregation and self-association with the negatively charged PBS-PFP copolymers, through electrostatic bonding interactions, to afford luminescent aggregates. The cationic PAH is a weak polyelectrolyte easily obtained by radical polymerization of allylamine hydrochloric

acid and whose charge can be modified by changing the pH [351], [352].

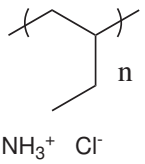

Figure 6.2.3: Structure of the cationic polyelectrolyte poly(allylamine hydrochloride).

This subchapter is focused on the stability of the polyelectrolyte complexes (PECs) between PBS-PFP copolymers and PAH as a function of the complex formation and hydrophobicity of the polyelectrolytes used. This is connected with the size, shape and structure of the PEC structures. PECs were investigated by fluorescence spectroscopy and time resolved emission measurements. Although the sulfonate groups of the PBS-PFP copolymers should behave as strong electrolytes, electrical conductivity measurements showed they behave like weak polyions, with conductivity values quite close to that of the solvent. Since both polyelectrolytes bare weakly ionic groups and have large differences in the molecular weight (PAH average Mw $\sim$ 15 000), it is expected that they will form sequential model complexes in solution [332].

Due to its low solubility in pure aqueous solution at neutral pH value (associated to free base formation), PAH had to be dissolved in a 0.01 M HCl solution (pH $\simeq$ 2) before being added to a water/dioxane (1:1, v/v) copolymer solution.

6.2.1 Steady state and time resolved fluorescence

6.2.1.1 PBS-PFP with on-chain PDI

It has previously been shown that CPE geometry can be modified by complexation with biomacromolecules, where conformational changes of the biomolecules inflict different conformations in the CPE backbone; leading to changes in the absorption and emission properties [353]. Complexation of CPEs with biological polyelectrolytes can be used for building materials and devices, through self-assembly [354] and, thus, to control the electronic properties by tuning the doping level of the conjugated polymer backbone [354]. A similar approach involving reference to biological macromolecule by a synthetic polyelectrolyte will be followed. In addition, it is expected to help understanding the complexation between two oppositely charged systems, both for fundamental and for practical reasons [355].

PBS-PFP has already been studied in the presence of various concentrations of the neutral polymer poly(ethylene glycol) (PEG), of PEG with hydrophobically modified end-cappers (HM-PEG) and of poly(propylene glycol) (PPG) [127]. In the PEG case, only small increases in the fluorescence intensity were seen with no significant shift in the emission band and no dependence on the PEG molecular weight. In contrast, a blue shift in the emission and an increase in the fluorescence quantum yield were seen with PPG and HM-PEG. The differences were explained via a balance between the hydrophobic and the hydrophilic effects, in the interaction of the water soluble polymers and PBS-PFP. The rigidity of the microenvironment in the region of the chromophore may also play an important role [127].

When PAH was added to the PBS-PFP-PDI copolymer solution, a strong emission quenching accompanied by a red-shift on the fluorescence emission maxima and a considerable diminution on the PLQY, were observed (Table 6.10 and Figure 6.2.4). To assist in the interpretation of the results, control experiments were performed on the homopolymer PBS-PFP in the presence of PAH and similar behavior was seen. In contrast with the cationic surfactants, the copolymer spectra do not lose their vibronic shape (Figure 6.2.5) and no clear indication of the PDI emission was detected, thought it may be expected in this water shielded media. The aggregation of polyfluorenes is often accompanied by a spectral broadening of the long wavelength absorption band, which was confirmed in the excitation spectra depicted in Figure 6.2.5 b). The photophysical data suggest that PAH addition leads to the formation of an aggregate with increased PBS-PFP-PDI interchain interaction and order.

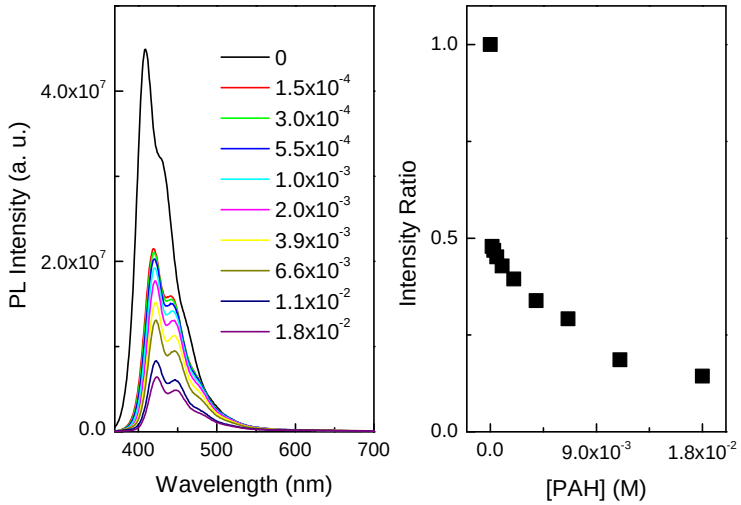

Figure 6.2.4: Emission spectra (right) and intensity ratio (left) of PBS-PFP-PDI with increasing PAH concentrations (M) in water/dioxane (1:1, v/v) mixture.

Table 6.10: Absorption and Emission Maxima and PLQY of PBS-PFP-PDI and PBS-PFP in water/dioxane (1:1, v/v) without and with PAH.

	0 M PAH			1.8×10^{-2} M PAH		
	Absorption (nm)	Emission (nm)	Φ_F	Absorption (nm)	Emission (nm)	Φ_F
PBS-PFP-PDI	360	408	0.55	366	424	0.12
PBS-PFP	372	410	0.52	376	426	0.10

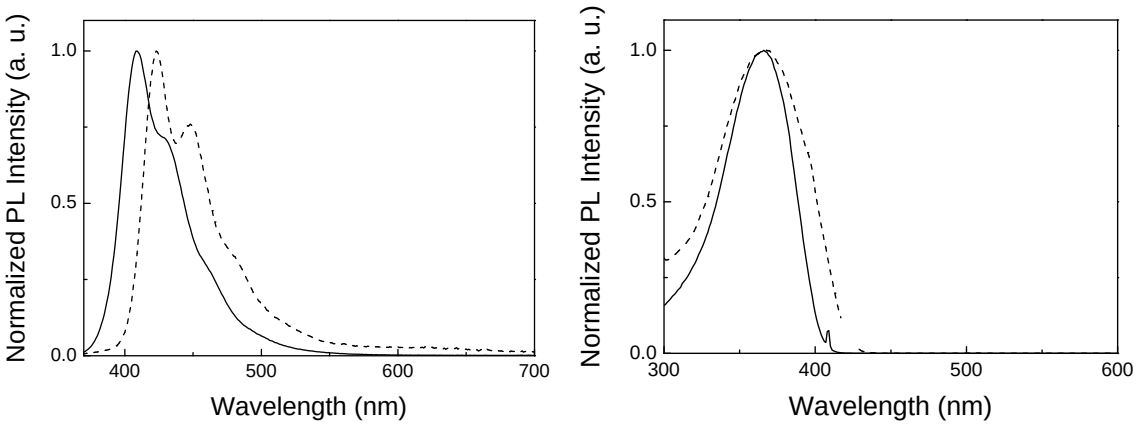

Figure 6.2.5: a) Emission and b) excitation spectra of PBS-PFP-PDI (5×10^{-6} M) in the presence (dashed line) and absence (solid line) of PAH in water/dioxane (1:1, v/v) mixture.

Time-resolved fluorescence experiments were carried out on solutions containing 0 and 18 mM of PAH (in terms of repeat units) at PBS-PFP-PDI solution (5×10^{-6} M, repeating unit) in water/dioxane (1:1, v/v), following excitation at 392 nm and collected at the PFP emission maxima. Though the decay is complex, it was fitted to a triexponential function. The longest lifetime, 360 ps, is assigned to the fluorescence lifetime of the isolated polymer chains of the PBS-PFP-PDI. This component shows a reduction in lifetime from 520 to 360 upon addition of PAH, Table 6.15. The shortening of the decay may either be due to the reduction of the polarity of the medium of the CPE environment by complex aggregate or aggregation, as proposed by Monkman and Liu [86], [356]. What is interesting is that τ_3 contribution to the overall decay is only 1%, compared with 92% in the absence of PAH (Figure 6.2.6).

Table 6.11: Fluorescence decay times (τ_i) and pre-exponential factors (a_{ij}) for the copolymer PBS-PFP-PDI in water/dioxane (1:1, v/v) with 0 and 18 mM PAH, obtained with excitation at 392 nm, emission at the wavelength maxima and T = 298.15 K.

[PAH] (mM)	λ_{em} (nm)	τ_1 (ns)	τ_2 (ns)	τ_3 (ns)	a_{i1}	a_{i2}	a_{i3}	χ^2
0	410	0.06	—	0.52	0.079	—	0.921	1.01
18	420	0.01	0.07	0.36	0.833	0.157	0.010	1.01

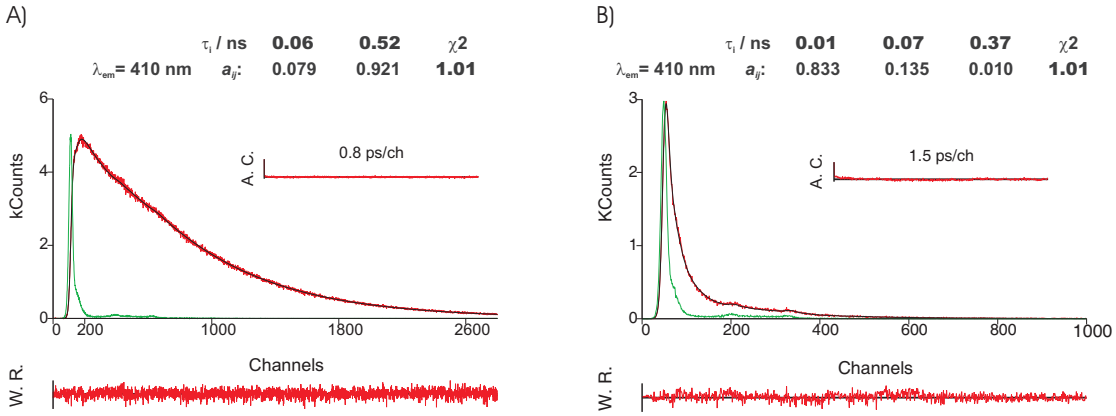

Figure 6.2.6: Fluorescence emission decay for PBS-PFP-PDI collected at the polymer emission maximum obtained with λ_{exc} 392 nm at 298.15 K in water/dioxane (1:1, v/v) mixture A) 0 mM PAH and B) 18 mM PAH. The green lines in the decays are the instrumental response function (IRF). For a better judgment of the quality of the fits weighted residuals (W.R., scale -3 $\leq \sigma \leq$ +3) autocorrelation functions (A.C.) and chi-square values (χ^2) are also presented.

Furthermore, two shorter decay lifetime components are detected (10 and 70 ps). The 10 ps component can be assigned to the exciton decay, quenched by the species in the copolymer/PAH aggregate, involving nonradiative inter and intrachain interactions; and that, in the presence of PAH, is the dominant decay component (83%). This is similar to observed by to Monkman *et al.*, where the polarity has a dramatic effect in thin films of fluorene CPE and where the shortest lifetime has the major role on the overall decay [86]. The decay component τ_2 is probably associated to variable size clusters/aggregates [85], [86], that in a less polar environment increase size and hence, quench τ_2 lifetime (200 - 70 ps [86]). In summary, PAH screens the solvent-copolymer interaction through complexation

with the CPE and reduces its fluorescence lifetime [356], by transforming the surrounding media into a solvent free environment that promptly increases CPE interchain interaction.

6.2.1.2 PBS-PFP with on-chain TBTT

As has previously been shown by Liu *et al.* interchain electronic energy transfer is more effective than intrachain FRET due, to the enhanced electronic coupling and increased dimensionality [271], [356]. Fluorescence quenching of water soluble PF-BTD copolymers in aqueous solution can also be attributed to the charge transfer interaction character of the excited states, due to the electron deficiency of the BTD units [271]. Based on the previous studies, aggregation induced between the PBS-PFP-$TBTT_x$ copolymers and the oppositely charged PAH macromolecule may be expected to favor interchain FRET from the fluorene segments to the TBTT, giving rise to fluorescence change from blue to red. This is confirmed in practice, as depicted in Figures 6.2.7 and 6.2.8.

With increasing PAH concentration, PBS-PFP-$TBTT_{10}$ exhibit a progressive increase in intensity in the PL spectra in the 600 - 700 nm region and a strong quenching in the PFP emission range. This effect is not that evident in the PBS-PFP-$TBTT_{16}$, because the copolymer aggregates easily in solution (see chapter 5). The increase on the TBTT emission and the quenching of the PFP emission, result from complex formation between the two oppositely charged polyelectrolytes. This subsequently creates a hydrophobic environment minimizing the contact between the PBS-PFP-$TBTT_x$ copolymers and the water molecules. The TBTT emission intensity of PBS-PFP-$TBTT_{10}$ and PBS-PFP-$TBTT_{16}$ reach a maximum at PAH concentrations of 1 mM and 11 mM, respectively, possibly indicating complex neutralization. The difference on the concentrations is explained by the copolymer solubility. PBS-PFP-$TBTT_{10}$ requires a lower polyelectrolyte complex (PEC) concentration due to its greater ability to interact with the PAH, similar to what was observed in the cationic surfactant presence (see subchapter 6.1.2). An example of a related complexation enhanced fluorescence, between an cationic PF-BTD copolymer with anionic biomacromolecule, has been described in by Liu [271].

The increase of interchain interactions provide a hydrophobic environment for the polymer against water invasion, that translates into the hight TBTT PLQY, Table 6.12. In solution and at low concentrations, the aggregation between two oppositely charge polyelectrolytes occurs with the formation of rather small particles or aggregates. The increase in polyelectrolyte concentration promotes the growth of the aggregates.

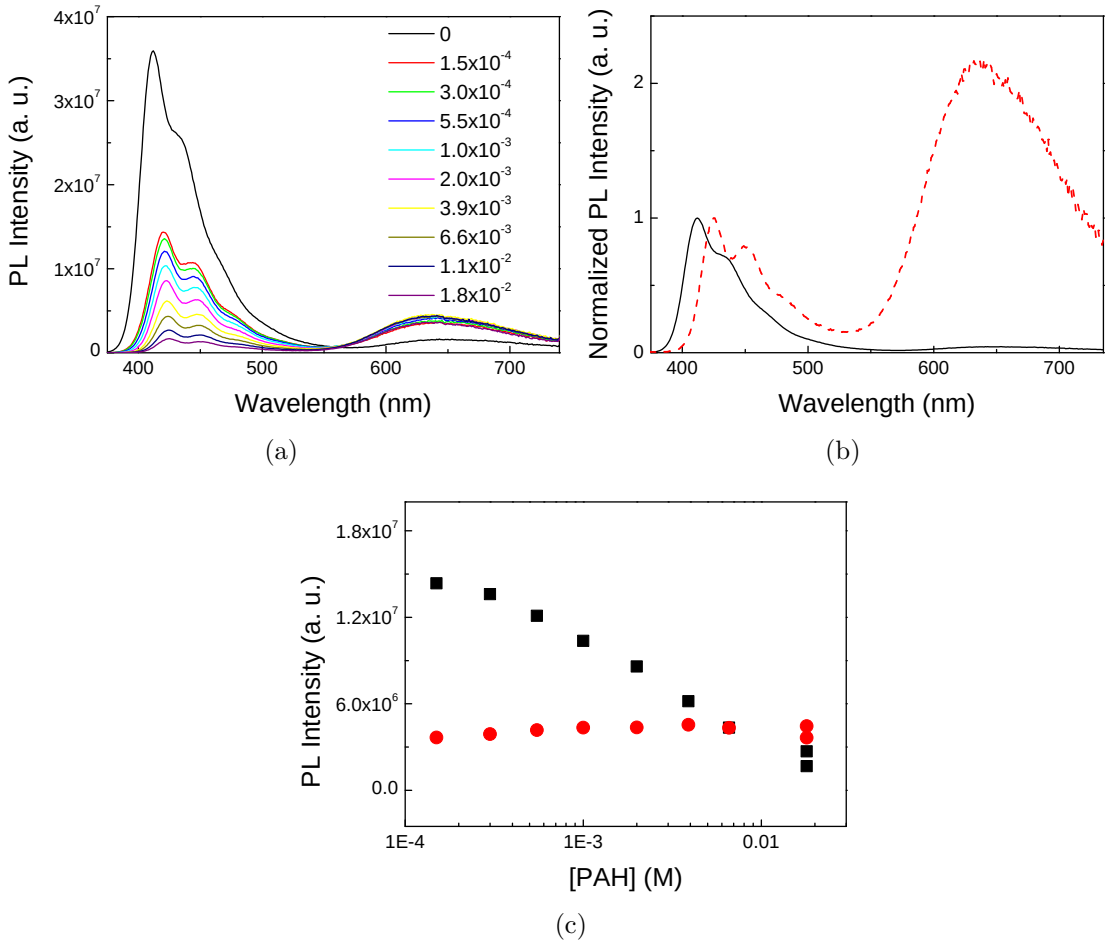

Figure 6.2.7: a) Emission spectra of PBS-PFP-TBTT$_{10}$ (5×10^{-6} M) with increasing PAH concentration (M) in water/dioxane (1:1, v/v) mixture. b) Normalized emission spectra in the absence (solid line) and presence of 18 mM PAH (dashed line). c) Photoluminescence intensity of PFP region (black squares) and TBTT region (red circles) upon addition of PAH (M). Excitation at 370 nm.

The formation of a polyelectrolyte complex, together with hydrogen bonding, van der Waals forces, hydrophobic and dipole interactions, lead the PBS-PFP-TBTT$_x$ copolymer to adopt an alternative conformation. The colorimetric effects in both polymers are explained in terms of conformational changes resultant of the PBS-PFP-TBTT$_x$/PAH interaction. Hence, upon increasing the PAH concentration a highly aggregated system is created, as shown by the red-shift in the absorption and emission spectra (Table 6.12). It is known that the PL efficiency of the BTD units in copolymer solutions at low pH are higher than at high pH [137], [271]. Thus the addition of small volumes of PAH dissolved in a 0.01 HCl M solution, could also contribute to the increased TBTT emission. However, the

PAH-copolymer interactions should be the major contribution for the PL changes observed.

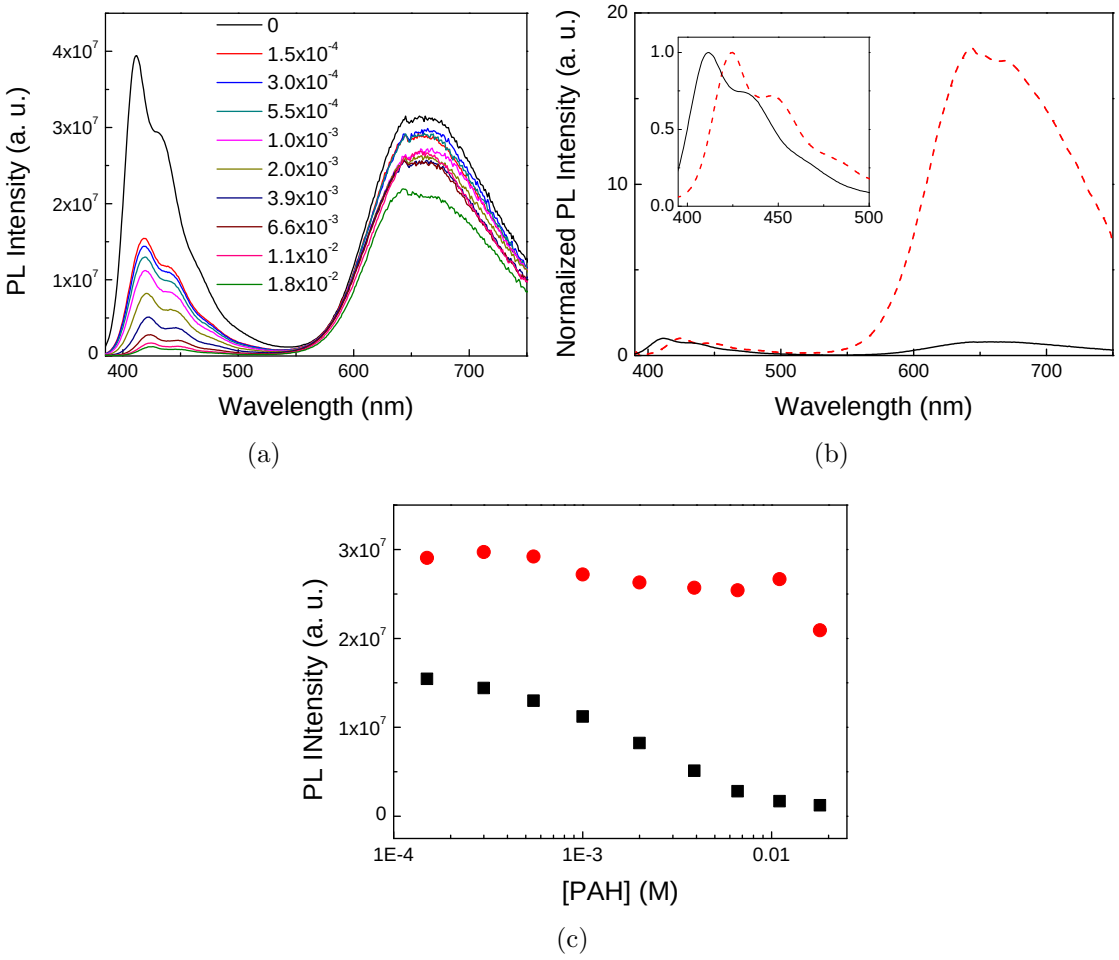

Figure 6.2.8: a) Emission spectra of PBS-PFP-TBTT$_{16}$ (5×10^{-6} M) with increasing PAH concentration (M) in water/dioxane (1:1, v/v) mixture. b) Emission spectra in the absence (solid line) and presence of 18 mM PAH (dashed line). The inset depicts the polyfluorene emission region. c) Photoluminescence intensity of PFP region (black squares) and TBTT region (red circles) upon addition of PAH (M). Excitation at 380 nm.

If the PAH encapsulates the copolymers in aggregates and affects the energy transfer efficiency, this should be reflected in the fluorescence lifetime measurements. The time-resolved data show the copolymers are quenched at a higher rate (Figure 6.2.9 and Table 6.13). Due to the complexity of the decay profile the data for the PBS-PFP-TBTT$_{16}$ copolymer is not shown.

Table 6.12: Absorption and Emission Maxima and PLQY of PBS-PFP-TBTT$_x$ in water/dioxane (1:1, v/v) and PAH.

	0 M PAH			1.8×10^{-2} M PAH		
	Absorption (nm)	Emission (nm)	Φ_F	Absorption (nm)	Emission (nm)	Φ_F
I[a]	370, 510	411, 650	0.43;[c] 0.02[d]	376, 520	424, 640	0.030;[a] 0.13[b]
II[b]	380, 520	411, 660	0.21;[c] 0.11[d]	382, 540	423, 660	0.004;[a] 0.16[b]

[a] PBS-PFP-TBTT$_{10}$
[b] PBS-PFP-TBTT$_{16}$
[c] Φ_F PFP
[d] Φ_F TBTT.

Table 6.13: Fluorescence decay times (τ_i) and pre-exponential factors (a_{ij}) for the copolymer PBS-PFP-TBTT$_{10}$ in water/dioxane (1:1, v/v) with 0 and 18 mM PAH, obtained with excitation at 392 nm, emission at the wavelength maxima and T = 298.15 K.

[PAH] (mM)	λ_{em} (nm)	τ_1 (ns)	τ_2 (ns)	τ_3 (ns)	τ_4 (ns)	a_{i1}	a_{i2}	a_{i3}	a_{i4}	χ^2
0	410	—	0.25	0.51	—	—	0.267	0.733	—	1.05
	650	—	—	0.45	2.52	—	—	0.470	0.530	1.06
18	424	0.01	0.06	0.33	—	0.860	0.134	0.006	—	0.95
	640	—	0.27	—	2.56	—	0.290	—	0.710	1.00

Following the idea of Monkman, the quenching is expected to arise from complex formation in the ground state [86], [110], through polyelectrolyte+CPE aggregation [357]. Three CPE components appear in the decay collected at the PFP emission region, with time constants of 10, 60 and 330 ps, whose attribution was already discussed for the PBS-PFP-PDI case (see subchapter 6.2.1.1). The decay component of 330 ps (PFP lifetime) is probably the most effective in the energy transfer process, as seen by both the decrease in lifetime wavelength and amplitude (almost 99%). Although from FRET, static quenching by complex formation in the ground state between the isolated copolymer chain and the PAH can also occur [85].

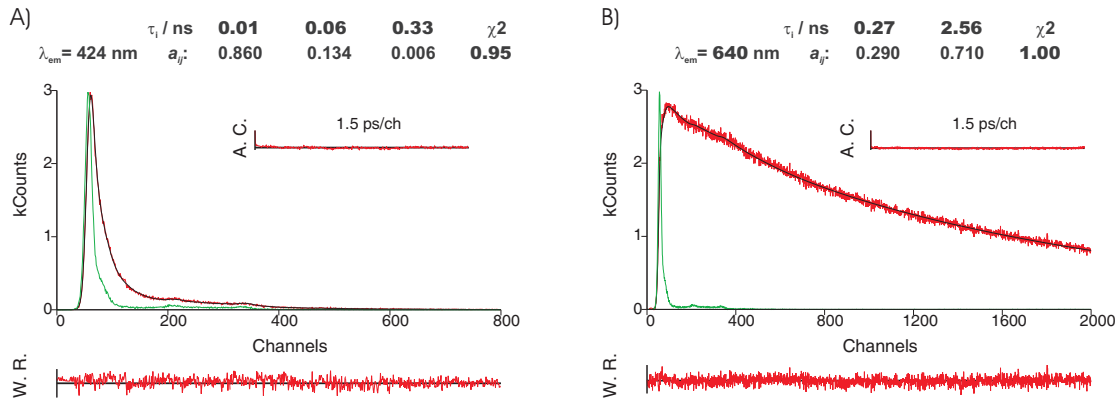

Figure 6.2.9: Fluorescence emission decay for PBS-PFP-TBTT$_{10}$ collected at the polymer emission maximum obtained with λ_{exc} 392 nm at 298.15 K in water/dioxane (1:1, v/v) mixture with 18 mM PAH. A) Emission at 424 nm. B) Emission at 660 nm. The green lines in the decays are the instrumental response function (IRF). For a better judgment of the quality of the fits weighted residuals (W.R., scale -3 $\leq \sigma \leq$ +3) autocorrelation functions (A.C.) and chi-square values (χ^2) are also presented.

When the decay is collected at 640 nm the emission first builds in with the fast time constant of 270 ps. Given the decay lifetime was measured in the red part of the fluorescence spectra (640 nm), this is expected to predominantly reflect energy transfer in the interchain species. Therefore, the 270 ps component should be related with the interchain transfer between PBS-PFP-TBTT$_x$ chains. The 270 ps component decays later with a 2.56 ns fluorescence lifetime. As discussed on chapter 5, the 2.56 ns is present only on the decays collected at 640 nm and is independent of the TBTT content and thus, is assigned to the on-cahin TBTT chromophore lifetime [270].

6.3 PBS-PFP copolymers and Aliquat 336

Ionic liquids are a group of organic salts that exist as liquids at a relatively low temperature, often below 100 °C. They are generally made of at least two organic components which can be varied (the anion and cation) and can be designed for a particular purpose, or to possess a particular set of properties. In general, ionic liquids are salts where one or both the ions are large, and the cation has a low symmetry [358], [359]. Ionic liquids are green solvents that have been applied as new reaction media for transition metal catalysis, where well known reactions can be accelerated with improved selectivities [360]. They have also been successfully used in various areas of analytical chemistry, with particular emphasis in analytes separation [361] and celulose dissolution [362].

A particular important, device application involve the use of ionic liquids in light emitting electrochemical cells (LECs) [363], [364]. In contrast to PLEDs, LECs require a solid state electrolyte, in addition to the conjugated polymer for their operation [365], [366]. In polymeric LECs, the anions and cations redistribute inside the active polymer layer under the influence of an applied electric field, leading to electrochemical redox doping, e. g. n-type near the cathode and p-type near the anode [367]. PLECs using a low concentration of an ionic liquid blended into a soluble PPV copolymer have already been reported [368]. Electrochemical activity of LECs can be improved by decreasing the number of components in the active material from the traditional choice of three: CP, salt, and ionic solvent. Two promising approaches envolve the employment of a single-component material, or of a binary mixture, comprised of a CP and an ionic liquid [369–372].

The modication of electronic conduction in conjugated polymers can also occur by field-effect methods. Only very recently, an alternative approach to apply the gate voltage through an electrolyte contact has achieve increased interest [373]; since patterning and deposition of active polymer materials are now possible. These new electrolyte-gated field effect transistors (EGOFETs) may use different electrolytes, such as polymer electrolytes, ion gels, ionic liquids and polyelectrolytes [373].

Manipulation of the electronic conductivity by electrochemical redox processes in conjugated polymers can be used to form new functions, like hybrid electronic and electrochemical devices, opening a window to new attractive properties for a variety of technological applications.

Control over the organization of synthetic supramolecular structures by tuning the assembly processes opens possibilities in the manipulation of material properties on the molecular scale. Among the best studied synthetic self-assembling polymeric systems are polyelectrolytes and oppositely charged small amphiphilic molecules (surfactants) [329]. Little has been studied on the self-assembly and material properties regarding the interaction of ionic liquids and polyelectrolytes, in particular CPEs. In this section is described the interaction between the ionic liquid, Aliquat 336, and various CPEs.

6.3.1 PBS-PFP-PDI and Aliquat 336

N-methyl-N,N-dioctyloctan-1-ammonium chloride, Aliquat 336, (Figure 6.3.1) was dissolved in dioxane and added to a solution of PBS-PFP-PDI (5×10^{-6} M, in terms of monomeric unit) in water/dioxane (1:1, v/v). The main objective was to test the dissolution and mixing capabilities of the ionic liquid with the PBS-PFP based copolymer.

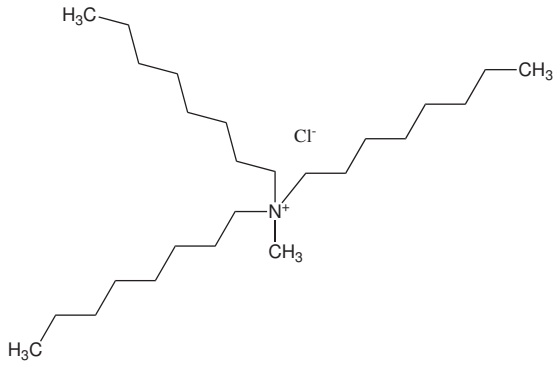

Figure 6.3.1: Structure of the ionic liquid Aliquat 336.

The driving force between Aliquat 336 and PBS-PFP-PDI will be considered to be the same as that of PBS-PFP in the presence of cationic single chains gemini surfactants: electrostatic interactions between the oppositely charged quaternary ammonium salt of the ionic liquid and the copolymer sulfonate group [374]. At a low concentration of Aliquat 336 PBS-PFP-PDI aggregates with the ionic liquid and an abrupt decrease in the PL intensity and PLQY of the copolymer is observed (Figure 6.3.2, Table 6.14). This quenching of the PL emission as well as the red-shift at low ionic liquid concentrations, Figure 6.3.2, are attributed to PBS-PFP-PDI aggregation, that increases the π-π interaction between the monomeric units inducing interchain excitation quenching.

Table 6.14: Absorption and Emission Maxima and PLQY of PBS-PFP-PDI and PBS-PFP in water/dioxane (1:1, v/v) with Aliquat 336.

	0 M Aliquat 336			1.8×10^{-2} M Aliquat 336		
	Absorption (nm)	Emission (nm)	Φ_F	Absorption (nm)	Emission (nm)	Φ_F
PBS-PFP-PDI	360	408	0.55	362	409	0.32
PBS-PFP	372	410	0.52	372	410	0.11

Further increments in the Aliquat 336 concentration (ca. 6.60 mM) enhance the PL emission. Such an effect is associated to the rupture of the polymer aggregates, with subsequent reduction of the interchain excitation quenching and a significant recovery of the copolymer emission (Figure 6.3.2 and Table 6.14). It is worth noting that the excitation and emission spectra, collected at the Aliquat 336 maximum concentration, match the inicial PBS-PFP-PDI initial spectra. That is indicative that more ordered and homogeneous poly-

mer configurations are obtained at higher Aliquat 336 concentrations [307]. Furthermore, no clear PDI emission band was observed during the experiment.

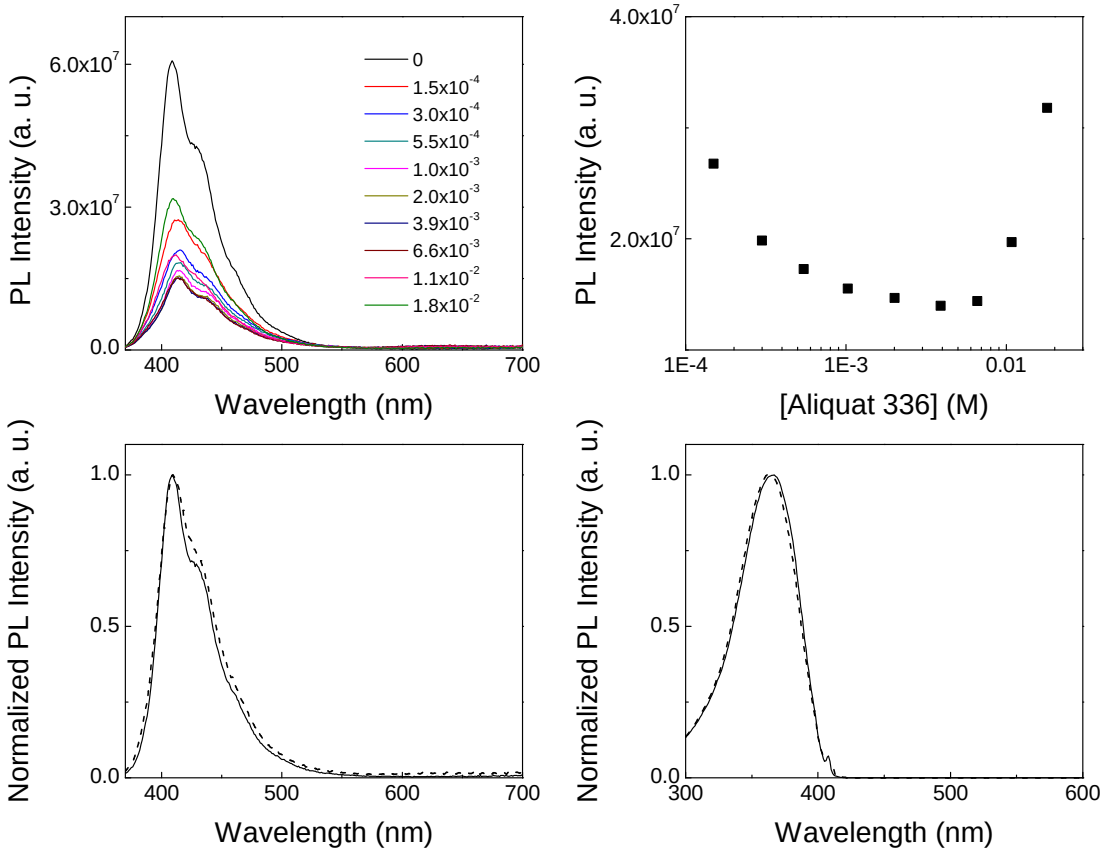

Figure 6.3.2: Emission spectra of PBS-PFP-PDI (5×10^{-6} M) with increasing Aliquat 336 concentration (M) in water/dioxane (1:1, v/v) mixture (top left). PL intensity of PBS-PFP-PDI with increasing Aliquat 336 concentration (M) (top right). Normalized emission spectra in the absence (solid line) and presence of 18 mM Aliquat 336 (dashed line) (bottom left). Normalized excitation spectra in the absence (solid line) and presence of 18 mM Aliquat 336 (dashed line) (bottom right).

In an attempt to understand the PL of the CPE in the ionic liquid, time-resolved fluorescence measurements were carried out (Table 6.15 and Figure 6.3.3). The relative contribution of the small decay time components enhances upon increasing Aliquat 336 concentration in solution. The fast component (40 ps) amplitude increase could be related to the reduction of the polarity of the polymer environment, due to the water screening effect as the ionic liquid concentration becomes greater [86]. It is interesting to note that the relative contribution of the long lifetime component also decreases from 92% (0 mM Aliquat 336) to 29% (18 mM Aliquat 336), in addition to the appearance of an intermediate

component of 140 ps.

Table 6.15: Fluorescence decay times (τ_i) and pre-exponential factors (a_{ij}) for the copolymer PBS-PFP-PDI in water/dioxane (1:1, v/v) with 0 and 18 mM Aliquat 336, obtained with excitation at 392 nm, emission at the wavelength maxima and T = 298.15 K.

[Aliquat 336] (mM)	λ_{em} (nm)	τ_1 (ns)	τ_2 (ns)	τ_3 (ns)	a_{i1}	a_{i2}	a_{i3}	χ^2
0	410	0.06	—	0.52	0.079	—	0.921	1.01
18	409	0.04	0.14	0.58	0.465	0.245	0.289	1.01

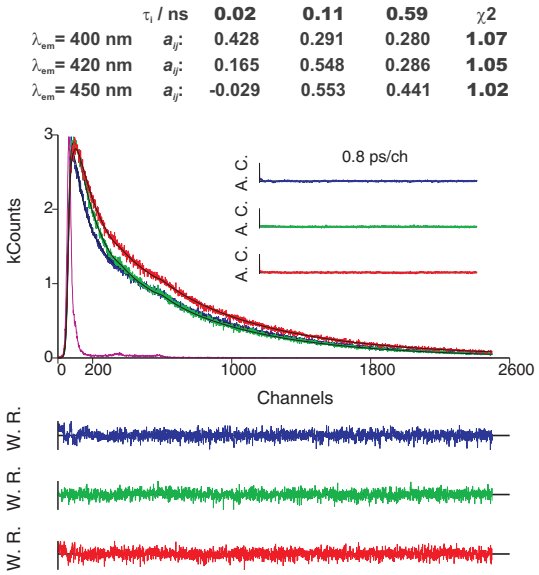

Figure 6.3.3: Fluorescence emission decay for PBS-PFP-PDI collected at the polymer emission maximum obtained with λ_{exc} 392 nm at 298.15 K in water/dioxane (1:1, v/v) mixture and 18 mM Aliquat 336. The magenta line in the decays is the instrumental response function (IRF). For a better judgment of the quality of the fits weighted residuals (W.R., scale -3 $\leq \sigma \leq$ +3) autocorrelation functions (A.C.) and chi-square values (χ^2) are also presented.

Figure 6.3.3 shows the fluorescence kinetics of the emission decay at a number of emission wavelengths over the range 400 - 450 nm. The longer and intermediate components always have a positive amplitude, with the short and intermediate ones (110 ps) giving rise to the main contribution in the overall emission decay. The wavelength effect of the

relative amplitudes of the faster component, 20 ps, reflect the superposition of two emitting species [45]. When the decay is collected in the blue edge of the emission spectra, 400 nm, the pre-exponential factor has a positive amplitude. This is valid until 420 nm, where it is transformed into an emission decay [45]. For lower energy values the fast component is associated with a negative amplitude, i.e., a risetime. The 20 ps component can then be assigned to the exciton decay quenched by the aggregate species ionic-liquid/CPE that arises from nonradiative inter and intrachain interactions [86]; to energy transfer towards PDI on-chain units [270]; or to a different conformational rearrangement [45]. Any energy transfer is too weak to be detected via fluorescence and time-resolved measurements and if it happens is followed by an electron transfer process [160]. Furthermore, the contribution of the 110 ps component increases with the emission wavelength and should be related to copolymer clusters or aggregates in solution [85].

6.3.2 PBS-PFP-TBTT and Aliquat 336

In the previous section, on the interaction of PBS-PFP bearing on-chain PDI with the Aliquat 336 interesting optical phenomena were revealed, due to different interactions within the copolymer chains. This cause chain aggregation at ionic liquid concentrations below 6.60 mM, while at 6.60 mM disruption of the copolymer aggregates/clusters is observed. It was also previously observed that the interaction of the oppositely charged polyelectrolyte, PAH, with PBS-PFP-TBTT based copolymers increases the energy transfer process, that leads to a dominant TBTT emission. Complexation with oppositely charge agents (polyelectrolytes or surfactants) brings together polymer segments and encourages energy migration to low energy emissive sites [356]. The above mentioned effect was also tested when Aliquat 336 is added to PBS-PFP-TBTT$_x$ solutions.

Analysis of the data in Table 6.16 illustrate there is no drastic effect on the spectral properties of either TBTT copolymers upon addition of Aliquat 336 maximum concentration. In fact, only the PLQY is affected, due to the PL emission quenching (Figures 6.3.4 and 6.3.5). However, Aliquat 336 favors the energy transfer process for the initial four concentrations, probably because aggregation is favored and a less hydrophobic environment around the chromophore units is created. For the same reason, the PF emission is highly affected, suffering a red-shift (Figure 6.3.4) and a decrease in the intensity of the emitted light (Figure 6.3.5). Upon increasing concentration of Aliquat 336, the intensity of the emitted light at 411 nm (PFP emission range) is further decreased and the band located at 640 - 650 nm (TBTT emission) starts losing intensity. Interestingly, Aliquat 336 acts in a similar way to the cationic surfactants and the interaction between the PBS-PFP-TBTT$_x$ and Aliquat 336 forces the copolymers chains to aggregate, as shown by the PL quenching

and low PLQY. Energy transfer towards the TBTT on-chain units is not further improved (Figures 6.3.4, 6.3.5 and Table 6.16).

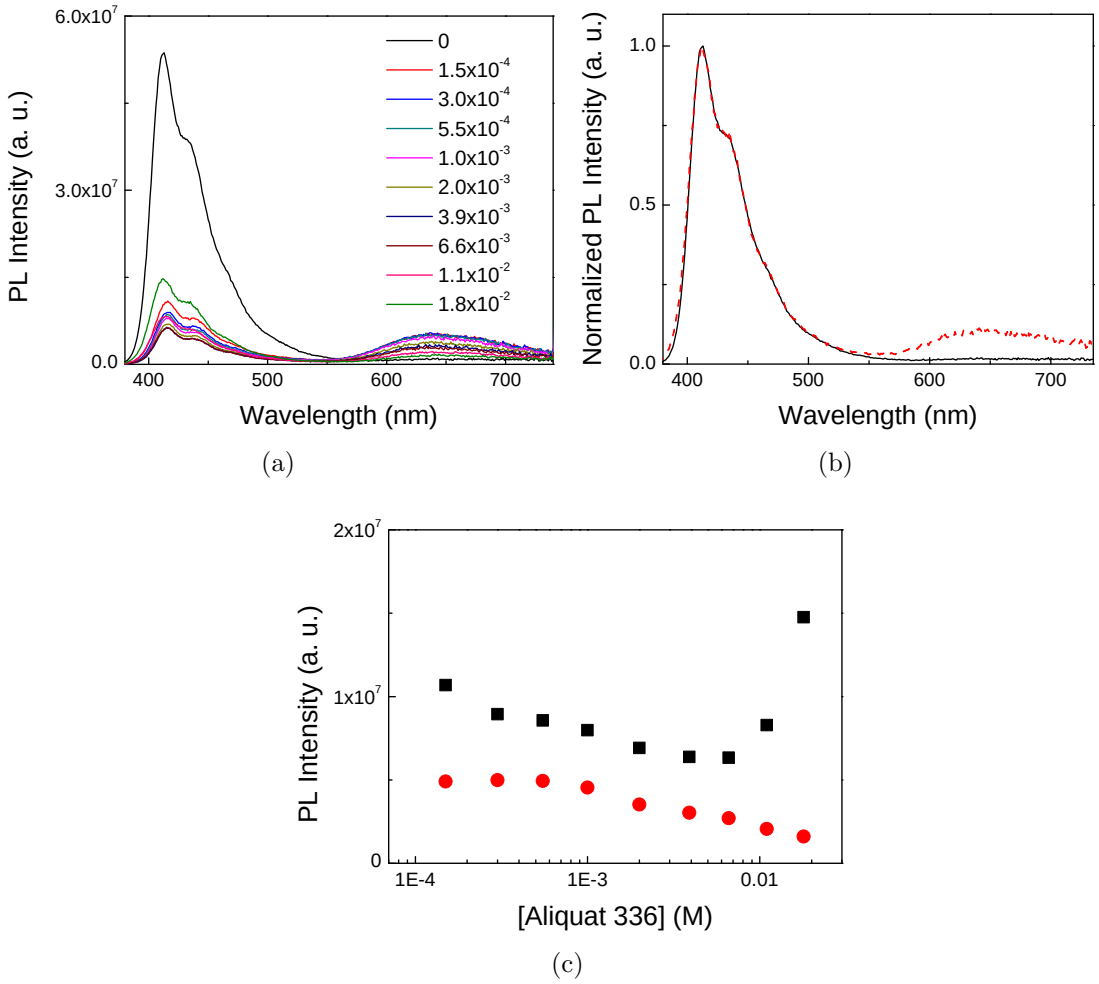

Figure 6.3.4: a) Emission spectra of PBS-PFP-TBTT$_{10}$ (5×10^{-6} M) with increasing Aliquat 336 concentration (M) in water/dioxane (1:1, v/v) mixture. b) Emission spectra in the absence (solid line) and presence of 18 mM Aliquat 336 (dashed line). c) Photoluminescence intensity of PFP region (black squares) and TBTT region (red circles) upon addition of Aliquat 336 (M).

Addition of a large amount of the cationic charged (6.60 mM) Aliquat 336 to the PBS-PFP-TBTT$_x$, induces new copolymer behavior in solution. The emission peak shifts back to a shorter wavelength (blue region of the spectra) and there is an increase in the PL intensity at 411 - 412 nm, especially in the PBS-PFP-TBTT$_{16}$ (the less "soluble" copolymer), Figure 6.3.5. The results strongly suggest that Aliquat 336 solubilizes the PBS-PFP-TBTT copolymers as isolated polymer chains in mixed polymer+Aliquat 336 complexes [319]. Being the

interactions responsible for the copolymers aggregation disrupted by both electrostatic and hydrophobic contributions [125, 145, 353].

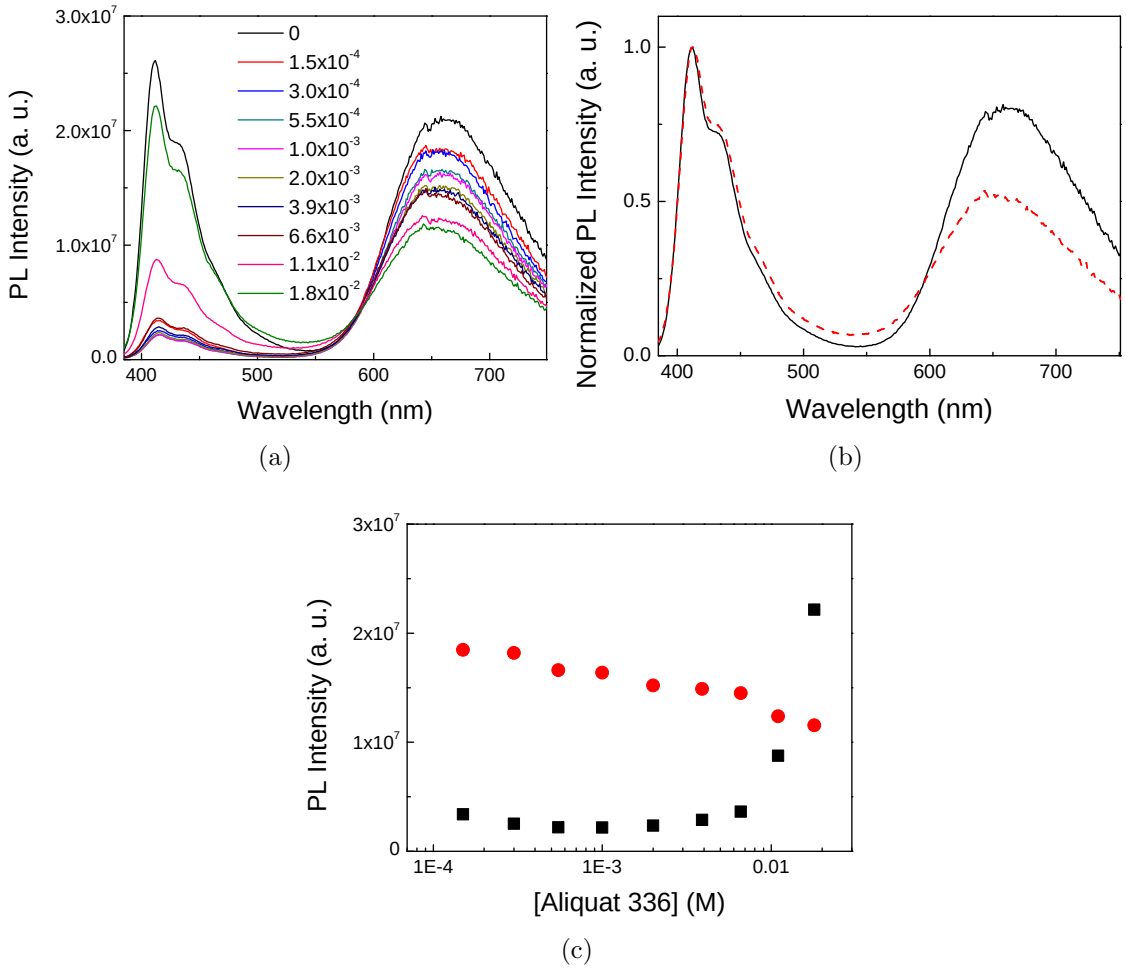

Figure 6.3.5: a) Emission spectra of PBS-PFP-TBTT$_{16}$ (5×10^{-6} M) with increasing Aliquat 336 concentration (M) in water/dioxane (1:1, v/v) mixture. b) Emission spectra in the absence (solid line) and presence of 18 mM Aliquat 336 (dashed line). c) Photoluminescence intensity of PFP region (black squares) and TBTT region (red circles) upon addition of Aliquat 336 (M).

Time-resolved fluorescence experiments show that, the decays at the emission maximum (411 and 412 nm for the PBS-PFP-TBTT$_{10}$ and PBS-PFP-TBTT$_{16}$, respectively) are dependent on the copolymer and hence, on the copolymer TBTT concentration. These could be fitted to biexponential or triexponential kinetics. The decays collected at 640 nm (PBS-PFP-TBTT$_{10}$) and 650 nm (PBS-PFP-TBTT$_{16}$) fit solely triexponential kinetics (Tables

6.17 and 6.18).

Table 6.16: Absorption and Emission Maxima and PLQY of PBS-PFP-TBTT$_x$ in water/dioxane (1:1, v/v) and Aliquat 336.

	0 M Aliquat 336			1.8×10^{-2} M Aliquat 336		
	Absorption (nm)	Emission (nm)	Φ_F	Absorption (nm)	Emission (nm)	Φ_F
I[a]	370, 510	411, 650	0.43;[a] 0.02[b]	376, 515	411, 640	0.15;[c] 0.03[d]
II[b]	380, 520	411, 660	0.21;[a] 0.11[b]	377, 530	412, 650	0.19;[c] 0.06[d]

[a] PBS-PFP-TBTT$_{10}$
[b] PBS-PFP-TBTT$_{16}$
[c] Φ_F PFP
[d] Φ_F TBTT.

Table 6.17: Fluorescence decay times (τ_i) and pre-exponential factors (a_{ij}) for the copolymer PBS-PFP-TBTT$_{10}$ in water/dioxane (1:1, v/v) with 0 and 18 mM Aliquat 336, obtained with excitation at 392 nm, emission at the wavelength maxima and T = 298.15 K.

[Aliquat 336] (mM)	λ_{em} (nm)	τ_1 (ns)	τ_2 (ns)	τ_3 (ns)	τ_4 (ns)	a_{i1}	a_{i2}	a_{i3}	a_{i4}	χ^2
0	410	—	0.25	0.51	—	—	0.267	0.733	—	1.05
	650	—	—	0.45	2.52	—	—	0.470	0.530	1.06
18	411	0.03	0.10	0.56	—	0.492	0.422	0.086	—	1.05
	640	0.04	—	0.61	3.06	-0.504	—	0.211	0.789	1.05

The emission decay collected at 411 nm for the copolymer PBS-PFP-TBTT$_{10}$, show two fast decay times of 30 and 100 ps and a long lifetime of 560 ps (Table 6.17 and Figure 6.3.6). This component, varying from 560 to 610 ps, appears as a decay time at both PFP and TBTT wavelengths and is more important at 411 nm than at 640 nm. This is clearly identified with the PFP lifetime [47]; while the shorter lifetime of 100 ps is attributed to polymer aggregates [145]. The effect of the Aliquat 336 concentration upon the emission intensity for the longest lifetime component is similar to that obtained in steady state experiments and decreases when the emission intensity of the shortest components increase

(Figure 6.3.6). The slower decay component (3.06 ns), collected at 640 nm, is only detected in the TBTT emission maximum and therefore assigned to the TBTT fluorescence lifetime [270]. Finally, the shortest decay component 30 - 40 ps appear as a decay time, positive amplitude, when the emission is collected at the PFP emission wavelength and as a risetime, negative amplitude, when the emission is collected at the TBTT emission wavelength (640 nm). Therefore, this component is related with the TBTT excited state population formation from the PFP moieties.

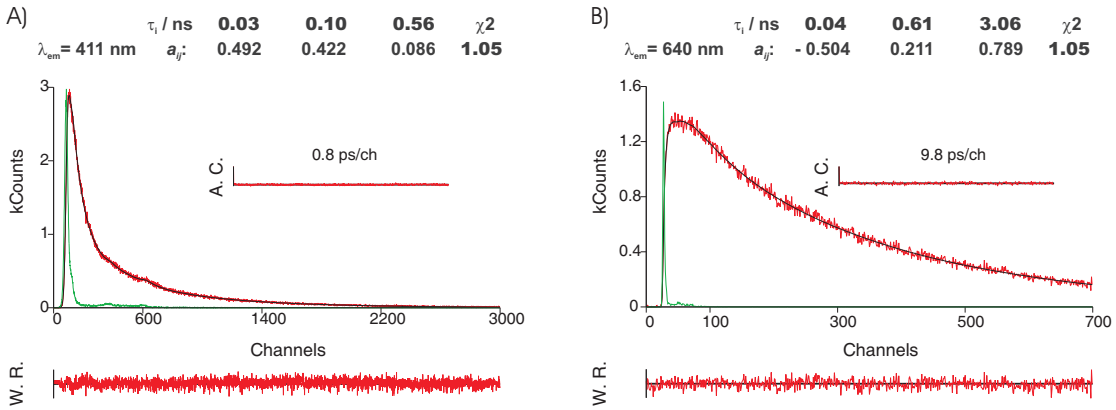

Figure 6.3.6: Fluorescence emission decay for PBS-PFP-TBTT$_{10}$ obtained with λ_{exc} 392 nm at 298.15 K in water/dioxane (1:1, v/v) mixture and collected at A) 411 nm and at B) 640 nm. The green lines in the decays are the instrumental response function (IRF). For a better judgment of the quality of the fits weighted residuals (W.R., scale -3 $\leq \sigma \leq$ +3) autocorrelation functions (A.C.) and chi-square values (χ^2) are also presented.

A similar approach can be made towards the interpretation of the PBS-PFP-TBTT$_{16}$ copolymer lifetime decays. The pre-exponential amplitude of the 10 - 20 ps component dominates the overall lifetime decay when collected at 412 nm and is related with the TBTT excited state population (Table 6.18). Indeed all the other lifetime components have the same previously ascribed attribution and only the following differences are observed. Direct comparison with the PBS-PFP-TBTT$_{10}$ lifetime measurements data clearly reveal a dependence of the fast component with the chromophore content (Table 6.18 and Figure 6.3.7).

Surprisingly, the decay fits into a biexponential equation and the 160 to 180 ps lifetime attributed to polymer aggregates, is no longer detected. Given that the polymer-ionic liquid interactions should involve electrostatic and hydrophobic contributions, it is possible that all the sulfonate side chains groups are neutralized by the ionic liquid and the copolymer is encapsulated in an hydrophobic media where it assumes an extended conformation. This

behavior/interaction assumes a major role in PBS-PFP-TBTT$_{16}$, with the higher TBTT on-chain concentration and subsequent increased hydrophobic effects.

Table 6.18: Fluorescence decay times (τ_i) and pre-exponential factors (a_{ij}) for the copolymer PBS-PFP-TBTT$_{16}$ in water/dioxane (1:1, v/v) with 0 and 18 mM Aliquat 336, obtained with excitation at 392 nm, emission at the wavelength maxima and T = 298.15 K.

[Aliquat 336] (mM)	λ_{em} (nm)	τ_1 (ns)	τ_2 (ns)	τ_3 (ns)	τ_4 (ns)	a_{i1}	a_{i2}	a_{i3}	a_{i4}	χ^2
0	410	0.02	0.18	0.47	—	0.422	0.245	0.333	—	0.96
	660	—	0.16	0.58	2.46	—	0.191	0.243	0.556	1.16
18	412	0.02	—	0.55	—	0.941	—	0.059	—	0.95
	650	0.01	—	0.47	2.72	-0.778	—	0.187	0.813	1.02

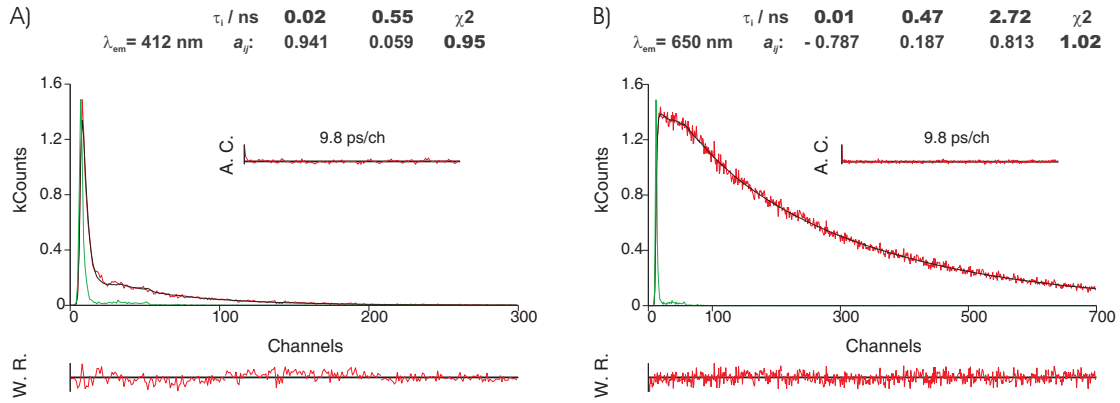

Figure 6.3.7: Fluorescence emission decay for PBS-PFP-TBTT$_{16}$ obtained with λ_{exc} 392 nm at 298.15 K in water/dioxane (1:1, v/v) mixture and collected at A) 412 nm and at B) 650 nm. The green lines in the decays are the instrumental response function (IRF). For a better judgment of the quality of the fits weighted residuals (W.R., scale -3 $\leq \sigma \leq$ +3) autocorrelation functions (A.C.) and chi-square values (χ^2) are also presented.

6.4 Conclusions

The FRET mechanism and aggregation behavior of anionic CPEs with on-chain chromophoric units in water/dioxane (1:1, v/v) mixture can be modulated through the interaction with cationic tetraalkylammonium surfactants, poly(allylamine hydrochoride) poly-

electrolyte (PAH) and the ionic liquid N-methyl-N,N-dioctyloctan-1-ammonium chloride (Aliquat 336). At low concentration of the cationic agents, nearly complete quenching of the PBS-PFP based copolymer emission is observed. While in nearly all of the systems studied, with PAH being the exception, the copolymers emission is recovered at high concentrations: above the surfactants cmc and above 6.60 mM Aliquat 336. The copolymer-cationic agents interactions are believed to involve both electrostatic and hydrophobic contributions.

Upon addition of C_{16}TAB to PBS-PFP-PDI solutions, a weak, long wavelength PDI-based PL component is seen. The low efficiency energy transfer is only observed in a nonpolar environment where the cationic C_{16}TAB molecules shield the copolymer from water, forming surfactant+CPE complexes. The collected data indicate that both energy and electron (or charge) transfer are possible with PBS-PFP-PDI upon excitation of the PFP copolymer units. In contrast, no long wavelength band was observed upon the addition of Aliquat 336 and PAH, although it is possible that electron or charge transfer dominates in the latter case, since PAH creates an almost solvent "free" environment.

The fluorescence intensity of the anionic PBS-PFP-TBTT$_x$ copolymers is quenched in the PFP region and enhanced on the chromophore TBTT region, upon addition of the cationic agents, due to induced polymer aggregation. In the cationic surfactant case, concentrations of C_{16}TAB, C_{18}TAB and C_{16}TAC above the surfactant micelle formation leads to break up of copolymer aggregates, as seen through the recovery of emission intensity in the PFP region and to a decrease in the TBTT light emission. C_{18}TAB is the least efficient in the copolymer solubilization process, possibly because in solution it forms elongated micelles easily. The counter ion effect is illustrated by comparison between the C_{16}TAC and C_{16}TAB results. Halide ions are known to quench fluorescence of aromatic hydrocarbons [375] and the quenching of the PFP emission band is more intense in C_{16}TAB than in C_{16}TAC. This may be due to a heavy atom effect or other mechanisms [41], [375]. Time-resolved fluorescence experiments show that, depending on the surfactant and copolymer, the decays can be fitted to either biexponential or triexponential kinetics. The intermediate component with lifetime 80 - 290 ps increases its contribution with the surfactant concentration, as a result of clusters/aggregates formation of PBS-PFP-TBTT$_x$/surfactants in solution. The longer decay component, associated with the TBTT lifetime remains unchanged, while the PFP component (470 - 660 ps) decreases amplitude, or disappears from the overall decay when collected at the chromophore emission maximum. Electrical conductivity measurements reveal that C_{16}TAB aggregates are favored by the copolymers presence and that both PBS-PFP-TBTT$_x$ copolymers influence the formation of bigger and compact aggregates, with the phenomena being more pronounced for PBS-PFP-TBTT$_{16}$. At surfactant concentration below the cac the extent of the PBS-PFP-TBTT$_{10}$ effect on

the surfactant conductivity is predominant and explained by differences in the copolymer solubility. PBS-PFP-$TBTT_{16}$ is suggested to undergo a dissolution like process above the psp. Molecular dynamics simulations indicate a strong tendency for the PBS-PFP-$TBTT_x$ copolymers to aggregate, driven by the interactions of the copolymer hydrophobic aromatic body and the hydrophilic adjacent chains. Equally important, is the C_{16}TAB effect on the oppositely charged CPE, that demonstrate the copolymer backbone becomes straightened as it is surrounded in a sheath of surfactant molecules, while the sulfonate group is exposed to water.

The backbone aggregation of the PBS-PFP based copolymers, can be switched by interactions with the synthetic PAH polyelectrolyte. The complex formation between the two polyelectrolytes will force the copolymers to adopt a non-planar conformation and the copolymer chains to aggregate. This has been detected by the optical measurement, in particular PFP red-shifted emission maximum and quenching. Additionally, in the case of the PBS-PFP-$TBTT_x$, an increase in the TBTT emission is observed, typical for highly aggregated systems, with increased interchain energy transfer. In the presence of PAH, the copolymer fluorescence decays decrease and the CPEs reveal optical properties of a solvent free media. The interaction is so strong, and it is possible that there may be an assembly of polyelectrolyte multilayers.

Aliquat 336, quenches the fluorescence of PFP-PFP-PDI, but in contrast to C_{16}TAB no new band at low energies (635 nm) is observed. As has previously been observed with the non-ionic surfactant $C_{12}E_5$, a marked blue shift of the absorption and emission maxima is seen. In this perspective, Aliquat 336 acts as a co-solvent in the solvent mixture. The PBS-PFP-PDI+Aliquat 336 interaction can, thus, be used to control the spectroscopic properties of the copolymer, which may have implications in its applications. The same behavior is observed for TBTT based copolymers, with the onset of interaction observed for Aliquat 336 concentrations above 6.60 mM, interpreted as resulting from Aliquat 336 induced breakup of copolymer clusters. Equally important, is the effect of the ionic liquid on the fluorescence decays of the PBS-PFP-$TBTT_x$ copolymers. Upon excitation in the PFP region the TBTT component is formed during the excited state population of the PFP lifetime, as shown by the rise time of the 10 - 40 ps component. The interaction between the ionic liquid and the CPEs demonstrate the tendency to form copolymer-Aliquat 336 complexes in which isolated chains of PBS-PFP based copolymers are included.

Chapter 7

Final remarks and future perspectives

Several conjugated polyelectrolytes have been synthesized in which the chromophore dyes are statistically distributed comonomers in the polymer backbone. The energy transfer was proven to be highly dependent upon the polymer morphology and environment and the molecular weight underestimated. The presence of aggregates in aqueous and co-solvent solution mixtures of the CPs occurs during solubilization and adversely affect the polymer optoelectronic properties: fluorescence spectra and photoluminescence quantum yield.

Efficient energy transfer where achieved with the PBS-PFP-$TBTT_x$ copolymers, due to the spectral overlap between the donor PFP and the acceptor TBTT chromophore and the concentration of the TBTT units in the polymer. Furthermore, the FRET mechanism can be modulated by the copolymer self-assembly with hexadecyltrimethylammonium bromide surfactants, PAH and Aliquat 336. Evidence that the copolymer aggregation enhances the energy transfer were given by the emission spectroscopy and TCSPC measurements; and further studies of electrical conductivity and molecular dynamic simulations provided information about different copolymer morphologies dependent upon the surfactants concentration. Nevertheless, SAXS and SANS studies are in progress to obtain more structural information on these systems.

The solvent polarity, intermolecular separation and relative orientations of the transition dipole densities on the donor and acceptor units, are key factors that hinder and determinate the rate of electronic excitation energy. Investigation of the photophysical properties of two CPEs systems: with on-chain porphyrin acceptor moieties (PBS-PFP-DPP) and self-assembled with an anionic porphyrin bound electrostatically by calcium ions (PBS-PFP-Ca^{2+}-TPPS), shown the energy transfer process is more efficient on the assembled system. The difference is attributed either to a lower porphyrin content in the PBS-PFP-DPP

copolymer when compared to PBS-PFP-Ca^{2+}-TPPS, to further deactivation (radiative decay of the singlet excitons photogenerated on the donor-acceptor segments), to copolymer solution conformational changes, or to the orientations of the dipole densities on the donor and acceptor moieties.

The dependence of the FRET process on the solvent polarity was studied in the PBS-PFP-PDI anionic copolymer. Time-resolved PL, femtosecond fluorescence and transient absorption experiments in water and water/dioxane mixture document the presence of fast PL decay components. Suggesting an efficient nonradiative decay pathway, that involves electron (or charge transfer) and subsequently quench both PFP and PDI emission. Therefore, the effect of adding the oppositely charged cationic surfactant, leads to the weak long wavelength PDI-based PL emission. Low efficiency energy transfer is only observed in a non-polar environment where the cationic CTAB molecules shield the copolymer for water, forming surfactant+polyelectrolyte complexes.

Effective photon propagation along the copolymer units and the level of electronic communication between adjacent subunits was also observed when the phenylene spacer is replaced by non-fully conjugated molecule. A notable feature is that each donor and acceptor subunits can be selectively excited. This length dependence is a consequence of the energy gap between donor and spacer units becoming smaller as the molecular length of the spacer is increased.

The photophysical properties of PBS-PFP revealed the copolymer tendency to aggregate in aqueous solution. The addition of a co-solvent (dioxane), or a non-ionic surfactant ($C_{12}E_5$) has proven to reduce aggregation and improve the copolymer sensitivity to quenching. The possibility of energy transfer of PBS-PFP using three different cationic conjugated oligoelectrolytes was investigated. Steady-state and time resolved luminescence data confirm efficient electronic energy transfer from the polyelectrolyte to the COEs, in water/dioxane (1:1, v/v) solution and in $C_{12}E_5$ micelles. Coulombic interactions and steric effects seem to be have an important role regarding quenching efficiency, as well as the COE chain length.

The results have provided a detailed photophysical characterization of a number of newly synthesized fluorene based conjugated polyelectrolytes containing on-chain chromophores. It was shown that they can be affected by solvent polarity, surfactants, polyelectrolytes and ionic liquids. Future work should concentrate on the characterization of the structures formed, and may also be directed to device fabrication (e. g. LEDs, LECs and photovoltaic systems) containing some of these materials.

Bibliography

[1] C. L. Chochos and S. A. Choulis *Prog. Polym. Sci.*, vol. 36, pp. 1326–1414, 2011.

[2] P. M. Beaujuge and J. M. J. Fréchet *J. Am. Chem. Soc.*, vol. 133, pp. 20009–20029, 2011.

[3] M. Muccini *Nature Materials*, vol. 5, pp. 605–613, 2006.

[4] D. J. Gundlach *Nature Materials*, vol. 6, pp. 173–174, 2007.

[5] F. Huang, H. Wu, and Y. Cao *Chem. Soc. Rev.*, vol. 39, pp. 2500–2521, 2010.

[6] K. P. Ghiggino, T. D. M. Bell, and E. N. Holley *Faraday Discuss.*, vol. 155, pp. 1–10, 2011.

[7] B. Schwartz *J. Annu. ReV. Phys. Chem.*, vol. 54, pp. 141–172, 2003.

[8] B. J. Schwartz *Nature Materials*, vol. 7, pp. 427–428, 2008.

[9] C. Ego, D. Marsitzky, S. Becker, J. Zhang, A. C. Grimsdale, K. Müllen, J. D. MacKenzie, C. Silva, and R. H. Friend *J. Am. Chem. Soc.*, vol. 125, pp. 437–443, 2003.

[10] A. Gutacker, N. Koenen, U. Scherf, S. Adamczyk, J. Pina, S. M. Fonseca, A. J. Valente, R. C. Evans, J. S. de Melo, H. D. Burrows, and M. Knaapila *Polymer*, vol. 51, pp. 1898–1903, 2010.

[11] R. Verduzco, I. Botiz, L. Deanna, L. Pickel, S. M. K. II, K. Hong, E. Dimasi, and S. B. Darling *Macromolecules*, vol. 44, pp. 530–539, 2011.

[12] T. Sugimoto, S. Habuchi, K. Ogino, and M. Vacha *J. Phys. Chem. B*, vol. 113, pp. 12220–12226, 2009.

[13] J.-M. Koenen, S. Jung, A. Patra, A. Helfer, and U. Scherf *Adv. Mater.*, vol. 24, pp. 681–686, 2012.

[14] A. W. Hains, Z. Liang, M. A. Woodhouse, and B. A. Gregg *Chem. Rev.*, vol. 110, pp. 6689–6735, 2010.

[15] R. H. Friend, R. W. Gymer, A. B. Holmes, J. H. Burroughes, R. N. Marks, C. Taliani, D. C. C. Bradley, D. A. D. Santos, J. L. Brédas, M. Lögdlund, and W. R. Salaneck *Nature*, vol. 397, pp. 121–128, 1999.

[16] A. P. Kulkarni, C. J. Tonzola, A. Babel, and S. A. Jenekhe *Chem. Mater.*, vol. 16, pp. 45556–4573, 2004.

[17] A. Dodabalapur *Solid State Commun.*, vol. 102, pp. 259–267, 1997.

[18] J. Huang, G. Li, E. Wu, Q. Xu, and Y. Yang *Adv. Mater.*, vol. 18, pp. 114–117, 2006.

[19] S. Brovelli, F. Meinardi, G. Winroth, O. Fenwick, G. Sforazzini, M. J. Frampton, L. Zalewski, J. A. Levitt, F. Marinello, P. Schiavuta, K. Suhling, H. L. Anderson, and F. Cacialli *Adv. Funct. Mater.*, vol. 20, pp. 272–280, 2010.

[20] E. Moons *J. Phys.: Condens. Matter*, vol. 14, pp. 12235–12260, 2002.

[21] M. T. Bernius, M. Inbasekaran, J. O'Brien, and W. Bernius *Adv. Mater.*, vol. 12, pp. 1737–1750, 2000.

[22] J. Liu, Q. Zhou, Y. Cheng, Y. Geng, L. Wang, D. Ma, X. Jing, and F. Wang *Adv. Funct. Mater.*, vol. 16, pp. 957–965, 2006.

[23] B. Zhang, C. Qin, J. Ding, L. Chen, Z. Xie, Y. Cheng, and L. Wang *Adv. Mater.*, vol. 20, pp. 2951–2957, 2010.

[24] S. K. Lee, D.-H. Hwang, B.-J. Jung, N. S. Cho, J. Lee, J.-D. Lee, and H.-K. Shim *Adv. Funct. Mater.*, vol. 15, pp. 1647–1655, 2005.

[25] A. Garcia, J. Z. Brzezinski, and T.-Q. Nguyen *J. Phys. Chem. C*, vol. 113, pp. 2950–2954, 2009.

[26] C. Deibel and V. Dyakonov *Rep. Prog. Phys.*, vol. 73, p. 096401 (39pp), 2010.

[27] C.-H. Hsieh, Y.-J. Cheng, P.-J. Li, C.-H. Chen, M. Dubosc, R.-M. Liang, and C.-S. Hsu *J. Am. Chem. Soc.*, vol. 132, pp. 4887–4893, 2010.

[28] R. Stalder, J. Mei, and J. R. Reynolds *Macromolecules*, vol. 43, pp. 8348–8352, 2010.

[29] H. Sirringhaus, M. Bird, T. Richards, and N. Zhao *Adv. Mater.*, vol. 22, pp. 3893–3898, 2010.

[30] A. Troisi and G. Orlandi *J. Phys. Chem. A*, vol. 110, pp. 4065–4070, 2006.

[31] H. Ma, H.-L. Yip, F. Huang, and A. K.-Y. Jen *Adv. Funct. Mater.*, vol. 20, pp. 1371–1388, 2010.

[32] T. Lei, Y. Cao, Y. Fan, C.-J. Liu, S.-C. Yuan, and J. Pei *J. Am. Chem. Soc.*, vol. 133, pp. 6099–6101, 2011.

[33] C. Bardeen *Science*, vol. 331, pp. 544–545, 2011.

[34] U. Mitschke and P. Bäuerle *J. Mater. Chem.*, vol. 10, pp. 1471–1507, 2000.

[35] T. A. Skotheim and J. R. Reynolds, *Conjugated Polymers: Theory, Synthesis, Properties and Characterization*. Florida: Taylor & Francis, 2007.

[36] J. U. Wallace and S. H. Chen, *Adv. Polym. Sci.* Berlin: Springer-Verlag, 2008.

[37] N. Miyaura and A. Suzuki *Chem. Rev.*, vol. 95, pp. 2457–2483, 1995.

[38] K. Müllen and U. Scherf, *Organic Light Emitting Devices Synthesis, Properties and Applications*. Weinheim: Wiley Verlag GmbH Co. KGaA, 2006.

[39] T. Yamamoto *Synlett*, vol. 4, pp. 235–450, 2003.

[40] B. Souharce, *Triphenylamine and Carbazole-Based Hole Transporting Materials and their Applications in Organic Field-Effect Transistors*. PhD thesis, Makromoleculare Chemie, Bergische Universität Wuppertal, 2008.

[41] N. J. Turro, *Modern Molecular Photochemistry*. Sausalito, California: University Science Books, 1991.

[42] J. R. Lakowicz, *Principles of Fluorescence Spectroscopy 3rd Ed.* Berlin Heidelberg New York: Springer, 2006.

[43] A. Monkman, C. Rothe, S. King, and F. Dias, *Adv. Polym. Sci.* Verlag Berlin Heidelberg: Springer, 2008.

[44] B. Valeur, *Molecular Fluorescence: Principles and Applications*. Weinheim: Wiley Verlag GmbH Co. KGaA, 2001.

[45] F. B. Dias, A. L. Maçanita, J. S. de Melo, H. D. Burrows, R. Guntner, U. Scherf, and A. P. Monkman *J. Chem. Phys.*, vol. 118, pp. 7119–7126, 2003.

[46] J. Cornil, A. J. Heeger, and J. L. Bredas *Chem. Phys. Lett.*, vol. 272, pp. 463–470, 1997.

[47] F. B. Dias, M. Knaapila, A. P. Monkman, and H. D. Burrows *Macromolecules*, vol. 39, pp. 1598–1606, 2006.

[48] D. Beljonne, G. Pourtois, C. Silva, E. Hennebicq, L. M. Herz, R. H. Friend, G. D. Scholes, S. Setayesh, K. Müllen, and J. L. Brédas *PNAS*, vol. 99, pp. 10982–10987, 2002.

[49] B. Albinsson and J. Mårtensson *J. Photochem. Photobiol. C: Photochem. Rev.*, vol. 9, pp. 138–155, 2008.

[50] I. Hwang and G. D. Scholes *Chem. Mater.*, vol. 23, pp. 610–620, 2011.

[51] K. F. Wong, B. Bagchi, and P. J. Rossky *J. Phys. Chem. A*, vol. 108, pp. 5752–5763, 2004.

[52] M. Montalti, A. Credi, L. Prodi, and M. T. Gandolfi, *Handbook of Photochemistry 3rd Ed.* Florida: Taylor & Francis, 2006.

[53] L.-O. Pålsson and A. P. Monkman *Adv. Mater.*, vol. 14, pp. 757–758, 2002.

[54] J. Pina, "Estudo Fotofísico de Dispositivos Moleculares e de Polímeros Condutores," Master's thesis, Departamento de Química, Universidade de Coimbra, 2004.

[55] J. S. de Melo and A. L. Maçanita *Chem. Phys. Lett.*, vol. 204, pp. 556–562, 1993.

[56] J. S. de Melo *Chem. Educ.*, vol. 10, pp. 29–35, 2005.

[57] J. S. de Melo and P. F. Fernandes *J. Mol. Struct.*, vol. 565-566, pp. 69–78, 2001.

[58] J. Pina, J. S. de Melo, H. D. Burrows, A. L. Maçanita, F. Galbrecht, T. Bünnagel, and U. Scherf *Macromolecules*, vol. 42, pp. 1710–1719, 2009.

[59] A. C. F. Ribeiro, A. J. M. Valente, V. M. M. Lobo, E. F. G. Azevedo, A. M. Amado, A. M. A. da Costa, M. L. Ramos, and H. D. Burrows *J. Mol. Struct.*, vol. 703, pp. 93–101, 2004.

[60] J. Barthel, F. Feuerlein, R. Neueder, and R. Wachter *J. Solut. Chem.*, vol. 9, pp. 209–219, 1980.

[61] M. W. Schmidt, K. K. Baldridge, J. A. Boatz, S. T. Elbert, M. S. Gordon, J. H. Jensen, S. Koseki, N. Matsunaga, K. A. Nguyen, S. J. Su, T. L. Windus, M. Dupuis, and J. A. Montgomery *J. Comput. Chem.*, vol. 14, pp. 1347–1363, 1993.

[62] A. D. Becke *J. Chem. Phys.*, vol. 98, pp. 5648–5653, 1993.

[63] C. Lee, W. Yang, and R. G. Parr *Phys. Rev. B*, vol. 37, pp. 785–789, 1988.

[64] A. W. S. D. M. F. van Aalten *Acta Crystallogr. D*, vol. 60, pp. 1355–1363, 2004.

[65] L. D. Schuler, X. Daura, and W. F. van Gunsteren *J. Comput. Chem.*, vol. 22, pp. 1205–1218, 2001.

[66] J. A. S. Almeida, E. F. Marques, A. S. Jurado, and A. A. C. C. Pais *Phys. Chem. Chem. Phys.*, vol. 12, pp. 14462–14476, 2010.

[67] B. Hess, H. Bekker, H. J. C. Berendsen, and J. G. E. M. Fraaije *J. Comput. Chem.*, vol. 18, pp. 1463–1472, 1997.

[68] W. Humphrey, A. Dalke, and K. Schulten *J. Molec. Graphics*, vol. 14, pp. 33–38, 1996.

[69] E. Scheler, E. Betthausen, and P. Strohriegl *Macromol. Chem. Phys.*, vol. 211, pp. 2081–2089, 2010.

[70] T. A. Carlson, *Photoelectron and Auger Spectroscopy.* London: Plenum Press, 1975.

[71] F. Huang, Y. Zhang, M. S. Liu, and A. K.-Y. Jen *Adv. Funct. Mater.*, vol. 19, pp. 2457–2466, 2009.

[72] X. Han, X. Chen, T. Gordon, and S. Holdcroft *Macromol. Rapid Commun.*, vol. 30, pp. 2089–2095, 2009.

[73] A. Bolognesi, F. Bertini, M. Marinelli, and W. Porzio *Macromol. Chem. Phys.*, vol. 202, pp. 3477–3483, 2001.

[74] S. H. Oh, S.-I. Na, J. Jo, B. Lim, D. Vak, and D.-Y. Kim *Adv. Funct. Mater.*, vol. 20, pp. 1–7, 2010.

[75] S. Kirmayer, E. Dovgolevsky, M. Kalina, E. Lakin, S. Cadars, J. D. Epping, A. Fernández-Arteaga, C. Rodríguez-Abreu, B. F. Chmelka, and G. L. Frey *Chem. Mater.*, vol. 20, pp. 3745–3756, 2008.

[76] R. C. Evans, A. G. Macedo, S. Pradhan, U. Scherf, L. D. Carlos, and H. D. Burrows *Adv. Mater.*, vol. 22, pp. 3032–3037, 2010.

[77] A. Duarte, K.-Y. Pu, B. Liu, and G. C. Bazan *Chem. Mater*, vol. 23, pp. 501–515, 2011.

[78] U. Scherf and E. J. W. List *Adv. Mater.*, vol. 14, pp. 477–487, 2002.

[79] J. C. D. Mello, H. F. Wittmann, and R. H. Friend *Adv. Mater.*, vol. 9, pp. 230–232, 1997.

[80] T. Wågberg, B. Liu, G. Orädd, B. Eliasson, and L. Edman *Eur. Polym. J.*, vol. 45, pp. 3230–3235, 2009.

[81] M. Knaapila and M. J. Winokur, *Adv. Polym. Sci.* Verlag Berlin Heidelberg: Springer, 2008.

[82] S. Gamerith, C. Gadermaier, U. Scherf, and E. J. W. List *Phys. Stat. Sol. (A)*, vol. 201, pp. 1132–1151, 2004.

[83] S. Budavari, M. O'Neil, A. Smith, P. Heckelman, and J. Obenchain, *The Merck Index 12th Ed.* Whitehouse Station NJ: Merck & Co, 1996.

[84] D. R. Lide, *Handbook Chemistry and Physics 85th Ed.* Boca Raton FL: CRC, 2004.

[85] H. A. A. Attar and A. P. Monkman *Adv. Funct. Mater.*, vol. 18, pp. 2498–2509, 2008.

[86] H. A. A. Attar and A. P. Monkman *J. Phys. Chem. B*, vol. 111, pp. 12418–12426, 2007.

[87] J. H. Snook, L. A. Samuelson, J. Kumar, K. Y.-G, and E. W. J *Organic Electronics*, vol. 6, pp. 55–64, 2005.

[88] F. Huang, H. Wu, and Y. Cao *Chem. Soc. Rev.*, vol. 39, pp. 2500–2521, 2010.

[89] G. Zhou, G. Qian, L. Ma, Y. Cheng, Z. Xie, L. Wang, X. Jing, and F. Wang *Macromolecules*, vol. 38, pp. 5416–5424, 2005.

[90] F. Huang, H. Wu, D. Wang, W. Yang, and Y. Cao *Chem. Mater.*, vol. 16, pp. 708–716, 2004.

[91] L. L. G. Justino, M. L. Ramos, M. Knaapila, A. T. Marques, C. J. Kudla, U. Scherf, L. Almásy, R. Schweins, H. D. Burrows, and A. P. Monkman *Macromolecules*, vol. 44, pp. 334–343, 2011.

[92] P. Lu, H. Zhang, M. Li, Y. Zheng, Y. Ma, X. Chen, and N. Tamai *Polym. Int.*, vol. 2008, pp. 987–994, 57.

[93] R. Stepanyan, A. Subbotin, M. Knaapila, O. Ikkala, and G. ten Brinke *Macromolecules*, vol. 36, pp. 3758–3763, 2003.

[94] J. Peet, E. Brocker, Y. Xu, and G. C. Bazan *Adv. Mater.*, vol. 20, pp. 1882–1885, 2008.

[95] M. H. Rahman, S.-C. Liao, H.-L. Chen, J.-H. Chen, V. A. Ivanov, P. P. J. Chu, and S.-A. Chen *Langmuir*, vol. 25, pp. 1667–1674, 2009.

[96] G. Fytas, H. G. Nothofer, U. Scherf, D. Vlassopoulos, and G. Meier *Macromolecules*, vol. 35, pp. 481–488, 2002.

[97] M. Knaapila, R. Stepanyan, M. Torkkeli, B. P. Lyons, T. P. Ikonen, L. Almásy, J. P. Foreman, R. Serimaa, R. Güntner, U. Scherf, and A. P. Monkman *Phys. Rev. E*, vol. 71, pp. 041802–13, 2005.

[98] M. H. Rahman, C.-Y. Chen, S.-C. Liao, H.-L. Chen, C.-S. Tsao, J.-H. Chen, J.-L. Liao, V. A. Ivanov, and S.-A. Chen *Macromolecules*, vol. 40, pp. 6572–6578, 2007.

[99] M. Knaapila, F. B. Dias, V. M. Garamus, L. Almásy, M. Torkkeli, K. Leppanen, F. Galbrecht, E. Preis, H. D. Burrows, U. Scherf, and A. P. Monkman *Macromolecules*, vol. 40, pp. 9398–9405, 2007.

[100] M. Knaapila, V. M. Garamus, F. B. Dias, L. Almásy, F. Galbrecht, A. Charas, J. Morgado, H. D. Burrows, U. Scherf, and A. P. Monkman *Macromolecules*, vol. 39, pp. 6505–6512, 2006.

[101] D. E. Discher and F. Ahmed *Annu. Rev. Biomed. Eng.*, vol. 8, pp. 323–341, 2006.

[102] C. R. Weitzel, T. A. Everett, and D. A. Higgins *Langmuir*, vol. 25, pp. 1188–1195, 2009.

[103] U. Scherf, S. Adamczyk, A. Gutacker, and N. Koenen *Macromol. Rapid Commun.*, vol. 30, pp. 1059–1065, 2009.

[104] G. Tu, H. Li, M. Forster, R. Heiderhoff, L. J. Balk, R. Sigel, and U. Scherf *Small*, vol. 3, pp. 1001–1006, 2007.

[105] F. Huang, Y.-H. Niu, Y. Zhang, J.-W. Ka, M. S. Liu, and A. K.-Y. Jen *Adv. Mater.*, vol. 19, pp. 2010–2014, 2007.

[106] Y. Zhang, F. Huang, Y. Chi, and A. K.-Y. Jen *Adv. Mater.*, vol. 20, pp. 1565–1570, 2008.

[107] Y. Zhang, F. Huang, Y. Chi, and A. K.-Y. Jen *Appl. Phys. Lett.*, vol. 92, p. 063303 (3pp), 2008.

[108] K.-Y. Pu, L. Cai, and B. Liu *Macromolecules*, vol. 42, pp. 5933–5940, 2009.

[109] F. Lv, X. Feng, H. Tang, L. Liu, Q. Yang, and S. Wang *Adv. Funct. Mater.*, vol. 21, pp. 845–850, 2011.

[110] L. Chen, D. W. McBranch, H.-L. Wang, R. Helgeson, and F. W. D. G. Whitten *PNAS*, vol. 96, pp. 12287–12292, 1999.

[111] B. Liu and G. C. Bazan *Chem. Mater.*, vol. 16, pp. 4467–4476, 2004.

[112] Z. Li, Z. L. X. Lou, and J. Qin *Appl. Mater. Interfaces*, vol. 1, pp. 232–234, 2009.

[113] O. R. Miranda, C.-C. You, R. Phillips, I.-B. Kim, P. S. Ghosh, U. H. F. Bunz, and V. M. Rotello *J. Am. Chem. Soc.*, vol. 129, pp. 9856–9857, 2007.

[114] Z. Chen, X.-D. Dang, A. Gutacker, A. Garcia, H. Li, Y. Xu, L. Ying, T.-Q. Nguyen, and G. C. Bazan *J. Am. Chem. Soc*, vol. 132, pp. 12160–12162, 2010.

[115] J. Fang, B. H. Wallikewitz, F. Gao, G. Tu, C. Müller, G. Pace, R. H. Friend, and W. T. S. Fang *J. Am. Chem. Soc.*, vol. 133, pp. 683–685, 2011.

[116] C. V. Hoven, H. Wang, M. Elbing, L. Garner, D. Winkelhaus, and G. C. Bazan *Nature Materials*, vol. 9, pp. 249–252, 2010.

[117] H. Jiang, P. Taranekar, J. R. Reynolds, and K. S. Schanze *Angew. Chem. Int. Ed.*, vol. 48, pp. 4300–4316, 2009.

[118] J. H. Seo, E. B. Namdas, A. Gutacker, A. J. Heeger, and G. C. Bazan *Appl. Phys. Letters*, vol. 97, p. 043303 (3pp), 2010.

[119] U. Scherf *Angew. Chem. Int. Ed.*, vol. 50, pp. 5016–5017, 2011.

[120] K.-Y. Pu, K. Li, X. Zhang, and B. Liu *Adv. Mater.*, vol. 22, pp. 4186–4198, 2010.

[121] A. Gutacker, S. Adamczyk, A. Helfer, L. E. Garner, R. C. Evans, S. M. Fonseca, M. Knaapila, G. C. Bazan, H. D. Burrows, and U. Scherf *J. Mater. Chem.*, vol. 20, pp. 1423–1430, 2010.

[122] L. Chen, S. Xu, D. McBranch, and D. Whitten *J. Am. Chem. Soc.*, vol. 122, pp. 9302–9303, 2000.

[123] H. D. Burrows, M. Knaapila, A. P. Monkman, M. J. Tapia, S. M. Fonseca, M. L. Ramos, W. Pyckhout-Hintzen, S. Pradhan, and U. Scherf *J. Phys.: Condens. Matter*, vol. 20, pp. 104210–104217, 2008.

[124] H. D. Burrows, V. M. M. Lobo, J. Pina, M. L. Ramos, J. S. de Melo, A. J. M. Valente, M. J. Tapia, S. Pradhan, and U. Scherf *Macromolecules*, vol. 37, pp. 7425–7427, 2004.

[125] M. J. Tapia, H. D. Burrows, A. J. M. Valente, S. Pradhan, U. Scherf, V. M. M. Lobo, J. Pina, and J. S. de Melo *J. Phys. Chem. B*, vol. 109, pp. 19108–19115, 2005.

[126] M. Knaapila, L. Almásy, V. M. Garamus, C. Pearson, S. Pradhan, M. C. Petty, U. Scherf, H. D. Burrows, and A. P. Monkman *J. Phys. Chem. B*, vol. 110, pp. 10248–10257, 2006.

[127] H. D. Burrows, M. J. Tapia, S. M. Fonseca, S. Pradhan, U. Scherf, C. L. Silva, A. A. C. C. Pais, A. J. M. Valente, K. Schillén, V. Alfredsson, A. M. Carnerup, M. Tomšič, and A. Jamnik *Langmuir*, vol. 25, pp. 5545–5556, 2009.

[128] H. D. Burrows, S. M. Fonseca, F. B. Dias, J. S. de Melo, A. P. Monkman, U. Scherf, and S. Pradhan *Adv. Mater.*, vol. 21, pp. 1155–1159, 2009.

[129] Q. Bricaud, R. M. Fabre, R. N. Brookins, K. S. Schanze, and J. R. Reynolds *Langmuir*, vol. 27, pp. 5021–5029, 2011.

[130] H. Y. Woo, B. Liu, B. Kohler, D. Korystov, A. Mikhailovsky, and G. C. Bazan *J. Am. Chem. Soc.*, vol. 127, pp. 14721–14729, 2005.

[131] L. E. Garner, J. Park, S. M. Dyar, A. Chworos, J. J. Sumner, and C. C. Bazan *J. Am. Chem. Soc.*, vol. 132, pp. 10042–10052, 2010.

[132] A. T. Marques, T. Costa, J. S. de Melo, H. D. Burrows, U. Scherf, L. E. Garner, A. W. Thomas, and G. C. Bazan *Self-assembly of poly{1,4-phenylene-[9,9-bis(4-phenoxybutylsulfonate)]fluorene-2,7-diyl} with amphiphilic phenylenevinylene oligoelectrolytes*, to be submitted.

[133] A. Suzuki *J. Organometallic Chem.*, vol. 576, pp. 147–168, 1999.

[134] S. Pradhan, *Ionic, Water-Soluble Polyfluorene-Type Copolymers*. PhD thesis, Makromoleculare Chemie, Bergische Universität Wuppertal, 2004.

[135] S. Wang and G. C. Bazan *Chem. Commun.*, vol. 21, pp. 2508–2509, 2004.

[136] C. Tan, M. R. Pinto, and K. S. Schanze *Chem. Commun.*, vol. 5, pp. 446–447, 2002.

[137] F. Wang and G. C. Bazan *J. Am. Chem. Soc.*, vol. 128, pp. 15786–15792, 2006.

[138] Y. Chen, K.-Y. Pu, Q.-L. Fan, X.-Y. Qi, Y.-Q. Huang, X.-M. Lu, and W. Huang *J. Polym. Sci. A: Polym. Chem.*, vol. 47, pp. 5057–5067, 2009.

[139] S. H. Lee, S. Kömürlü, X. Zhao, H. Jiang, G. Moriena, V. D. Kleiman, and K. S. Schanze *Macromolecules*, vol. 44, pp. 4742–4751, 2011.

[140] H. D. Burrows, V. M. M. Lobo, J. Pina, M. L. Ramos, J. S. de Melo, A. J. M. Valente, M. J. Tapia, S. Pradhan, U. Scherf, S. Hintschich, C. Rothe, and A. P. Monkman *Colloids and Surfaces A: Physicochem. Eng. Aspects*, vol. 270-271, pp. 61–66, 2005.

[141] M. J. Tapia, M. Monteserín, A. Costoyas, H. D. Burrows, A. T. Marques, A. A. C. C. Pais, A. J. M. Valente, R. Mallavia, U. Scherf, A. Pinazo, L. Pérez, and M. C. Morán *J. Mol. Liq.*, vol. 156, pp. 18–27, 2010.

[142] M. J. Tapia, H. D. Burrows, M. Knaapila, A. P. Monkman, A. Arroyo, S. Pradhan, U. Scherf, A. Pinazo, L. Pérez, and M. C. Morán *Langmuir*, vol. 22, pp. 10170–10174, 2006.

[143] K. Holmberg, B. Jönsson, B. Kronberg, and B. Lindman, *Surfactants and Polymers in Aqueous Solutions 2nd Ed.* England: John Wiley & Sons Ltd, 2003.

[144] S. M. Pinto, H. D. Burrows, M. M. Pereira, S. M. Fonseca, F. B. Dias, R. Mallavia, and M. J. Tapia *J. Phys. Chem. B*, vol. 113, pp. 16093–16100, 2009.

[145] M. Monteserín, H. D. Burrows, A. J. M. Valente, V. M. M. Lobo, R. Mallavia, M. J. Tapia, I. X. García-Zubiri, R. E. D. Paolo, and A. L. Maçanita *J. Phys. Chem. B*, vol. 111, pp. 13560–13569, 2007.

[146] M. Monteserín, H. D. Burrows, A. J. M. Valente, R. Mallavia, R. E. D. Paolo, A. L. Maçanita, and M. J. Tapia *J. Phys. Chem. B*, vol. 113, pp. 1294–1302, 2009.

[147] L. Arnaut, S. Formosinho, and H. Burrows, *Chemical Kinetics: From Molecular Structure to Chemical Reactivity.* Amsterdam: Elsevier, 2007.

[148] M. Liu, P. Kaur, D. H. Waldeck, C. Xue, and H. Liu *Langmuir*, vol. 21, pp. 1687–1690, 2005.

[149] D. Wang, X. Gong, P. S. Heeger, F. Rininsland, G. C. Bazan, and A. J. Heeger *J. Proc. Natl. Acad. Sci. U.S.A*, vol. 99, pp. 49–53, 2002.

[150] C. Fan, K. W. Plaxco, and A. J. Heeger *J. Am. Chem. Soc.*, vol. 124, pp. 5642–5643, 2002.

[151] C. B. Murphy, Y. Zhang, T. Troxler, V. Ferry, J. J. Martin, and W. E. J. Jr. *J. Phys. Chem. B*, vol. 108, pp. 1537–1543, 2004.

[152] J. I. T. da Costa, S. M. Fonseca, C. L. Silva, A. J. M. Valente, A. A. C. C. Pais, and H. D. Burrows, *Book of Proceedings: 2nd RICI, Colloids and Interfaces*. Coimbra Portugal: SPQ, 2007.

[153] H. Jiang, X. Zhao, and K. S. Schanze *Langmuir*, vol. 22, pp. 5541–5543, 2006.

[154] J. H. Ortony, T. Chatterjee, L. E. Garner, A. Chworos, A. Mikhailovsky, E. J. Kramer, and G. C. Bazan *J. Am. Chem. Soc.*, vol. 133, pp. 8380–8387, 2011.

[155] S.-A. Chen, H.-H. Lu, and C.-W. Huang, *Adv. Polym. Sci.* Verlag Berlin Heidelberg: Springer, 2008.

[156] E. Xu, H. Zhong, H. Lai, D. Zeng, J. Zhang, W. Zhu, and Q. Fang *Macromol. Chem. Phys.*, vol. 211, pp. 651–656, 2010.

[157] J. Morgado, F. Cacialli, R. H. Friend, R. Iqbal, G. Yahioglu, L. R. Milgrom, S. C. Moratti, and A. B. Holmes *Chem. Phys. Lett.*, vol. 325, pp. 552–558, 2000.

[158] E. J. W. List, C. Creely, G. Leising, N. Schulte, A. D. Schluter, U. Scherf, K. Müllen, and W. Graupner *Chem. Phys. Lett.*, vol. 325, pp. 132–138, 2000.

[159] J. Hofkens, M. Cotlet, T. Vosch, P. Tinnefeld, K. D. Weston, C. E. A. Grimsdale, K. Müllen, D. Beljonne, J. L. Brédas, S. J. G. Schweitzer, M. Sauer, and F. D. Schryver *PNAS*, vol. 100, pp. 13146–13151, 2003.

[160] E. Fron, A. Deres, S. Rocha, G. Zhou, K. Müllen, F. C. D. Schryver, M. Sliwa, U. Hiroshi, J. Hofkens, and T. Vosch *J. Phys. Chem. B*, vol. 325, pp. 1277–1287, 2010.

[161] Z. Yuan, J. Li, Y. Xiao, Z. Li, and X. Qian *J. Org. Chem.*, vol. 75, pp. 3007–3016, 2010.

[162] M. Supur, M. E. El-Khouly, J. H. Seok, J. H. Kim, K.-Y. Kay, and S. Fukuzumi *J. Phys. Chem. C*, vol. 114, pp. 10969–10977, 2010.

[163] D. Gosztola, M. P. Niemczyk, and W. Svec *J. Phys. Chem. A*, vol. 104, pp. 6545–6551, 2000.

[164] T. Kircher and H.-G. Löhmannsröben *Phys. Chem. Chem. Phys.*, vol. 1, pp. 3987–3992, 1999.

[165] C. Kirmaier, H. eun Song, E. Yang, J. K. Schwartz, E. Hindin, J. R. Diers, R. S. Loewe, K. ya Tomizaki, F. Chevalier, L. Ramos, R. R. Birge, J. S. Lindsey, D. F. Bocian, and D. Holten *J. Phys. Chem. B*, vol. 114, pp. 14249–14264, 2010.

[166] C. Flors, I. Oesterling, T. Schnitzler, E. Fron, G. Schweitzer, M. Sliwa, A. Herrmann, M. van der Auweraer, F. C. de Schryver, K. Müllen, and J. Hofkens *J. Phys. Chem. C*, vol. 111, pp. 4861–4870, 2007.

[167] T. Cordes, J. Vogelsang, M. Anaya, C. Spagnuolo, A. Gietl, W. Summerer, A. Herrmann, K. Müllen, and P. Tinnefeld *J. Am. Chem. Soc.*, vol. 132, pp. 2404–2409, 2010.

[168] R. Gomez and C. S. J. L. Segura *J. Org. Chem.*, vol. 75, pp. 5099–5108, 2010.

[169] E. Zhou, J. Cong, Q. Wei, K. Tajima, C. Yang, and K. Hashimoto *Angew. Chem. Int. Ed.*, vol. 50, pp. 2799–2803, 2011.

[170] D. M. Russell, A. C. Arias, R. H. Friend, C. Silva, C. Ego, A. C. Grimsdale, and K. Müllen *Appl. Phys. Lett.*, vol. 80, pp. 2204–2206, 2002.

[171] R. Gómez, D. Veldman, R. Blanco, C. Seoane, J. L. Segura, and R. A. J. Janssen *Macromolecules*, vol. 40, pp. 2760–2772, 2007.

[172] H. Langhals *Heterocycles*, vol. 40, pp. 477–500, 1995.

[173] M. W. Holman, R. Liu, L. Zang, P. Yan, S. A. DiBenedetto, R. D. Bowers, and D. M. Adams *J. Am. Chem. Soc.*, vol. 126, pp. 16126–16133, 2004.

[174] F. Jaiser, D. Neher, A. Meisel, H.-G. Nothofer, T. Miteva, A. Herrmann, K. Müllen, and U. Scherf *J. Chem. Phys.*, vol. 129, p. 114901 (9pp), 2008.

[175] J. Morgado, F. Cacialli, R. Iqbal, S. C. Moratti, A. B. Holmes, G. Yahioglu, L. R. Milgrom, and R. H. Friend *J. Mater. Sci. - Mater. Electron.*, vol. 11, pp. 97–103, 2000.

[176] W. E. Moerner and D. P. Fromm *Rev. Sci. Instrum.*, vol. 74, pp. 3597–3619, 2003.

[177] P. Dedecker and J. Hofkens *Nature Chemistry*, vol. 2, pp. 157–159, 2010.

[178] F. D. Schryver, T. Vosch, M. Cotlet, M. V. der Auweraer, K. Müllen, and J. Hofkens *Acc. Chem. Res.*, vol. 38, pp. 514–522, 2005.

[179] P. Dedecker, B. Muls, A. Deres, H. Uji-i, J. Hotta, M. Sliwa, J.-P. Soumillion, K. Müllen, J. Enderlein, and J. Hofkens *Adv. Mater.*, vol. 21, pp. 1079–1090, 2009.

[180] M. P. Gordon, T. Ha, and P. R. Selvin *PNAS*, vol. 101, pp. 6462–6465, 2004.

[181] F. Delport, A. Deres, J. i. Hotta, B. Verbruggen, B. Sels, J. Hofkens, and J. Lammertyn *Langmuir*, vol. 26, pp. 1594–1597, 2010.

[182] M. Tong, C. X. Chen, and Z. V. Vardeny *Phys. Rev. B*, vol. 75, p. 125207 (10pp), 2007.

[183] B. Kraabel, V. I. Klimov, R. Kohlman, S. Xu, H. L. Wang, and D. W. MacBranch *Phys. Rev. B*, vol. 61, p. 8501 (14pp), 2000.

[184] T. Virgili, D. G. Lidzey, and D. D. C. Bradley *Synthetic Metals*, vol. 111-112, pp. 203–206, 2000.

[185] T. Virgili, D. Marinotto, C. Manzoni, G. Cerullo, and G. L. G *Phys. Rev. Lett.*, vol. 94, p. 117402 (4pp), 2005.

[186] S. M. King, D. Dai, C. Rothe, and A. P. Monkman *Phys. Rev. B*, vol. 76, pp. 085204–7, 2007.

[187] R. Kersting, U. Lemmer, M. Deussen, H. J. Bakker, R. F. Mahrt, H. Kurz, V. I. Arkhipov, H. Bassler, and E. O. Gobel *Phys. Rev. Lett.*, vol. 73, pp. 1440–1443, 1994.

[188] E. M. Conwell and H. A. Mizes *Phys. Rev. B*, vol. 51, pp. 6953–6958, 1995.

[189] D. Gosztola, M. P. Niemczyk, W. A. Svec, A. S. Lukas, and M. R. Wasielewski *J. Phys. Chem. A*, vol. 104, pp. 6545–6551, 2000.

[190] F. B. Dias, M. Maiti, S. I. Hintschich, and A. P. Monkman *J. Chem. Phys.*, vol. 122, p. 054904 (11pp), 2005.

[191] E. Zojer, A. Pogantsch, E. Hennebicq, D. Beljonne, J. L. Bredas, P. S. de Freitas, U. Scherf, and E. J. W. List *J. Chem. Phys.*, vol. 117, pp. 6794–6802, 2002.

[192] H. D. Burrows, J. S. de Melo, M. Forster, R. Güntner, U. Scherf, A. P. Monkman, and S. Navaratnam *Chem. Phys. Lett.*, vol. 385, pp. 105–110, 2004.

[193] S. Fratiloiu, S. M. Fonseca, F. C. Grozema, H. D. Burrows, M. L. Costa, A. Charas, J. Morgado, and L. D. A. Siebbeles *J. Phys. Chem. C*, vol. 111, pp. 5812–5820, 2007.

[194] E. E. Neuteboom, S. C. J. Meskers, E. H. A. Beckers, S. Chopin, and R. A. J. Janssen *J. Phys. Chem. A*, vol. 110, pp. 12363–12371, 2006.

[195] M. L. Davies, P. Douglas, H. D. Burrows, M. da Graça Miguel, and A. Douglas *J. Phys. Chem. B*, vol. 115, pp. 6885–6892, 2011.

[196] C. Li and Z. Bo *Polymer*, vol. 51, pp. 4273–4294, 2010.

[197] P. Dutta, R. Rai, and S. Pandey *J. Phys. Chem. B*, vol. 115, pp. 3578–3587, 2011.

[198] A. Hagfeldt, G. Boschloo, L. Sun, L. Kloo, and H. Pettersson *Chem. Rev.*, vol. 110, pp. 6595–6663, 2010.

[199] R. K. Lammi, R. W. Wagner, A. Ambroise, J. R. Diers, D. F. Bocian, D. Holten, and J. S. Lindsey *J. Phys. Chem B.*, vol. 105, pp. 5341–5352, 2001.

[200] J. Song, N. Aratani, P. Kim, D. Kim, H. Shinokubo, and A. Osuka *Angew. Chem. Int. Ed.*, vol. 49, pp. 3617–3620, 2010.

[201] B. J. Campo, J. Duchateau, C. R. Ganivet, B. Ballesteros, J. Gilot, M. M. Wienk, W. D. Oosterbaan, L. Lutsen, T. J. Cleij, G. de la Torre, R. A. J. Janssen, D. Vanderzande, and T. Torres *Dalton Trans.*, vol. 40, pp. 3979–3988, 2011.

[202] M. J. Zöllner, J. S. Frähmcke, M. Elstner, U. Jahn, P. G. Jones, E. Becker, W. Kowalsky, and H.-H. Johannes *Macromol. Chem. Phys.*, vol. 211, pp. 359–371, 2010.

[203] P. Kim, J. Sung, H. Uoyama, T. Okujima, H. Uno, and D. Kim *J. Phys. Chem. B*, vol. 115, pp. 3784–3792, 2011.

[204] T. Yoneda, S. Saito, H. Yorimitsu, and A. Osuka *Angew. Chem. Int. Ed.*, vol. 50, pp. 3475–3478, 2011.

[205] P. A. Liddell, M. G. Gervaldo, J. W. Bridgewater, A. E. Keirstead, S. Lin, T. A. Moore, A. L. Moore, and D. Gust *Chem. Mater.*, vol. 20, pp. 135–142, 2008.

[206] L. J. Twyman, A. Ellis, and P. J. Gittins *Macromolecules*, vol. 44, pp. 6365–6369, 2011.

[207] S. Prathapan, T. E. Johnson, and J. S. Lindsey *J. Am. Chem. Soc.*, vol. 115, pp. 7519–7520, 1993.

[208] J. Seth, V. Palaniappan, T. E. Johnson, S. Prathapan, J. S. Lindsey, and D. F. Bocian *J. Am. Chem. Soc.*, vol. 116, pp. 10578–10592, 1994.

[209] R. Takahashi and Y. Kobuke *J. Am. Chem. Soc.*, vol. 125, pp. 2372–2373, 2003.

[210] I. K. Martin and L. Twyman *J. Tetrahedron Lett.*, vol. 42, pp. 1119–1121, 2001.

[211] M. A. Castriciano, A. Romeo, N. Angelini, N. Micali, A. Longo, A. Mazzaglia, and L. M. Scolaro *Macromolecules*, vol. 39, pp. 5489–5496, 2006.

[212] S. Saini, G. Srinivas, and B. Bagchi *J. Phys. Chem. B*, vol. 113, pp. 1817–1832, 2009.

[213] W. Tang, J. Hai, Y. Dai, Z. Huang, B. Lu, F. Yuan, J. Tang, and F. Zhang *Solar Energy Materials & Solar Cells*, vol. 94, pp. 1963–1979, 2010.

[214] B. Li, X. Xu, M. Sun, Y. Fu, G. Yu, Y. Liu, and Z. Bo *Macromolecules*, vol. 39, pp. 456–461, 2006.

[215] W. Wang, H. Wang, Y. Yang, Y. He, L. Zhang, Y. Li, and X. Li *Macromolecules*, vol. 43, pp. 709–715, 2010.

[216] B. P. Lyons, R. P. Jackson, K. S. Wong, and A. P. Monkman *Synthetic Metals*, vol. 135-136, pp. 367–368, 2003.

[217] B. J. Littler, M. A. Miller, C.-H. Hung, R. W. Wagner, D. F. O'Shea, P. D. Boyle, and J. S. Lindsey *J. Org. Chem.*, vol. 64, pp. 1391–1396, 1999.

[218] S. G. DiMagno, V. S.-Y. Lin, and M. J. Therien *J. Org. Chem.*, vol. 58, pp. 5983–5993, 1993.

[219] X. Zhou, P. Shen, B. Zhao, P. Jiang, L. Deng, and S. Tan *J. Polym. Sci., Part A: Polym. Chem.*, vol. 49, pp. 2685–2692, 2011.

[220] X. Xu, H. Chen, E. H. X. Cai, and Y. Ying *Polymer Bulletin*, vol. 60, pp. 7–14, 2008.

[221] H. Huang, C. Zhu, S. Zhang, W. Li, Y. Guo, X. Zhan, Y. Liu, and Z. Bo *Macromolecules*, vol. 41, pp. 6895–6902, 2008.

[222] M. Gouterman *J. Mol. Spectrosc.*, vol. 6, pp. 138–163, 1961.

[223] J. S. de Melo, A. J. F. N. Sobral, A. M. d'A. R. Gonsalves, and H. D. Burrows *J. Photochem. Photobiol. A: Chemistry*, vol. 172, pp. 151–160, 2005.

[224] C. J. P. Monteiro, M. M. Pereira, S. M. A. Pinto, A. V. C. Simões, G. F. F. Sá, L. G. Arnaut, S. J. Formosinho, S. Simões, and M. F. Wyatt *Tetrahedron*, vol. 64, pp. 5132–5138, 2008.

[225] K. Holmberg, B. Jönsson, B. Kronberg, and B. Lindman, *Surfactants and Polymers in Aqueous Solution, 2nd Edition.* West Sussex, England: John Wiley & Sons Ltd, 2003.

[226] M. Fujitsuka, A. Okada, S. Tojo, F. Takei, K. Onitsuka, S. Takahashi, and T. Majima *J. Phys. Chem. B*, vol. 108, pp. 11935–11941, 2004.

[227] R. Iqbal, S. C. Moratti, A. B. Holmes, G. Yahioglu, L. F. Milgrom, F. Cacialli, J. Morgado, and R. H. Friend *J. Mater. Sci. - Mater. Electron.*, vol. 11, pp. 97–103, 2000.

[228] J. Morgado, F. Cacialli, R. Iqbal, S. C. Moratti, A. B. Holmes, G. Yahioglu, L. R. Milgrom, and R. H. Friend *J. Mater. Chem.*, vol. 11, pp. 278–283, 2001.

[229] C. Tan, E. Atas, J. G. Müller, M. R. Pinto, V. D. Kleiman, and K. S. Schanze *J. Am. Chem. Soc.*, vol. 126, pp. 13685–36949, 2004.

[230] J. G. Müller, E. Atas, C. Tan, K. S. Schanze, and V. D. Kleiman *J. Am. Chem. Soc.*, vol. 128, pp. 4007–4016, 2006.

[231] W. Tang, L. Ke, L. Tan, T. Lin, and T. K. Z.-K. Chen *Macromolecules*, vol. 40, pp. 6164–6171, 2007.

[232] E. Lim, B.-J. Jung, and H.-K. Shim *J. Polym. Sci., Part A: Polym. Chem.*, vol. 44, pp. 243–253, 2006.

[233] J. Bouffard and T. M. Swager *Macromolecules*, vol. 41, pp. 5559–5562, 2008.

[234] A. P. Kulkarni and Y. Z. S. A. Jenekhe *Macromolecules*, vol. 38, pp. 1553–1563, 2005.

[235] J. Mei, N. C. Heston, S. V. Vasilyeva, and J. R. Reynolds *Macromolecules*, vol. 42, pp. 1482–1487, 2009.

[236] K.-C. Li, J.-H. Huang, Y. C. Hsu, P.-J. Huang, C.-W. Chu, J.-T. Lin, K.-C. Ho, K.-H. Wei, and H.-C. Lin *Macromolecules*, vol. 42, pp. 3681–3693, 2009.

[237] J.-M. Raimundo, P. B. H. Brisset, S. Akoudad, and J. Roncali *Chem. Commun.*, pp. 939–940, 2000.

[238] K. R. J. Thomas, J. T. Lin, M. Velusamy, Y.-T. Tao, and C.-H. Chuen *Adv. Funct. Mater.*, vol. 14, pp. 83–90, 2004.

[239] B. Burkhart, P. K. Khlyabich, T. C. Canak, T. W. LaJoie, and B. C. Thompson *Macromolecules*, vol. 44, pp. 1242–1246, 2011.

[240] K.-H. Ong, S.-L. Lim, H.-S. Tan, H.-K. Wong, J. Li, Z. Ma, L. C. H. Moh, S.-H. Lim, J. C. de Mello, and Z.-K. Chen *Adv. Mater.*, vol. 23, pp. 1409–1413, 2011.

[241] D. Kabra, L. P. Lu, M. S. Song, H. J. Snaith, and R. H. Friend *Adv. Mater.*, vol. 22, pp. 3194–3198, 2010.

[242] J. Gilot, R. Abbel, G. Lakhwani, E. W. Meijer, A. P. H. J. Schenning, and S. C. J. Meskers *Adv. Mater.*, vol. 22, pp. 131–134, 2010.

[243] Z. Chen, J. Fang, F. Gao, T. J. K. Brenner, K. K. Banger, X. Wang, W. T. S. Huck, and H. Sirringhaus *Organic Electronics*, vol. 12, pp. 461–471, 2011.

[244] E. Lim, B.-J. Jung, and H.-K. Shim *Macromolecules*, vol. 36, pp. 4288–4293, 2003.

[245] E. Lim, B.-J. Jung, J. Lee, H.-K. Shim, J.-I. Lee, Y. S. Yang, and L.-M. Do *Macromolecules*, vol. 38, pp. 4531–4535, 2005.

[246] M. J. Kang, I. Doi, H. Mori, E. Miyazaki, K. Takimiya, M. Ikeda, and H. Kuwabara *Adv. Mater.*, vol. 23, pp. 1222–1225, 2011.

[247] J. Huang, Y. Niu, W. Yang, Y. Mo, M. Yuan, and Y. Cao *Macromolecules*, vol. 35, pp. 6080–6082, 2002.

[248] S.-H. Jung, H. K. Kim, S.-H. Kim, S.-H. Kim, Y. H. Kim, S. C. Jeoung, and D. Kim *Macromolecules*, vol. 33, pp. 9277–9288, 2000.

[249] M. Jayakannan, P. A. V. Hal, and R. A. J. Janssen *J. Polym. Sci.: Part A: Polym. Chem.*, vol. 40, pp. 251–261, 2002.

[250] M. Jayakannan, P. A. V. Hal, and R. A. J. Janssen *J. Polym. Sci.: Part A: Polym. Chem.*, vol. 40, pp. 2360–2372, 2002.

[251] M. Karikomi, C. Kitamura, S. Tanaka, and Y. Yamashita *J. Am. Chem. Soc.*, vol. 117, pp. 6791–6792, 1995.

[252] Y. Zhu, R. D. Champion, and S. A. Jenekhe *Macromolecules*, vol. 39, pp. 8712–8719, 2006.

[253] Y. Zhang, Q. Hou, Q.-L. Niu, S.-W. Zheng, S.-T. Li, M. He, and G.-H. Fan *Chin. Phys. Lett.*, vol. 26, pp. 077811–077815, 2009.

[254] B. Friedel, C. R. McNeill, and N. C. Greenham *Chem. Mater.*, vol. 22, pp. 3389–3398, 2010.

[255] E. Bundgaard and F. C. Krebs *Macromolecules*, vol. 39, pp. 2823–2831, 2006.

[256] C. Wu, Y. Jin, T. Schneider, D. R. Burnham, P. B. Smith, and D. T. Chiu *Angew. Chem., Int. Ed.*, vol. 49, pp. 9436–9440, 2010.

[257] C. Wu, T. Schneider, M. Zeigler, J. Yu, P. G. Schiro, D. R. Burnham, J. D. McNeill, and D. T. Chiu *J. Am. Chem. Soc.*, vol. 132, pp. 15410–15417, 2010.

[258] F. Ye, C. Wu, Y. Jin, Y.-H. Chan, X. Zhang, and D. T. Chiu *J. Am. Chem. Soc.*, vol. 133, pp. 8146–8149, 2011.

[259] K.-P. Tseng, F.-C. Fang, J.-J. Shyue, K.-T. Wong, G. Raffy, A. D. Guerzo, and D. M. Bassani *Angew. Chem. Int. Ed.*, vol. 50, pp. 7032–7036, 2011.

[260] A. Garcia and T.-Q. Nguyen *J. Phys. Chem. C*, vol. 112, pp. 7054–7061, 2008.

[261] I.-B. Kim and U. H. F. Bunz *J. Am. Chem. Soc.*, vol. 128, pp. 2818–2819, 2006.

[262] T. M. Swager *Acc. Chem. Res.*, vol. 41, pp. 1181–1189, 2008.

[263] Y.-Q. Huang, Q.-L. Fan, X.-M. Lu, C. Fang, S.-J. Liu, L. Yu-Wen, L.-H. Wang, and W. Huang *J. Polym. Sci., Part A: Polym. Chem.*, vol. 44, pp. 5778–5794, 2006.

[264] D.-L. Jiang, C.-K. Choi, K. Honda, W.-S. Li, T. Yuzawa, and T. Aida *J. Am. Chem. Soc.*, vol. 126, pp. 12084–12089, 2004.

[265] B. Zhu, Y. Han, M. Sun, and Z. Bo *Macromolecules*, vol. 40, pp. 4494–4500, 2007.

[266] F. S. Mancilha, B. A. D. S. Neto, A. S. Lopes, P. F. M. Jr., F. H. Quina, R. S. Gonçalves, and J. Dupont *Eur. J. Org. Chem.*, pp. 4924–4933, 2006.

[267] Q. Hou, Y. Xu, W. Yang, M. Yuan, J. Peng, and Y. Cao *J. Mater. Chem.*, vol. 12, pp. 2887–2892, 2002.

[268] K. Pilgram, M. Zupan, and R. Skiles *J. Heterocycl. Chem.*, vol. 7, pp. 629–633, 1970.

[269] W. Li, R. Qin, Y. Zhou, M. Andersson, F. Li, C. Zhang, B. Li, Z. Liu, Z. Bo, and F. Zhang *Polymer*, vol. 51, pp. 3031–3038, 2010.

[270] F. D. Dias, K. T. Kamtekar, T. Cazati, G. Williams, M. B. Bryce, and A. P. Monkman *ChemPhysChem*, vol. 10, pp. 2096–2104, 2009.

[271] K.-Y. Pu and B. Liu *Adv. Funct. Mater.*, vol. 19, pp. 277–284, 2009.

[272] L. Stryer *Ann. Rev. Biochem.*, vol. 47, pp. 819–846, 1978.

[273] A. Harriman, L. J. Mallon, K. J. Elliot, A. Haefele, G. Ulrich, and R. Ziessel *J. Am. Chem. Soc.*, vol. 131, pp. 13375–13386, 2009.

[274] T. Ishiyama, M. Murata, and N. Miyaura *J. Org. Chem.*, vol. 60, pp. 7508–7510, 1995.

[275] A. Harriman, A. Khatyr, R. Ziessel, and A. C. Benniston *Angew. Chem. Int. Ed.*, vol. 39, pp. 4287–4289, 2000.

[276] Z. S. Romanova, K. Deshayes, and P. Piotrowiak *J. Am. Chem. Soc.*, vol. 123, pp. 11029–11036, 2001.

[277] S. Tannert, E. A. Ermilov, J. O. Vogel, M. T. M. Choi, D. K. P. Ng, and B. Röder *J. Phys. Chem. B*, vol. 111, pp. 8053–8062, 2007.

[278] A. C. Benniston, A. Harriman, P. Li, and C. A. Sams *J. Am. Chem. Soc.*, vol. 127, pp. 1553–2564, 2005.

[279] H.-C. Chen, Z.-Q. You, and C.-P. Hsu *J. Chem. Phys.*, vol. 129, p. 084798 (10pp), 2008.

[280] R. F. Kelley, S. J. Lee, T. M. Wilson, Y. Nakamura, D. M. Tiede, A. Osuka, J. T. Hupp, and M. R. Wasielewski *J. Am. Chem. Soc*, vol. 130, pp. 4277–4284, 2008.

[281] B. V. Averbeke and D. Beljonne *J. Phys. Chem. A*, vol. 113, pp. 2677–2682, 2009.

[282] A. Olaya-Castro, C. F. Lee, F. F. Olsen, and N. F. Johnson *Phys. Rev. B*, vol. 78, p. 085115 (7pp), 2008.

[283] L. Brizhik, A. Eremko, B. Piette, and W. Zakrzewski *Chem. Phys.*, vol. 324, pp. 259–266, 2006.

[284] P. E. Shaw, A. Ruseckas, and I. D. W. Samuel *Phys. Rev. B*, vol. 78, p. 245201 (5pp), 2008.

[285] K. Kilså, J. Kajanus, J. Mårtensson, and B. Albinsson *J. Phys. Chem. B*, vol. 103, pp. 7329–7339, 1999.

[286] K. D. Jordan and M. N. Paddon-Row *Chem. Rev.*, vol. 92, pp. 395–410, 1992.

[287] J. Pina, J. S. de Melo, H. D. Burrows, T. W. Bünnagel, D. Dolfen, C. J. Kudla, and U. Scherf *J. Phys. Chem. B*, vol. 113, pp. 15928–15936, 2009.

[288] M. Wohlgenannt, X. M. Jiang, and Z. V. Vardeny *Phys. Rev. B*, vol. 69, p. 241204 (4pp), 2004.

[289] C. Rothe, K. Brunner, I. Bach, S. Heun, and A. P. Monkman *J. Chem. Phys.*, vol. 122, p. 084706 (6pp), 2005.

[290] J. Casado, R. G. Hicks, V. Hernández, D. J. T. Myles, M. C. R. Delgado, and J. T. L. Navarrete *J. Chem. Phys.*, vol. 118, pp. 1912–1920, 2003.

[291] M. S. Liu, X. Jiang, P. Herguth, S. Liu, and A. K.-Y. Jen *SPIE*, vol. 4800, pp. 130–137, 2003.

[292] J. J. Intemann, J. F. Mike, M. Cai, S. Bose, T. Xiao, T. C. Mauldin, R. A. Roggers, J. Shinar, R. Shinar, and M. Jeffries-EL *Macromolecules*, vol. 44, pp. 248–255, 2011.

[293] C. J. Tonzola, M. M. Alam, B. A. Bean, and S. A. Jenekhe *Macromolecules*, vol. 37, pp. 3554–3563, 2004.

[294] E. Jeong, S. E. Kim, I. H. Jung, Y. Xia, L. K, H. Suh, H.-K. Shim, and H. Y. Woo *J. Polym. Sci.: Part A: Polym. Chem.*, vol. 47, pp. 3467–3479, 2009.

[295] S. K. Lee, B.-J. Jung, T. Ahn, Y. K. Jung, J.-I. Lee, I.-N. Kang, J. Lee, J.-H. Park, and H. K. Shim *J. Polym. Sci.: Part A: Polym. Chem.*, vol. 45, pp. 3380–3390, 2007.

[296] J. Liu, Z. Xie, Y. Cheng, Y. Geng, L. Wang, X. Jing, and F. Wang *Adv. Mater.*, vol. 19, pp. 531–535, 2007.

[297] J. Liu, Q. Zhou, Y. Cheng, Y. Geng, L. Wang, D. G. Ma, X. B. Jing, and F. S. Wang *Adv. Mater.*, vol. 17, pp. 2974–2978, 2005.

[298] L. S. Fuller, B. Iddon, and K. A. Smith *J. Chem. Soc. Perkin Trans. 1*, pp. 3465–3470, 1997.

[299] J. Luo, X. Li, Q. Hou, J. Peng, W. Yang, and Y. Cao *Adv. Mater.*, vol. 19, pp. 1113–1117, 2007.

[300] J. Luo, J. Peng, and Y. Cao *Appl. Phys. Lett.*, vol. 87, pp. 261103–30, 2005.

[301] Y.-J. Cheng, S.-H. Yang, and C.-S. Hsu *Chem. Rev.*, vol. 109, pp. 5868–5923, 2009.

[302] X. Xu, H. Chen, E. Huo, X. Cai, Y. Li, and Q. Jiang *Polymer Bulletin*, vol. 60, pp. 7–14, 2008.

[303] E. Zhou, K. Tajima, C. Yang, and K. Hashimoto *J. Mater. Chem.*, vol. 20, pp. 2362–2368, 2010.

[304] P. Piyakulawat, A. Keawprajak, A. Chindaduang, A. Helfer, and U. Asawapirom *E-Polymers*, vol. 071, 2010.

[305] P. P. Nefedov, M. A. Lazareva, B. G. Belenkii, S. Y. Frenkel, and M. M. Koton *J. Chromatogr.*, vol. 170, pp. 11–24, 1979.

[306] E. López-Cabarcos, J. R. Retama, V. Sholin, and S. A. Carter *Polym. Int.*, vol. 56, pp. 588–592, 2007.

[307] M. Laurenti, J. Rubio-Retama, F. Garcia-Blanco, and E. López-Cabarcos *Langmuir*, vol. 24, pp. 13321–13327, 2008.

[308] H. A. Ho, K. Doré, M. Boissinot, M. G. Bergeron, R. M. Tanguay, D. Boudreau, and M. Leclerc *J. Am. Chem. Soc.*, vol. 127, pp. 12673–12676, 2005.

[309] B. S. Gaylord, A. J. Heeger, and G. C. Bazan *PNAS*, vol. 99, pp. 10954–10957, 2002.

[310] H.-A. Ho, A. Najari, and M. Leclerc *Acc. Chem. Res.*, vol. 41, pp. 168–178, 2008.

[311] P. S. Heeger and A. J. Heeger *PNAS*, vol. 96, pp. 12219–12221, 1999.

[312] J. J. Lavigne, D. L. Broughton, J. N. Wilson, B. Erdogan, and U. H. F. Bunz *Macromolecules*, vol. 36, pp. 7409–7412, 2003.

[313] B. Liu, B. S. Gaylord, S. Wang, and G. C. Bazan *J. Am. Chem. Soc.*, vol. 125, pp. 6705–6714, 2003.

[314] K.-Y. Pu, K. Li, X. Zhang, and B. Liu *Adv. Funct. Mater.*, vol. 22, pp. 4186–4189, 2010.

[315] X. Xu, B. Han, J. Chen, J. Peng, H. Wu, and Y. Cao *Macromolecules*, vol. 44, pp. 4204–4212, 2011.

[316] R. Yang, Y. Xu, X.-D. Dang, T.-Q. Nguyen, Y. Cao, and G. C. Bazan *J. Am. Chem. Soc.*, vol. 130, pp. 3282–3283, 2008.

[317] A. Chakrabarty, P. Das, A. Mallick, and N. Chattopadhyay *J. Phys. Chem. B*, vol. 112, pp. 3684–3692, 2008.

[318] S. M. Fonseca, M. E. Eusébio, C. R, H. D. Burrows, M. J. Tapia, and U. Olsson *J. Colloid Interface Sci*, vol. 315, pp. 805–809, 2007.

[319] H. D. Burrows, M. J. Tapia, S. M. Fonseca, A. J. M. Valente, V. M. M. Lobo, L. L. G. Justino, S. Qiu, S. Pradhan, U. Scherf, N. Chattopadhyay, M. Knaapila, and V. M. Garamus *Appl. Mater. Interfaces*, vol. 1, pp. 864–874, 2009.

[320] H. D. Burrows, M. J. Tapia, C. L. Silva, A. A. C. C. Pais, S. M. Fonseca, J. Pina, J. S. de Melo, Y. Wang, E. F. Marques, M. Knaapila, A. P. Monkman, V. M. Garamus, S. Pradhan, and U. Scherf *J. Phys. Chem. B*, vol. 111, pp. 4401–4410, 2007.

[321] J. W. Goodwin, *Colloids and Interfaces with Surfactants and Polymers - An Introduction.* West Sussex, England: John Wiley & Sons Ltd, 2004.

[322] J. Mata, D. Varade, and P. Bahadur *Thermochimica Acta*, vol. 428, pp. 147–155, 2008.

[323] A. C. F. Ribeiro, V. M. M. Lobo, A. J. M. Valente, E. F. G. Azevedo, M. G. Miguel, and H. D. Burrows *Colloid Polym. Sci.*, vol. 283, pp. 277–283, 2004.

[324] K. Maiti, I. Chakraborty, S. C. Bhattacharya, A. K. Panda, and S. P. Moulik *J. Phys. Chem. B*, vol. 111, pp. 14175–14185, 2007.

[325] S. P. Moulik and B. K. Paul *Adv. Colloid Interface Sci.*, vol. 78, pp. 99–105, 1998.

[326] P. Kaur, H. Yue, M. Wu, M. Liu, J. Treece, and D. H. Waldeck *J. Phys. Chem. B*, vol. 111, pp. 8589–8596, 2007.

[327] H. Yue, M. Wu, C. Xue, S. Velayudham, H. Liu, and D. H. Waldeck *J. Phys. Chem. B*, vol. 112, pp. 8218–8226, 2008.

[328] K. N. Bakeev, Y. M. Shu, A. B. Zezin, and V. A. Kabanov *Macromolecules*, vol. 29, pp. 1320–1325, 1996.

[329] W. J. MacKnight, E. A. Ponomarenko, and D. A. Tirrell *Acc. Chem. Res.*, vol. 31, pp. 781–788, 1998.

[330] K. C. Tam and E. Wyn-Jones *Chem. Soc. Rev.*, vol. 35, pp. 693–709, 2008.

[331] Y. Morishima, M. Mizusaki, K. Yoshida, and P. L. Dubin *Colloids Surf.*, vol. 147, pp. 149–159, 1999.

[332] T. Radeva, *Physical Chemistry of Polyelectrolytes.* New York, USA: Marcel Dekker, Inc., 2001.

[333] C. L. Mesa *J. Colloid Interface Sci.*, vol. 286, pp. 148–157, 2005.

[334] J. Yan, D. Wang, F. Bu, and F. F. Yang *J. Sol. Chem.*, vol. 39, pp. 1501–1508, 2010.

[335] P. Mukerjee and K. J. Mysels, *Critical Micelle Concentration of Aqueous Surfactant Systems*. Washington D.C., USA: National Bureau of Standards, 1971.

[336] M. A. Mougán, A. Coello, A. Jover, F. Meijide, and J. V. Tato *J. Chem. Educ.*, vol. 72, pp. 284–286, 1995.

[337] G. Akerlof and O. A. Short *J. Am. Chem. Soc.*, vol. 58, pp. 1241–1243, 1936.

[338] E. Somma, B. Loppinet, C. Chi, G. Fytas, and G. Wegner *Phys. Chem. Chem. Phys.*, vol. 8, pp. 2773–2887, 2006.

[339] Z. Weican, L. Ganzuo, M. Jianhai, S. Qiang, Z. Liqiang, L. Haojun, and W. Chi *Chinese Sci. Bull.*, vol. 45, pp. 1854–1857, 2000.

[340] S. B. Velegol, B. D. Fleming, S. Biggs, E. J. Wanless, and R. D. Tilton *Langmuir*, vol. 16, pp. 2548–2556, 2000.

[341] S. M. C. Silva, F. E. Antunes, J. J. S. Sousa, A. J. M. Valente, and A. A. C. C. Pais *Carbohydr. Polym.*, vol. 86, pp. 35–44, 2011.

[342] D. Zanette, A. A. Ruzza, S. J. Froehner, and E. Minati *Colloid Surface A*, vol. 108, pp. 91–100, 1996.

[343] J. Koetz and S. Kosmella, *Polyelectrolytes and nanoparticles*. Berlin Heidelberg, Germany: Springer, 2007.

[344] S. Schwarz, W. Jaeger, S. Bratskayaa, J. Bohrisch, T. Schimmel, M. Mende, M. Oelmann, and V. Boyko *ColloidsandSurfacesA:Physicochem. Eng. Aspects*, vol. 276, pp. 65–71, 2006.

[345] N. Beheshti, K. Zhu, and A.-L. Kjøniksen *Colloid Polym. Sci.*, vol. 288, pp. 1121–1130, 2010.

[346] J. Koetz, H. Koepke, G. Schmidt-Naake, P. Zarras, and O. Vogl *Polymer*, vol. 37, pp. 2775–2781, 1996.

[347] L. Zhang and J. Sun *Macromolecules*, vol. 43, pp. 2413–2420, 2010.

[348] D. M. Kaschak and T. E. Mallouk *J. Am. Chem. Soc.*, vol. 118, pp. 4222–4223, 1996.

[349] D. V. Pergushov, V. A. Izumrudov, A. B. Zezin, and V. A. Kabanov *Polymer Science Ser. A*, vol. 35, pp. 844–849, 1993.

[350] D. V. Pergushov, V. A. Izumrudov, A. B. Zezin, and A. V. Kabanov *Vysokomol. Soedin.*, vol. 37, pp. 1739–1746, 1995.

[351] H. Oie, A. Sudo, and T. Endo *J. Polym. Sci.: Part A: Polym. Chem.*, vol. 49, pp. 3174–3183, 2011.

[352] S. Harada and S. Hasegawa *Macromol. Rapid Commun.*, vol. 5, pp. 27–31, 1984.

[353] K. P. R. Nilsson, J. Rydberg, L. Baltzer, and O. Inganäs *PNAS*, vol. 100, pp. 10170–10174, 2003.

[354] P. Björk, A. Herland, I. G. Scheblykin, and O. Inganäs *Nano Lett.*, vol. 5, pp. 1848–1953, 2005.

[355] B. Nandy and P. K. Maiti *J. Phys. Chem. B*, vol. 115, pp. 217–230, 2011.

[356] B. Liu and G. C. Bazan *J. Am. Chem. Soc.*, vol. 126, pp. 1942–1943, 2004.

[357] B. Liu and G. C. Bazan *J. Am. Chem. Soc.*, vol. 129, pp. 1188–1196, 2006.

[358] S. Zhu, Y. Wu, Q. Chen, Z. Yu, C. Wang, S. Jin, Y. Dinga, and G. Wu *Green Chem.*, vol. 8, pp. 325–327, 2006.

[359] M. J. Earle and K. R. Seddon *Pure Appl. Chem.*, vol. 72, pp. 1391–1398, 2000.

[360] P. Wasserscheid and W. Keim *Angew. Chem. Int. Ed.*, vol. 39, pp. 3772–3789, 2000.

[361] J. f. Liu, J. A. Jönsson, and G. b. Jiang *Trend. Anal. Chem.*, vol. 24, pp. 20–27, 2005.

[362] R. P. Swatloski, S. K. Spear, J. D. Holbrey, and R. D. Rogers *J. Am. Chem. Soc.*, vol. 124, pp. 4974–4975, 2002.

[363] Q. Pei, G. Yu, C. Zhang, Y. Yang, and A. J. Heeger *Science*, vol. 269, pp. 1086–1088, 1995.

[364] Q. Pei, Y. Yang, G. Yu, C. Zhang, and A. J. Heeger *J. Am. Chem. Soc.*, vol. 118, pp. 3922–3929, 1996.

[365] G. Mauthner, U. Scherf, and E. J. W. List *Appl. Phys. Letters*, vol. 91, p. 133501 (3pp), 2007.

[366] D. B. Rodovsky, O. G. Reid, L. S. C. Pingree, and D. S. Ginger *ACS Nano*, vol. 4, pp. 2673–2680, 2010.

[367] Y. Shao, G. C. Bazan, and A. J. Heeger *Adv. Mater.*, vol. 20, pp. 1191–1193, 2008.

[368] Y. Shao, G. C. Bazan, and A. J. Heeger *Adv. Mater.*, vol. 19, pp. 365–370, 2007.

[369] J.-H. Shin, S. Xiao, Å. Fransson, and L. Edman *Appl. Phys. Lett.*, vol. 87, p. 043506 (3pp), 2005.

[370] L. Edman, J. Swensen, D. Moses, and A. J. Heeger *Appl. Phys. Lett.*, vol. 84, p. 3744 (2pp), 2004.

[371] V. Cimrová, W. Schmidt, R. Rulkens, M. Schulze, W. Meyer, and D. Neher *Adv. Mater.*, vol. 8, pp. 585–588, 1996.

[372] D. Vak, S.-H. Oh, and D.-Y. Kim *Appl. Phys. Lett.*, vol. 94, p. 243305 (3pp), 2009.

[373] O. Ingamäs *Chem. Soc. Rev.*, vol. 39, pp. 2633–2642, 2010.

[374] M. J. Tapia, M. Monteserín, A. J. M. Valente, H. D. Burrows, and R. Mallavia *Adv. Colloid Interface Sci.*, vol. 158, pp. 94–107, 2010.

[375] A. R. Watkins *J. Phys. Chem.*, vol. 78, pp. 2555–2558, 1974.